Université de Strasbourg
en cotutelle avec l'Université de Bologna

École Doctorale des Sciences Chimiques

ISIS (UMR 7006)

Thèse

présentée par Thomas Botzung

soutenue le 6 décembre 2019

pour obtenir le grade de: **Docteur de l'Université de Strasbourg**
Discipline/Spécialité: **Physique**

Study of strongly correlated one-dimensional systems with long-range interactions

THÈSE dirigée par:
Pr. PUPILLO Guido Professeur, Université de Strasbourg
Pr. ERCOLESSI Elisa Professeur, Université de Bologna

RAPPORTEURS :
Pr. CIUTI Cristiano Professeur, Université Paris Diderot
Pr. SCARDICCHIO Antonello Professeur, Abdus Salam ICTP, Trieste

Université de Strasbourg

EDSC École Doctorale des Sciences Chimiques

Thomas Botzung

Study of strongly correlated one-dimensional systems with long-range interactions

Résumé Durant cette thèse, nous étudions des systèmes unidimensionnels avec des couplages longue-portée. Dans la première partie, nous démontrons que ces couplages entraînent une décroissance algébrique des corrélations dans des fils quantiques désordonnés. Deuxièmement, nous analysons un modèle étendu de Hubbard où les particules interagissent via un potentiel « soft-core » générant de nouvelles phases exotiques. Dans le troisième chapitre, nous démontrons que restaurer l'extensivité a une influence sur les propriétés de basse énergie de modèle quantique dans la limite thermodynamique. Finalement, nous présentons des résultats préliminaires sur la modification de la localisation d'Anderson en présence d'un couplage avec une cavité.

Mots clés: Systèmes quantiques à N corps, Physique de la matière condensée, Méthodes numériques, Interactions à longue portée.

Abstract During this Ph.D, we studied one-dimensional systems with long-range couplings. In the first part, we demonstrate that power-law couplings lead to an algebraic decay of correlations at long distances in disordered quantum wires. In the second chapter, we analysed an extended Hubbard model where particles interact via a finite-range potential that induces frustration and new exotic phases. In the third chapter, we demonstrated that restoring energy extensivity has an influence on the low-energy properties of quantum model in the thermodynamic limit. Finally, we provide preliminary results on the modification of Anderson localization due to the coupling to a cavity mode.

Keywords: Quantum Many-Body Systems, Condensed Matter Physics, Numerical Methods, Long-Range Interactions.

Résumé

Les interactions à longue-portée sont intrinsèques à une myriade de systèmes physiques, allant des amas auto-gravitants des matériaux ferromagnétiques, des plasmas non-neutres, des systèmes de cavités-QED ou encore des chaines d'atomes/spins à 1D. En raison de leurs fascinantes propriétés, elles jouent un rôle prépondérant dans la recherche actuelle, aussi bien sur le plan théorique qu'expérimental. Récemment, de nombreux travaux théoriques ont mis en lumière des effets intriguant pour ces systèmes, incluant par exemple des nouvelles phases quantiques, des propagations anormales des fonctions de corrélations et de l'intrication quantique. En outre, de nos jours, les récents progrès pour réaliser des réseaux artificiels de gaz d'atomes froids offrent une plateforme idéale pour créer et étudier une variété de modèles longue-portée fortement corrélés, qui sont utilisés en matière condensée. En particulier, les modèles unidimensionnels constituent souvent un candidat fantastique pour explorer à la fois le rôle des interactions et révéler de nouveaux phénomènes. Qui plus est, utiliser une dimensionnalité réduite rend généralement le problème suffisamment simple pour être résolu à l'aide de méthode spécifique telle la bosonization. De surcroît, des simulations numériques de haute précision peuvent être réalisées via la méthode de Density Matrix Renormalisation Group (DMRG) afin de caractériser les phases quantiques exotiques à une dimension. Cette thèse est axée autour de quatres thèmes essentiels : (i) une étude de l'impact des couplages longue-portée sur le phénomène de la localisation d'Anderson, (ii) la recherche de phase quantique exotique induite par une interaction à portée finie et par effet de frustration, et enfin (iii) la compréhension de l'extensivité de l'énergie sur les phases quantiques dans des systèmes à une dimension avec des interactions de longue-portée.

La localisation d'Anderson [1], à savoir la localisation des ondes électroniques de Bloch dûe aux interférences dans un milieu désordonné, est un phénomène fondamental dans la nature. En particulier, la présence d'un désordre suffisamment important peut mener à une complète absence de diffusion dans l'échantillon désordonné, où les ondes quantiques sont alors localisées exponentiellement. Bien que pour les systèmes avec interaction à courte-portée cette description ait été confirmée par pléthore d'études expérimentales et théoriques, une question cependant émerge, que deviennent les propriétés des modèles localisés en présence de couplages longue-portée ? Récemment, cette question a reçu un intérêt considérable, déclenché par la possibilité expérimentale de contrôler à la fois la portée et la forme de l'interaction. Par exemple, le modèle d'Ising avec des interactions de spins en loi de puissance $1/l^{\alpha}$ où l'exposant α est contrôlable entre 0 et 3, a été réalisé dans des expériences révolutionnaires en utilisant des réseaux d'ions froids générés par un laser [2–6] ou également avec des atomes piégés par un guide d'ondes à cristaux photoniques [7, 8]. Afin d'examiner plus en détail cette question, dans la première partie de la thèse nous analysons l'interdépendance entre le désordre et les potentiels longue-portée dans des fils quantiques de fermions et de spins où l'interaction décroît avec la distance l comme une loi de puissance. Plus spécifiquement, nous nous concentrons en premier lieu sur un modèle sans interaction de fermions sans spin où les particules peuvent sauter de sites en sites (seulement entre plus proches voisins) et sont soumises à un appariement longue-portée. Par souci de complétude, nous considérons un modèle avec du désordre

dans le terme de saut ou dans le terme d'appariement, que nous nommons modèle I et modèle II, respectivement. Ces systèmes correspondent à une extension du modèle de Kitaev avec des appariements longue-portée, qui ont déjà été étudié dans [9]. Ce dernier a l'avantage significatif de rester quadratique en terme d'opérateur fermionique et ce faisant de rester exactement soluble. En combinant des résultats analytiques et numériques, nous nous sommes concentrés sur les fonctions de corrélations à un corps et deux corps, découvrant plusieurs nouvelles caractéristiques : (i) les fonctions de corrélations décroissent algébriquement à longue distance dans toutes les phases localisées et ce pour tout α. (ii) L'exposant caractérisant la décroissance dépend exclusivement de α et non par exemple de la force du désordre. Ce dernier point a été notamment démontré par un résultat analytique, en parfait accord avec le numérique. (iii) De manière intéressante, nous avons également trouvé que la fonction d'onde, habituellement localisée exponentiellement dans le phénomène de localisation d'Anderson, présente ici une localisation algébrique à longue distance. Finalement, nous avons étudié un système avec interaction via le modèle d'Ising longue-portée dans un champ transverse. Puisque ce dernier n'est pas intégrable, nous avons utilisé un algorithme de Density Matrix Renormalisation Group pour résoudre le problème. De façon tout à fait remarquable, nous avons noté que les mêmes prédictions analytiques restent valides pour les corrélations de la chaine d'Ising. Ces résultats apparaissant parallèlement dans des modèles sans et avec interaction suggèrent l'existence d'un comportement universel dû aux couplages longue-portée.

En général, les systèmes à une dimension sont décrits par la classe universelle des Tomonaga-Luttinger Liquids (TLL). Dans cette théorie, le comportement à basse énergie des modèles interagissant de fermions, bosons et spins peuvent être transposé sur un modèle de boson libre. Cette description est souvent la clef pour comprendre la plupart des systèmes de matière condensée à une dimension. Ces derniers comprennent diverses systèmes tels que des matériaux organiques, des nano-fils, des nanotubes de carbone, les modes de bords dans des matériaux à effet Hall quantique. Cependant, des travaux récents [10–14] ont signalé une possible défaillance de la théorie TLL. En outre, une question cruciale demeure, comprendre la robustesse du paradigme conventionnel TLL dans des systèmes soumis à différents types de potentiel. Dans la deuxième partie de la thèse, nous investigons méthodiquement le diagramme de phase à température nulle ($T = 0$) d'une variante étendue du modèle de Hubbard à une dimension dans laquel un système de fermions avec spin peut interagir à la fois avec un potential sur site U mais également avec un potentiel répulsif V fini dans une certaine region de longueur r_c. Le cas pour une interaction entre proches voisins ($rc = 1$) est effectivement bien décrit par la théorie de TLL, toutefois, quand la portée de l'interaction est étendue sur quelques sites ($rc > 1$), un effet de frustration peut apparaître et la situation devient alors dramatiquement différente. En effet, la commensurabilité entre la densité de particule et la portée du potentiel peut mener à la formation d'amas de particules qui sont alors libres de se déplacer dans leur ensemble, conduisant à un nouveau type de phases non-gappées que nous définissons comme un TLL d'amas, et nommons ces dernières Cluster Luttinger Liquid (CLL). En variant la force des interactions U et V (assumées répulsives $U, V > 0$), nous sommes amenés à rencontrer différents type d'amas et ce faisant différentes type de phases CLL. Les sim-

ulations numériques ont été réalisées via un algorithme de DMRG [15], néanmoins en raison du haut degré de frustration inhérent au modèle et au fait qu'il se trouve toujours dans une phase critique, atteindre une haute précision au sein de ces simulations est un challenge considérable. Malgré ces contraintes, nous avons démontré que pour des faibles valeurs de U et V la phase est bien décrite par un liquide standard TLL. Par contre, pour $U < V$, nous trouvons une phase CLL dans laquelle les amas contiennent une particule ou un couple de particule proches voisins. A contrario dans le cas $V < U$, nous avons une phase avec des doublons, ou les amas peuvent être constitués d'une particle ou d'un site doublement occupé. Ces deux phases sont respectivement dénommées CLLnn et CLLd (c.f. figure 4). Au niveau semi-classique, nous avons trouvé que la transition entre ces deux liquides apparait à $V = 2/3U$. De plus, en réalisant un étude intensive de l'entropie d'intrication et des degrés de liberté de basse énergie au point critique de la transition entre le liquide conventionnel TLL et CLLnn , nous y avons prouvé l'émergence d'un mode super-symétrique. Autrement dit, en ce point critique, les vitesses des modes bosonic et fermionic deviennent équivalentes. Finalement, nous avons noté que pour de faibles valeurs U et fortes/intermédiaires magnitudes de V , le système a tendance à former un liquide avec seulement des sites doublement occupés. Ces travaux vont être publiés à SciPost dans les semaines à venir.

Dans la troisième partie, nous portons notre attention vers l'étude des étonnantes propriétés émergeantes dans le régime de « forte » longue-portée. Un système physique est dit interagissant à longue-portée quand le potentiel V entre les particules décroît comme une loi de puissance avec la distance r : $V(r) \propto 1/r^{\alpha}$ avec $\alpha > 0$. Plus particulièrement, le régime de « forte » longue-portée pour un système d-dimensionnel avec un volume $\mathcal{V}$ est atteint quand $\alpha < d$. Ce dernier est typiquement associé avec des propriétés thermodynamiques inhabituelles telle que la non-extensivité de l'énergie $E \sim \mathcal{V}^{2-\frac{\alpha}{d}}$, menant notamment à une limite thermodynamique mal défini. De manière intéressante, ces systèmes présentent aussi une non-additivité, c'est-à-dire que l'énergie totale ne peut pas être obtenue en sommant les énergies des différents sous-systèmes comme c'est généralement le cas en présence d'interaction à courte-portée [16]. Tandis que cette non-additivité apparaît comme une propriété essentielle pour les systèmes longue-portée [16, 17], l'extensivité quant à elle peut être restaurée en appliquant un rescale du potentiel d'interaction avec un facteur Λ dépendant du volume, connu sous le nom de la prescription de Kac. Cette dernière est par exemple systématiquement utilisée pour étudier les propriétés thermodynamiques des modèles classiques de spin avec interactions à longue-portée. Dans les systèmes quantiques de matière condensée, cependant, le rescaling de Kac n'est habituellement pas considéré, ce qui pose l'intéressante et ouverte question de savoir si l'extensivité de l'énergie peut modifier les propriétés fondamentales des systèmes quantiques longue-portée. Pour ce faire, nous analysons les propriétés de l'état fondamental d'un modèle à une dimension de boson de coeur dur interagissant via un potentiel longue-portée en utilisant la méthode de DMRG. Nous avons démontré que restaurer l'extensivité de l'énergie dans le système, via la prescription de Kac, a une profonde influence sur les propriétés de basse énergie du système. Dans la limite thermodynamique, il apparaît en effet qu'en absence de rescale la phase est isolante tandis qu'en appliquant la pre-

scription sus-mentionnée la phase est métallique pour toute valeur finie de l'interaction. Nous avons réalisé notre analyse en combinant des résultats issus à la fois de la théorie de Luttinger et du numérique. Nous démontrons également que le mode de plasmon est supprimé quand l'extensivité de l'énergie est restaurée tout en préservant le caractère longue-portée du potentiel.

Finalement dans la dernière partie de cette thèse, nous étudions la modification de la localisation d'Anderson en présence d'un couplage avec un mode de cavité. Nous choisissons un modèle d'Anderson composé de N émetteurs quantiques sur un réseau cubique en trois dimensions. En premier lieu, nous analysons plusieurs observables telle que la probabilité de retour, ou l'inverse du ratio de participation. Ces deux quantités, nous donnent des mesures qualitatives du degré de localisation dans notre système. Nous montrons des différences importantes dans le régime de fort désordre ($W \gg J$) et de couplage fort ($g\sqrt{N} \gg W/2$), que nous caractérisons comme une phase semi-localisée (à opposer à la phase localisée sans couplage avec une cavité). En effet, dans ce régime, la statistique des niveaux montre un comportement Semi-poissonien, caractérisée par une repulsion de niveau (comme dans la phase métallique) et un comportement exponentiel dans la partie à longue distance (comme dans la phase localisée). Qui plus est, en traitant le désordre comme une perturbation, nous avons obtenu des estimations analytiques pour les vecteurs propres et valeurs propres de notre systèmes. Ces dernières reproduisent parfaitement le comportement de la statistique des niveaux dans la phase semi-localisée. Enfin, dans l'optique d'étudier les propriétés de transport au sein de ce système, nous nous concentrons sur la diffusion (c'est à dire l'évolution temporelle de l'écart quadratique moyen), que nous analysons à la fois numériquement et analytiquement. Nous trouvons que les polaritons determinent l'évolution à court terme tandis que les états sombres sont responsables d'une évolution anormale (sous-diffusif) à long terme. Nous terminons notre discussion par l'analyse de la moyenne (sur le désordre) de la probabilité de transfert d'une excitation. En séparant les contributions des polaritons et des états sombres, nous montrons que les polaritons se comportent en $\sim 1/N^2$ et les états sombres en $\sim 1/N$. Ces derniers rappellent notamment le comportement des fonctions de Bloch dans les systèmes localisés. Ainsi, la phase semi-localisée présente à la fois des propriétés localisées similaire à ceux d'un isolant et des propriétés de transfert d'excitations similaire à une phase délocalisée.

Dans cette thèse, nous avons mis en lumière des nouveaux phénomène induits par des couplages longue-portée dans des systèmes à une dimension inspirés de la physique AMO (Atomic Molecular Optic). En premier lieu, nous avons établi qu'un couplage en loi de puissance peut fortement modifier la localisation d'Anderson, donnant lieu à une localisation algébrique. Puis, en explorant le diagramme de phase d'un modèle étendu de Hubbard avec des interactions « soft-shoulder », nous avons démontré l'existence de nouvelles phases exotiques de liquides quantiques. Ensuite, nous nous sommes concentrés sur une propriété intrinsèque des systèmes longue-portée, nommément la non-extensivité de l'énergie.Nous avons notamment montré que restaurer l'extensivité a un impact profond sur les phases des systèmes quantiques. Finalement, nous avons étudié la modification

de la localisation d'Anderson en présence d'un couplage avec un mode de cavité. Nous avons notamment démontré l'apparitions d'une nouvelle phase semi-localisée aux propriétés partagées entre ceux d'un isolant et d'une phase délocalisée.

Riassunto

Le interazioni a lungo raggio sono intrinseche ad una miriade di sistemi fisici, a partire da cluster auto-gravitanti, materiali ferromagnetici, plasmi non neutri, fino a sistemi QED in cavità o a catene di atomi o spin monodimensionali. A causa delle loro affascinanti proprietà, queste svolgono un ruolo preponderante nella ricerca attuale, sia teorica che sperimentale. Recentemente numerosi lavori teorici hanno messo in luce effetti nuovi ed intriganti per questi sistemi, tra cui, ad esempio, nuove fasi quantistiche o una propagazione anormale delle funzioni di correlazione e dell'entanglement quantistico. Inoltre, i recenti progressi nella realizzazione di reticoli artificiali di gas atomici freddi offrono al giorno d'oggi una piattaforma ideale per la creazione e lo studio di una molteplice varietà di modelli a lungo raggio altamente correlati di interesse per la fisica della materia condensata. In particolare, i modelli monodimensionali sono spesso ottimi candidati per l'esplorazione del ruolo delle interazioni e per rivelare nuovi fenomeni. Inoltre, l'utilizzo della ridotta dimensionalità di solito rende il problema abbastanza semplice da poter essere risolto utilizzando metodi specifici come, ad esempio, la bosonizzazione. Per questi sistemi, è inoltre possibile eseguire simulazioni numeriche di alta precisione utilizzando il metodo DMRG (Density Matrix Renormalization Group) per caratterizzare nuove ed esotiche fasi quantistiche. Questa tesi si concentra su quattro argomenti essenziali: (i) uno studio sull'impatto degli accoppiamenti a lungo raggio sul fenomeno della localizzazione di Anderson, (ii) la ricerca di fasi quantistiche esotiche indotte da interazioni a raggio finito e dall'effetto della frustrazione, ed infine (iii) la comprensione dell'estensività dell'energia sulle fasi quantistiche nei sistemi monodimensionali con interazioni a lungo raggio.

La localizzazione di Anderson [1], ovvero la localizzazione delle onde elettroniche di Bloch a causa di interferenze in un ambiente disordinato, è un fenomeno fondamentale in natura. In particolare, la presenza di un disordine sufficientemente grande può portare a una completa mancanza di diffusione nel campione disordinato, in cui le onde quantistiche sono quindi localizzate in modo esponenziale. Sebbene per i sistemi con interazione a corto raggio questa descrizione sia stata confermata da numerosi studi sperimentali e teorici, emerge tuttavia un'importante domanda: cosa succede alle proprietà dei modelli localizzati in presenza di accoppiamenti a lungo raggio? Recentemente, questa domanda ha suscitato notevole interesse, innescato dalla possibilità di controllare, negli esperimenti, sia il raggio che la forma dell'interazione. Ad esempio, il modello Ising con interazioni di spin che decadono algeibraicamente con la distanza come $1/l^{\alpha}$ in cui l'esponente α è controllabile tra 0 e 3, è stato realizzato in esperimenti rivoluzionari utilizzando reticoli di ioni freddi generati da un laser [2–6] o ancora con atomi intrappolati da una guida d'onda a cristalli fotonici [7, 8]. Al fine di esaminare in maniera più dettagliata questa domanda, nella prima parte della tesi analizziamo l'interdipendenza tra disordine e potenziali a lungo raggio nei fili quantistici di fermioni e di spin in cui l'interazione diminuisce algebraicamente con la distanza l. Più specificamente, ci concentriamo dapprima su un un modello di fermioni senza spin in assenza di interazioni. In questo modello le particelle possono saltare tra i diversi siti (solo tra siti primi vicini) e sono soggette ad un accoppiamento a lungo raggio. Per completezza, consideriamo un modello con disordine nel

termine di salto o nel termine di accoppiamento, che chiamiamo rispettivamente Modello I e Modello II. Questi sistemi corrispondono ad un'estensione del modello di Kitaev con accoppiamenti a lungo raggio, che sono già stati studiati in [9]. Questo modello ha il vantaggio significativo di rimanere quadratico in termini degli operatori fermionici e quindi di essere esattamente solubile. Combinando sia risultati analitici che numerici, ci siamo concentrati su funzioni di correlazione ad singolo corpo e a due corpi scoprendo diverse nuove caratteristiche: (i) le funzioni di correlazione diminuiscono algebricamente su lunghe distanze in tutte le fasi localizzate per tutti i valori di α. (ii) L'esponente che caratterizza il decadimento dipende esclusivamente da α e non, ad esempio, dalla intensità del disordine. Quest'ultimo punto è stato dimostrato in particolare da un risultato analitico, in perfetto accordo con i risultati numerici. (iii) È interessante notare che abbiamo anche scoperto che la funzione d'onda, solitamente localizzata esponenzialmente nel fenomeno della localizzazione di Anderson, presenta in questo caso una localizzazione algebraica a lungo raggio. Infine, abbiamo studiato un sistema con interazione tramite il modello Ising a lungo raggio in campo trasversale. Poiché quest'ultimo non è integrabile, abbiamo usato un algoritmo di Density Matrix Renormalization Group per risolvere il problema. Abbastanza sorprendentemente, abbiamo notato che le stesse previsioni analitiche rimangono valide per le correlazioni della catena Ising. Questi risultati, che appaiono in parallelo nei modelli senza e con interazione, suggeriscono l'esistenza di un comportamento universale a causa di accoppiamenti a lungo raggio.

In generale, i sistemi monodimensionali sono descritti dalla classe universale dei liquidi Tomonaga-Luttinger (Tomonaga Luttinger Liquid o TLL). In questa teoria, il comportamento a bassa energia dei modelli interagenti di fermioni, bosoni e spin può essere trasposto su un modello a bosone libero. Questa descrizione è spesso la chiave per comprendere la maggior parte dei sistemi unidimensionali di materia condensata. Questi includono vari sistemi come materiali organici, nanofili, nanotubi di carbonio, modalità edge nei materiali quantistici di Hall. Tuttavia, recenti lavori [10–14] hanno riportato un possibile fallimento della teoria TLL. Inoltre, un importante questione rimane ancora aperta: comprendere la solidità del paradigma TLL convenzionale nei sistemi soggetti a diversi tipi di potenziale. Nella seconda parte della tesi, analizziamo metodicamente il diagramma di fase a temperatura zero ($T = 0$) di una variante estesa del modello unidimensionale di Hubbard in cui un ensemble di fermioni con spin può interagire sia on-site (con intensità U) sia con un potenziale repulsivo V in una determinata regione di raggio r_c. Il caso di un'interazione tra primi vicini ($r_c = 1$) è in effetti ben descritto dalla teoria TLL, tuttavia, quando l'ambito dell'interazione viene esteso su alcuni siti ($r_c > 1$), possono entrare in gioco effetti di frustazione che rendono la situazione drammaticamente diversa. In effetti, la commensurabilità tra densità delle particelle e intervallo potenziale può portare alla formazione di gruppi di particelle che sono quindi liberi di muoversi insieme, portando a un nuovo tipo di fase gapless che definiamo come un TLL di cluster e quindi denominiamo come Cluster Luttinger Liquid (CLL). Variando la forza delle interazioni U e V (nel caso repulsivo $U, V > 0$), siamo portati ad incontrare diversi tipi di cluster e quindi ad osservare diversi tipi di fasi CLL. Le simulazioni numeriche sono state eseguite tramite un algoritmo DMRG [15], tuttavia a causa dell'elevato grado di

frustrazione insito nel modello e del fatto che si trova ancora in una fase critica, ottenere un'alta precisione all'interno di queste simulazioni diventa una sfida considerevole. Nonostante questi vincoli, abbiamo dimostrato che per bassi valori di U e V la fase è ben descritta da un liquido TLL standard. D'altra parte, per $U \gg V$, troviamo una fase CLL in cui i cluster contengono una particella o una coppia di particelle prime vicine. Al contrario, nel caso $V \gg U$, abbiamo una fase con *doublons*, in cui i cluster possono essere costituiti da una o da due particelle sullo stesso sito. Queste due fasi sono rispettivamente chiamate CLL_{nn} e CLL_d (vedi Figura 4). A livello semi-classico, abbiamo dimostrato che la transizione tra questi due liquidi appare a $V = 2/3U$. Inoltre, conducendo uno studio intensivo sull'entropia entanglement e sui gradi di libertà a bassa energia nel punto critico della transizione tra il fluido TLL e CLL_{nn} convenzionale, abbiamo dimostrato l'emergenza di un modo supersimmetrico. In altre parole, in questo punto critico, le velocità dei modi bosonico e fermionico diventano equivalenti. Infine, abbiamo notato che per bassi valori di U e forti o intermedie magnitudini di V, il sistema tende a formare un liquido con solo siti doppiamente occupati. Questo lavoro sarà pubblicato su SciPost nelle prossime settimane.

Nella terza parte, rivolgiamo la nostra attenzione allo studio di incredibili proprietà emergenti nel cosiddetto regime forte per le interazioni a lungo raggio. Si dice che un sistema fisico interagisca a lungo raggio quando il potenziale V tra le particelle diminuisce come una legge di potenza con la distanza r: $V(r) \propto 1/r^\alpha$ con $\alpha > 0$. In particolare, per queste interazioni, il cosiddetto regime "forte" a lungo raggio per un sistema d-dimensionale con un volume $\mathcal{V}$ viene raggiunto quando $\alpha < d$. Quest'ultimo è in genere associato a insolite proprietà termodinamiche come la non estensibilità dell'energia $E \sim \mathcal{V}^{2-\frac{\alpha}{d}}$, portando in particolare ad un limite termodinamico mal definito. È interessante notare che questi sistemi sono anche non additivi, vale a dire che l'energia totale non può essere ottenuta sommando le energie di diversi sottosistemi, come generalmente accade in presenza di interazioni a corto raggio [16]. Mentre questa non additività appare come una proprietà essenziale per i sistemi a lungo raggio, l'estensività può essere ripristinata applicando un rescaling al potenziale di interazione con un fattore, Λ, dipendente dal volume e noto con il nome nome di *prescrizione Kac*. Quest'ultima è ad esempio sistematicamente utilizzata per studiare le proprietà termodinamiche dei modelli di spin classici con interazioni a lungo raggio [16, 17]. Nei sistemi quantistici di materia condensata, tuttavia, il rescaling di Kac di solito non viene preso in considerazione. Ciò solleva l'interessante e aperta questione di come l'estensività dell'energia possa alterare le proprietà fondamentali dei sistemi quantistici a lungo raggio. Per provare a rispondere a questa domanda, in questa parte della tesi, utilizziamo il metodo DMRG per analizzare le proprietà dello stato fondamentale di un modello unidimensionale di bosoni *hardcore* che interagiscono attraverso un potenziale a lungo raggio. Così facendo siamo riusciti a dimostrare che il ripristino dell'estensività dell'energia nel sistema, attraverso la prescrizione di Kac, ha una profonda influenza sulle proprietà a bassa energia del sistema. Nel limite termodinamico, sembra infatti che in assenza di tale rescaling la fase sia isolante mentre applicando la suddetta prescrizione la fase è metallica per qualsiasi valore finito dell'interazione. Abbiamo eseguito la nostra analisi combinando i risultati sia della teoria di Luttinger che nu-

merici. Dimostriamo anche che i modi plasmonici vengono soppressi quando l'estensività dell'energia viene ripristinata preservando il potenziale a lungo raggio.

Infine, nell'ultima parte di questa tesi, studiamo l'alterazione del fenomeno della localizzazione di Anderson in presenza di un accoppiamento con i modi normali di una cavità. Scegliamo un modello Anderson costituito da N emettitori quantistici su un reticolo cubico tridimensionale. Innanzitutto, analizziamo diversi osservabili come la probabilità di ritorno o l'inverso del rapporto di partecipazione. Queste due quantità ci forniscono misure qualitative del grado di localizzazione nel nostro sistema. Mostriamo importanti differenze nel regime forte disordine ($W \gg J$) e forte accoppiamento ($g\sqrt{N} \gg W/2$), che caratterizziamo come una fase semi-localizzata (a contrasto con la fase localizzata senza accoppiamento con una cavità). Infatti, in questo regime, le statistiche dei livelli mostrano un comportamento semi-poissoniano, caratterizzato da una repulsione di livello (come nella fase metallica) e da un comportamento esponenziale nella parte a lunga distanza (come nella fase localizzata). Inoltre, trattando il disordine in modo perturbativo, abbiamo ottenuto stime analitiche per gli autovettori e gli autovalori del nostro sistema. Questi ultimi riproducono perfettamente il comportamento delle statistiche dei livelli nella fase semi-localizzata. Infine, al fine di studiare le proprietà di trasporto all'interno di questo sistema, ci concentriamo sulla diffusione (ovvero l'evoluzione temporale dello scarto quadratico medio), che analizziamo sia numericamente e analiticamente. Scopriamo che i polaritoni determinano l'evoluzione a breve termine mentre gli stati *dark* sono responsabili dell'evoluzione anormale (sub-diffusiva) a lungo termine. Terminiamo la nostra discussione analizzando la media (sul disordine) della probabilità di trasferimento di una singola eccitazione. Separando i contributi dei polaritoni e degli stati oscuri, mostriamo che i polaritoni si comportano come $\sim 1/N^2$ e gli stati oscuri come $\sim 1/N$. Questi ultimi richiamano in particolare il comportamento delle funzioni di Bloch nei sistemi localizzati. Pertanto, la fase semi-localizzata ha proprietà localizzate simili a quelle di un isolante e proprietà di trasferimento di eccitazione simili a una fase delocalizzata.

In questa tesi, abbiamo messo in evidenza nuovi fenomeni indotti da accoppiamenti a lungo raggio in sistemi monodimensionali ispirati alla fisica AMO (Atomic Molecular Optic). In primo luogo, abbiamo stabilito che un accoppiamento della legge di potenza può modificare fortemente il fenomeno della localizzazione di Anderson, dando origine a una localizzazione algebrica. Quindi, esplorando il diagramma di fase di un modello Hubbard esteso con interazioni soft-shoulder, abbiamo dimostrato l'esistenza di nuove fasi esotiche di liquidi quantistici. Successivamente, ci siamo concentrati su una proprietà intrinseca dei sistemi a lungo raggio, vale a dire la non estensibilità dell'energia. In particolare, abbiamo dimostrato che il ripristino dell'estensività ha un profondo impatto sulle fasi dei sistemi quantistici. Infine, abbiamo studiato l'alterazione del fenomeno della localizzazione di Anderson in presenza di un accoppiamento con i modi normali di una cavità. In particolare, abbiamo dimostrato la comparsa di una nuova fase semi-localizzata con proprietà condivise tra quelle di un isolante e una fase delocalizzata.

Contents

Introduction

> *Begin at the beginning, the King said, very gravely, and go on till you come to the end: then stop.*
>
> Lewis Carroll, Alice in Wonderland

A physical system is said to be long-range interacting when the coupling between its constituents decays slowly, e.g., algebraically with the distance separating them. Long-range interactions naturally appear in the fundamental laws governing the universe such as gravitational and electromagnetic forces. Electromagnetism describes interactions between charged particles and plays a fundamental role in the cohesion of matter in solids. The latter typically consist of severals atoms, ions, or molecules forming a lattice and bound together via molecular (dipole-dipole and Van der Waals interactions), ionic, or covalent bondings. These interactions lie at the heart of condensed matter physics.

In classical physics governing the dynamics of gravitational systems, the presence of long-range interactions leads to the emergence of exotic statistical and dynamical properties compared to systems with short-range interactions [18, 19]. When the potential experienced by two particles decays with an exponent smaller than the dimension of the space, the thermodynamic limit is ill-defined due to the energy non-extensivity [20, 21]. Another property of this *strong long-range regime* is referred to as non-addivity, i.e., the total energy of the system can not be obtained by summing up the energies of different subsystems. Non-addivity typically leads to unusual behaviors including the breaking of ergodicity, the existence of slow relaxation processes towards the thermodynamic equilibrium, and the inequivalence of statistical ensembles [22–24]. These properties have been widely studied in the context of classical spin models with long-range interactions, which are used to describe magnetism in solids. At low temperature, however, quantum theory is needed to describe certain magnetic properties due to, e.g., itinerant electrons [25–27]. Indeed, quantum fluctuations play a crucial role in this case because the De Broglie wavelength of the electrons is typically larger than the lattice spacing.

The development of quantum mechanics across the twentieth century has led to remarkable successes in the description of condensed matter systems. The band theory for electrons in solids is a canonical example. For instance, most of metallic materials are rather well described by independent electron models treating Coulomb interactions as a perturbation [28–30]. Nevertheless, each order of the perturbative series diverges due to the long-range character of the Coulomb potential. This issue was solved with the "random phase approximation" (RPA) which consists of summing up the most divergent terms resulting in a finite limit [31–34]. This method in fact captures the collective response of

the electron gas, linear combination of the individual excitations, which is responsible for the screening of electrostatic potentials that become effectively short-range [35]. More generally, the relevance of perturbative approaches relies on the concept of quasi-particle introduced by Landau in 1956 [36]. The main idea is here to focus on the low-energy properties of the system which are governed by independent electrons "dressed" by their mutual interactions. Within this paradigm called "Fermi liquid", correlations between particles are completely neglected.

Strongly correlated phases of matter beyond the Fermi liquid description have been identified since the seminal paper of Bardeen, Cooper, and Schrieffer (BCS) in 1957 [37]. In 1911, K. Onnes discovered that the resistivity of mercury suddenly dropped to zero below a certain critical temperature of about 4 K [38]. The BCS theory interpreted this phenomenon as a phase transition where electrons spontaneously form "Cooper" pairs below the critical temperature. In parallel, the phenomenological description of such phase transitions was provided by Ginzburg and Landau who interpreted them as resulting from a spontaneous symmetry breaking and the emergence of a local order parameter [39]. Another famous example is the transition from a paramagnetic to a ferromagnetic state below the Curie temperature. In strongly anisotropic magnetic materials, such a transition can be described by the simple Ising model for 1/2 spins aligned along a given axis with nearest neighbor couplings [40, 41]. At zero temperature, Coulomb interactions can solely drive a material that is metallic according to band theory towards an insulating phase where electrons can not move due the strong repulsion, which is denoted as Mott insulator transition [42]. The simplest model which features such a *quantum phase transition* is called the *Hubbard model*, where particles in a two-dimensional lattice can tunnel between nearest neighboring sites and experience an on-site interaction. When the latter is repulsive and tuned above a critical value the system undergoes a metal-insulator transition [43–47]. All these developments introduced the fundamental idea that some emergent properties of condensed-matter systems can not be described by perturbative approaches based on Fermi liquid theory.

Strongly correlated phases arise in particular in low-dimensional materials. For instance, in one dimension all excitations are collective since an electron cannot move without affecting the motion of *all* the other ones. In addition, the screening of the Coulomb potential typically becomes less efficient as the dimensionality is reduced, and one recovers the issues related to the divergence of the perturbative series. Theoretical descriptions of these materials have been notably developed by Tomonaga and Luttinger in 1950s [48, 49], who realized that the low-energy sector of one-dimensional metals fall into a new universal class referred to as *Luttinger Liquids*. A useful microscopic description was later introduced by Haldane in 1981 [50], who expressed the collective excitations of many fermions in one dimension in terms of bosonic modes. For this reason this approach is nowadays denoted as bosonization. The latter has been successfully applied to quasi-dimensional materials which include organic conductors such as Bechgaard salts [51], carbon nanotubes [52–54], as well as the edge states of quantum Hall systems [55, 56]. This Luttinger liquid behavior has also been observed in artificial materials using cold gases

of atoms [57–60]. Over the past decades, developments of efficient numerical techniques such as the density matrix renormalization group for one-dimensional systems [61, 62] and the quantum Monte Carlo algorithm [63, 64] for bosons in higher dimensions, have allowed better understanding of strongly correlated materials.

The work of Haldane in the 80's has led to the identification of another type of phase transitions that are not captured by the Ginzburg-Landau theory, the so-called topological phase transitions associated with non-local order parameters [65]. A famous example at finite temperature is the Berezinsky-Kosterlitz-Thouless transition in two dimensions that is not associated to any spontaneous symmetry breaking and where topological excitations are vortices [66]. Another model has been introduced by Kitaev in 2001 and consists of one-dimensional spinless fermions with *nearest-neighbor* hopping and pairing terms [67]. This model was shown to feature a topologically ordered phase characterized by two or more degenerate low-energy states localized at the edges of the open chain, which correspond to topologically protected *Majorana fermions*. This phase can be seen as a superconductor exhibiting Cooper pairs with p-wave symmetry. The Kitaev model with long pairing has been addressed in recent work [9]. It was found that starting from the paramagnetic phase where the system features a short-range order for nearest neighbor electron pairing, increasing the range of this pairing term leads to the emergence of a quasi long-range order at large distance [9, 68].

In the last decades, advances [69, 70] in cooling and trapping neutral atoms, ions, and molecules, have opened the possibility of quantum emulation of strongly correlated materials [71–74]. A quantum simulator is a controllable quantum system that mimics the dynamics or static properties of a quantum model that cannot be simulated efficiently with a classical computer [75]. For instance, optical lattices [76, 77], which are artificial crystals created by standing wave light, are an ideal platform to engineer large arrays of atoms or molecules (100-10^6) due to the ac-Stark effect, and to confine them in a variety of low-dimensional lattice geometries. Furthermore, the possibility of controlling the microscopic parameters via external lasers and magnetic fields (with, e.g., Feshbach resonances [78]) allows to explore experimentally many quantum phases and quantum phase transitions. An illustrative example is provided by the realization of the Hubbard model for bosons and the associated transition from a superfluid to a Mott insulating phase [79].

Cold atoms experiments are also an ideal platform to simulate certain transport properties of condensed-matter systems. For instance, the *localization* phenomena introduced by Anderson in 1957 is characterized by an absence of diffusion stemming from the interference between multiple scattering paths of quantum waves moving in a disordered lattice [1]. Since this effect relies on quantum coherence, cold atomic gases with long coherence time ($\sim$ 100 ms) have emerged as ideal candidates to observe Anderson localization experimentally, in contrast to condensed-matter systems where the excitation lifetime is strongly limited by electron-phonon and electron-electron interactions. Such metal-insulator transition purely induced by disorder was reported in Ref [80, 81]. In the experiment of Ref. [81], the one-dimensional model originally introduced by Anderson

was simulated by a bichromatic lattice. A main standing wave was used to generate the optical lattice trap for the atoms, while changing its intensity allows to control the tunnelling rate. A second optical lattice with a different period that is non-commensurate with the first one was then added to induce a disorder potential. Note that the impact of Coulomb interactions on the Anderson localization phenomena is a complicated issue that is still actively debated [82, 83].

Cold atomics gases also offer the possibility to tune the range and the shape of the interactions. In particular, contact-like interactions (e.g. Van der Waals $\sim r^{-6}$) can lead to a rich variety of phenomena and has been notably used to realize Bose Einstein condensates (BEC) [84–87] and degenerate Fermi gases of atoms experimentally. In addition, long-range dipole-dipole interactions ($\sim r^{-3}$) can be engineered by manipulating the large permanent dipole moments naturally present in heteronuclear polar molecules [88–94] and magnetic atoms [95, 96]. Other examples include pairwise interactions between Rydberg atoms in their excited states [97–101]. Rydberg atoms are also an ideal platform to study intermediate regimes between long-range and short-range interactions, e.g., finite-range ($\sim$ few sites) interactions by exploiting the Rydberg blockade mechanism [102–106]. The latter stems from the suppression of simultaneous excitations of two atoms in the Rydberg excited state within a finite-range. This type of potential has been recently shown to lead to highly frustrated regimes in many-body systems of trapped particles where the ground state is degenerate. This *frustration* can generate phases featuring a self-assembly of clusters of particles and intertwined orders, e.g., crystalline and superfluid, which is referred to as a supersolid phase [107–110]. Moreover, following earlier theoretical works [111, 112], analogue quantum simulation of long-range interacting spin systems have been realized in recent experiments with cold trapped ions. Electrically confined cold ions in, e.g., a Penning trap, naturally form a stable crystal due to Coulomb repulsion, and some of their internal states can be selected to act as effective spins. These internal states can then mediate a spin-spin interaction via collective vibrational modes of the Coulomb crystal that can be tuned by lasers. Effective long-range interactions with power law exponent $0 < \alpha < 3.5$ have been for instance generated in arrays of laser-driven cold ions [2–6]. These effective spin models can be mapped onto interacting hard-core bosons with hopping and/or density-density interaction in the strong long-range regime.

Another type of systems where long-range couplings can be achieved is provided by cavity quantum electrodynamics (cavity-QED), which is the study of the interaction between light and atoms confined in a cavity. In a famous experiment, S. Haroche used Rydberg atoms with long coherence time ($\sim$ 10 ms) embedded in a superconducting high-finesse cavity [113], and demonstrated that an energy exchange between the atomic cloud and the cavity takes place when the atom-cavity coupling exceeds the decay rates. This regime is denoted as *strong coupling* [114]. In the dispersive regime where the detuning between the atomic transition and the cavity mode is larger than the coupling strength, it is possible to generate an effective interaction between the atoms mediated by the cavity mode [7, 8, 115, 116]. For instance, the case $\alpha = 0$ (infinite-range potential) is typically obtained when the extent of the atomic cloud is much smaller that the cavity

mode wavelength [117–119].

During my Ph.D, I studied different many-body one-dimensional systems with long-range couplings. I investigated how these long-range couplings can affect the ground state quantum phases and lead to exotic transport properties and new type of orders in strongly correlated models. The manuscript is organized as follows.

- In the first chapter, we analyze the effects of disorder on the correlation functions in extensions of the Kitaev and Ising models in one dimension with long-range couplings and interactions. Using a combination of analytical and numerical results, we demonstrate that power-law couplings generally lead to an algebraic decay of correlations at long distances in disordered-localized phases. We also demonstrate that the decay exponent of the correlations is insensitive to the disorder strength and depends only of the power law exponent. The decay of the wave functions in the Kitaev model is also shown to present an algebraic behavior.

- In the second chapter, we investigate the zero temperature phase diagram of a variant of the one-dimensional extended Hubbard model where particles interact via a finite-range soft-shoulder potential. We show that this type of potential typically gives rise to frustration in the system, leading to the emergence of new phases that are not captured by the conventional Luttinger Liquid theory. Using a full numerical analysis based on the density matrix renormalization group, we demonstrate that these phases consist of liquids made of clusters of particles.

- The third chapter is devoted to a study of one-dimensional hard-core bosons interacting via a variable long-range repulsive potential in the strong long-range regime. We demonstrate that restoring energy extensivity in the system, which is done by rescaling the interaction potential with a suitable size-dependent factor known as Kac's prescription, has a profound influence on the low-energy properties in the thermodynamic limit. Using the density matrix renormalization group, we find that while an insulating phase occurs in the absence of Kac's rescaling, the latter leads to a new metallic phase that does not fall into the conventional Luttinger liquid paradigm.

- In the last chapter, we consider a disordered spin model with nearest neighbor couplings and where the spins interact with a common cavity mode. We provide preliminary results on the modification of Anderson localization due to the coupling to the cavity. By computing observables characteristic of the Anderson localization phenomenon using exact diagonalization in the single excitation subspace, we find that the coupling to the cavity gives rise to a novel *semi-localized* phase with peculiar level spacing distribution. Further physical insights are obtained using a perturbative treatment of the disorder. We also demonstrate that this new phase exhibits transport properties close to the ones of a delocalized phase.

The results respectively presented in the first, second, and third chapters of this thesis have been published in the three following papers:

- Thomas Botzung, Davide Vodola, Piero Naldesi, Markus Müller, Elisa Ercolessi, Guido Pupillo *Algebraic Localization from Power-Law Interactions in Disordered Quantum Wires* arXiv:1810.09779

- Thomas Botzung, Guido Pupillo, Pascal Simon, Roberta Citro, Elisa Ercolessi *One-dimensional extended Hubbard model with soft-core potential*

- Thomas Botzung, David Hagenmüller, Guido Masella, Jérôme Dubail, Nicolò Defenu, Andrea Trombettoni, Guido Pupillo *Effects of energy extensivity on the quantum phases of long-range interacting systems* arXiv:1909.12105

The work presented in the fourth chapter is still in progress and will lead to a first publication in the next months.

Chapter 1

Algebraic localization from power-law couplings in disordered quantum wires

It is not good to try to stop knowledge from going forward. Ignorance is never better than knowledge.

Enrico Fermi

Anderson localisation, the localisation of electronic Bloch waves due to interference in disordered potentials, is one of the fundamental phenomena in nature. Since the first seminal work [1] much theoretical interest has been devoted to the appearance of localized phases and of localization-delocalization phase transitions in non-interacting and interacting systems [120–137].

While for short-range couplings, it is well etablished that disordered one-dimensional systems feature localization phenomena, recent experiments with cold magnetic atoms, electronically excited Rydberg atoms and polar molecules have raised the question of the nature of localisation in the presence of long-range interactions that decay algebraically with distance ℓ as $1/\ell^{\alpha}$. These long-range interactions are now subjected to an intense research as they provide novel physical effects and can be engineered in a variety of systems ranging from ground-state neutral atoms [138–141], where dipolar-type $1/\ell^3$ or van-der-Waals-type $1/\ell^6$ have been experimentally demonstrated, to Rydberg atoms [97, 98, 101, 105, 106, 142–151], polar molecules [88–90], ions and nuclear spins [152]. In solid state materials, power-law hopping is of interest for, e.g., excitonic materials [153–165]; long-range $1/\ell$ coupling is found in helical Shiba chains [166, 167], made of magnetic impurities on an s-wave superconductor, while planar arrays of Josephson Junctions [168, 169] can effectively realize long-range extensions of the Kitaev chain for spinless fermions [67].

In the absence of disorder, theory and experiments have provided evidence for novel enticing static and dynamic phenomena in these systems, such as, e.g., the non-local propagation of correlations [170–173], time crystal phases [174], novel topological effects [175–180], and exotic behaviors of equal-time correlations, such as hybrid exponential and power-law decays within gapped phases, related to the violation of the area law for the entanglement entropy [9, 181–183]. However, in many of these systems, disorder - in particles' positions, local energies, or coupling strengths - is an intrinsic feature. Understanding its effects on the above phenomena and in the context of single-particle and many-body localization remains a fundamental open question.

For non-interacting models, it is generally expected that long-range hopping induces delocalization in the presence of disorder for $\alpha < d$, while for $\alpha > d$ all wave-functions are exponentially localized [1, 184–190]. However, recent theoretical works with posi-

tional [191] and diagonal [190] disorder have demonstrated that localization can survive even for $\alpha < d$. Surprisingly, wave-functions were found to be localized only algebraically in these models, in contrast to the usual Anderson-type exponential localization expected from short-range models. How these finding translate to the behavior of wave-functions and, crucially, correlation functions in many-particle systems is not known.

This chapter is devoted to studying the interplay between disorder and long-range potential in quantum wires of fermions and spins. In this way, it has been natural to choose models providing both physical insights of the long-range effect and immediate experimental interest. These are extensions of the Kitaev chain with long-range pairing [9, 68, 168] and the Ising model in a transverse field [192]. In the Sec. 1.1 we first introduce the models of interest, namely the disordered long-range Kitaev models (LRK) and the random long-range Ising Hamiltonian in a transverse field (LRI). We then turn to the localized properties of the fermionic Hamiltonians by looking at the inverse participation, the entanglement entropy of excited states, and the energy scaling. In the Sec. 1.3, we give particular attention to the properties of the correlations functions and the wave function within the localized phases, providing clear evidence, both analytically and numerically, of an algebraic localization in non-interacting and interacting models.

1.1 Disordered models

We consider the following Hamiltonians for one-dimensional long-range fermionic models

$$H_{\mathrm{I,II}} = H_0 + V_{\mathrm{I,II}} \tag{1.1}$$

where H_0 is a homogeneous Hamiltonian given by

$$\begin{aligned} H_0 = &-t\sum_{j=1}^{L}\left(a_j^\dagger a_{j+1} + \mathrm{H.c.}\right) + \mu\sum_{j=1}^{L} n_j \\ &+ \sum_{j,\ell}\frac{\Delta}{\ell^\alpha}\left(a_j a_{j+\ell} + \mathrm{H.c.}\right) \end{aligned} \tag{1.2}$$

that describes a p-wave superconductor with a long-range pairing, and the indices I, II refer to the two different types of Hamiltonians we consider, namely

$$V_{\mathrm{I}} = \sum_{j=1}^{L} W_j\left(a_j^\dagger a_{j+1} + \mathrm{H.c.}\right) \tag{1.3}$$

that corresponds to a random hopping and

$$V_{\mathrm{II}} = \sum_{j,\ell}\frac{W_j}{\ell^\alpha}\left(a_j a_{j+\ell} + \mathrm{H.c.}\right) \tag{1.4}$$

that corresponds to a random long-range pairing. In the previous equations, $a_j^\dagger$ (a_j) is a fermionic creation (annihilation) operator on-site j, μ is the chemical potential, Δ is the strength of the fermion p-wave pairing, $n_j = a_j^\dagger a_j$ and W_j are i.i.d random variables

drawn from a uniform distribution of width 2 and zero mean value. In the following, we will also assume open boundary condition. The Hamiltonian 1.1, even with long-range pairing and disorder is still quadratic and thus exactly solvable. By diagonalizing it and averaging over several realizations of disorder, we are able to determine the phase diagram and to analyze the correlation functions and the wave-function within the localized regions.

As an interacting model, we introduce the following random long-range Ising Hamiltonian in transverse field,

$$H_{\mathrm{LRI}} = \sum_{j,\ell} (\sin\theta + B_{j,j+\ell}) \frac{\sigma_j^x \sigma_{j+\ell}^x}{\ell^\alpha} + \sum_{j=1}^{L} (\cos\theta + W_j)\sigma_j^z, \tag{1.5}$$

where σ_j^ν ($\nu = x, z$) are Pauli matrices for a spin-1/2 at site j and $B_{j,j+\ell}$ are i.i.d. random variables drawn from a uncorrelated uniform distribution of width $2B$ and zero mean value. We choose open boundary condition and $\theta = \pi/5$, corresponding to a paramagnetic phase for $B_{j,j+\ell} = W_j = 0$ [9]. Different values of θ will not change the results we find in the following. Since this class of Ising models appears in a variety of natural context, many localization properties have already been studied. First of all, in the limit, of $\alpha \to \infty$ the LRI (and LRK) model reduces to an exactly nearest-neighbors Ising model and the system is known to be an Anderson insulator. When the value of the exponent $\alpha \geq 2d$ (d is the dimensionality) the model Eq. (1.5) has been shown to display a many-body localized (MBL) phase [193–196]. For $\alpha \leq 2d$, recent studies [197, 198] seems to corroborate the absence of localization. However, since this work aims at studying the interplay between the long-range interaction and the *localization* induced by disorder, we restrict the analysis to any $\alpha \geq 2$.

1.2 Localized phases of disordered fermions

We start our analysis by first determining the regime of localization for the disordered fermionic systems (Eq. (1.2)). By combining information from the numerical calculation of the inverse participation (IPR), the entanglement entropy, and an energy scaling analysis, we draw a complete phase diagram of the models.

1.2.1 Inverse participation ratio

Let us consider the IPR, which gives a measure of the localization with respect to a preferential basis by providing information about the spatial extension of single-particle states. It is defined as:

$$\mathrm{IPR}(E_n) = \frac{\sum_{i=1}^{L} |\Psi_n(x_i)|^4}{(\sum_{i=1}^{L} |\Psi_n(x_i)|^2)^2}, \tag{1.6}$$

where $\Psi_n(x_i)$ is the wave function corresponding to the energy E_n. Using the integrability of the fermionic model, the IPR can be compute semi-analytically. Indeed, the random

hamiltonian 1.2 can be cast in the diagonal form by means of a generalized Bogoliubov transformation [199]:

$$\eta_q = \sum_j (g_{q,j} a_j + h_{q,j} a_j^\dagger). \tag{1.7}$$

In this basis, the hamiltonian read as:

$$\mathcal{H}_{I,II} = \sum_{q=0}^{L-1} \Lambda_q \eta_q^\dagger \eta_q \tag{1.8}$$

with Λ_q the energies of the single-particle states labelled by q. The ground state $|\Omega\rangle$ is then the vacuum of all quasi-particles η_q and the matrix elements $g_{q,j}$ and $h_{q,j}$ can be identified with the wave functions of the two fermionic modes $\eta_q^\dagger$ and η_q, respectively. Thus, the IPR in the diagonal basis 1.8 becomes:

$$\mathrm{IPR}_q = \sum_{j=1}^{L} [|g_{q,j}|^4 + |h_{q,j}|^4], \tag{1.9}$$

for a normalized state with energy Λ_q. The IPR constitutes a measurement of the degree of localization in a system. It has two different behavior, (i) for extended states, the IPR tends to zero for increasing the system size L while (ii) for localized states it remains finite. So it is crucial to realize a finite-size scaling analysis to conclude about the nature of the phase. Furthermore, if a value for the energies Λ_q exists that separates extended states from localized states the system is said to display a (single-particle) mobility edge. In order to compare the IPR of states with different energies (due to the randomness), we define a dimensionless relative energy from the Λ_q (obtained for approximatively 200 disorder realizations) according to

$$\epsilon_q = \frac{\Lambda_q - \Lambda_{\min}}{\Lambda_{\max} - \Lambda_{\min}}, \tag{1.10}$$

with $\Lambda_{\max}$ ($\Lambda_{\min}$) the maximum (minimum) value of the energies Λ_q. We then bin the different levels into groups with equal energy width and we average the IPR within each bin. Finally, to obtain the phase diagrams, we perform a finite-size scaling of the obtained IPR with size L as large as $L = 10^4$.

In Fig. 1.1, we present the IPR for a fixed system size $L = 2000$ as a function of W and ϵ for model Eqs. (1.1) (I) [for $\alpha = 3$ and 0.8 in panels (a) and (b), respectively], and (II) [for $\alpha = 3$ in panel (c)] together with examples of finite-size scaling [panels (d-e)]. In the first model with disordered hopping for $\alpha > 1$ [panel(a)] essentially all states are localized for a finite value of the disorder. This behavior presents strong similarity with the one expected for purely short-range interactions ($\alpha \to \infty$) and the usual Anderson localization phenomenon in 1D. However, in the same system, when the interaction becomes truly long-range, i.e. for $\alpha < 1$ panel (b)] , we notice that, at W fixed, there seems to exist a surprising mobility edge below (above) which all the states are localized (delocalized). Regarding the second model [panel (c)] with disordered pairing, we see that when $\alpha > 1$ localized states are present at all energies if $W \gtrsim 2$, while we find a mobility edge for $\alpha > 1$ and $W \lesssim 2$ fixed: all states are delocalized at low energy ϵ and localized for

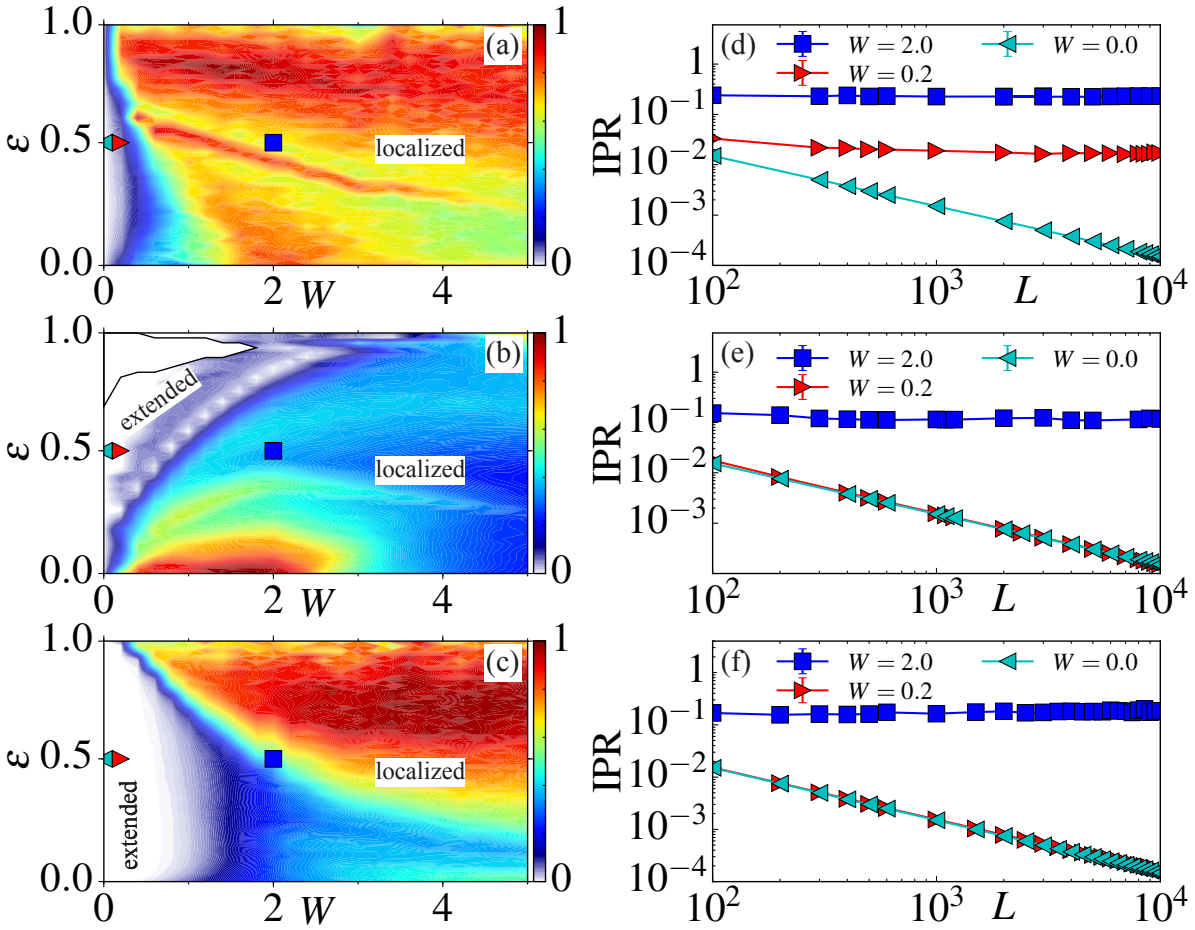

Figure 1.1: Left panels: IPR in the thermodynamic limit as a function of the disorder strength W and the rescaled energy ϵ for (a) $\alpha = 3$ and (b) $\alpha = 0.8$ for the model (I) with random hopping and (c) for $\alpha = 3.0$ for the model (II) with random pairing. In panel (b) the solid black line marks the region where the number of extended states is too low for a meaningful data analysis. Only in these panels, for drawing purpose, the IPR has been rescaled to 1 in correspondence of its maximum value. Right panels: Scaling of the IPR as a function of the system size L for $\epsilon = 1/2$ and different W for (d) $\alpha = 3$ and (e) $\alpha = 0.8$ for the model (I) and (f) for $\alpha = 3.0$ for the model (II). In panels (a-c) the symbols indicate the values of W and ϵ we choose to plot the IPR in panels (d-f).

higher ϵ. In relation to the panel (a)-(c), the finite-size analysis presented in panel (e)-(f) corroborate the aforementioned phases.

While, in general, one-dimensional models can not exhibit a single-particle mobility edge, as all states are localized for any finite disorder strength (e.g. panel (a) and panel (d)), we remark that single-particle mobility edges have also been observed in other 1D models, e.g. in the presence of quasi-periodic potential [127, 200–202] or correlated disorder [203]. So, it is a crucial question to confirm the existence or the absence of this mobility-edge with different approaches. In what follows, we focus arbitrarily on the model (I) and study in-depth the presence of the single particle mobility-edge. In order to do so, we combine information from the entanglement entropy and the energy scaling analysis.

1.2.2 Entanglement entropy

Further insight on the localization properties of the states of Hamiltonians (I) can be extract by analysing the entanglement properties of their eigenmodes. Measures of entanglement have been widely used to characterise the properties of ground state of many-body quantum systems [204] as well as to quantify the degree of localisation for ground- and excited states of disordered models [135]. A non-trivial measure of the rate of entanglement for a state $|\phi\rangle$ is the von Neumann entropy

$$S_{\mathrm{vN}}(\phi,\ell) = -\operatorname{Tr}\rho_\ell \log_2 \rho_\ell, \tag{1.11}$$

where $\rho_\ell = \operatorname{Tr}_{L\setminus\ell}|\phi\rangle\langle\phi|$ is the reduced density matrix of the state $|\phi\rangle$ that contains ℓ sites of the entire lattice. S_{vN} is known to follow an area-law scaling for localized states ψ_{loc} [i.e. $S_{\mathrm{vN}}(\psi_{\mathrm{loc}},\ell)\sim\ell^0$], while for extended states ψ_{ext} it follows a volume law, e.g. it scales as $S_{\mathrm{vN}}(\psi_{\mathrm{ext}},\ell)\sim\ell$ [129, 205, 206]. Previously we have seen that some high excited states in the model (I) remains extended despite the presence of impurities, suggesting the appearance of a single particle mobility edge. In order to confirm this observation, we study the entanglement entropy for a particular class of excited states. In the following, we compute S_{vN} semi-analytically for a bipartition of the chain into two equal halves ($\ell = L/2$) for the excited states. An excited state of the Hamiltonians $H_{\mathrm{I,II}}$ is defined by assigning a set of occupied modes $\mathbf{n} = \{n_1, n_2, \ldots, n_L\}$ with $n_q = 0, 1$ and then creating single quasi-particles $\eta_q^\dagger$ on the ground state $|\Omega\rangle$ if the mode q is occupied

$$|\mathbf{n}\rangle = \prod_{q=0}^{L-1} [\eta_q^\dagger]^{n_q} |\Omega\rangle\,. \tag{1.12}$$

In the thermodynamic limit the set of occupied mode can be approximated by a occupation density $\mathcal{N}(\theta)$ such that $\mathcal{N}(\theta)\mathrm{d}\theta$ is the number of states with momentum between θ and $\theta+\mathrm{d}\theta$. In particular in [207], they derive a scaling law for a general eigenstates of a translational invariant Hamiltonian. This scaling for a single block ℓ read as :

$$S(\phi,\ell) = A\ell + B\log(\ell) + C, \tag{1.13}$$

with

$$A = \frac{1}{2\pi}\int_{-\pi}^{\pi} f(1, 2\mathcal{N}(\theta)-1)\mathrm{d}\theta, \tag{1.14}$$

where

$$f(x,y) = -\frac{x+y}{2}\log\left(\frac{x+y}{2}\right) - \frac{x-y}{2}\log\left(\frac{x-y}{2}\right) \tag{1.15}$$

From the previous equation, we can see directly that $S(\phi,\ell)$ has a term proportional to the block length ℓ (A), as expected from an extensive quantity as entropy, a logarithmic contribution (B) specific to one dimensional critical systems [208] and a finite contribution C. Interestingly, we notice that if the coefficient A goes to zero for some peculiar states, the volume law scaling will not be observable. This happens precisely when $N(\theta) = 0$ or $N(\theta) = 1$, corresponding respectively to a state with no single excitation and maximum occupation. As a consequence, we compute the entanglement entropy for a particular class of excited states where A is finite.

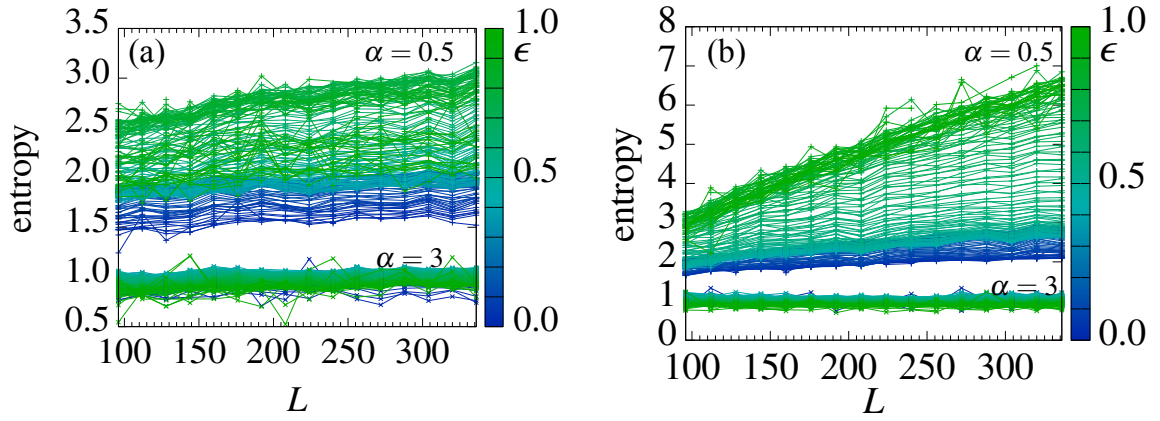

Figure 1.2: von Neumann entropy $S_{\rm vN}$ for the many-particle excited states of Hamiltonian (I) as a function of the system size L for different energies ϵ and $W = 1$: (a) states $|\mathbf{n}\rangle$ from Eq. (1.16), (b) states $|\mathbf{n}'\rangle$ from Eq. (1.17). For $\alpha = 3.0$, as all single-particle modes are localized, the entropy of the states for all energies does not depend on the system size (i.e the von Neumann entropy satisfies an area law). For $\alpha = 0.5$, the scaling of the entanglement entropy depends on the energy of the excited states $|\mathbf{n}\rangle$ and $|\mathbf{n}'\rangle$: it goes from approximately constant for the low-energy states (depicted in blue), while it is found to follow a volume law (i.e., $S_{\rm vN} \sim L$) for the high-energy ones (depicted with green lines).

The two classes of excited states that we consider for computing the von Neumann entropy are given by

$$|\mathbf{n}_\nu\rangle = |\underbrace{0\dots0}_{\nu}\underbrace{11\dots11}_{L/4}0\dots0\rangle \tag{1.16}$$

$$|\mathbf{n}'_\nu\rangle = |\underbrace{0\dots0}_{\nu}\underbrace{1010\dots1010}_{L/4}0\dots0\rangle\,. \tag{1.17}$$

We study the scaling of the von Neumann entropy as a function of the energy $e(\nu) = \sum_q n_q \Lambda_q$ and the system size L.

Following Ref. [209], we compute the entropy of the excited states as a function of their energy and, by changing ν, we can explore the whole energy spectrum. This will provide a complete understanding of the different scalings of $S_{\rm vN}$ with L for high- and low-energy states.

In order to compare the entropies of different eigenmodes, we first rescale the energies by introducing $\epsilon = [e(\nu) - E_{\rm min}]/(E_{\rm max} - E_{\rm min})$, where $E_{\rm min}$ ($E_{\rm max}$) is the minimum (maximum) among the energies of the excited states of Eqs. (1.16) or (1.17). We then average the entropies, after binning them into groups of equal energy width.

In Fig.. 1.2 we show the entanglement entropy of the excited states of Hamiltonian (I) as a function of the system size L for a given choice of $W = 1$ and for $\alpha = 3$ and $\alpha = 0.5$. Panel (a) shows the entropy for the excited states $|\mathbf{n}\rangle$ defined in Eq. (1.16) while panel (b) shows the entropy for the excited states $|\mathbf{n}'\rangle$ defined in Eq. (1.17). For $\alpha = 3$, the entropy shows an area-law behavior (i.e., $S_{\rm vN} \sim L^0$) for both the types of excited states at all energies. That behavior can be explained by the localisation of all single-particle

modes. For $\alpha = 0.5$, instead, the scaling of the entanglement entropy depends on the energy of the excited states $|\mathbf{n}\rangle$ and $|\mathbf{n}'\rangle$: it goes from approximately constant for the low-energy states (depicted in blue), while it is found to follow a volume law (i.e., $S_{\text{vN}} \sim L$) for the high-energy ones (depicted with green lines). We notice that the changing in the behavior of the entropy from area law to volume law is enhanced for the states $|\mathbf{n}'\rangle$. This behaviour is compatible with the presence of a mobility edge for all $\alpha < 1$ that separates localized low-energy states from extended high-energy ones.

1.2.3 Energy scaling analysis

In addition to the numerical analysis, we give now an analytical insight (based principally on Ref. [188]) on the different behaviors of the IPR (plotted in Fig. 1.1) of the single-particle states for the Hamiltonians 1.2 when $\alpha > 1$ and $\alpha < 1$. The key idea is to compare the magnitude of the scattering matrix, which couples bared extended states and the level spacing of the homogenous hamiltonian.

We consider a closed translationally invariant ring which let us to use a Fourier transform for the fermionic operator $a_j^\dagger = \frac{1}{\sqrt{N}} \sum_k e^{\mathrm{i}kj} a_k^\dagger$ and impose anti-periodic boundary condition. Then, we express Eq. 1.2 as the sum of a homogeneous part H_0 and of a random part V_{I}:

$$H = H_0 + \sum_{kk'} J_{k,k'} (e^{\mathrm{i}k} a_k^\dagger a_{k'} + e^{-\mathrm{i}k'} a_{k'}^\dagger a_k) \equiv H_0 + V_{\text{I}} \tag{1.18}$$

where $J_{k,k'} = -\sum_j e^{\mathrm{i}(k-k')j} W_j / L$ and a_k ($a_k^\dagger$) are the fermionic operators in the space of quasi-momenta k, with $k = 2\pi(n + 1/2)/L$ and $0 \leq n < L$.

In appendix 1.A, we show how the homogeneous Hamiltonian H_0 can be diagonalised via Fourier and Bogoliubov transformation as $H_0 = \sum_k \lambda_\alpha(k) \xi_k^\dagger \xi_k$, where ξ_k are Bogoliubov quasi-particles with extended eigenmodes of energies and $\lambda_\alpha(k)$ is the spectrum of excitation. The random term V_{I} couples the bare (extended) eigenmodes of H_0 to each others and it can lead to localization if the mean fluctuation σ_{I} of $J_{k,k'}$ is much larger than the level spacing $\delta\lambda_\alpha$ of the energies $\lambda_\alpha(k)$ of H_0. Consequently, we see that:

- when the inequality $\sigma_{\text{I}} \ll \delta\lambda_\alpha$ holds, states are weakly coupled and delocalized over the whole systems.
- when the reverse inequality, $\sigma_{\text{I}} \gg \delta\lambda_\alpha$, is verified, the disorder strongly mixes states and localized them within a region smaller than the system size.
- the equality $\sigma_{\text{I}} \sim \delta\lambda_\alpha$ defines the single particle mobility edge.

First of all, the (square) mean fluctuation of the disorder σ_{I}^2 of $J_{k,k'}$ is defined as the mean value of is square:

$$\sigma_{\text{I}}^2 := \langle J_{k,k'}^2 \rangle_W \tag{1.19}$$

where the brakets mean average on the uniform disorder distribution. After some algebra, we obtain

$$\langle J_{k,k'}^2 \rangle = \frac{1}{L^2} \sum_{i,\ell} \langle W_j W_\ell \rangle e^{\mathrm{i}(k-k')j} e^{\mathrm{i}(k-k')j}. \tag{1.20}$$

The disorder is uncorrelated and knowing that the (squared) standard deviation for a uniform disorder is $\sigma^2_{\rm uni} = 2W^2/12$, we deduce that $\langle W_j W_\ell \rangle = \delta_{j,\ell} W^2/3$ and we have

$$\sigma_{\rm I}^2 = \delta_{k,k'} \frac{W^2}{3L}. \tag{1.21}$$

It is important that $\sigma_{\rm I}^2$ scales inversely proportional to L.

We now turn to the level spacing $\delta\lambda_\alpha$ which can be computed analytically from $\lambda_\alpha(k)$ (c.f. Appendix 1.A) and it strongly depends on α:

- If $\alpha > 1$, $\lambda_\alpha(k)$ is finite for all k and we obtain $\lambda_\alpha(k) \sim k^2$ both at the minimum and at the maximum of the band. The corresponding level spacing thus scales with L as $\delta\lambda_{\alpha>1} \sim 1/L^2$ and it decays faster than $\sigma_{\rm I}$. In this case the extended states of H_0 are coupled by the random part of $V_{\rm I}$ and they will be localized. No mobility edge is then expected for $\alpha > 1$. The IPR computed for this case is shown in Fig. 1.1(a).

- If $\alpha < 1$ the energy diverges for $k \to 0$ as

$$\lambda_\alpha(k) \sim \cos\frac{\pi\alpha}{2} \frac{|\Gamma(1-\alpha)|}{|k|^{1-\alpha}}. \tag{1.22}$$

  and the level spacing for the high-energy states grows as $\delta\lambda_{\alpha<1} \sim L^{1-\alpha}$. The fluctuation of the random couplings $\sigma_{\rm I} \sim 1/\sqrt{L}$ is thus suppressed by $\delta\lambda_{\alpha<1}$ and the high-energy states of H_0 remain extended. As the lowest-energy states can be localised, a single-particle mobility edge can be then expected for all $\alpha < 1$.

By the equality $\delta\lambda_{\alpha<1} \sim \sigma_{\rm I}$ that defines the single-particle mobility edge, it is possible to show that the number of extended states increases with L as $N_{\rm ext} \sim L^{(3/2-\alpha)/(2-\alpha)}$. However, the fraction of delocalized states (found at high energy) $N_{\rm ext}/L$ vanishes as $\sim 1/L^{1/(4-2\alpha)}$ and approach the band edge for $L \to \infty$ [189]. This result implies that the single-particle mobility-edge is defined only for a finite-system. The IPR for this case is shown Fig. 1.1 (b).

The apparent discrepancy between the qualitative argument and the numerics can be explained as follows: for finite system size and due to the necessity to average over small energy windows, we always have a finite number of high energy states. These latter are effectively delocalized as suggested by the entanglement entropy and the IPR. Nevertheless, the fact that their fraction vanishes in the thermodynamic limit leads ultimately to the disappearance of the bandwidth in the usual sense and consequently of the mobility edge.

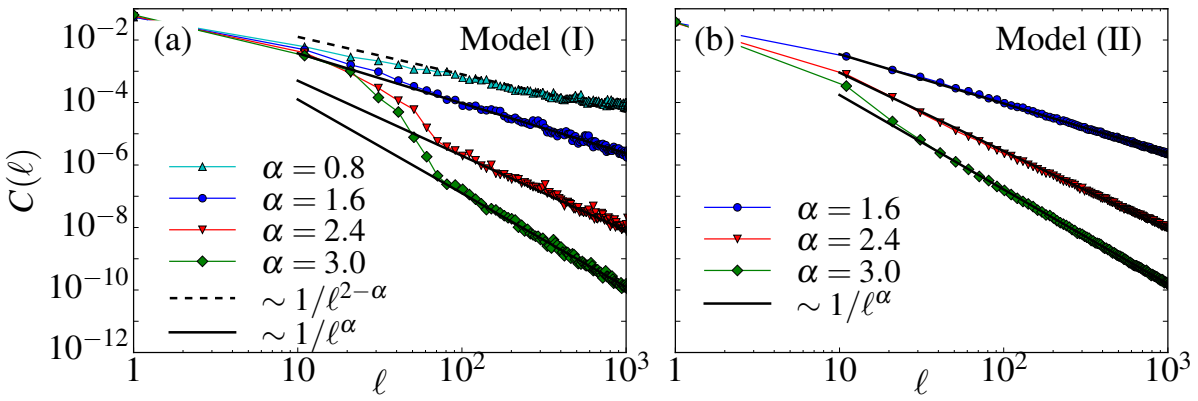

Figure 1.3: (a) Correlation function $C(\ell)$ for the model (I) as a function of the lattice site ℓ for different values of α and for $W = 5$, $L = 2000$ and 400 disorder realizations. The power-law tails are fit by the black lines scaling as $1/\ell^{2-\alpha}$ (dashed) and $1/\ell^{\alpha}$ (solid) in agreement with the analytical results in Eq. (1.56). (b) Same as panel (a) but for the model (II).

1.3 Algebraic localization

So far we have drawn a general phase diagram of the localized phase in the fermionic models, which enables us now to turn back to our primary goal, namely providing an in-deep study of the decay of the correlations functions and the wave functions into the phases mentioned above. Here, we would like to demonstrate that all these quantities decay algebraically at large distance, for both interacting and non-interacting system. By exploiting the integrability of the fermionic model (LRK), we extract insight of the long-range effects and show that some of those results can still be exported to non-solvable models (LRI).

1.3.1 Correlation functions in fermionic models

We consider the single-particle correlator

$$C(j,\ell) = \langle a_j^\dagger a_{j+\ell} \rangle_W \,, \tag{1.23}$$

for the two free-fermionic models of Eqs. (1.2) in the localized phases and where the subscript W indicates averaging over the disorder distribution. Furthermore, we compute the density-density correlation functions from the single-particle correlators $\langle a_j^\dagger a_{j+\ell} \rangle$ and $\langle a_j^\dagger a_{j+\ell}^\dagger \rangle$ via the Wick's theorem

$$G(j,\ell) = [\langle n_j n_{j+\ell} \rangle - \langle n_j \rangle \langle n_{j+\ell} \rangle]_W = [|\langle a_j a_{j+\ell} \rangle|^2 - \left|\langle a_j^\dagger a_{j+\ell} \rangle\right|^2]_W. \tag{1.24}$$

It is known that for disordered systems with short-range interactions, the correlation functions decay exponentially with the distance. Here, we are interested in the effects of long-range interactions.

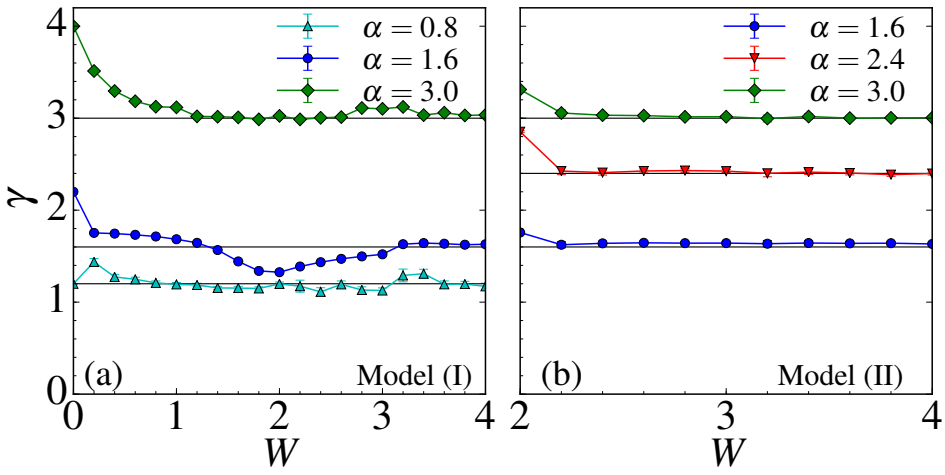

Figure 1.4: (a) Decay exponent γ of the long-distance tail of the correlation function $C(\ell)$ for the model (I) as a function of W and for $\alpha = 0.8$ (cyan triangles), $\alpha = 1.6$ (blue circles), $\alpha = 3.0$ (green diamonds). If $W > 0$, the decay exponent satisfies $\gamma \sim \alpha$ for $\alpha > 1$ and $\gamma \sim 2 - \alpha$ for $\alpha < 1$ and it does not show significance dependence on W. These data are obtained by computing the correlation function $C(\ell)$ numerically from the full random Hamiltonian in Eq. (1.25) and then by fitting the long-range decaying tail of $C(\ell)$ with $1/\ell^{\gamma}$. The black lines represent the expected exponents: $\gamma = 1.2$ for $\alpha = 0.8$, $\gamma = 1.6$ for $\alpha = 1.6$, $\gamma = 3.0$ for $\alpha = 3.0$. (b) Same as panel (a) but for the localized phase (for $W \gtrsim 2$) of model (II).

We begin by looking numerically to the different correlations and focus in the localized regime found in Sec. 1.2. Panel (a) and (b) of Fig. 1.3 show the correlator $C(j_0, \ell)$ for models $H_{\rm I}$ and $H_{\rm II}$, respectively, for different values of α, a disorder strength $W = 5$ and $L = 2000$. We impose $j_0 = L/4$ far from the edges in order to minimize boundary effects and average over 400 realizations. We observe that the tail at long-distance always decays algebraically as $C(\ell) \sim \ell^{-\gamma}$ for all α within localized phases. For $\alpha > 1$, both models present an hybrid behavior that is exponential at short distance and power-law at large distance, with a decay exponent $\gamma \sim \alpha$, e.g. panels (a) and (b). For the model I and $\alpha < 1$, the decay is essentially algebraic at all distance with $\gamma \sim 2 - \alpha$. Remarkably, we notice that the values of the decay exponents of the power-law tails do not depend on the disorder strength W as shown in Fig. 1.4 where we plot the decay exponents of $C(\ell)$ as a function of W for different values of α. For completeness we show also the decay exponent of the correlation function $C(\ell)$ for the model (II) with random long-range pairing.

Finally, examples of $G(\ell) = G(j_0, \ell)$ with $j_0 = L/4$ are shown in Fig. 1.5 for a system of $L = 2000$ sites and for a disorder strength $W = 5$. Expectedly, we find that in the localized phases for model (I) when $\alpha < 1$, $G(\ell) \sim 1/\ell^2$ while for both models $G(\ell) \sim 1/\ell^{2\alpha}$ when $\alpha > 1$. The first behaviour with a decay exponent that does not depend on α has been already observed in Refs. [9, 68], while the second can be explained by looking at the $\ell \to \infty$ scaling of $|C(\ell)|^2 \sim 1/\ell^{2\alpha}$ in Sec. 1.3.2 Eq. (1.56).

It has to be stressed that these data demonstrated an algebraic tail only for the ground state. In order to demonstrate that this behavior is typical also for higher excited states,

we build excited states as $\eta_q^\dagger|\Omega\rangle$ and compute the corresponding correlation function $C_{\rm ex}(j,\ell) = \langle\Omega|\eta_q\ a_j^\dagger a_\ell\ \eta_q^\dagger|\Omega\rangle$. The correlator for an excited state that lies in the middle of the energy band for both the models (I) and (II) is plotted in Fig. 1.6, for the same set of parameters of Fig. 1.3. Unambiguously, we see that the power-law decay is also present in this case.

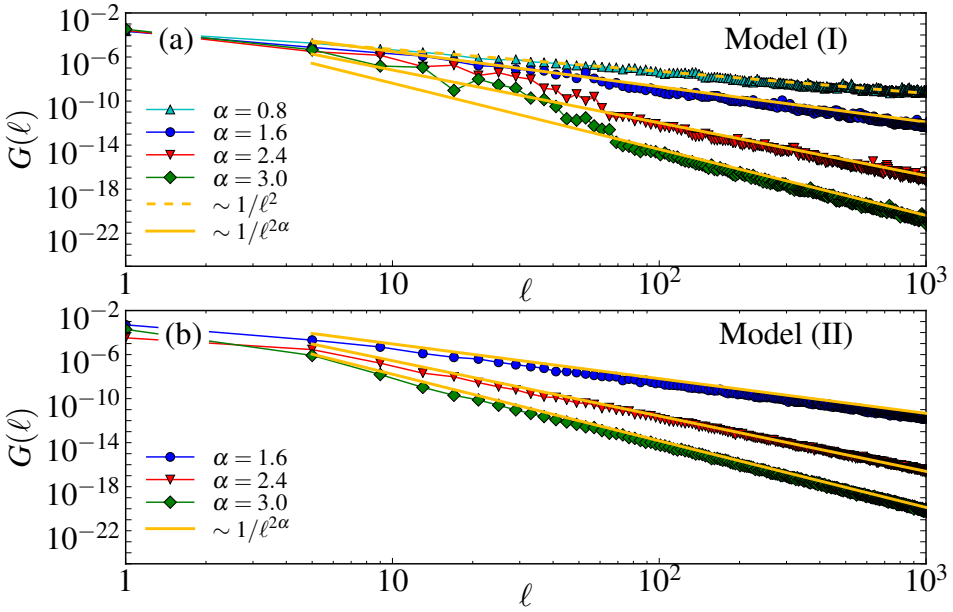

Figure 1.5: (a) Density-density correlation function $G(\ell)$ for the model (I) as a function of the lattice site ℓ for different values of α and for $W = 5$, $L = 2000$ and 400 disorder realizations. The power-law tails are fit by the yellow lines scaling as $1/\ell^2$ (dashed) and $1/\ell^{2\alpha}$ (solid). (b) Same as panel (a) but for the model (II).

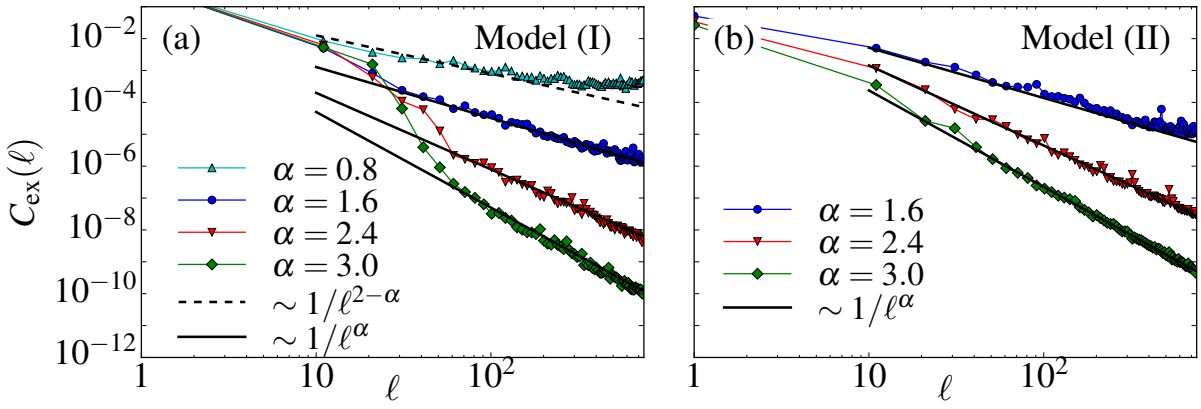

Figure 1.6: Correlation function $C_{\rm ex}(\ell)$ computed on the an excited state at the middle of the energy band for the model (I) as a function of the lattice site ℓ for different values of α and for $W = 5$, $L = 1000$ and 200 disorder realizations. The continuous lines are guides to the eye and show that the power-law tails scales as $1/\ell^{2-\alpha}$ (dashed) and $1/\ell^{2\alpha}$ (solid) also for that excite state. (b) Same as panel (a) but for the model (II).

1.3.2 Perturbation theory

To understand in more detail the decay of the correlation, we take advantage of the integrability of the fermionic models and we use a previous method developed in [9]. In the following, we will provide an extension of the method by computing the correlations functions analytically treating the disorder as a pertubation. Here we focus on the model (I) and we recall that the Hamiltonian $H_{\rm I}$ in Eq. 1.2 of the main text is formed by two parts:

$$H_{\rm I} = H_0 + V_{\rm I} \tag{1.25}$$

where

$$H_0 = -t\sum_{j=1}^{L}\left(a_j^\dagger a_{j+1} + \text{H.c.}\right) + \mu\sum_{j=1}^{L} a_j^\dagger a_j + \sum_{j,\ell}\frac{\Delta}{\ell^\alpha}\left(a_j a_{j+\ell} + \text{H.c.}\right), \tag{1.26}$$

and

$$V_{\rm I} = -t\sum_{j=1}^{L} W_j\left(a_j^\dagger a_{j+1} + \text{H.c.}\right). \tag{1.27}$$

In order to compute the correlation function $C(j,i) = \langle\Omega|a_j^\dagger a_i|\Omega\rangle$ on the ground state $|\Omega\rangle$ of $H_{\rm I}$ in Eq. (1.25), we first find the first-order correction $|\delta\Omega_0\rangle$ to the ground state $|\Omega_0\rangle$ of H_0 by treating $V_{\rm I}$ as a perturbation.

The first-order correction $|\delta\Omega_0\rangle$ to the ground state $|\Omega_0\rangle$ of the Hamiltonian H_0 due to the perturbation $V_{\rm I}$ is given by [210]

$$|\delta\Omega_0\rangle = \sum_{\mathbf{n}_0}\frac{\langle\mathbf{n}_0|V_{\rm I}|\Omega_0\rangle}{E(\mathbf{n}_0) - E_0}|\mathbf{n}_0\rangle \tag{1.28}$$

where the quantities $E(\mathbf{n}_0)$ and E_0 are the energy of the states $|\mathbf{n}_0\rangle$ and of $|\Omega_0\rangle$, respectively and $|\mathbf{n}_0\rangle$ indicates an excited state of the homogeneous Hamiltonian H_0 that can be diagonalized via Fourier and Bogoliubov transformations as

$$H_0 = \sum_k \lambda_\alpha(k)\xi_k^\dagger\xi_k. \tag{1.29}$$

The ground state $|\Omega_0\rangle$ of H_0 is then the vacuum of all extended Bogolioubov quasi-particles ξ_k. In Eq. (1.29) we have defined the single-particle energy

$$\lambda_\alpha(k) = \left[(\cos k - \mu)^2 + 4f_\alpha^2(k)\right]^{1/2} \tag{1.30}$$

and the Bogolioubov quasi-particles ξ_k that are related to the original fermionic operators $\tilde{a}_k$ in momentum space via

$$\tilde{a}_k = v_k\xi_k - u_k\xi_{-k}^\dagger \tag{1.31}$$

with $v_k = \cos\varphi(k)$ and $u_k = \mathrm{i}\sin\varphi(k)$ where $\tan 2\varphi(k) = f_\alpha(k)/[\mu - \cos k]$ and $f_\alpha(k) = \sum_{\ell=1}^{L-1}\sin(k\ell)/\ell^\alpha$. We notice that the functions $f_\alpha(k)$ when $L\to\infty$ become $f_\alpha(k) = \left[\mathrm{Li}_\alpha(\mathrm{e}^{\mathrm{i}k}) - \mathrm{Li}_\alpha(\mathrm{e}^{-\mathrm{i}k})\right]/(2\mathrm{i})$, with $\mathrm{Li}_\alpha(z) = \sum_j z^j/j^\alpha$ a polylogarithm of order α. The excited states $|\mathbf{n}_0\rangle$ are defined by assigning a set of occupied modes $\mathbf{n}_0 = \{n_1, n_2, \ldots, n_L\}$

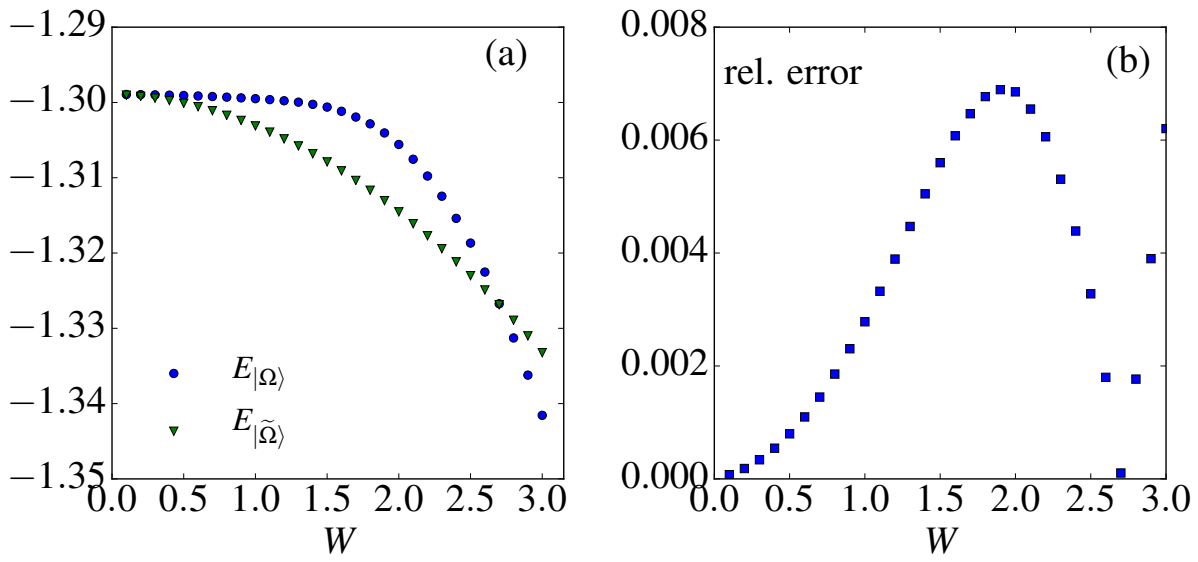

Figure 1.7: (a) Energy density $E_{|\Omega\rangle}/L$ of the ground state of the Hamiltonian $H_{\rm I}$ computed numerically (blue circles) and the energy $E_{|\widetilde{\Omega}_0\rangle}/L$ (green triangles) computed by perturbation theory. (b) Relative error defined as $\left|1 - E_{|\widetilde{\Omega}\rangle}/E_{|\Omega\rangle}\right|$. It is possible to see that the difference between the true ground state energy and the perturbed one is bounded by $8 \cdot 10^{-3}$ when the disorder strength satisfies $0 \leq W \leq 3$. For both panels we consider $\alpha = 3.0$ and a system of $L = 400$ sites and after averaging 200 disorder realizations.

with $n_q = 0, 1$ and then creating single quasi-particles $\xi_q^\dagger$ on the ground state $|\Omega_0\rangle$ if the mode q is occupied

$$|\mathbf{n}_0\rangle = \prod_{q=0}^{L-1} [\xi_q^\dagger]^{n_q} |\Omega_0\rangle \,. \tag{1.32}$$

The first-order correction $|\delta\Omega_0\rangle$ can now be obtained from Eq. (1.28) and the true ground state $|\Omega\rangle$ becomes

$$\begin{aligned} |\Omega\rangle &= |\widetilde{\Omega}\rangle + \mathcal{O}(W^2) \\ &= |\Omega_0\rangle + |\delta\Omega_0\rangle + \mathcal{O}(W^2) \\ &= |\Omega_0\rangle - \textstyle\sum_{kk'} J_{k,k'} A(k,k') \xi_k^\dagger \xi_{k'}^\dagger |\Omega_0\rangle + \mathcal{O}(W^2), \end{aligned} \tag{1.33}$$

where we have defined $J_{k,k'} = -\sum_j e^{\mathrm{i}(k-k')j} W_j/L$ and $A(k,k') = 2(\mathrm{e}^{\mathrm{i}k} + \mathrm{e}^{-\mathrm{i}k'}) v_k u^*_{k'}/[\lambda(k) + \lambda(k')]$.

Validity of the perturbation theory

Before going further in the calculation, it is convenient here to check the validity of the perturbation theory. To this end, we will compare the energy $E_{|\Omega\rangle}$ of the ground state of the Hamiltonian $H_{\rm I}$ computed numerically with the energy $E_{|\widetilde{\Omega}\rangle}$ of the state $|\widetilde{\Omega}\rangle = |\Omega_0\rangle + |\delta\Omega_0\rangle$ coming from the first order correction given in Eq. (1.33).

The energy $E_{|\widetilde{\Omega}\rangle}$ can be obtained by considering that the first order correction to a wave function gives a second order correction to the energy [211]. Therefore, the energy

for the perturbed state $|\widetilde{\Omega}\rangle$ is given by

$$E_{|\widetilde{\Omega}\rangle} = E_{|\Omega_0\rangle} + \sum_{\mathbf{n}_0} \frac{|\langle\Omega_0|V_{\mathrm{I}}|\mathbf{n}_0\rangle|^2}{E_{|\Omega_0\rangle} - E_{|\mathbf{n}_0\rangle}} \tag{1.34}$$

where $E_{|\Omega_0\rangle}$ is the ground state energy of the Hamiltonian H_0, $|\mathbf{n}_0\rangle$ denotes the excited states of H_0 from Eq. (1.32) and $E_{|\mathbf{n}_0\rangle}$ denotes their energy.

By computing the scalar product $\langle\mathbf{n}_0|V_{\mathrm{I}}|\Omega_0\rangle$ we get

$$E_{|\widetilde{\Omega}\rangle} = E_{|\Omega_0\rangle} - \sum_{q_1,q_2} \frac{|\mathcal{E}_{q_1,q_2}|^2}{\lambda_\alpha(q_1) + \lambda_\alpha(q_2)} \tag{1.35}$$

where $\mathcal{E}_{q_1,q_2} = 2J_{q_1,q_2}\mathrm{e}^{\mathrm{i}q_1}v_{q_1}u^*_{q_2} +$ h.c. where v_{q_1} and u_{q_2} are defined after Eq. (1.31) and J_{q_1,q_2} after Eq. (1.33). The left panel of Fig.. 1.7 shows the values of the energy density $E_{|\Omega\rangle}/L$ of the ground state of the Hamiltonian H_{I} computed numerically (blue circles) with the energy $E_{|\widetilde{\Omega_0}\rangle}/L$ (green triangles), while the right panel shows the relative error defined as $\left|1 - E_{|\widetilde{\Omega}\rangle}/E_{|\Omega\rangle}\right|$ for a system of $L = 400$ sites and after averaging 200 disorder realizations for $\alpha = 3.0$. It is possible to see that the difference between the true ground state energy and the perturbed one is bounded by $8 \cdot 10^{-3}$ when the disorder strength satisfies $0 \leq W \leq 3$. Note that the minimum around $W \simeq 2.5$ corresponds in fact to a accidental change of sign of the difference $E_{|\widetilde{\Omega}\rangle} - E_{|\Omega\rangle}$.

As seen, the perturbation theory is a valid approximation in a large range of W. We now continue the derivation in order to obtain an analytical form for the different correlators. Considering Eq. 1.33 for a single disorder realization, the correlation function $\langle\Omega|a_j^\dagger a_i|\Omega\rangle$ takes the form

$$\langle\Omega|a_j^\dagger a_i|\Omega\rangle = \langle\Omega_0|a_j^\dagger a_i|\Omega_0\rangle + \langle\delta\Omega_0|a_j^\dagger a_i|\Omega_0\rangle + \langle\Omega_0|a_j^\dagger a_i|\delta\Omega_0\rangle + \langle\delta\Omega_0|a_j^\dagger a_i|\delta\Omega_0\rangle\,. \tag{1.36}$$

If we now average Eq. (1.36) over many disorder realizations, the cross terms $\langle\delta\Omega_0|a_j^\dagger a_i|\Omega_0\rangle$ and $\langle\Omega_0|a_j^\dagger a_i|\delta\Omega_0\rangle$ vanish as, due to the correction $|\delta\Omega_0\rangle$, only one random term W_j (that has mean value zero) appears in them. Therefore we get

$$\langle\Omega|a_j^\dagger a_i|\Omega\rangle_W = \langle\Omega_0|a_j^\dagger a_i|\Omega_0\rangle + \langle\delta\Omega_0|a_j^\dagger a_i|\delta\Omega_0\rangle_W\,. \tag{1.37}$$

The first term of the r.h.s. of Eq. (1.37) corresponds to the correlator for a homogenous translationally-invariant system. By rewriting $a_j^\dagger$ and a_i in momentum space and by using Eq. (1.31) recalling that $\xi_k\,|\Omega_0\rangle = 0$ we obtain

$$C_0(\ell) := \langle\Omega_0|a_j^\dagger a_i|\Omega_0\rangle = \frac{1}{L}\sum_k \mathrm{e}^{\mathrm{i}k\ell}R_0(k) \tag{1.38}$$

where $\ell = j - i$ and $R_0(k) = |u_k|^2$.

In the second term of the r.h.s. of Eq. (1.37), as we are averaging on the disorder configurations, we can expect that the disorder average $\langle\delta\Omega_0|a_j^\dagger a_i|\delta\Omega_0\rangle_W$ will be translationally invariant, i.e. it will depend on the relative distance $\ell = j - i$ while the terms

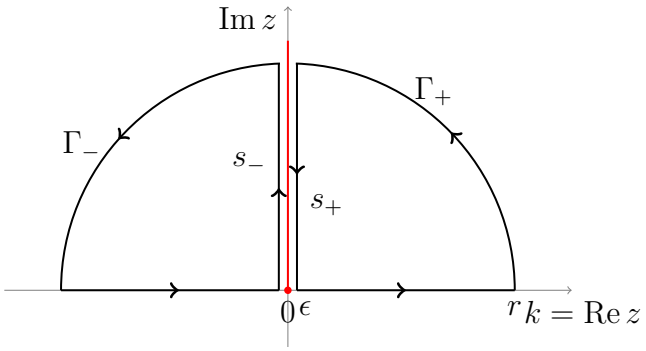

Figure 1.8: Integration contour for evaluating the asymptotic behaviors of the correlators $C_0(\ell)$ in Eq. (1.47) and $C_1(\ell)$ in Eq. (1.53).

that depend on i and j separately will average out to zero (see §6.5 in Ref. [212] or §12.3 in Ref. [213]). By keeping only the terms that depend on ℓ, after rewriting $a_j^\dagger$ and a_i in momentum space and using again Eq. (1.31) recalling that $\xi_k |\Omega_0\rangle = 0$, the second term becomes

$$C_1(\ell) := \langle \delta\Omega_0 | a_j^\dagger a_i | \delta\Omega_0 \rangle_W = \frac{W^2}{3L} \sum_k \mathrm{e}^{\mathrm{i}k\ell} R_1(k) \tag{1.39}$$

where

$$R_1(k) = c|u_k|^2 + U(k)|u_k|^2 - V(k)|v_k|^2, \tag{1.40}$$

$$c = \sum_p A(p,p)^2 - \sum_{p_1 p_2} A(p_1,p_2)A(p_2,p_1), \tag{1.41}$$

$$U(k) = 2\sum_p A(p,-k)A(-k,p) = -\frac{f_\alpha(k)}{\lambda_\alpha(k)} \sum_p \frac{2+2\cos(p-k)}{(\lambda_\alpha(k)+\lambda_\alpha(p))^2} \frac{f_\alpha(p)}{\lambda_\alpha(p)}, \tag{1.42}$$

$$V(k) = 2\sum_p A(p,k)A(k,p) = \frac{f_\alpha(k)}{\lambda_\alpha(k)} \sum_p \frac{2+2\cos(p+k)}{(\lambda_\alpha(k)+\lambda_\alpha(p))^2} \frac{f_\alpha(p)}{\lambda_\alpha(p)}. \tag{1.43}$$

We note that the quantity c does not depend on k.

Asymptotic behaviour

Finally, we show how the correlators $C_0(\ell)$ and $C_1(\ell)$ behave asymptotically for $\ell \to \infty$.

Let us consider $C_0(\ell)$ in Eq. (1.38) first. In the limit $L \to \infty$ we can replace the summation with an integral

$$C_0(\ell) = \frac{1}{2\pi} \int_{-\infty}^{\infty} \mathrm{d}k\ \mathrm{e}^{\mathrm{i}k\ell} R_0(k). \tag{1.44}$$

The asymptotic behavior of $C_0(\ell)$ for $\ell \to \infty$ can be computed by considering the integrals I_0^+ and I_0^- on the complex plane in Fig. 1.8 that are

$$I_0^+ = \frac{1}{2\pi} \int_{s_+} \mathrm{d}z\ \mathrm{e}^{\mathrm{i}z\ell} R_0(z) + \frac{1}{2\pi} \int_{\Gamma_+} \mathrm{d}z\ \mathrm{e}^{\mathrm{i}z\ell} R_0(z) + \frac{1}{2\pi} \int_0^{\infty} \mathrm{d}k\ \mathrm{e}^{\mathrm{i}k\ell} R_0(k) \tag{1.45}$$

$$I_0^- = \frac{1}{2\pi} \int_{s_-} \mathrm{d}z\ \mathrm{e}^{\mathrm{i}z\ell} R_0(z) + \frac{1}{2\pi} \int_{\Gamma_-} \mathrm{d}z\ \mathrm{e}^{\mathrm{i}z\ell} R_0(z) + \frac{1}{2\pi} \int_{-\infty}^{0} \mathrm{d}k\ \mathrm{e}^{\mathrm{i}k\ell} R_0(k) \tag{1.46}$$

where we have chosen to put the branch cut of the complex logarithm [see the expansion of the polylogarithm in Eq. (1.48)] on the imaginary positive axis.

By sending the radius r of the circles $\Gamma_\pm$ to infinity and by neglecting possible residues inside the integration contour that will contribute only with exponential decaying terms we have

$$\begin{aligned} C_0(\ell) &= -\frac{1}{2\pi}\int_{s_+} \mathrm{d}z\ \mathrm{e}^{\mathrm{i}z\ell} R_0(z) - \frac{1}{2\pi}\int_{s_-} \mathrm{d}z\ \mathrm{e}^{\mathrm{i}z\ell} R_0(z) \\ &= \frac{\mathrm{i}}{2\pi}\int_0^\infty \mathrm{d}y\ \mathrm{e}^{-y\ell} R_0(\epsilon+\mathrm{i}y) - \frac{\mathrm{i}}{2\pi}\int_{-\infty}^0 \mathrm{d}y\ \mathrm{e}^{-y\ell} R_0(-\epsilon+\mathrm{i}y) \\ &= \frac{1}{\pi}\int_0^\infty \mathrm{d}y\ \mathrm{e}^{-y\ell}\,\mathrm{Im}\, R_0(\mathrm{i}y) \end{aligned} \tag{1.47}$$

where on the lines $s_\pm$ the complex variable is $z = \pm\epsilon + \mathrm{i}y$ with ϵ a small positive parameter that we send to zero.

We are able now to evaluate the asymptotic behavior of $C_0(\ell)$ by computing the $y \to 0$ part of $\mathrm{Im}[R_0(\mathrm{i}y)]$ and then integrating the last equality in Eq. (1.47). This is done by recalling that the polylogarithm admits the series expansion [214, 215] for a general complex number z as

$$\mathrm{Li}_\alpha(z) = \Gamma(1-\alpha)\left(\ln\frac{1}{z}\right)^{\alpha-1} + \sum_{n=0}^\infty \zeta(\alpha-n)\frac{(\ln z)^n}{n!} \tag{1.48}$$

that makes them non-analytical due to the presence of the complex logarithm and the power-law. In Eq. (1.48), $\Gamma(x)$ and $\zeta(x)$ are the Euler gamma function and the Riemann zeta function, respectively.

By using the series expansion of the polylogarithms from Eq. (1.48) that yields

$$\mathrm{Li}_\alpha(\mathrm{e}^{-y}) - \mathrm{Li}_\alpha(\mathrm{e}^{y}) = \Gamma(1-\alpha)\left(1+\mathrm{e}^{\mathrm{i}\pi\alpha}\right) y^{\alpha-1} - 2\sum_{n\ \mathrm{odd}}^\infty \frac{\zeta(\alpha-n)}{n!} y^n \tag{1.49}$$

we can obtain the function $R_0(\mathrm{i}y)$ on the imaginary axis:

$$\begin{aligned} R_0(\mathrm{i}y) &= \frac{\mu-\cosh y}{2\lambda_\alpha(\mathrm{i}y)} \\ &\sim \frac{\mu-1}{2\sqrt{(\mu-1)^2 - \Gamma^2(1-\alpha)(\mathrm{e}^{\mathrm{i}\pi\alpha}+1)^2 y^{2\alpha-2} - 4\Gamma(1-\alpha)(\mathrm{e}^{\mathrm{i}\pi\alpha}+1)\zeta(\alpha-1)y^\alpha}}. \end{aligned} \tag{1.50}$$

The previous equation in the limit $y \to 0$ gives

$$\mathrm{Im}\, R_0(\mathrm{i}y) = \begin{cases} y^{1-\alpha} & \text{for } \alpha < 1 \\ y^{2\alpha-2} & \text{for } 1 < \alpha < 2 \\ y^\alpha & \text{for } \alpha > 2 \end{cases} \tag{1.51}$$

and, after performing the last integral in Eq. (1.47), the asymptotic behavior of C_0 turns out to be

$$C_0(\ell) \sim \begin{cases} 1/\ell^{2-\alpha} & \text{for } \alpha < 1 \\ 1/\ell^{2\alpha-1} & \text{for } 1 < \alpha < 2 \\ 1/\ell^{\alpha+1} & \text{for } \alpha > 2. \end{cases} \tag{1.52}$$

For the correlator $C_1(\ell)$ in Eq. (1.39) we can use the same contour in Fig. 1.8 and get

$$C_1(\ell) = \frac{W^2}{3\pi} \int_0^\infty \mathrm{d}y \; \mathrm{e}^{-y\ell} \, \mathrm{Im}\, R_1(\mathrm{i}y). \tag{1.53}$$

For the asymptotic behaviour of $C_1(\ell)$, we need again the $y \to 0$ part of $R_1(\mathrm{i}y)$. Let us start by noting that from Eqs. (1.42) and (1.43) the $y \to 0$ part of both $U(\mathrm{i}y)$ and $V(\mathrm{i}y)$ is given by

$$\mathrm{Im}[U(\mathrm{i}y)|u_{\mathrm{i}y}|^2] \sim \mathrm{Im}[V(\mathrm{i}y)|v_{\mathrm{i}y}|^2] \sim \mathrm{Im}\, \frac{f_\alpha(\mathrm{i}y)(\mu - \cosh y)}{\lambda_\alpha^2(\mathrm{i}y)} \sim \begin{cases} y^{1-\alpha} & \text{for } \alpha < 1 \\ y^{\alpha-1} & \text{for } \alpha > 1. \end{cases} \tag{1.54}$$

The previous equation, by considering also the contribution coming from $c|u_{\mathrm{i}y}|^2$ [see Eq. (1.40)], gives

$$\mathrm{Im}\, R_1(\mathrm{i}y) \sim \begin{cases} y^{1-\alpha} & \text{for } \alpha < 1 \\ y^{\alpha-1} & \text{for } \alpha > 1 \end{cases} \tag{1.55}$$

and after integrating Eq. (1.53), we finally get the correlator

$$C_1(\ell) = \begin{cases} W^2/\ell^{2-\alpha} & \text{for } \alpha < 1 \\ W^2/\ell^{\alpha} & \text{for } \alpha > 1. \end{cases} \tag{1.56}$$

The asymptotic behavior coming from Eqs. (1.52), (1.56) can be checked by computing the correlator $C(\ell)$ numerically as reported in Fig. 1.3.

The discussion above demonstrates the following surprising results:

- For $\alpha < 1$ disorder does not modify the power of the algebraic decay of correlations, rather it affects its strength.
- For $\alpha > 1$, the decay of correlations due to disorder is always algebraic, with an exponent that is smaller than for the homogeneous case with $W_j = 0$. This implies that disorder enhances the algebraic localization in these gapped models.
- For $\alpha \leq 2$ we find the duality relation $\gamma(\alpha) = \gamma(2-\alpha)$ in the exponents of the algebraic decay. This is reminiscent of the duality recently found for the decay exponent of the wave functions of long-range non-interacting spin models with positional disorder [191].

1.3.3 Correlations in LRI

We now consider the random interacting long-range Ising model within the MBL phase with $\alpha > 1$, and compute the spin-spin correlation function

$$S_\nu(j,\ell) = \left[\langle \sigma_j^\nu \sigma_{j+\ell}^\nu \rangle - \langle \sigma_j^\nu \rangle \langle \sigma_{j+\ell}^\nu \rangle\right]_W, \quad (\nu = x, z). \tag{1.57}$$

To calculate the correlation $S_\nu(j_0,\ell)$ ($\nu = x, z$), we make use of a the density matrix renormalization group (DMRG) as introduced in [61, 216]. Here we choose $j_0 = L/10$ and for the simulations, we use up to 400 local DMRG states, 16 sweeps and we average $S_\nu(\ell)$

over 100 disorder realizations. Strikingly, we find that $S_\nu(\ell)$ decays algebraically with ℓ as $S_\nu(\ell) \sim \ell^{-\gamma}$ with an exponent that is consistent with $\gamma = \alpha$, in complete agreement with the discussion above for non-interacting theories. As an example, Fig. 1.9(a) shows $S_x(\ell)$ for different values of α, $W = 5\sin(\pi/5) \approx 2.93$ and $B = 0$, while Fig. 1.9(b) shows $S_z(\ell)$ for different values of α, $W = 0$ and $B = 5\sin(\pi/5)$. The corresponding fits (continuous lines) with $1/\ell^\alpha$ perfectly match the numerical results.

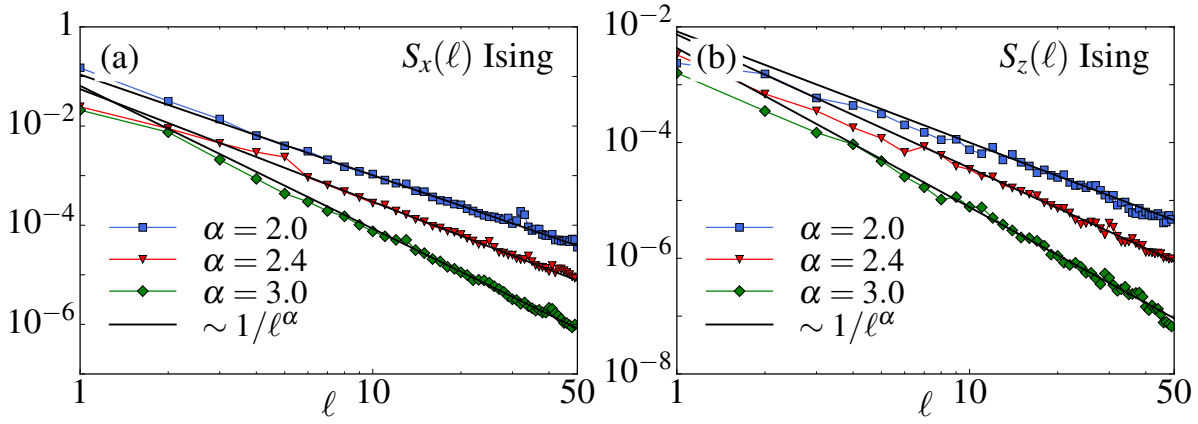

Figure 1.9: (a) Correlation function $S_x(\ell)$ for the long-range Ising model with a random transverse field [$W = 5\sin(\pi/5)$] and a constant interaction term ($B = 0$) for a system of $L = 100$ spins and 50 disorder realizations. (b) Correlation function $S_z(\ell)$ for the long-range Ising model with a random interaction [$B = 5\sin(\pi/5)$] and a constant magnetic field ($W = 0$). In both panels, the power-law tails are fit by the black lines scaling as $1/\ell^\alpha$.

The demonstration of algebraic localization found in long-range couplings in the presence of disorder is a central result of this work. We argue that the fact that these results are found both for non-interacting and interacting models strongly suggests the existence of a universal behavior due to long-range coupling.

1.3.4 Localization of the wave function

Further insight of the localised properties is given by the analysis of the decay of the single particle-wave functions. While in the conventional Anderson model, the latter are exponentially localized, here we expect changes due to the power law potential. Our numerical results on the decay of the single-particle wave functions are obtained by considering the mean value $\Phi(\ell) = \sum_{q=1}^{N} |g_{q,\ell-j_M}|/N$ where we average $N = L/4$ wave functions $g_{q,\ell}$ with lowest energies, shifted by the quantity j_M that corresponds to the lattice site where $|g_{q,\ell}|$ shows its maximum value. We average $\Phi(\ell)$ also over several disorder realizations (of the order of 500).

Fig. 1.10 shows typical results of the decay of $\Phi(\ell)$ as a function of the distance ℓ within the localized phases of models (I) and (II) of Eqs. (1.1) [panels (a,b) and (c,d), respectively].

Remarkably, we find that the wave functions decay algebraically at long distances regardless of the strength W of the disorder, mimicking the scaling of the correlation

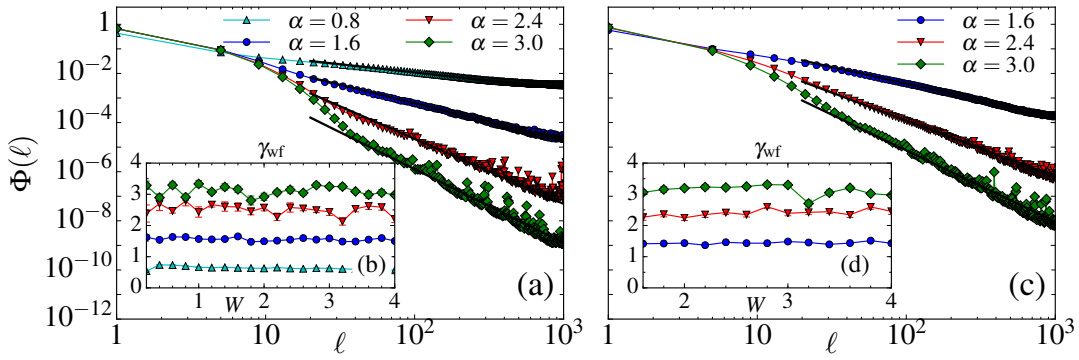

Figure 1.10: (a) Decay of the averaged wave function $\Phi(\ell)$ (absolute value, see text) of localized states for the model (I): If $\alpha > 1$ we find an hybrid exponential and power-law behaviour. If $\alpha < 1$ the exponential part is suppressed and only the power-law tail is visible. The black lines correspond to fit of the data scaling as $1/\ell^{\gamma_{\rm wf}}$. (b) Decay exponent $\gamma_{\rm wf}$ for the model (I) of the long-distance tail of $\Phi(\ell)$ as a function of W for different values of α. The decay exponent satisfies $\gamma_{\rm wf} \sim \alpha$ and does not show significance dependence on W. (c-d) Same as (a-b) but for the model (II) with random long-range pairing.

functions discussed above. However, for all α, i.e. both $\alpha > 1$ and $\alpha < 1$, $\Phi(\ell)$ decays at large distances as $\Phi(\ell) \sim \ell^{-\gamma_{\rm wf}}$, with an exponent $\gamma_{\rm wf}$ consistent with $\gamma_{\rm wf} \sim \alpha$. This is different from the results of Ref. [191] with positional disorder, where for $\alpha < 1$ one gets $\gamma_{\rm wf} \sim 2 - \alpha$. For sufficiently large $\alpha > 1$ this algebraic decay is preceded by an exponential decay at short distances, reminiscent of the exponentially localized states of short-range random Hamiltonians.

1.4 Conclusion

In this chapter, motivated by recent experimental advances in engineering long-range couplings, we have analyzed the effect of disorder on the correlation functions of one-dimensional quantum models of fermions and spins with long-range interactions, finding several novels features. These include a new mechanism to create high-energy protected states against localization at finite size and disordered phases where the tails of correlation functions exhibit algebraic decay.

In the first part of the study, using a combination of analytical and numerical technics, we have determined the phase diagram of the fermionic models, showing a non-trivial interplay between long-range and disorder. In particular, we have demonstrated the presence of an *effective* single-particle mobility edge that vanishes in the thermodynamic limit. In the second part, we have investigated long-range interaction effect on the decay of the correlations and the waves functions within the localized phases.

We have notably demonstrated that couplings that decay as a power-law with distance induce an algebraic decay of correlation functions and wave functions both in non-interacting and interacting models in the presence of disorder. This behavior is in stark contrast to results expected from short-range models and generalizes recent results for the decay of wave-functions in quadratic models.

Appendices

1.A Exact diagonalization and level spacing

Exact diagonalization

In this Appendix, we will review some results on the exact diagonalization of the Long-range Kitaev model [9]. We consider the following quadratic Hamiltonian:

$$\begin{aligned} H_0 = -t\sum_{j=1}^{L}\left(a_j^\dagger a_{j+1} + \text{H.c.}\right) + \mu\sum_{j=1}^{L} n_j \\ + \sum_{j,\ell}\frac{\Delta}{d_\ell^\alpha}\left(a_j a_{j+\ell} + \text{H.c.}\right) \end{aligned} \tag{1.58}$$

where $a_j^\dagger$ (a_j) is a fermionic creation (annihilation) operator on site j, $n_j = a_j^\dagger a_j$, t the tunneling rate and μ the chemical potential. Δ is the strength of the p-wave pairing and we can set without lost of generality that $\Delta = 2t$, different value of Δ/t simply rescale the fermi velocity. The function d_ℓ specifies the distance between two fermions.

In the next, we consider a ring which is invariant by translation ($d_\ell = \min(\ell, L-\ell)$), and we impose anti-periodic condition ($a_j = -a_{j+L}$). This choice of the boundary condition directly comes from the pairing term. Indeed, because of the ring geometry, the term $a_j a_{j+\ell}$ and $a_{j+\ell}a_{j+\ell+L}$ connect two fermions with the same distance. Then, if we choose periodic boundary condition ($a_j = a_{j+L}$), these two terms, and so the pairing term, will cancel out due to the anti-commutation of fermionic particles.

Now one can rewrite the hamiltonian 1.58 by using a Fourier transform of the fermionic operators $a_j^\dagger = \frac{1}{\sqrt{N}}\sum_k e^{\mathrm{i}kj}a_k^\dagger$. It takes the form

$$\begin{aligned} H = -\sum_n\left(t\cos k_n + \frac{\mu}{2}a_{k_n}^\dagger a_{k_n} + a_{-k_n}^\dagger a_{-k_n}\right) \\ + i\Delta\sum_n f_\alpha(k_n)\left(a_{k_n}a_{-k_n} - a_{-k_n}^\dagger a\dagger_{k_n}\right) \end{aligned} \tag{1.59}$$

where $k_n = \frac{2\pi}{L}(n+\frac{1}{2})$ and $f_\alpha(k_n) = \sum_{\ell=1}^{L-1}\frac{\sin(k_n\ell)}{\ell^\alpha}$.

Formally, we can write our Hamiltonian into a more compact form as:

$$H = \frac{1}{2}\sum_{n=0}^{L-1}\begin{pmatrix} a_{k_n}^\dagger & a_{-k_n}\end{pmatrix}\begin{pmatrix} -(2t\cos k_n + \mu) & i\Delta f_\alpha(k_n) \\ -i\Delta f_\alpha(k_n) & (2t\cos k_n + \mu)\end{pmatrix}\begin{pmatrix} a_{k_n} \\ a_{-k_n}^\dagger\end{pmatrix} \tag{1.60}$$

By means of a Bogolyubov transformation each blocks of momentum k_n can be diagonalized:

$$\begin{pmatrix} a_{k_n} \\ a^\dagger_{-k_n} \end{pmatrix} = \mathrm{U}^\dagger \begin{pmatrix} \xi_{k_n} \\ \xi^\dagger_{-k_n} \end{pmatrix} \tag{1.61}$$

with

$$\mathrm{U} = \begin{pmatrix} \cos\varphi_{k_n} & i\sin\varphi_{k_n} \\ i\sin\varphi_{k_n} & \cos\varphi_{k_n} \end{pmatrix} \tag{1.62}$$

and φ_{k_n} is given by

$$\tan(2\varphi_{k_n}) = -\frac{\Delta f_\alpha(k_n)}{2t\cos k_n + \mu} \tag{1.63}$$

Finally, in the Bogolyubov basis the hamiltonian read as:

$$H = \frac{1}{2}\sum_{n=0}^{L-1} \lambda(k_n)\xi^\dagger_{k_n}\xi_{k_n} \tag{1.64}$$

and its single-particle energy

$$\lambda(k_n) = \sqrt{(2t\cos k_n + \mu)^2 + (\Delta f_\alpha(k_n))^2} \tag{1.65}$$

Level spacing and polylogarithmic

In order to qualitatively understand the level spacing, we should analyse in more details the spectrum of excitations. While the first part corresponds to the usual free fermions, the second part with function $f_\alpha(k)$ contains all the informations about the long-range. Below, we focus on some mathematical properties of this function.

The series defining $f_\alpha(k)$ is :

$$f_\alpha(k) = \sum_{\ell=1}^{L-1} \frac{\sin(k\ell)}{\ell^\alpha} \tag{1.66}$$

When $L \to \infty$, i.e in the thermodynamic limit, $f_\alpha(k)$ reads as

$$f_\alpha(k) = \frac{1}{2i}\sum_{\ell=1}^{\infty} \frac{e^{i\ell k} - e^{-i\ell k}}{\ell^\alpha} = -\frac{i}{2}(\mathrm{Li}_\alpha(e^{ik}) - \mathrm{Li}_\alpha(e^{-ik}), \tag{1.67}$$

with

$$\mathrm{Li}_\alpha(z) = \sum_{\ell=1}^{\infty} \frac{z}{\ell^\alpha} \tag{1.68}$$

the polylogarithm of complex z of order α. Interestingly, in our case, $z = e^{ik}$ and $|z| = 1$, the convergence of the previous serie is α dependent. For $\alpha > 1$, the serie converges,

whereas for $\alpha < 1$, the serie converge only for $z \neq 0$, i.e for $k \neq 0$ but diverges for $k = 0$. For two particular case, $\alpha = 0$ and $\alpha = 1$, one can obtained for $\mathrm{Li}_\alpha(z)$:

$$\mathrm{Li}_0(z) = \frac{z}{z-1} \qquad \mathrm{Li}_1(z) = \ln(1-z) \tag{1.69}$$

and $f_\alpha(k)$

$$f_0(k) = \cot\left(\frac{k}{2}\right) \qquad f_1(k) = \pi - k. \tag{1.70}$$

Let us consider, the maximum $k = \pi$ and the minimum $k = 0$ of the band:

(i) for $\alpha > 1$, for $k \to 0$ and $k \to \pi$, $f_\alpha(k) \to 0$. In this case, the dispersion relation is close to the one of free fermions, and we obtain $\lambda_\alpha(k) \sim k^2$

(ii) For $\alpha < 1$, at the minimum of the band ($k = \pi$) , $f_\alpha(k = \pi) \to 0$. However, as mentioned previously the series diverge for $k \to zero$.

In the following we study the divergence $k \to 0$ when $\alpha < 1$. We start by introducing the series expansion:

$$\mathrm{Li}_\alpha(e^{ik}) = \Gamma(1-\alpha)(-ik)^{\alpha-1} + \sum_{n=0}^{\infty} \frac{\zeta(\alpha-n)}{n!}(ik)^n \tag{1.71}$$

$$\mathrm{Li}_\alpha(e^{-ik}) = \Gamma(1-\alpha)(ik)^{\alpha-1} + \sum_{n=0}^{\infty} \frac{\zeta(\alpha-n)}{n!}(-ik)^n \tag{1.72}$$

valid for all not integer α and where $\zeta(s)$ is the zeta Riemann function. Then we have,

$$f_\alpha(k) = 2\cos\frac{\pi\alpha}{2}\Gamma(1-\alpha)(k)^{\alpha-1} + 2\sum_{n=1}^{\infty} \sin\frac{\pi n}{2}\frac{\zeta(\alpha-n)}{n!}(k)^n \tag{1.73}$$

and

$$\begin{aligned} f_\alpha^2 k) = {} & 4\cos^2\frac{\pi\alpha}{2}\Gamma^2(1-\alpha)(k)^{2\alpha-2} + 8\cos\frac{\pi\alpha}{2}\zeta(\alpha)\Gamma(1-\alpha)k^\alpha \\ & + 4\zeta^2(\alpha)k^2 + \mathcal{O}(k^3) \end{aligned} \tag{1.74}$$

In this way when $\alpha < 1$ and $k \to 0$, we have

$$\lambda_\alpha(k) \sim \cos\frac{\pi\alpha}{2}\frac{|\Gamma(1-\alpha)|}{|k|^{1-\alpha}}. \tag{1.75}$$

1.B Correlation functions of the clean long-range models

1.B.1 LRK

In this appendix, we briefly review the method introduced in [9, 217] to compute the ground state correlation functions of the Long-range Kitaev model 1.58. In particular, we will show, that the correlations present a hybrid behavior for $\alpha > 1$ and a purely algebraic decay for $\alpha < 1$. We focus on the single-particle Green function $\langle a_R^\dagger a_0 \rangle$ and the

anomalous one $\langle a_R^\dagger a_0^\dagger \rangle$. As the hamiltonian is quadratic, higher-order correlations, such as density-density correlations $\langle n_R n_0 \rangle$ can easily be built via the Wick's theorem, e.g

$$\begin{aligned} \langle n_R n_0 \rangle &= \langle a_R^\dagger a_R a_0^\dagger a_0 \rangle \\ &= \langle n_R \rangle \langle n_0 \rangle - \langle a_R^\dagger a_0^\dagger \rangle \langle a_R a_0 \rangle + \langle a_R^\dagger a_0 \rangle \langle a_R a_0^\dagger \rangle \end{aligned} \tag{1.76}$$

In the limit $L \to \infty$, both correlators take the form of an integral on the Brillouin zone:

$$\langle a_R^\dagger a_0 \rangle = -\frac{1}{2\pi} \int_0^{2\pi} \mathrm{d}k \, e^{ikR} \, \mathcal{G}_\alpha(k), \tag{1.77}$$

and

$$\langle a_R^\dagger a_0^\dagger \rangle = \frac{1}{2\pi} \int_0^{2\pi} \mathrm{d}k \, e^{ikR} \, \mathcal{F}_\alpha(k) \tag{1.78}$$

with

$$\mathcal{G}_\alpha(k) = \frac{\cos k + \mu}{2\lambda_\alpha(k)} \quad \text{and} \quad \mathcal{F}_\alpha(k) = i \, \frac{f_\alpha(k)}{2\lambda_\alpha(k)} \tag{1.79}$$

In the following, we remind the main ideas and results of the calculations, neglecting most of the technical details that the interested readers can found in [217]. We first consider the one-body correlation function $\langle a_R^\dagger a_0 \rangle$. In order to evaluate the integral in Eq. (1.77), we apply the Cauchy Theorem to a contour in the complex plane which is defined in Fig. 1.11,

$$\langle a_R^\dagger a_0 \rangle = -\frac{1}{2\pi} \lim_{M \to \infty} \left(\int_{\mathcal{C}_0} + \int_{\mathcal{L}_-} + \int_{\mathcal{L}_+} + \int_{\mathcal{C}_{2\pi}} \right) \mathrm{d}z \, e^{izR} \, \mathcal{G}_\alpha(z) \tag{1.80}$$

with M specified in Fig. 1.11.

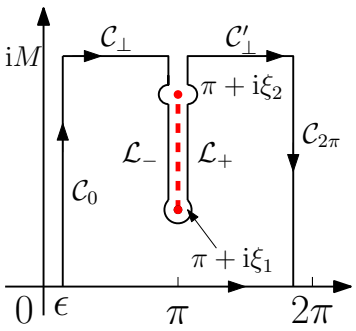

Figure 1.11: Deformed integration contour to evaluate the integral in Eq. (1.77). The dashed line is the branch cut of the square root in the denominator of the integrand.

The contours $\mathcal{L}_\pm$ are chosen in accordance with the square root in denominator of Eq. (1.79) which is a multivalued function and displays two complex roots $\pi + i\,\xi_{1,2}$ given by the solutions of the equation

$$(\mu - \cosh \xi_{1,2})^2 + f_\alpha(\pi + i\xi_{1,2})^2 = 0. \tag{1.81}$$

A branch cut arises between the roots above, as shown in Fig. 1.11. Here, different contributions can be inferred from the various path on the contour integration. First of all, the contributions from $\mathcal{C}_\perp$ and $\mathcal{C}'_\perp$ vanish when $M \to \infty$, thus we can neglect them. Then, we distinguish two main contributions that we analyze separately.

Power law part

The contribution parts coming from the momenta $k \to 0$ ($\mathcal{C}_0$) and $k \to 2\pi$ ($\mathcal{C}_{2\pi}$) are responsible for the power law decay at long distance. The integral on the line $\mathcal{C}_0$ read as

$$I_{\mathcal{C}_0} = -\frac{1}{2\pi}\int_{\mathcal{C}_0} e^{izR}\,\mathcal{G}_\alpha(z)\mathrm{d}z = -\frac{i}{2\pi}\int_0^\infty e^{-yR}\,\mathcal{G}_\alpha(\epsilon+iy)\mathrm{d}y, \tag{1.82}$$

while on $\mathcal{C}_{2\pi}$ (with $z = 2\pi - \epsilon + iy$)

$$I_{\mathcal{C}_{2\pi}} = -\frac{1}{2\pi}\int_{\mathcal{C}_{2\pi}} e^{izR}\,\mathcal{G}_\alpha(z)\mathrm{d}z = \frac{i}{2\pi}\int_0^\infty e^{-yR}\,\mathcal{G}_\alpha(2\pi-\epsilon+iy)\mathrm{d}y. \tag{1.83}$$

The sum on the integrals lines on $\mathcal{C}_0$ and $\mathcal{C}_{2\pi}$ gives

$$I_{\mathcal{C}_0} + I_{\mathcal{C}_{2\pi}} = \frac{1}{\pi}\int_0^\infty \mathrm{d}y\, e^{-yR}\,\mathrm{Im}(\mathcal{G}_\alpha(iy)). \tag{1.84}$$

An explicit calculation of the previous integral can be obtained by integrating in the $y \to 0$ and gives

$$I_{\mathcal{C}_0} + I_{\mathcal{C}_{2\pi}} = \mathcal{B}_\alpha(\mu)\cdot\begin{cases}\dfrac{1}{R^{\alpha+1}} & \text{if } \alpha > 2;\\[2ex] \dfrac{1}{R^{2\alpha-1}} & \text{if } 1<\alpha<2;\\[2ex] \dfrac{1}{R^{2-\alpha}} & \text{if } 0<\alpha<1.\end{cases} \tag{1.85}$$

Exponential part

The $\mathcal{L}_\pm$ parts with $k \to \pi$ are responsible for the exponential decay at short distance. If $\xi_1 < y < \xi_2$ we have $\mathcal{G}_\alpha(\pi^+ + iy) = \mathcal{G}^*_\alpha(\pi^- + iy)$ due to the branch cut of the square root in Eq. (1.79). The integrals on the two lines $\mathcal{L}_-$ and $\mathcal{L}_+$ give

$$I_{\mathcal{L}_-} + I_{\mathcal{L}_+} = \frac{e^{i\pi R}e^{-\xi_1 R}}{\pi}\int_0^{\xi_2} \mathrm{d}y\, e^{-yR}\,\mathrm{Im}\mathcal{G}_\alpha(\pi^+ + i(y+\xi_1)). \tag{1.86}$$

Evaluating this integral yields

$$I_{\mathcal{C}_0} + I_{\mathcal{C}_{2\pi}} = \mathcal{A}_\alpha(\mu)\frac{e^{i\pi R}}{\sqrt{\pi}}\frac{e^{-\xi_1 R}}{\sqrt{R}} \tag{1.87}$$

By collecting all the contributions we finally obtain:

$$\langle a_R^\dagger a_0 \rangle = \mathcal{A}_\alpha(\mu)\frac{e^{i\pi R}}{\sqrt{\pi}}\frac{e^{-\xi_1 R}}{\sqrt{R}} + \mathcal{B}_\alpha(\mu)\cdot\begin{cases}\dfrac{1}{R^{\alpha+1}} & \text{if } \alpha > 2;\\ \dfrac{1}{R^{2\alpha-1}} & \text{if } 1<\alpha<2;\\ \dfrac{1}{R^{2-\alpha}} & \text{if } 0<\alpha<1.\end{cases} \tag{1.88}$$

The parameter ξ_1 is the smallest real solution of $\lambda_\alpha(\mathrm{i}\pi+\xi_1)=0$ and depend on μ and α in an implicit way and the coefficients $\mathcal{A}(\alpha,\mu)$ and $\mathcal{B}(\alpha,\mu)$ can be found in Ref. [217]. It is possible to see that the correlation function shows a hybrid decay, i.e. exponential at short distances, followed by an algebraic tail whose decaying exponent depends on α.

Anomalous correlation function and other correlations

The anomalous correlation function $\langle a_R^\dagger a_0^\dagger\rangle$, which is given by the Eq. 1.78, can be computed along the same line. Using the same integration contour as for $\langle a_R^\dagger a_0\rangle$, we get:

$$\langle a_R^\dagger a_0^\dagger\rangle = \frac{e^{i\pi R}e^{-\xi_1 R}}{\pi}\int_0^\infty \mathrm{d}y\, e^{-yR}\mathcal{F}_\alpha(\pi^+ + i(y+\xi_1)) - \frac{1}{\pi}\int_0^\infty \mathrm{d}y\, e^{-yR}\,\mathrm{Im}\mathcal{F}_\alpha(iy), \tag{1.89}$$

showing both the exponential and the power-law contributions. In Eq. (1.89) ξ_1 is again the smallest solution of Eq. (1.81). One obtains finally

$$\langle a_R^\dagger a_0^\dagger\rangle = \mathcal{A}_\alpha^{\mathrm{ano}}(\mu)\frac{e^{i\pi R}}{\sqrt{\pi}}\frac{e^{-\xi_1 R}}{\sqrt{R}} + \mathcal{B}_\alpha^{\mathrm{ano}}(\mu)\cdot\begin{cases}\dfrac{1}{R^{\alpha}} & \text{if } \alpha > 1;\\ \dfrac{1}{R} & \text{if } 0<\alpha<1.\end{cases} \tag{1.90}$$

Furthermore, by combining the correlators, $g_1(R)$ and $g_1^a(R)$ one can now compute the two-point connected correlation function $g_2^c(R) = \langle n_R n_0\rangle - \langle n_R\rangle\langle n_0\rangle$. We find that the latter behave as

$$g_2^c(R) \sim \begin{cases}\dfrac{1}{R^{2\alpha}} & \text{if } \alpha > 1;\\ \dfrac{1}{R^2} & \text{if } 0<\alpha<1.\end{cases} \tag{1.91}$$

Fig. 1.12 shows a comparison between analytical estimation and fitted decay exponent of the one-body (γ) and two body (δ) correlators as function of α. These results are in perfect agreement with the numerical simulation of Eq. 1.80.

It has to be stressed that for $\alpha < 1$, even though the correlation functions have still two contributions, one can show that the exponential part tends to zero and we effectively notice that this one is unobservable.

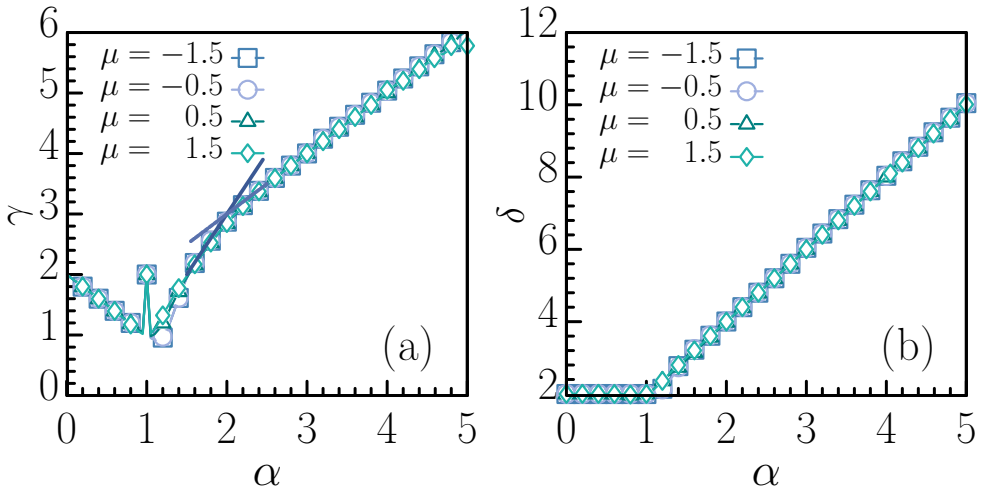

Figure 1.12: Exponents (a) γ and (b) δ of the algebraic decay of the one-body and two-body correlation functions vs. α, obtained by fitting with power-law functions, namely, $g_1(R) \sim R^{-\gamma}$ and $g_2(R) \sim R^{-\delta}$. The equations of the two straight lines in (a) are $2\alpha - 1$ and $\alpha + 1$.

1.B.2 LRI model

For completeness, we also compute the correlation functions of the long-range Ising model in a transverse field without disorder. Specifically, we focus on the correlation on the type

$$S_\nu(j,\ell) = \left[\langle \sigma_j^\nu \sigma_{j+\ell}^\nu \rangle - \langle \sigma_j^\nu \rangle \langle \sigma_{j+\ell}^\nu \rangle\right]_W , \quad (\nu = x, z). \tag{1.92}$$

with $\nu = x, z$. An example is shown in Fig. 1.13(a) for $S_x(R) \equiv S_x(R, 0)$. The exponent γ_x [shown in Fig. 1.13(b)] of the long-distance decay displays three difference behaviours:
(i) for $\alpha > 2$ it fulfils $\gamma_x = \alpha$;
(ii) for $1 < \alpha < 2$ a hybrid decay is observed and the algebraic tail decays with an exponent γ that depends linearly on α with a slope consistent with ~ 0.55;
(iii) for $\alpha \lesssim 1$, $\gamma_x \sim 0.25\alpha$. The correlator $S_z(R)$ is shown in Fig. 1.13(c) and it also displays an algebraic tails that decays as $1/R^{\gamma_z}$ where $\gamma_z \sim 2\alpha$ for $\alpha > 1$.

1.C Entropy from correlation function

In this Appendix, we give some details on the technique for computing the entanglement spectrum and the von Neumann entropy for a fermionic quadratic Hamiltonian. We follow closely Ref. [218–222].

Consider a fermionic quadratic Hamiltonian,

$$H = \sum c_i^\dagger t_{ij} c_j + \left(c_i^\dagger U_{ij} c_j^\dagger + \text{h.c.} \right) \tag{1.93}$$

one expects that the density matrix of the ground state has the same functional form:

$$\rho = \frac{\mathrm{e}^{-\mathcal{H}}}{Z} \tag{1.94}$$

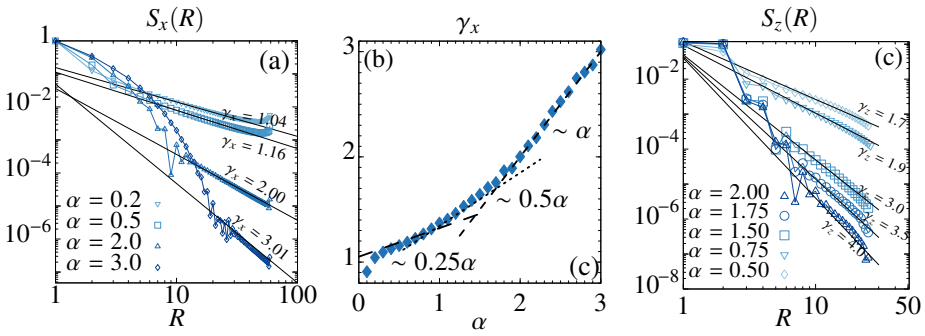

Figure 1.13: (a) $S_x(R)$ correlation for the long-range Ising model (Eq. (5) of the main text) for $B_{ij} = W_{ij} = 0$ ($\theta = 0.2\pi$ and $L = 60$), showing the hybrid exponential and power-law behavior for $\alpha \gtrsim 1$ and a purely power-law for $\alpha \lesssim 1$. (b) Decaying exponent γ_x of the algebraic tail of $S_x(R)$ fitted as $1/R^{\gamma_x}$. Three different behaviours for γ_x, corresponding to the three dashed black lines are observed. (c) $S_z(R)$ correlation for the long-range Ising model (Eq. (5) of the main text) for $B_{ij} = W_j = 0$ and $\theta = 0.207\pi$, $L = 100$ and different α.

with

$$\mathcal{H} = \sum c_i^\dagger A_{ij} c_j + \left(c_i^\dagger B_{ij} c_j^\dagger + \text{h.c.} \right) \tag{1.95}$$

to reproduce the expectation value in the ground state.

This means that all the information about the density matrix is encoded in the correlator matrices

$$C_{ij} = \langle c_i^\dagger c_j \rangle \qquad F_{ij} = \langle c_i^\dagger c_j^\dagger \rangle \,. \tag{1.96}$$

They are easily computed from the ground state of the Hamiltonian (1.93), as the latter is readily diagonalized with a Bogoliubov transformation.

Then, one can relate the correlation matrices with the eigenvalues of the "Hamiltonian" (1.95) and so with the density matrix ρ.

To compute those matrices, we first diagonalize (1.95) with a Bogoliubov transformation:

$$\begin{pmatrix} \eta \\ \eta^\dagger \end{pmatrix} = \begin{pmatrix} g & h \\ h & g \end{pmatrix} \begin{pmatrix} c \\ c^\dagger \end{pmatrix} \tag{1.97}$$

where g and h are $N \times N$ real matrices, satisfying, because of the anticommutation relations:

$$g g^T + h h^T = \mathbb{1} \tag{1.98}$$

$$g h^T + h g^T = \mathbb{0} \tag{1.99}$$

g^T means the transpose of the matrix g.

The "Hamiltonian" $\mathcal{H}$ takes the form

$$\mathcal{H} = \sum \varepsilon_k \eta_k^\dagger \eta_k \tag{1.100}$$

and the density matrix $\rho = \otimes \rho_k$, with :

$$\rho_k = \frac{\mathrm{e}^{-\varepsilon_k \eta_k^\dagger \eta_k}}{1 + \mathrm{e}^{-\varepsilon_k}} = \begin{pmatrix} (1 + \mathrm{e}^{\varepsilon_k})^{-1} & 0 \\ 0 & (1 + \mathrm{e}^{-\varepsilon_k})^{-1} \end{pmatrix} \tag{1.101}$$

as the particles are independent.

Now to compute the correlation matrices, we have to invert the Bogoliubov transformation:

$$\begin{pmatrix} c \\ c^\dagger \end{pmatrix} = \begin{pmatrix} g^T & h^T \\ h^T & g^T \end{pmatrix} \begin{pmatrix} \eta \\ \eta^\dagger \end{pmatrix} \tag{1.102}$$

and we have to note that

$$\langle \eta_k^\dagger \eta_{k'} \rangle = \mathrm{Tr}\left[\rho\, \eta_k^\dagger \eta_{k'}\right] = \frac{\mathrm{e}^{-\varepsilon_k}}{1+\mathrm{e}^{\varepsilon_k}} \delta_{kk'} \tag{1.103}$$

We define C the matrix $\langle c_i^\dagger c_j \rangle$ and F the matrix $\langle c_i^\dagger c_j^\dagger \rangle$, so we have

$$C = g^T \Lambda g + h^T \bar{\Lambda} h \tag{1.104}$$

$$F = g^T \Lambda h + h^T \bar{\Lambda} h \tag{1.105}$$

where $\Lambda, \bar{\Lambda}$ are diagonal matrices with elements

$$\Lambda_{ij} = \frac{\delta_{ij}}{1+\mathrm{e}^{\varepsilon_i}} \qquad \bar{\Lambda}_{ij} = \frac{\delta_{ij}}{1+\mathrm{e}^{-\varepsilon_i}} \tag{1.106}$$

Note that $\Lambda + \bar{\Lambda} = \mathbb{1}$. Let us define $\Delta = \Lambda - \bar{\Lambda}$, so, by using (1.98) we can write the correlators as

$$C = \frac{\mathbb{1}}{2} + \frac{1}{2}\left(g^T \Delta g - h^T \Delta h\right) \tag{1.107}$$

$$F = \frac{1}{2}\left(g^T \Delta h - h^T \Delta g\right) \tag{1.108}$$

Now, from the anticommutation relations (1.98), one has (note that $\Delta_{ij} = -\tanh(\varepsilon_i/2)\,\delta_{ij}$)

$$W \equiv \left(C - \frac{\mathbb{1}}{2} + F\right)\left(C - \frac{\mathbb{1}}{2} - F\right) = \frac{1}{4}(g-h)^T \Delta^2 (g-h) \tag{1.109}$$

By defining a matrix $\psi = g - h$ one has $\psi^T \psi = \mathbb{1}$ so ψ is orthogonal and, from the previous equation one has

$$W = \frac{1}{4}\psi^T \Delta^2 \psi \tag{1.110}$$

that is the eigenvalues of W are $\zeta_i = \frac{1}{4}\tanh^2(\frac{\varepsilon_i}{2})$. From these one gets the eigenvalues of $\mathcal{H}$:

$$\varepsilon_i = 2\,\mathrm{arctanh}\left(2\sqrt{\zeta_i}\right) \tag{1.111}$$

Entropies

Von Neumann entropy

From the entanglement spectrum and the density matrix (1.101), the von Neumann entropy is defined as

$$\mathrm{S_{vN}} = -\mathrm{Tr}\rho \log_2 \rho = -\sum_{\mathrm{m}=1}^{\ell} \mathrm{Tr}\rho_{\mathrm{m}} \log_2 \rho_{\mathrm{m}} \tag{1.112}$$

with

$$\rho_m \log_2 \rho_m = \begin{pmatrix} \frac{1}{1+\mathrm{e}^{\varepsilon_m}} \ln \frac{1}{1+\mathrm{e}^{\varepsilon_m}} & 0 \\ 0 & \frac{1}{1+\mathrm{e}^{-\varepsilon_m}} \ln \frac{1}{1+\mathrm{e}^{-\varepsilon_m}} \end{pmatrix} \tag{1.113}$$

and the entropy take the form

$$S_m^{\mathrm{vNe}} = -\sum_{m=1}^{\ell} \left[\frac{\ln(1+\mathrm{e}^{\varepsilon_m})}{1+\mathrm{e}^{\varepsilon_m}} + \frac{\ln(1+\mathrm{e}^{-\varepsilon_m})}{1+\mathrm{e}^{-\varepsilon_m}} \right] \tag{1.114}$$

Rényi entropy

The Rényi entropy of order α reads as follows

$$S_{m,\alpha}^{\mathrm{Re}} = \frac{1}{1-\alpha} \ln \mathrm{Tr}\, \rho_m^{\alpha}$$

$$with \rho_m^{\alpha} = \begin{pmatrix} (1+\mathrm{e}^{\varepsilon_m})^{-\alpha} & 0 \\ 0 & (1+\mathrm{e}^{-\varepsilon_m})^{-\alpha} \end{pmatrix} \tag{1.115}$$

and becomes

$$S_{m,\alpha}^{\mathrm{Re}} = \frac{1}{1-\alpha} \ln \left[(1+\mathrm{e}^{\varepsilon_m})^{-\alpha} + (1+\mathrm{e}^{-\varepsilon_m})^{-\alpha} \right] \tag{1.116}$$

Entropy of excited states

In the previous section we have only considered entropy for the ground state. Let us consider excited state $|E\rangle$ which is defined by assigning a set of occupied modes $\mathcal{K} = |n_1, n_2, \ldots, n_L\rangle$ with $n_j = 0, 1$ and then creating single quasi-particles $\eta_n^{\dagger}$ on the ground state $|\Omega\rangle$ of Hamiltonian (1.93)

$$|E\rangle = \prod_{n \in \mathcal{K}} \eta_n^{\dagger} |\Omega\rangle \tag{1.117}$$

For computing the entanglement entropy for this state one needs the correlation functions evaluated on the state $|E\rangle$ by means of the Bogoliubov transformation:

$$\langle E|c_i^{\dagger} c_j|E\rangle = \sum_{\substack{n \in \mathcal{K} \\ n=1}} g_{in} g_{nj} + \sum_{\substack{n \in \mathcal{K} \\ n=0}} h_{in} h_{nj} \tag{1.118}$$

Chapter 2

One-dimensional extended Hubbard model with soft-core potential

Laughter and tears are both responses to frustration and exhaustion. I myself prefer to laugh, since there is less cleaning do to do afterward.

Kurt Vonnegut

In general, one-dimensional interacting models fall into the universal class of the Tomonaga-Luttinger Liquids (TLL) [223]. There the low energy behavior of interacting fermionic, bosonic, and spin models can be mapped onto free bosonic ones [50, 223–227]. One remarkable example of 1d phenomenon that can be inferred from the TLL theory is the so-called spin-charge separation [228–233], i.e., uncoupled collectives modes of spins and charges excitations. The decoupled nature of these modes notably implies that the spin and charge degrees of freedom can propagate independently along the chain [223, 234]. Such a picture allows us to understand the low-energy behavior of the majority of fermionic quantum models in one-dimension. However, this framework is mainly verified for short-range systems such as the Hubbard model and its extension. Understanding the robustness of the TLL paradigm over various type of potential remains a crucial question. In particular, models with finite-range interactions were shown to provide a pathway to the realization of novel quantum phases beyond the TLL description [10, 235, 236]. That emergent phase arises from a combination of the commensurability and frustration effect that concurs to stabilize a new liquid phase, where the fundamental elements of the liquid are not single-particles but rather clusters of particles.

The present chapter is intended to study an extended version of the Hubbard model on a chain, where fermions with spin can tunnel between neighboring sites with tunneling amplitude t and interact via both an on-site U-potential and an off-site repulsion of strength V, which is finite within a spatial range of length r_c. The case for $r_c = 1$ has been the subject of intense investigations and is known has the extended Hubbard model [237]. The most interesting features of this model generally arise at commensurate filling (e.g. half filling or quarter filling) and where lattice effects play a role. A little attention has been devoted to small lattice filling, since the presence of empty sites seems to lead irremediably to a standard metallic phase. However, when the range of the interaction is extended to few inter-particles distance ($r_c > 1$), frustration effect can appear and the situation is then drastically different. Such effects lie at the heart of this chapter.

We start by introducing the model in Sec. 2.1, and emphasize its relevance in Rydberg-dressed cold gases in Sec. 2.1.1. We then focus on the classical limit ($t = 0$) of our model

in Sec. 2.1.2, which provides physical insights on the frustration mechanisms at play and allows to predict some of the phases in our system. In Sec. 2.1.3, we introduce the observables, such as the static structure factor, the low-energy degrees of freedom and the entanglement entropy, which are used to describe the ground state of the quantum model. In Sect. 2.2, we analyse in details the different phases in the whole-range of parameter U, V, by computing numerically the different observables introduced in the previous section, leading to the complete phase diagram of the model. In particular, we demonstrate that the ground state corresponds to a standard TLL phase for low values of U and V, while it consists of new types of liquids made of clusters of particles for large U and large V, in agreement with the classical prediction (Secs. 2.2.1 and 2.2.2). We investigate in details the transition between the different phases for an intermediate value of U in Sec. 2.2.3, and show in Sec. 2.2.4 that for very low U and intermediate V, the system tends to form a liquid phase that features more doubly occupied sites than the standard TLL phase and is not captured by the classical approximation. Details on the numerical analysis are provided in Appendix 2.A.

2.1 The model

In this work, we consider an extended Hubbard chain with on-site and finite-range soft-shoulder repulsion, described by the Hamiltonian

$$\mathcal{H} = -t \sum_{i,\sigma} (c^\dagger_{i,\sigma} c_{i+1,\sigma} + \text{h.c}) + U \sum_i n_{i\uparrow} n_{i\downarrow} + V \sum_i \sum_{\ell=1}^{r_c} n_i n_{i+\ell}, \tag{2.1}$$

where $c^\dagger_{i\sigma}$, $c_{i\sigma}$ are creation/annihilation operators of fermionic particles with spin $\sigma =\uparrow,\downarrow$ on the site i and $n_i = n_{i,\uparrow} + n_{i,\downarrow}$. The coefficient t represents the tunneling matrix element (and will be taken to be unitary in the following), while U gives the strength of the on-site interaction between two fermions on the same site (and opposite spin) and V that of the soft-core density-density interaction. This density-density interaction yields a contribution V only if two occupied sites lie within a distance r_c of each other, and zero otherwise. Here, we assume only purely repulsion interactions with $U, V > 0$ and impose antiperiodic boundary condition.

2.1.1 Soft-core potential in Rydberg-dressed atoms

The Hamiltonian Eq. (2.1) mimics the soft-core interaction achieved experimentally in Rydberg-dressed cold gases [99].

Rydberg atoms [238, 239] are highly excited atoms with one or two valence electrons in orbit with a large principal quantum number $n \gg 1$. Due to these large electronic orbitals, the effect of the nucleus and ionic core electrons are well approximated by an elementary positive point charge. Hence, they display properties close to the hydrogen atoms. Moreover, the typical size of the electronic wave function scales with $n \sim n^2$, giving rise to numerous outstanding properties, e.g. a large atomic size (of the order of 10^{-6} m for $n \sim 100$), a long lifetime, scaling as n^3, and a significant dipole moment

$\mu \sim n^2$. These latter give to the Rydberg atoms an extreme sensitivity to external field and make them polyvalent to generate a wide variety of potential between atoms. For instance, an external electric field can induce permanent electric dipole moments in the excited states, leading to a strong dipole-dipole interaction scaling $\sim r^{-3}$. On the contrary, when no external field is applied, the Rydberg-Rydberg interactions are given by Van-der-Waals (VdW) forces, scaling as C_6/r^6, where $C_6 \sim n^{11}$. Because of the strong $C_6 \sim n^{11}$ scaling of the VdW coefficient, such Rydberg-Rydberg atom interactions are orders of magnitude larger than those of ground state atoms.

In the next, we will only consider a repulsive interaction (attractive interaction can also be engineered by choosing different Rydberg states) and as a further assumption, we describe the Rydberg atoms as a two-level system, with a ground state $|g\rangle$ coupled to an excited state $|e\rangle$ with a resonant Rabi laser frequency Ω and detuning Δ.

An essential consequence of the strong interactions between Rydberg atoms is the *Rydberg excitation blockade* phenomenon, which inhibits double excitation within a specific range. Roughly speaking, in a case of two atoms, the ground state $|gg\rangle$ can be resonantly coupled to a state containing a single excitation, e.g. $|eg\rangle$ or $|ge\rangle$. However, the doubly-excited $|ee\rangle$ is shifted out of resonant by the strong VdW interactions between the two atoms. This mechanism prevents a simultaneous excitation for small enough distance between the atoms.

The Rydberg blockade can notably be used to generate Rydberg-dressed states [107, 240–244], i.e. superposition of ground state and excited states. In particular, in the weak-dressed regime, $\Omega << \Delta$ and with red detuning ($\Delta < 0$), the effective resulting interaction as function of the distance r can be obtained via perturbative expansion in Ω/Δ [100, 241] and is given by:

$$V_{\mathrm{dd}}(r) = \frac{\Omega^4}{8\Delta^3} \frac{1}{1 + (\frac{r}{r_c})^6}, \tag{2.2}$$

where $r_c = (C_6/2|\Delta|)^{1/6}$ and r the interatomic distance. Experimental realisations of this interaction between spins have been reported in Refs. [145, 150]. At large distance $r \gg r_c$, the potential $V_{\mathrm{dd}}(r)$ turn into the usual VdW interaction, reduce by the factor $\frac{\Omega^4}{8\Delta^3}$ to excite both atom at the same time. However, for $r < r_c$, due to the blockade, double excitation is forbidden and $V_{\mathrm{dd}}(r)$ saturates to a constant value for $r \to 0$. Fig. 2.1 shows the Rydberg potential (blue) and the approximate box potential used in Eq. (2.1) (red).

2.1.2 Classical analysis

Before going into the detailed analysis of the quantum phase diagram of Eq. (2.1), it is convenient to first consider the exact solution of the ground state in the classical limit ($t = 0$). In this regime, the main physics can be inferred by looking at the competition between the soft-shoulder potential, the on-site interaction and the two relevant length scales, namely the cut-off radius r_c and the mean spacing between particles $r^* = 1/\rho$, where $\rho = N/L$ is the particle density (N and L are the total number of particles and the size of the chain, respectively).

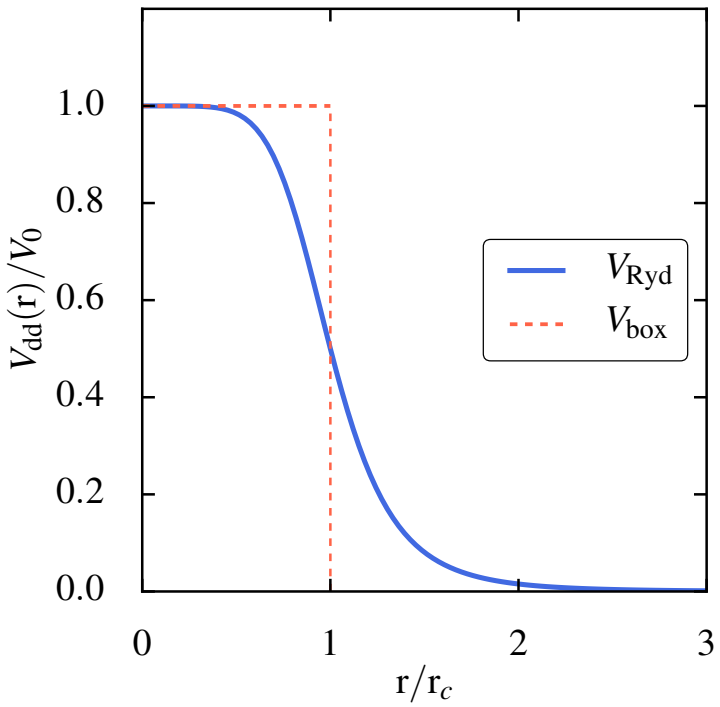

Figure 2.1: The blue line is the Rydberg potential as function of the interatomic distance in the weak-dressed regime $\Omega << \Delta$ and with red detuning ($\Delta < 0$). The red dotted line is the approximate box potential used in Eq. (2.1).

Let us first consider the regime $U \gg V$ which prevents double occupancy. In this case, the model becomes substantially the same as a spinless fermionic model. It was shown in Ref. [10] that the latter exhibits a rich phase diagram with three different phases:
(i) for $r^* > r_c$, the particle density is small and the ground state corresponds to a liquid type phase.
(ii) for $r^* = r_c$, particles are equally space every $r_c + 1$ lattice site, corresponding to a crystalline order.
(iii) The most interesting situation occurs for $r^* < r_c$, the competition between r^* and r_c leads to frustration and particles have tendency to self-assemble into clusters (blocks). These effects result in the formation of a highly degenerate ground state because these different types of clusters can be assembled in many different ways, thus leading to a liquid of clusters.

In order to describe the classical ground state of (iii) in a one-dimensional system, we extend the *cluster exchange model* introduced in [10]. The key idea is to identify the cluster of particles and holes in the configuration with lowest energy. First, the block with zero energy consists of one particle followed by a number of r_c of empty sites. We denote this cluster as A [see Fig. 2.2].

Secondly, we want to identify the blocks with the smallest finite energy. To do so, we have to take the competition between the on-site (U) and soft-core (V) potentials into account. When $U \gg V$, a cluster made by two nearest-neighbors followed by r_c empty sites is energetically favoured, with an energy V. The latter is denoted as cluster B [see

Fig. 2.2]. When $U \ll V$, the cluster made of a doubly occupied site followed by r_c empty sites is favoured with an energy U. We refer to this cluster as B' [see Fig. 2.2]. Other blocks with higher energy are discarded. Since exchanging two of these blocks let the energy unchanged, the classical ground state thus consist of all permutations of blocks A and B or A and B' (e.g. [ABAB],[AABB], or [AB'AB'],[AB'B'A]...). Introducing the total number of blocks M for a system of length L as

$$M = L(1-\rho)/\mathrm{r_c}, \tag{2.3}$$

the ground state degeneracy grows exponentially with M (see below). Furthermore, the blocks themselves are degenerate due to the presence of the additional spin degree of freedom. This is responsible for an increase of the ground state degeneracy compared to the spinless case [see Fig. 2.2].

In this work, we focus on the case $r_c = 2$ and choose a particle density $\langle n_\uparrow \rangle = \langle n_\downarrow \rangle = 1/5$. A convenient graphical representation illustrating the classical ground state configurations for $\mathrm{r_c} = 2$ is presented in Fig. 2.3. This specific density corresponds to a ratio of n_A block A and n_B block B or $n_{\mathrm{B}'}$ block B' equal to $n_\mathrm{B}/n_\mathrm{A} = n_{\mathrm{B}'}/n_\mathrm{A} = 1/2$. As already mentioned the presence of the on-site interaction will slightly modify the classical picture. In particular, a transition can occur between a liquid made of clusters AB and a liquid made of clusters AB'. To gain physical insight, we define the energetical gain to transform all $\mathrm{B} \to \mathrm{B}'$ by $\Delta_{\mathrm{B}\to\mathrm{B}'} = n_\mathrm{B}V - n_{\mathrm{B}'}U$. When $\Delta_{\mathrm{B}\to\mathrm{B}'} < 0$ (> 0) , B'(B)-clusters are favoured. One can note that the size of cluster B' $(r_c + 1)$ is one site smaller than cluster B $(r_c + 2)$. Thus, changing 3 cluster B to 3 cluster B' gives 3 vacant spaces, which corresponds precisely to the size of cluster A with zero energy. As a consequence, the 3 B cluster effectively transform into 2 cluster B' and 1 cluster A, lowering the energy by $\Delta_{\mathrm{B}\to\mathrm{B}'} = 3V - 2U$ and changing the ratio $n_{\mathrm{B}'}/n_\mathrm{A} = 1/4$. The transition is therefore found at $V = \frac{2}{3}U$. In the same manner one can find a generalization for arbitrary r_c with the transition given by $V = \frac{r_c}{r_c+1}U$. From this argument, two situations can arise:

(i) $V < \frac{2}{3}U$, the cluster type B is favored with respect to the B'. The classical blocks configuration can be ordered in many different ways leading to an exponential degeneracy of the ground state $d = M!/[(M/3)!(2M/3)!]$, without considering the spin degeneracy. Fig. 2.3, panel (a), presents the corresponding cluster exchange.

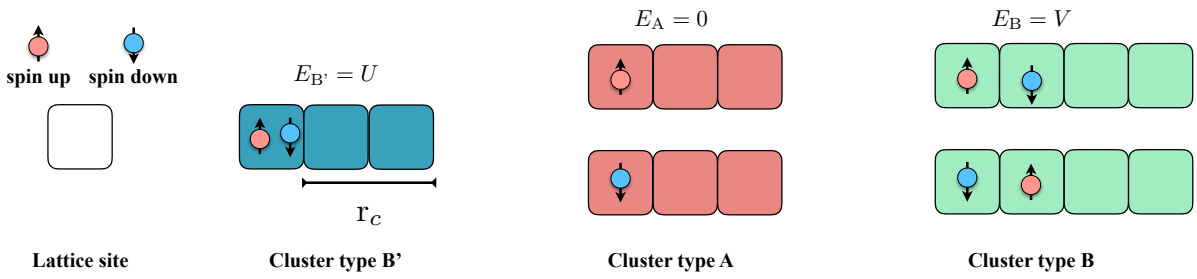

Figure 2.2: Graphical representation of the different possible blocks structure for the case $\mathrm{r}_c = 2$.

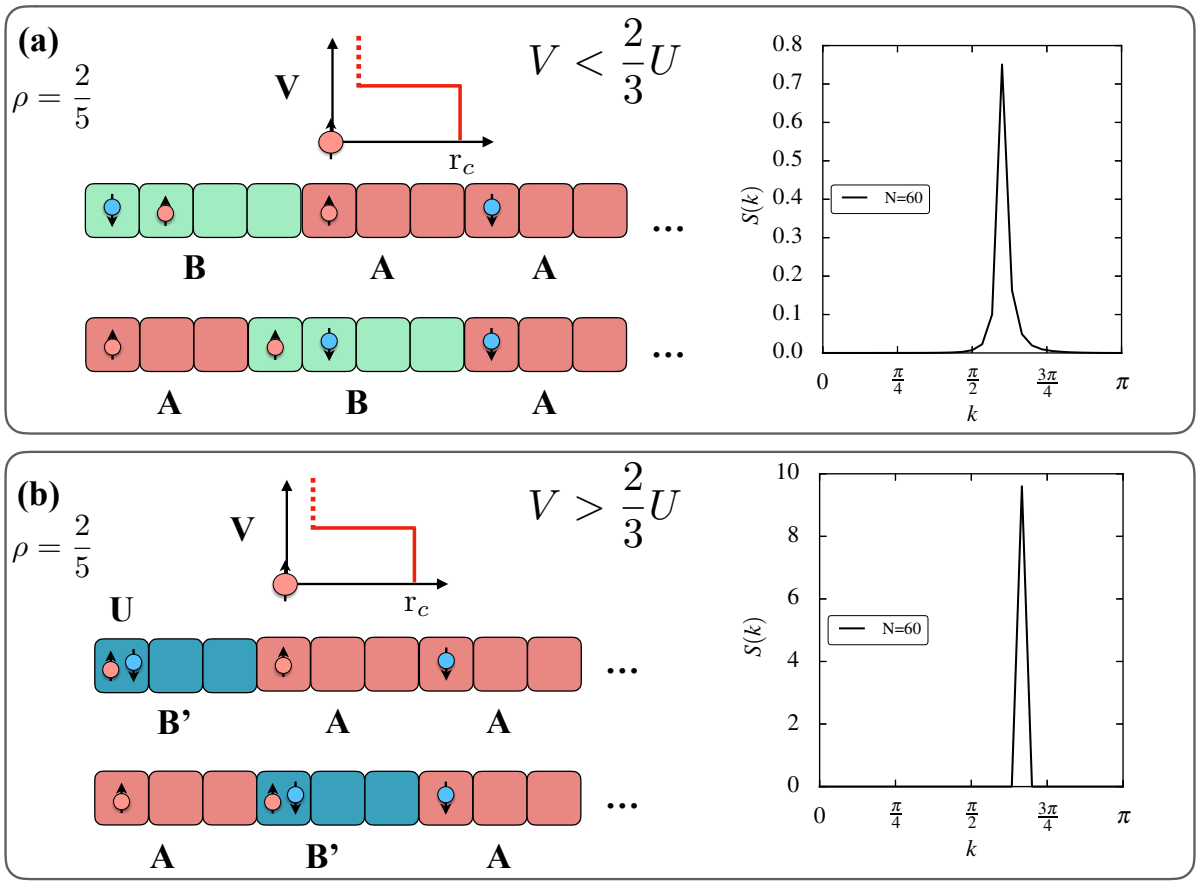

Figure 2.3: Graphical representation of a classical ground state configuration for the CLL_{nn} phase in panel (a) and the CLL_{d} phase in panel (b). As an example, we show in each panel, the corresponding peak in the structure factor.

(ii) $V > \frac{2}{3}U$, B'-clusters of double occupied sites are now favoured, with the same exponentially degenerate ground state. This case is presented in Fig. 2.3 panel(b).

For the rest of this chapter, we will denote (i) $\mathrm{CLL}_{\mathrm{nn}}$ the phase with nearest-neighbor (B) cluster whereas (ii) the phase with doubly occupied sites will be refer to $\mathrm{CLL}_{\mathrm{d}}$. Clearly commensurability between the size of the clusters and the total size of the system is important. In the following analytical and numerical calculations we always assume that L contains an integer number of clusters, namely $L = 20, 30, 40, 50, 60$.

2.1.3 Observables

Before investigating the influence of quantum fluctuation ($t = 1$) on the phase diagram in Sec. 2.2, we first introduce the different observables targeting both the spin and the charge sectors such as the structure factor, the low-energy degrees of freedom, and the entanglement entropy. In particular, we provide a classical interpretation of these observables when possible.

Structure factor

Two-points correlations between particles or spins are known to give valuable information about the order and dynamics in condensed matter systems. The Fourier transform of the correlations in real space, namely the structure factor, reveals the relevant length scales, e.g., the periodicity along one and/or several axis arising from spontaneous symmetry breaking. In particular, a peak in the structure factor at a specific momentum indicates a precise spatial period.The charge and the spin structure functions are given by:

$$S_\nu(k) = \frac{1}{L}\sum_{\ell,j} e^{ik(l-j)} g_{2,\nu}(\ell - j)$$

with $g_{2,\nu}(\ell - j)$ the connected correlation function in the charge or spin sector ($\nu = c, s$), which reads:

$$\begin{aligned} g_{2,c}(\ell - j) &= \langle n_\ell n_j\rangle - \langle n_\ell\rangle\langle n_j\rangle \\ g_{2,s}(\ell - j) &= \langle S^z_\ell S^z_j\rangle - \langle S^z_\ell\rangle\langle S^z_j\rangle \end{aligned} \tag{2.4}$$

We expect that the formation of the clusters phases should be well captured by the charge structure factor. Indeed, the charge modulation in the classical phase already provides an estimate of the momentum peak's position of the charge structure factor. Within our classical approximation, we see in Fig. 2.3 that $S_c(k)$ exhibits a peak located at $k_{nn} = 2\pi M/L = 3\pi/5$ for the $\mathrm{CLL_{nn}}$ [Fig. 2.3 (a)] and a peak at $k_d = 2\pi/3$ for the $\mathrm{CLL_d}$ [Fig. 2.3 (b)] .

Low-energy degrees of freedom

The behaviour of the low-energy excitations is well captured by the charge and spin gaps defined as:

$$\begin{aligned} \Delta_c &= E^{(\uparrow=\downarrow)}_{N+2}(L) + E^{(\uparrow=\downarrow)}_{N-2}(L) - 2E^{(\uparrow=\downarrow)}_{N}(L) \\ \Delta_s &= E^{(\uparrow=\downarrow+2)}_{N}(L) - E^{(\uparrow=\downarrow)}_{N}(L) \end{aligned} \tag{2.5}$$

where $E^{(\uparrow=\downarrow)}_N(L)$ is the ground state energy in the case of $N_\uparrow = N_\downarrow = L\rho$, $E^{(\uparrow=\downarrow)}_{N\pm2}(L)$ is the energy of the state obtained by adding/removing two particles with opposite spin and $E^{(\uparrow=\downarrow\pm2)}_N(L)$ is the energy of the state obtained by flipping the spin of one particle. Also, we consider the single particle gap:

$$\Delta_{sp} = E^{(\uparrow=\downarrow\pm1)}_{N+1}(L) + E^{(\uparrow=\downarrow\pm1)}_{N-1}(L) - 2E^{(\uparrow=\downarrow)}_{N}(L) \tag{2.6}$$

where $E^{(\uparrow=\downarrow\pm1)}_N(L)$ is the energy of the state obtained by adding/removing one particle.

In the usual LL, all these gaps are expected to vanish. However, this is different in the cluster phase. In the following, we first compute these gaps in the classical limit ($t = 0$) from the solution introduced in Sec. 2.1.2. For clarity, a graphical representation for the single-particle and spin gap is presented in Fig. 2.4 (a) and (b).

(i) In the $\mathrm{CLL_{nn}}$ phase, we consider a system size $L = 10\ell$ commensurate with the cluster formation, $n_A = 2\ell$ and $n_B = \ell$ (see Sec), where ℓ labels the number of building blocks. The classical energy of the system reads

$$E_N^{(\uparrow=\downarrow)}(L) = n_B V = \ell V. \tag{2.7}$$

(a) Single particle gap. Now, upon adding/removing one particle we obtain,

$$E_{N+1}^{(\uparrow=\downarrow\pm1)}(L) = \ell V + 2V \qquad E_{N-1}^{(\uparrow=\downarrow\pm1)}(L) = (\ell-1)V \tag{2.8}$$

as the states cannot rearange properly due to the frustration. Thus, the single particle gap is given by

$$\Delta_{sp} = \ell V + 2V + (\ell-1)V - 2\ell V = V, \tag{2.9}$$

which implies that the single particle gap is always open within the CLL_{nn} [see Fig. 2.4 (a)].

(b) Spin gap. We see that upon a spin flip, classical energy remains unchanged. Consequently the spin gap is always closed in this phase [see Fig. 2.4 (a)].

(c) charge (cluster) gap. Here, the situation is remarkably different, since extracting/adding two particles allows the system to rearrange properly his configuration. For instance, if we consider a ground state of the form BAABAABAABAA, extracting two particles changes 3 clusters B to 4 clusters A creating the new configuration AAAAAAAAABAA, and lowering the energy by an amount $3V$. Instead, the opposite process, i.e. doping with two particles, changes 4 clusters A to 3 clusters B, thus increasing the energy by $3V$:

$$E_{N+2}^{(\uparrow=\downarrow)}(L) = \ell V + 3V \qquad E_{N-2}^{(\uparrow=\downarrow)}(L) = V - 3V. \tag{2.10}$$

The contributions associated to the insertion and extraction of a single cluster gap therefore cancel out.

(ii) In the $\mathrm{CLL_d}$ phase, we consider a system size $L = 3 \times 10\ell$ commensurate with the cluster formation, again we have $n_A = 2\ell$ and $n_B = \ell$, where ℓ labels the number of building blocks, which yields to a classical energy:

$$E_N^{(\uparrow=\downarrow)}(L) = n_{\mathrm{B}'} U = 2\ell U. \tag{2.11}$$

(a) Single particle gap. Unlike the $\mathrm{CLL_{nn}}$ phase, in this case, adding/removing a particle cost exactly the same energy to the system, U. Because, we choose $\langle n_\uparrow \rangle = \langle n_\downarrow \rangle$, this effect is independent of the spin considered, and thus the single particle gap vanishes [see Fig. 2.4 (b)].

(b) Spin gap. Due to the double occupancy, at first glance we expect spin effect to be relevant. Nevertheless, since the number of cluster A is twice the number of clusters B', the system can be (at least classically) rearranged to have both spin flip contribution exactly cancelling out. The spin gap is also zero in that phase [see Fig. 2.4 (b)].

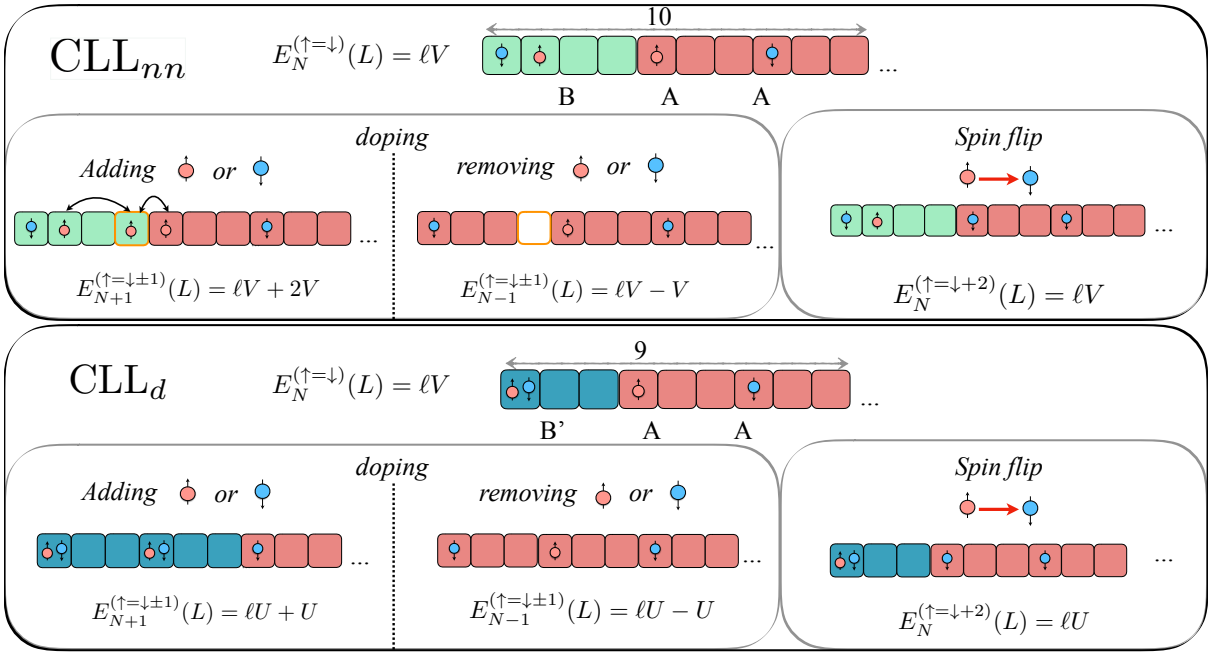

Figure 2.4: Graphical representation of the one-particle doping and spin-flip processes in the two clusters phases, CLL$_{nn}$ in (a) and CLL$_d$ in (b).

(c) Charge (cluster) gap. In the same manner as the single particle gap, both contribution will exactly cancel, leading to a vanishing cluster gap.

This investigation indicates that there must be a transition between the CLL$_{nn}$ phase and the TLL where the single-particle gap Δ_{sp} opens linearly with V, while the cluster gap and spin gap remain gapless. The second transition between the CLL$_{nn}$ and the CLL$_d$, predicted at $V = \frac{2}{3}U$ in Sec. 2.1.2, is characterized by the fact that single-particle gap closes while the other gaps remain unchanged. We will show in the next Sec. 2.2 that quantum fluctuations ($t \neq 0$) lead to qualitatively similar physical properties.

Gaps / Phases	Δ_{sp}	Δ_c	Δ_s
TLL	0	0	0
CLL$_{nn}$	V	0	0
CLL$_d$	0	0	0

Table 2.1: Summary table of the expected values of the gap inferred from the classical analysis.

Von Neumann entropy

Entanglement plays a fundamental role in the study of strongly correlated systems and is widely used to characterize their critical properties. In particular, a change in the ground state entanglement allows to understand and locate a quantum phase transition. The

most common way to measure entanglement between two parts of a system is provided by the Von Neumann entropy $S_L(\ell)$, which is also called entanglement entropy. If we consider a system of L sites that is divided into two subsystems A and B containing ℓ and $L-\ell$ sites, respectively, $S_L(\ell)$ is given by:

$$S_L(\ell) = -\mathrm{Tr}\rho_\ell \log \rho_\ell, \tag{2.12}$$

where ρ_ℓ is the reduced density matrix of the sub-interval ℓ with respect of the rest of the chain.

In the thermodynamic limit, we have generally two different behaviors:

1. For gapped phases $S_L(\ell)$ follows an area law, i.e. is proportional to the surface of the block ℓ which is thus constant in 1D.

2. In critical gapless phases, the entropy diverges logarithmically, $S_L(\ell) \sim \log(\ell)$. In particular, for a conformal invariant one-dimensional system with periodic boundary condition, the entropy satisfies the following universal scaling law [208]:

$$S_L(\ell) = \frac{c}{3} \ln \left[\frac{L}{\pi} \sin(\pi \ell / L) \right] + a_0 + \mathcal{O}(1/\ell^\alpha), \tag{2.13}$$

where L is the system size of the system, c the central charge of the theory, a_0 a non-universal constant and ℓ the block length. There is also additional correction of the form $1/\ell^\alpha$. From Eq. 2.13, we can extract the value of the central charge of the underlying conformal field theory, which roughly speaking is a measure of the degrees of freedom of the system, e.g., for a boson $c = 1$ and for a fermion $c = 1/2$. Since the low-energy degrees of freedom of both the TLL and the CLL phases [10] are described by a conformal field theory, we use Eq. 2.13 to obtain the entanglement properties of the ground state. Note that the TLL theory predicts a separation of the spin and charge degrees of freedom, which implies a central charge $c = 2$.

2.2 The phase diagram

We now study how the physical properties found in the previous section with our classical approximation are modified in the presence of the tunneling term $t \neq 0$. We use a Density Matrix Renormalization Group (DMRG) algorithm [15] to investigate the quantum phase diagram at zero temperature ($T = 0$) of the soft-shoulder Hubbard model (Eq. (2.1)) in the whole range of the parameters $U/t, V/t$ (where t is set to unity), for a potential range $r_c = 2$ and a fermionic density of $\rho = 2/5$[see Fig. 2.5]. In Sec. 2.2.1, we first characterize the nearest-neighbor cluster phase (CLL_{nn}) obtained in the large-U limit. In Sec. 2.2.2, we then study the doublon cluster phase (CLL_d) occuring for large V. In the next Sec. 2.2.3,, we consider the intermediate value of $U = 10$ and study the different phase transition (TLL $\rightarrow$ CLL_{nn} and $\mathrm{CLL}_{nn} \rightarrow \mathrm{CLL}_d$) occuring as V is increased. Finally, Sec. 2.2.4 is devoted to the study of the TLL_d phase, found for small U for all V. Due to the high degree of frustration inherent to the model, reaching a high precision in numerical simulations is very challenging. Details on the numerical analysis are provided in the appendix 1.4.

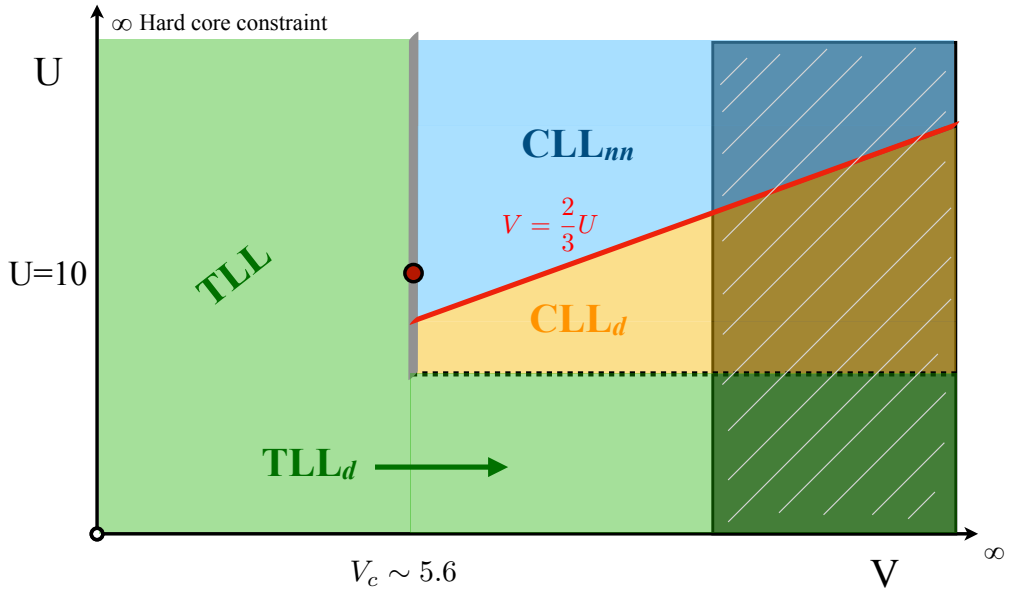

Figure 2.5: Sketch of phase diagram of the extended Hubbard model with soft-core potential. We choose a potential range $r_c = 2$ and a fermionic density of $\rho = 2/5$. The properties of the different phases will be discussed in the Sec. 2.2 . The shaded area indicates where the numerical results are particularly hard to extract.

2.2.1 The large U-limit and the nearest-neighbor cluster phase (CLL$_{nn}$)

Classically, we have shown in Sec. 2.1 that the CLL$_{nn}$ phase appears when the on-site interaction U is on a factor 3/2 larger than the soft-shoulder repulsion V. To observe this phase, we consider a regime with $U \gg V \gg t$, and we therefore expect the spin gap to be closed, as in the standard Hubbard model. Since, in this limit, double occupancy is strongly avoided, the charge sector of our models mimics essentially a spinless fermionic model with a density of particles given by $\rho = \langle n_\uparrow \rangle + \langle n_\downarrow \rangle$, i.e., the model considered in Ref. [235]. In order to see that the formation of the block structure introduced in Sec. 2.1 survives with quantum fluctuation, we look at the numerical calculation of the (static) charge structure function $S_c(k)$, which should develop a peak at $k_{nn} = 2\pi M/L$ where M is the total number of clusters. In this case, denoted CLL$_{nn}$ in Sec. 2.1, we have $M/L = 3/10$, so that $k_{nn} = (3/5)\pi$. In Fig.(2.6) panel (a), we show the behaviour of $S_c(k)$ for $U = 50$ and different values of V. The emergence of the peak is evident.

2.2.2 The large V-limit and the doublon cluster phase (CLL$_d$)

We now turn to the second phase predicted in the classical limit, which appears for $V \gg U \gg t$. Since the one-site interaction is finite it is necessary to take into consideration the fact that we have two species of fermions and that we might now have double occupied sites. Similarly to the previous case, we have to respect a certain density constraint implying that $n_A = 4n_{B'}$ and we can order clusters of type A and B' in many different ways, leading to a liquid cluster phase which contains doubled occupied states.

This phase was refer to the doublon cluster phase (CLL_d) in Sec.2.1. A pictorial representation of it is shown in the panel (b) of Fig. 2.3. One can check that now $M/L = 1/3$ (see Eq. (2.3)) for commensurate system size, we thus expect to see a peak in the charge structure function at $k_d = 2\pi M/L = (2/3)\pi$.
At the semiclassical level ($t = 0$), the discontinuity in the energy between the CLL_{nn} and the CLL_d phases suggests a first order transition at $3V = 2U$. Of course, strong renormalization on the localization of the critical point is expected due to the presence of the hopping term in the hamiltonian, nevertheless these phases should be qualitatively the same. This can be checked, by examining what happens for an intermediate values of V, say $V = 8$ and two different values of U, one large (say $U = 50$) corresponding to a CLL_{nn} phase and one intermediate (e.g. $U = 10$) corresponding to a CLL_d phase. Moreover, we choose a system size $L = 30$ which exactly commensurates with both clusters configuration. The predicted shift of the peak in the charge structure function is indeed numerically verified as shown in Fig.2.6, panel (b).

It is essential to notice that the position of the different peaks indicates a clear breakdown of the TLL theory. Indeed, bosonization predicts a peak in the charge structure factor independently of r_c at

$$k_c = 2\pi\rho \tag{2.14}$$

with ρ the total density. For a hard-core particle model [235], it has been established that this breakdown is rooted in the classical frustration inherent from this type of finite-range potential [see also Sec. 2.1.2]. Here, we have thus confirmed and extended this result to fermionic models, and we have demonstrated that the spin degree of freedom can lead to

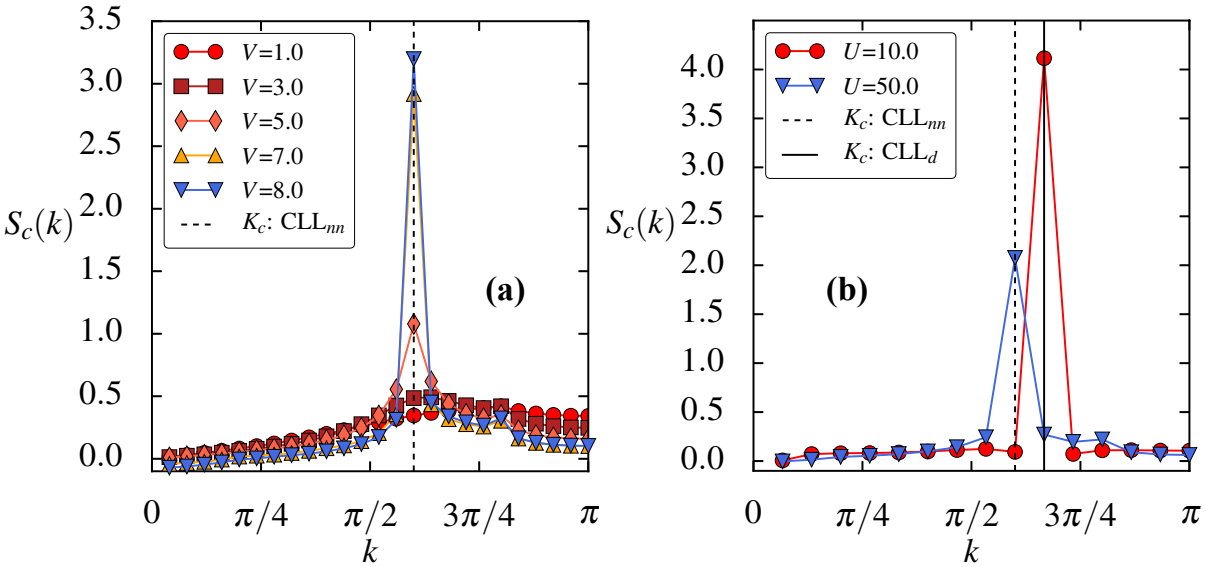

Figure 2.6: Panel (a): The charge structure function $S_c(k)$, evaluated for $U = 50$ and $V = 1, 3, 5, 8$. The numerical simulation is performed with $L = 50$, a size allowing for an exact number of clusters. Panel (b): The charge structure function $S_c(k)$, evaluated for $V = 8$ and $U = 10, 50$. The numerical simulation is performed with $L = 30$, a size allowing for an exact number of clusters for both the CLL_{nn} and the CLL_d phases.

a novel type of cluster phase. To go further in the analysis, we would like to see if the presence of the spin degree of freedom also influences the transition between a TLL and a CLL_{nn}.

2.2.3 The phases for intermediate values of U

In the two previous subsections, we have confirmed the existence of the different cluster phases inferred from the classical limit. Now, we would like to study in details the transition between the different aforementioned phases. In particular, we would like to see possible novels effects on the transition TLL $\rightarrow$ CLL_{nn} due to the presence of a spin. To do so, in this subsection, we fix the on-site interaction to the intermediate value $U = 10$ and study in details the characteristics of the different cluster phases encounter by varying V. As mentioned previously, we expect now to find three phases: the TLL, the CLL_{nn} and the CLL_d, in order of increasing values of V. In the first place, we distinguish TLL, the CLL_{nn} and the CLL_d phases by looking at the peak in charge structure factor. In Fig. 2.7 (a), we find that the position k_c of the maximum peak in $S_c(k)$ indicates the three phases. First, at small V, k_c is located at $4\pi/5$ in agreement with a TLL liquid, see Eq. (2.14). For an intermediate V, $k_c = 3\pi/5$, corresponds to the classical charge modulation of the CLL_{nn} (see Fig. 2.3). Finally at strong V, k_c is equal to $\pi/3$, which corresponds to the CLL_d phase (see Fig. 2.3). In general, a specific ordered phase is characterized by a finite non-zero value of $S_c(k_c)/L$ in the thermodynamical limit. In order to see that this is the case, we have examined the finite size scaling of the charge structure factor $S_c(k)/L$. This is shown for instance in Fig. 2.7 panel (b) for several values of V. Dotted lines are best fits of the form $a + b/L + c/L^2$, where we have arbitrary considered size correction up to the second order. From these data, it is evident that $S_c(k)/L$ is finite in the thermodynamic limit for $V \geq 5.5$, whereas it goes to zero for smaller values of the interaction. In Fig. 2.7 panel (c), we present the extrapolated infinite size $S_c(k_c)$ value as a function of the interaction strength V.

To better understand the nature of the cluster phases, we now focus on the spin structure function $S_s(k)$. By looking at Fig. 2.8 panel (a) and panel (b), we notice that, at small and intermediate V, the position k_c of the maximum peak of $S_s(k)$ is located at $k_0 = (2/5)\pi$ in correspondence with the one-particle density $n = 1/5$ and the TLL theory (see Eq. (2.14)). In addition, with increasing V we observe the gradual increase of $S_s(\pi)$ which becomes dominant for large V. From that we can clearly conclude that:
i) In the CLL_{nn} phase AF order is enhanced. This result can be easily understood if we consider strong-coupling corrections to the large U limit. Indeed, for infinite U when double occupancy is strictly avoided and the hopping term can be neglected, the different spin sectors are exactly degenerate. For large but finite U, the spin configuration that allows for the maximum energy gain due to hopping is indeed the one in which two spins that are separated only by empty sites are AF ordered. However, this effect does not correspond to a true long range order, as it can be inferred from the fact that the peak

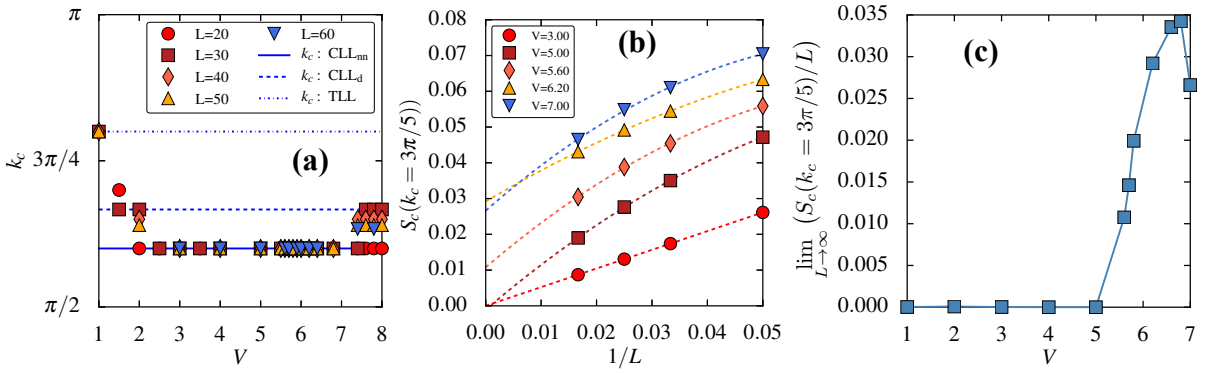

Figure 2.7: Panel (a) shows the position of the maximum momentum peak of $S_c(k)$ vs V. Lines are guides for eyes and correspond to the theoretical prediction of the momentum peak for the LL (dotted), CLL$_{\rm nn}$ (full) and CLL$_{\rm d}$ (dash-dotted). Panel (b): Finite size scaling of the density-density structure factor $S_c(k_c)$ for different values of V. The extrapolated values are shown in panel (c). All simulations are performed at $U = 10$.

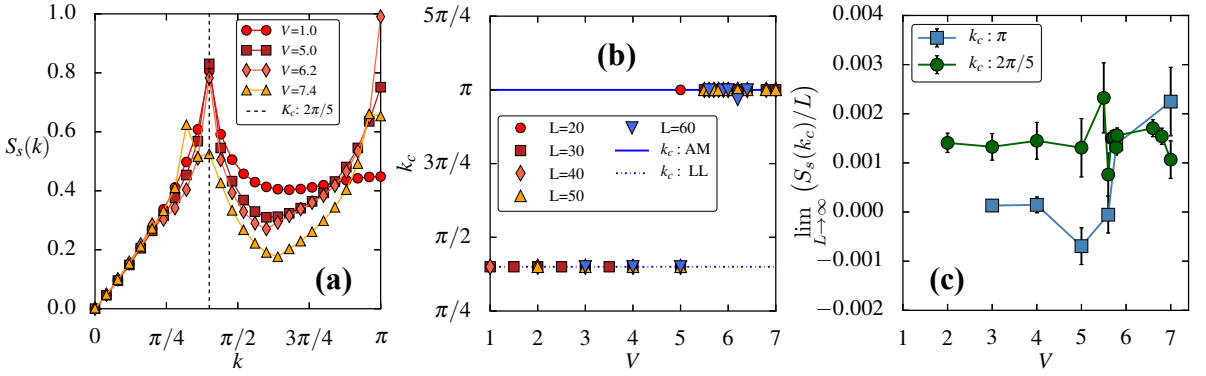

Figure 2.8: Panel (a): Spin-spin structure factor evaluated at $U = 10$ for different interaction strength V. Panel (b) shows the position of the maximum momentum peak of $S_s(k)$ vs V. Lines are guides for eyes and correspond to the theoretical prediction of the momentum peak for the LL (dotted), CLL$_{\rm nn}$ (full) and CLL$_{\rm d}$. Panel (c): The extrapolated values of $S_s(k)$ in the infinite-size limit are presented for $k_c = \pi$ and $k_c = 3\pi/5$.

at $k = \pi$ goes to zero (or a very small value) in the thermodynamic limit, e.g. see panel (c) of Fig. 2.8.

ii) In the CLL$_d$ phase the peak corresponding to the total density of (single) particles is shifted to smaller values of the momentum, signalling that there is a formation of a certain number of double occupied sites, effectively reducing the (single particle) spin density. To confirm the latter point, we study the doubly occupancy d, defined as:

$$d = \frac{1}{L}\sum_i n_{i,\uparrow}n_{i,\downarrow} - \rho, \tag{2.15}$$

where $n_{i,\sigma}$ is the occupation of one species particle, and ρ the total average density. Fig. 2.9 (a) shows the double occupancy as function of V. We find that the double occupancy increases continuously with V up to a discontinuous jump around $V \sim 7.5$, which could indicate a first order transition between the CLL$_{nn}$ and the CLL$_d$ phases. In

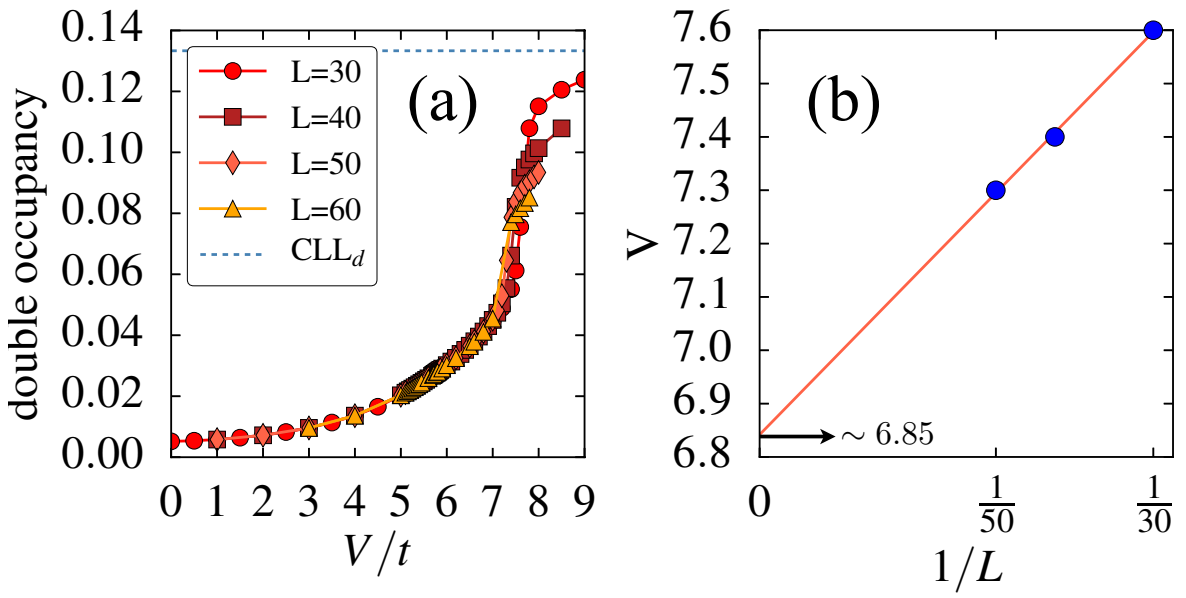

Figure 2.9: Panel (a) : the double occupancy (d) versus V for an on-site interaction $U = 10$. We see that d increases with V, a jump occurs at $V \sim 7.5$, indicating a possible first-order transition. The dotted blue line is the expected doubly occupancy within the CLL$_d$ phase. Panel (b): finite size analysis of the critical point extracted from the maximum of the first derivative $\mathrm{d}(d)/\mathrm{d}V$.

Fig. 2.9 (b), we report the critical $V_c(L)$ extracted from the maximum of the first derivative $\mathrm{d}(d)/\mathrm{d}V$ as a function of $1/L$. We then extrapolate the V_c in the thermodynamic limit by doing a fit of the form $\frac{a}{L} + b$. We obtain $V_c \approx 6.85$, in agreement with the semi classical prediction $V = 2U/3 \approx 6.66$.

Further insight can be obtained by looking at the ground state entanglement properties of the system. We consider the bipartite von Neumann entropy and extract the central charge of the system according to formula (2.13). As said before, the numerical calculations are very challenging: due to large frustration, convergence is very slow and size effects are very strong (cf. appendix). Here we summarize our results in Fig. 2.10, where we show the infinite size extrapolation of the central charge for different values of $V = 1 - 8$. From a detailed analysis of the scaling, we can conclude that:
i) the LL phase has $c = 2$, as it is expected from bosonisation which, for small values of U and V, predicts a liquid of two bosonic species, with spin and charge separation;
ii) the CLL$_{nn}$ phase has also $c = 2$ (cf. caption in Fig. 2.10 and appendix): the liquid is made up of clusters with only single occupied sites, with two species of fermions;
iii) the critical point separating the LL and the CLL$_{nn}$ phases is located at $V_c \simeq 5.7$, where the central charge jumps to $c = 5/2$;
iv) even if numerical difficulties limit our simulations to values of V not larger than 9, we see a second critical point $V \simeq 7.4$ at which the central charge is very high.

In order to understand the properties of the different low energy degrees of freedom, we calculate the gaps in the CLL$_{nn}$ phase. Both the charge and the spin gaps are zero

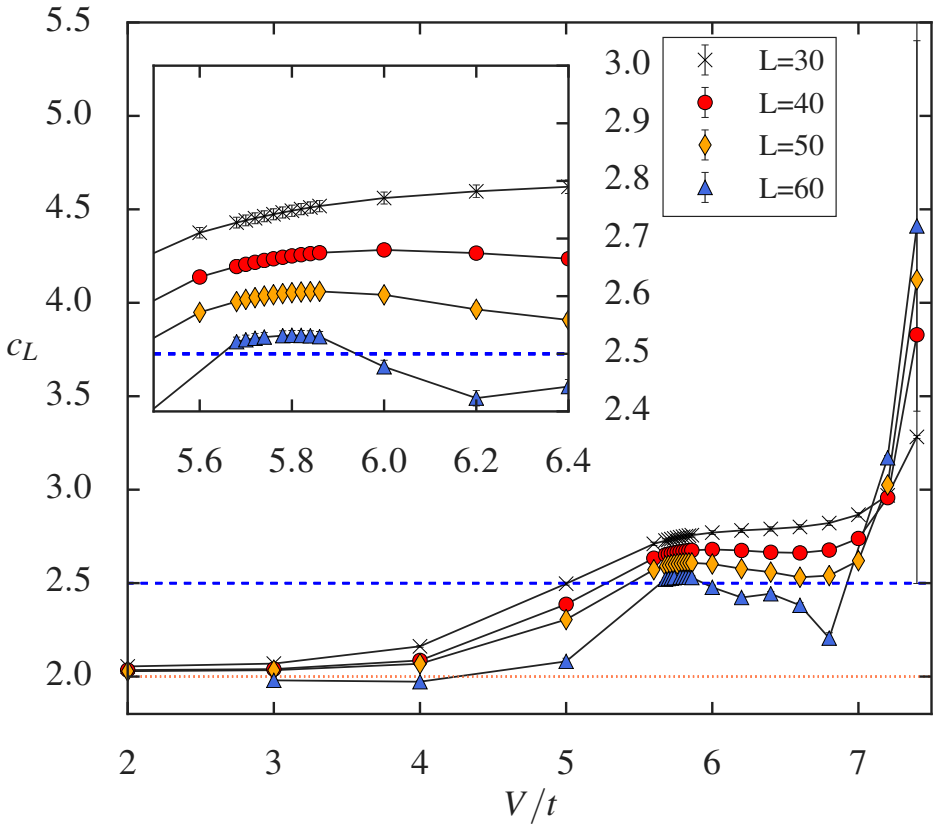

Figure 2.10: Central charge obtained from formula (2.13). The data show a phase transition at $V_c \simeq 5.7$ and a possible extended critical region up to $V \sim 7$ (inset). For clarity, in the appendix, we present an in-depth analysis of a point inside the critical extended region, showing that c_L goes back to 2. The critical point is characterised by a central charge that in the thermodynamic limit is given by $c = 5/2$ (the blue dotted line is a guide for the eye). A second transition is predicted for $V \simeq 7.4$.

in the thermodynamic limit, showing that indeed we are in a massless phase in both the spin and charge sectors. As an example, the finite size behaviour of the spin gap and its extrapolation in the thermodynamic limit are shown in Fig. 2.11 panel (a) and panel (b), respectively. On the contrary, we can observe the opening of the single particle gap, as shown in Fig. 2.12 (a) and (b). In Fig. 2.12 (a), we show the finite-size analysis in the vicinity of the critical point where we perform a fit of the form $a_1/L^{a_2} + a_0$ to extrapolate the single-particle gaps in the thermodynamic limit. We report these extrapolated values in the Fig. 2.12 (b) as function of V and we see the linear opening of the single particle gap. Then, we use the formula $\Delta \sim (V - V_c)^\nu$ in order to extract the critical exponent at the transition point. In the inset of Fig. 2.12 we show our numerical data, from which we can extract the estimate $\nu \simeq 1$, a value suggesting a transition belonging to university class of 2D Ising model, which is compatible with the central charge behaviour seen before.

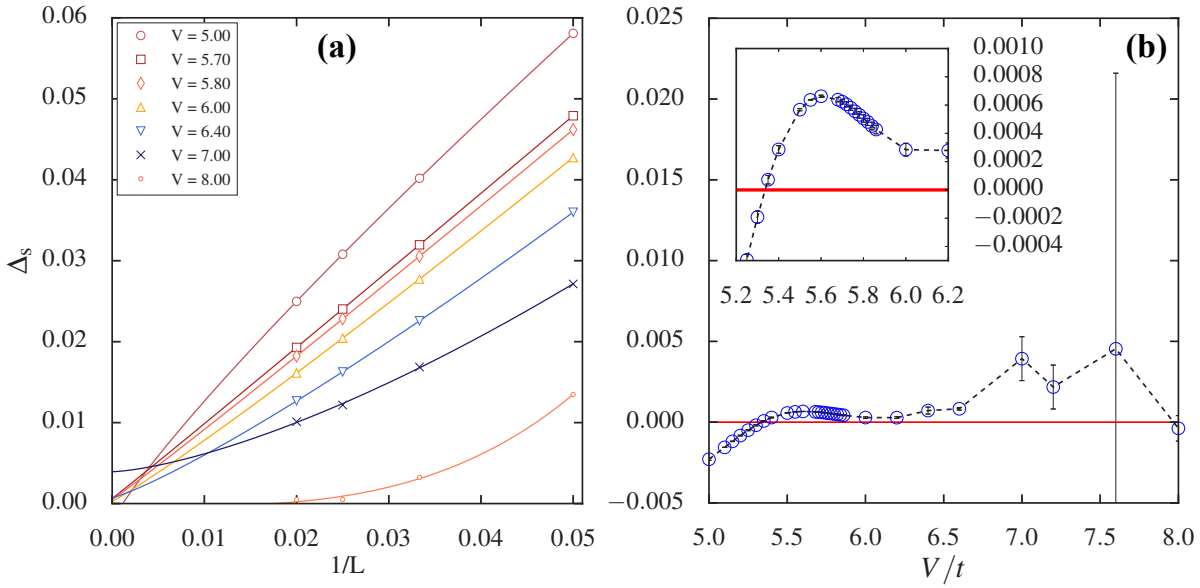

Figure 2.11: Panel (a): Finite-size scaling of the spin gap for different magnitude V . Lines are the best fit of the form $a_1/L^{a_2} + a_0$, with a_0, a_1 and a_2 constant. Panel (b): The thermodynamic extrapolation of the single particle gap as function of the interaction strength. Errors are estimated with the least-square method and are of the order of 10^{-2} for large V.

We come now to the interpretation of the numerical results reported above.
First of all, let us notice that they are consistent with the fact that spin and charge degrees of freedom are separated at all values of the interaction parameters, so extending the prediction of (standard) bosonisation which describes the TLL phase.
Second, we also see that they are in agreement with what happens for the single species case [235]. In the latter case, both the TLL and the CLL phase are characterised by a central charge $c = 1$. The extended Hubbard model we consider here contains two species of fermions and we find for both CLL phases a value of the central charge $c = 2$. Also, at the TLL-CLL$_{nn}$ transition point ($V_c \simeq 5.7$), the value of the central charge is enhanced by a factor of 1/2, signalling that an additional (real) fermionic degree of freedom is

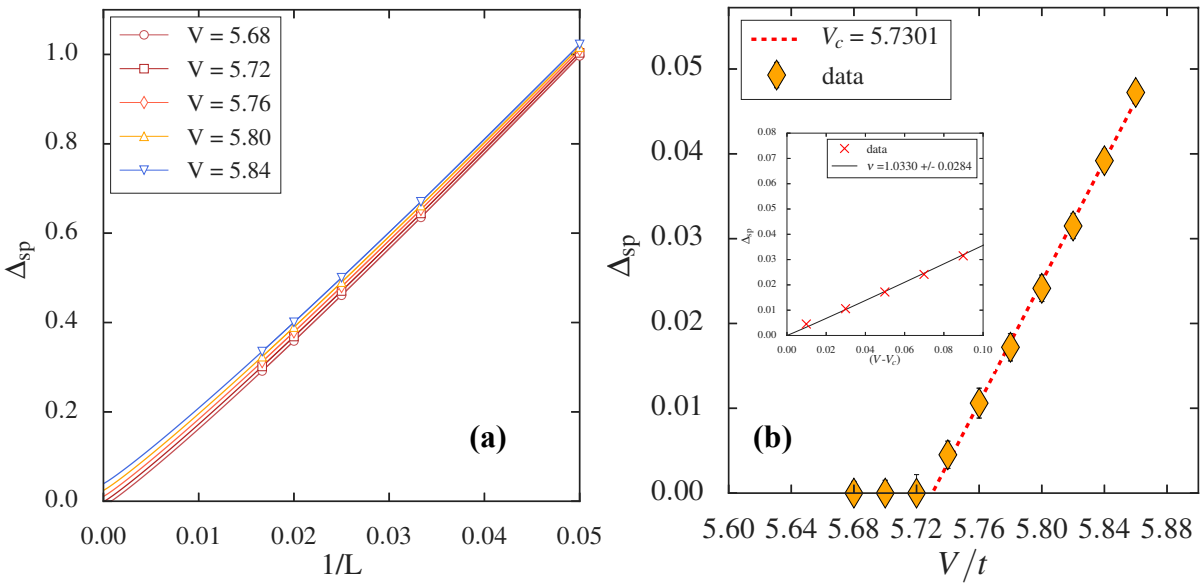

Figure 2.12: Panel (a): Finite-size scaling of the single particle gap near to the transition point. Lines represent a best fit of the form $a_1/L^{a_2} + a_0$, with a_0, a_1 and a_2 constant. Panel (b): The thermodynamic extrapolation of the single particle gap as function of the interaction strength. The red dotted line is a linear fit; its intersection with the horizontal axis yields the critical point $V_c \simeq 5.73$. Errors are estimated with the least-square method and are of the order of the marker size. The inset shows the estimation of the critical exponent ν at the LL-CLL$_{\text{nn}}$ transition point.

becoming massless. For the single particle case, this sudden increase of the central charge was interpreted [235] as a signal of an emergent supersymmetry between the compactified bosonic degree of freedom of the liquid phase and of an Ising fermionic one that becomes massless at the critical point. We can confirm that this is what happens also in our case by looking at the sound velocities of the bosonic and fermionic modes at the transition. We can define the sound velocities v_c, v_s, v_{sp} respectively according to [245]:

$$\begin{aligned} \Delta_c/2 &= \frac{2\pi v_c d_c}{L} \\ \Delta_s/2 &= \frac{2\pi v_s d_s}{L} \\ \Delta_{sp} &= \frac{2\pi v_{sp} d_{sp}}{L} \end{aligned} \tag{2.16}$$

where d_α is the conformal dimension of the corresponding vertex operator in the conformal field theory that describes the low-energy continuum limit of our model. Notice that we put a factor $1/2$ in the formulae for the charge and spin gaps because their definition implies the action of two vertex operators. The charge and spin bosonic modes are each described by a $c = 1$ conformal field theory, which is completely fixed by the Luttinger parameter $K_{c,s}$ through the formula: $d_{c,s} = 1/4K_{c,s}$ [223, 246]. The $SU(2)$ spin symmetry implies that we should assume $K_s = 4$. If we also assume so for the charge sector $K_c = 4$,

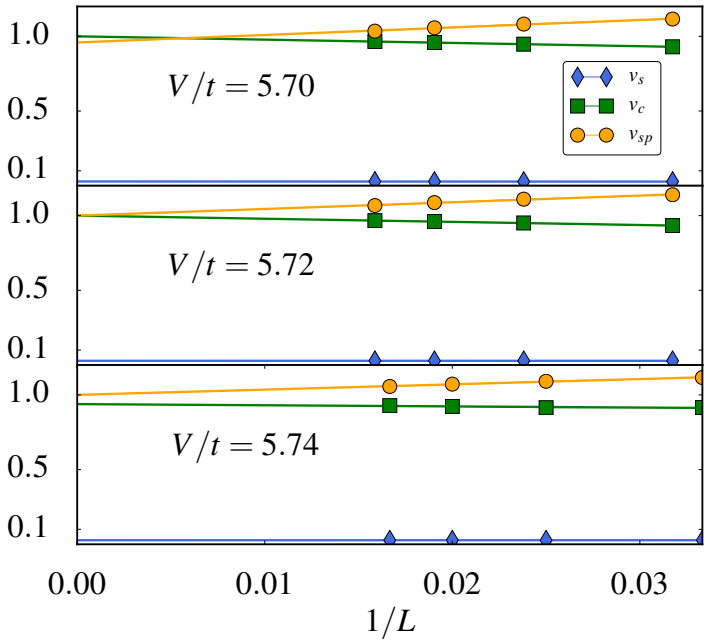

Figure 2.13: Rescaled sound velocities $v_\alpha^r = v_\alpha/v_m$, where v_m is the maximum of the three sound velocities in the $L \to \infty$ limit, as extracted from the low-energy spectrum.

then we can say that:

$$\begin{aligned} v_c &= \frac{4\Delta_c L}{\pi} \\ v_s &= \frac{4\Delta_s L}{\pi} \end{aligned} \tag{2.17}$$

For the single particle gap, we use instead the conformal dimension of the first vertex operator in the Ising model, $x_{sp} = 1/8$, to get:

$$v_{sp} = \frac{8\Delta_{sp} L}{\pi} \tag{2.18}$$

As shown in Fig. 2.13, our numerical data confirms that all sound speeds become the same at the TLL-CLL transition point, which is a signature of an emergent supersymmetry, i.e. a symmetry between bosons and fermions. At a supersymmetric point, the number of bosonic and fermionic modes is equal, and a boson can be transformed into a fermion under specific transformations known as supersymmetric transformations [129, 247, 248]. In our case, approaching the critical point, the granularity of the liquid changes from a single-particle (fermionic mode) to a cluster of particles (bosonic mode), which leads to a peculiar symmetry precisely at the critical point.
As a final remark, we want to comment on the value of the central charge at the second transition $V \simeq 7.4$. Here numerical simulations are particularly hard and we can see from Fig. 2.10 that we have not reached convergence yet, since $c(L)$ is still increasing very fast with the size of the system. Thus, within the accuracy of our data, we are not able to say whether it is converging to a finite value. A divergent central charge might be the signal that this transition is first order, as it is predicted by semi-classical considerations.

2.2.4 The phases for small values of U

In the following, we consider the case of small on-site interaction by fixing U = 1.5. We start our analysis by looking at the charge structure factor $S_c(k)$ for several magnitudes of the interaction V, presented in Fig. 2.14 panel (a). We observe (i) the usual TLL phase (no peak) at small V, and, (ii) surprisingly, the emergence of a new peak at intermediate value of V, see e.g $V = 4, 7$ in Fig. 2.14.

To understand in-depth the nature of the phase, we perform a finite-size scaling of the peak of the charge structure factor $S_c(k)/L$. Fig. 2.14 panel (b) shows examples of the scaling, where solid lines are linear fits. Our data show that $S_c(k_c)/L$ goes to zero in the thermodynamic limit, signaling a liquid phase. Furthermore, as shown in Fig. 2.14 panel (c) the double occupancy increases with the interaction strength. We interpret these combined results as an emergence of a "new" liquid phase where particles have the tendency of forming pairs, which we call TLL_d. Finally, in Fig. 2.15, we present the central charge, extrapolated in the thermodynamic limit, as a function of the interaction strength V. While for large V, the frustration prevents any real conclusion, at small and intermediate V, the central charge is equal to 2, as expected for a TLL.

We notice that TLL_d and CLL_d appears to be distinct phases. In both cases, due to the small value of the on-site interaction, clusters with doubly occupied sites ($|200\rangle$) are favored with respects to the ones with nearest neighbors. However, qualitatively in the TLL_d region, since U are on the same order of t ($U \gtrsim t$), extra pairs and thus vacant spaces are easily formed. This effect provides higher mobility for the single-particles via first or second-order hopping processes. In contrast, in CLL_d, $U \gg t$ and the system tries to minimize every cluster's formation. In this case, the mobility of clusters can only be assured by higher-order hopping processes as in [235].

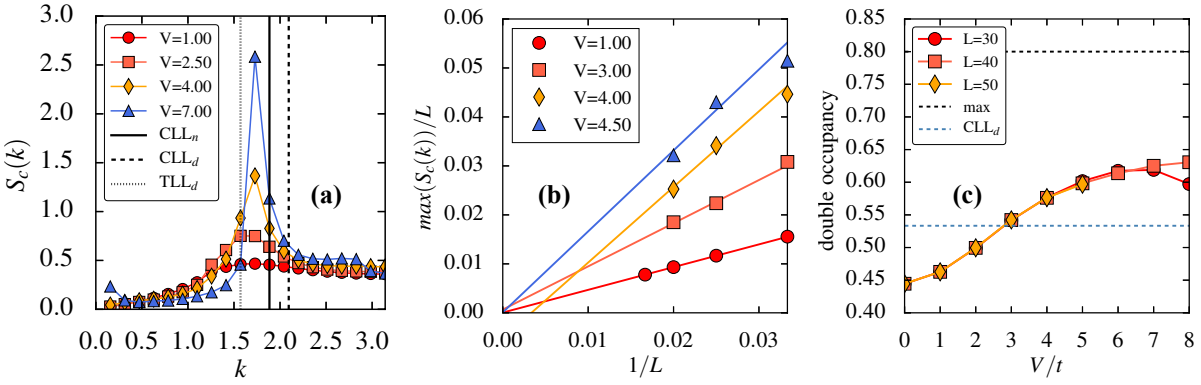

Figure 2.14: Panel (a): Density-density structure factor for a system size $L = 40$. The black solid line indicates the semi-classical prediction for the CLL_{nn} phase, the dashed one for the CLL_{d} phase and the dotted line for the TLL_d. In panel (b), examples of the finite-size scaling for the peak are shown, where the solid lines are a linear fit of the form $\frac{a}{L} + b$. In panel (c), we present the double occupancy for different values of V/t. The dashed lines are guide for the eye and represent the maximum ratio of double occupancy for the fix density $\rho = 2/5$ (black) and the expected value in the CLL_d phase (blue), respectively.

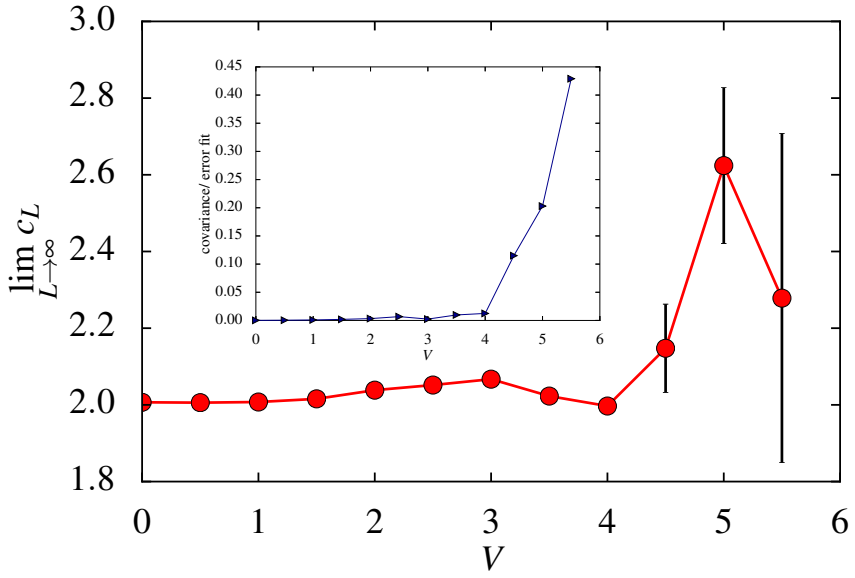

Figure 2.15: The extrapolated central charge obtained from the Cardy-Calabrese formula for $U = 1.5$ for different values of $V = 0 - 6$.

2.3 Conclusion

In this work, we have studied in details the ground state phase diagram of a 1D Hubbard model, where particles interact via soft-shoulder potential.

In the first part of the study, we have focused on the classical limit of our model ($t = 0$), for which we have described the frustration mechanisms at play. We have notably shown that these effects lead to the appearance of two cluster type phases, one already known as the cluster luttinger liquid (CLL) and a second one made of on-site pairs (CLL$_d$). Interestingly, these phases are not captured by the standard TLL theory, and we have found that the transition between the CLL$_{nn}$ and CLL$_d$ occurs at $V = 2U/3$ at this classical level.

In the second part of this work, using the DMRG method, we have studied the phase diagram of our quantum ($t \equiv 1$) model in the whole range of the parameters U, V by analysing in detail the properties of the different phases. We have notably demonstrated that the standard TLL phase is the ground state for low values of U, V. At large U or at large V, we have confirmed the existence of the cluster phases predicted classically. Then, focusing on an intermediate value of U, we have characterized in more details the different phases and the transition between them. In particular, we have shown that all the phases present in our model are characterized by a central charge $c = 2$, consistent with the separation of the spin and charge degrees of freedom in the TLL theory. However, in the CLL$_{nn}$ we have shown that the single-particle excitation is gapped; hence we have interpreted this phase as a TLL made of composite clusters particles. At low on-site interaction U and intermediate V, we have found the presence of a liquid phase characterized by the formation of more one-site pairs as compared to the standard TLL, which we have qualitatively attributed to a strong competition between the tunneling and the on-site repulsion.

At the critical point between the conventional TLL and the CLL_{nn}, we have carried out an extensive investigation of the entanglement entropy and the low-lying energy degree of freedom, providing evidence of an enhance of the central charge to $c = 5/2$ compared to the usual TLL, indicating an emergent supersymmetry. Regarding the last point, we have confirmed that the renormalized sound velocities of the emergent bosonic and fermionic modes are indeed equivalent at the critical point within numerical accuracy. Finally, we have shown numerically that the classical prediction for the transition between the CLL_{nn} and CLL_{d} holds.

Appendices

2.A Details about the numerics

In this appendix, we give an insight into the real computational challenge inherent to frustrated systems considered in this work. Indeed, numerical results are hard to extract with high precision, even with the state of art of techniques such as DMRG. In this work, we use a DMRG code provided by ITENSOR [15], and we impose anti-periodic boundary conditions to reduce boundary effects, keeping up to 9000 states per block and up to 20 sweeps. Furthermore, in order to keep commensurability with the cluster structure (CLL_{nn}), we considered only chains of size $L = 10, 20, 30, 40, 50, 60$. For comparison, in the usual short-range Hubbard model convergence is reached with few hundred states and few sweeps.

We now give an example of the problems we encountered, by showing how we tackled the problem of extracting the central charge. As an instance, we consider the point $U = 10, V = 6.4$, which lies inside the CLL_{nn} phase. Here, we compare the results of the entanglement entropy by varying some numerical parameters, such as the bond dimensions and the block length of Eq. 2.13. Using this approach, we are able to extrapolate the central charge in the limit of infinite bond dimension and in the thermodynamic limit. As we will see, the data strongly suggest that the central charge is equal to 2.

In Fig. 2.16 panel (a), we show the central charge versus the minimum block length ℓ used in Eq. (2.13) for various D and fix $L = 50$. The strong dependence on the bond dimension and the block length is evident. In particular, we find that keeping tiny blocks in the Eq. (2.13) leads to an overestimation of the central charge, signaling the importance of the non-universal effects. It is possible to estimate the central charge in the limit of infinite number of local states by fitting with a function $c(1 - be^{-aD})$, see e.g. Fig. 2.16 panel (b). This limit is reported as the black line in Fig. 2.16 panel (a).

In order to calculate the central charge in the thermodynamic limit, we now perform a finite-size analysis at fixed block length $\ell \leq 7$ to avoid non-universal effects. In Fig. 2.17 panel (a), we plot the central charge as a function of $1/L$ for different bond dimensions. Then, we extrapolate $c_{L\to\infty}$ with a fit of the form $c + \frac{a}{L} + \frac{b}{L^2}$. As mentioned before, the black line corresponds to the infinite bond limit and gives us a first estimation for the central charge around ~ 1.8. Numerically, we find here that convergence is particularly hard to reach. The value of the central charge is still underestimated by considering 9000 states per block. Finally, in Fig. 2.17 panel (b), we show $c_{L\to\infty}$ as a function of the local states D. By fitting with a function $c(1-be^{-ax})$ (blue line), we obtain a second estimation of the central charge in the limit of infinite size and infinite local states: $c \sim 2.3$. These combined results indicate a central charge equal to 2 in the CLL_{nn} region.

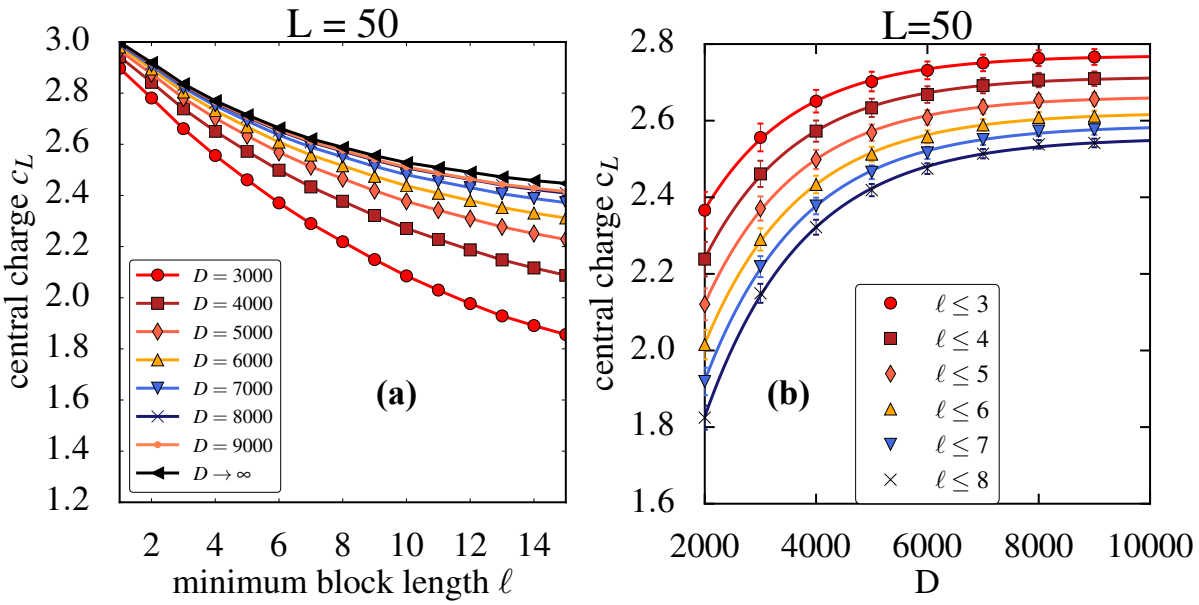

Figure 2.16: Panel (a): central charge as function of the different block length kept for different local bond dimension. The black line corresponds to an extrapolation in the infinite local states limit. Panel (b): central charge versus D, the solid lines are fits of the form $c(1 - be^{-aD})$, providing an extrapolated value of c_L in the limit of infinite D.

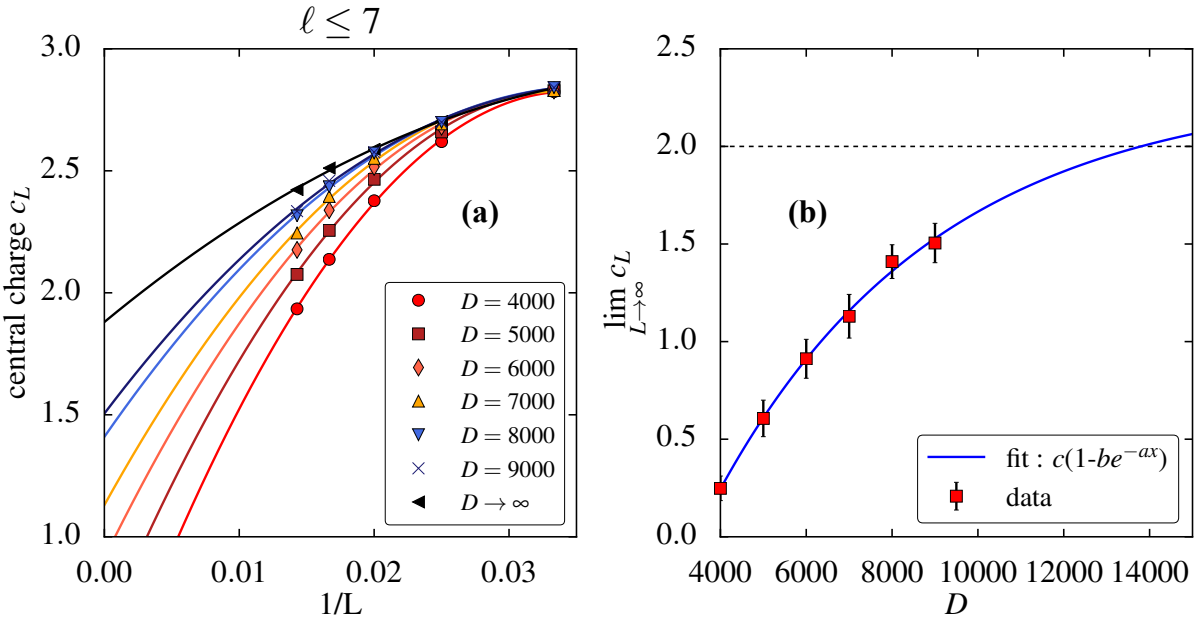

Figure 2.17: Panel (a) is the finite-size scaling, for block length ≥ 7, for different bond dimension (colours cf. legend). As previously the black line is the infinite bond dimension limit. In panel (b), we present the extrapolated central charge as function of the local bond dimension.

Chapter 3

Effects of energy extensivity on the quantum phases of long-range interacting one-dimensional systems

Laws of Thermodynamics:
- This is the game
- You can't win
- You can't break even
- You can't get out of the game

C.P. Snow

Long-range (LR) interacting systems are characterized by highly non-local couplings between their constituents, typically decaying as a power law for large distances between them. LR models feature a wide variety of applications including self-gravitating clusters [249], ferromagnetic materials [250], non-neutral plasmas [251], cavity-QED systems [117], and 1D quantum wires [252]. Recent progress in the realization of artificial lattices of cold gases with sizable LR interactions has stimulated considerable interest [3–6, 8, 93, 112, 115, 139, 253–260]. In parallel, theoretical studies of the ground state of LR spin models have revealed anomalous critical exponents [261–263] and decay of correlations [264–269], as well as the existence of new quantum phases [9, 110, 270–273].

The *strong* LR regime for a d-dimensional system with volume $\mathcal{V}$ is achieved when the power-law exponent α entering the potential $V(r) \propto 1/r^{\alpha}$ experienced by two particles separated by the distance r is such that $0 \leq \alpha \leq d$. This regime is typically associated to unusual thermodynamic properties such as a non-extensive energy $E \sim \mathcal{V}^{2-\frac{\alpha}{d}}$ leading to an ill-defined thermodynamic limit [18]. Furthermore, the total energy cannot be obtained by summing up the energies of different subsystems as is usually the case for short-range interactions [16, 274]. This non-additivity appears as a fundamental property of LR models and leads to exotic behaviors including the breaking of ergodicity, the existence of slow relaxation processes, and the inequivalence of statistical ensembles [19, 22–24]. In contrast, extensivity can be restored by rescaling the interaction potential with an appropriate volume-dependent factor Λ, which is known as Kac's prescription [275]. The latter is systematically used to study the thermodynamic properties of classical spin models with LR interactions [17, 276–279]. In condensed-matter quantum systems, however, Kac's rescaling is usually not considered, and it is therefore an open and interesting question to investigate whether energy extensivity can modify the fundamental properties of LR quantum systems.

In this chapter, we focus on the impact of non-extensivity in quantum systems interacting via repulsive potentials in the strong LR regime. In Sec 3.1, we start by reviewing the different regimes of LR interacting systems, as well as their specific thermodynam-

ics and dynamical properties. We then introduce the Kac's prescription and explain its relevance for classical systems. In Sec. 3.3, we investigate a specific LR quantum model, namely a 1D periodic chain of hard-core bosons interacting via a repulsive potential in the strong LR regime at half-filling. A particular case of this model ($\alpha = 1$) has been already studied in the context of 1D quantum wires and features interesting properties due to its long-range nature. [280–288]. In Sec. 3.4 and 3.5, we use the Luttinger liquid (LL) theory combined with Density Matrix Renormalization Group (DMRG) calculations [15] for large system sizes ($\gtrsim 200$ sites) to analyse the quantum phases of this model with and without Kac's prescription. We find that the latter has a profound influence on the low-energy properties in the thermodynamic limit. In the absence of Kac's rescaling, the ground state is in a gapped insulating phase in the thermodynamic limit in the whole range $0 < \alpha \leq 1$, extending the results of Ref. [286] in the marginal case $\alpha = 1$. In stark contrast, we demonstrate that Kac's rescaling leads to a metallic phase for any finite strength of the interaction in the thermodynamic limit for $0 \leq \alpha \leq 1$. This finding raises fundamental questions on how to study the thermodynamics of LR interacting quantum systems, since different phases are obtained depending on whether Kac's prescription is used or not. Furthermore, we study the validity of the Luttinger Liquid theory in Sec. 3.6 by computing the Luttinger parameters from the single-particle correlation function, the structure factor, the charge gap, and the charge stiffness. Interestingly, we find a discrepancy between the results that make this metallic phase incompatible with a conventional LL. Finally, in Sec. 3.7, we show that restoring extensivity eliminates the plasmon modes while preserving the LR character of the potential, and with it some inherent properties of the strong LR regime such as non-addivity.

3.1 Long-range system

In the two following sections, we briefly review the peculiar thermodynamic properties of LR systems. In most physical systems with short-range interactions, the connection between microscopic and macroscopic descriptions relies on the introduction of different statistical ensembles, which in principle give equivalent predictions. However, one of the most fascinating properties of LR systems is that these statistical ensembles are not always equivalent. This discrepancy stems from the non-additivity and the non-extensivity of the energy. Both are intimately related, as we will see in the section below.

3.2 Non-extensivity and non-additivity

In order to define more precisely what do we mean by a (truly) LR system, we consider a model with N particles in a d-dimensional volume $\mathcal{V}$ interacting via a potential V decaying as a power law of the inter-particle distance r: $V(r) \propto 1/r^{\alpha}$, $\alpha > 0$. When $\alpha > d$, the interaction potential decays rapidly at large distance, and the thermodynamic and dynamical properties correspond to those of short-range systems. This regime is usually referred to as *weak* LR. In contrast, the potential for $\alpha < d$ varies slowly with the distance and has a more pronounced effect. In this case, the system is said to be truly long-range or in the *strong* LR regime. To illustrate this point, we examine the potential

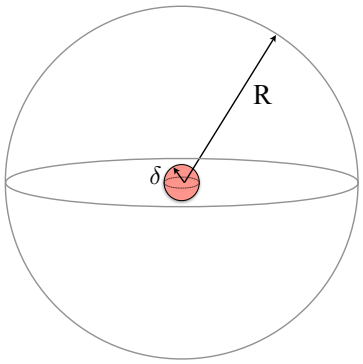

Figure 3.1: Schematic picture of the domain considered for the evaluation of the energy ϵ of a particle: A spherical shell of outer radius R and inner radius δ.

energy ϵ of a system consisting of one particle placed in the center of a sphere of radius R, and an homogeneous particle density with density ρ. We exclude the small volume around the central particle to regularize the potential at short distance (see Fig. 3.1) [17, 278]. The energy reads:

$$\epsilon = \int_{\delta}^{R} \mathrm{d}^d r \frac{V}{r^\alpha} = \rho V \Omega_d \int_{\delta}^{R} \frac{1}{r^{1+\alpha-d}} dr = \frac{\rho V \Omega_d}{d-\alpha}\left[\frac{1}{R^{\alpha-d}} - \frac{1}{\delta^{\alpha-d}}\right], \tag{3.1}$$

where Ω_d is the angular volume in dimension d. In the weak LR regime $\alpha > d$, the energy ϵ tends to a finite value when increasing the radius R, and one can check that the energy is extensive, i.e. it scales linearly with the volume $\mathcal{V}$. In contrast, the energy scales superlinearly with the volume as $E \sim \mathcal{V}^{2-\frac{\alpha}{d}}$ (or logarithmically in the marginal case $\alpha = 1$) in the strong LR regime $\alpha < d$. This implies that the system is non-extensive, which leads to an ill-defined thermodynamic limit. Indeed, extensivity is responsible for the competition between energy and entropy. This can be seen by introducing the free energy $F = E - TS$. Since the entropy always scales linearly with the volume, the free energy is dominated by the energy part which leads to a trivial thermodynamics [16, 274]. The thermodynamic limit can be however studied using a simple trick known as the Kac's prescription. This prescription restores energy extensivity and consists of rescaling the potential by a volume dependent factor $\Lambda_\alpha = \mathcal{V}^{1-\frac{\alpha}{d}}$. Note that in a simple case where we neglect the kinetic term, either the potential energy or the temperature T can be equivalently rescaled.

Non-additivity is another inherent property of the strong LR regime and can be defined as follows. Considering a system divided in two macroscopic parts 1 and 2 with energy E_1 and E_2, the total energy of the system cannot be obtained by summing the energy of each part, i.e., $E_{\text{tot}} \neq E_1 + E_2$. This property stems from the energy E_{int} due to interactions between the different parts of the system, which cannot be neglected in the strong LR regime causing the system to be intrinsically non-additive. In contrast, in most physical systems with short-range interactions (or in the weak LR regime), this interaction energy

$E_{\rm int}$ goes to zero in the thermodynamic limit and the systems is thus said to be additive, i.e., $E_{\rm tot} = E_1 + E_2$.

One can check that the energy scales linearly with the volume when $E_{\rm int}$ is neglected. In other words, additivity implies extensivity. Note also that while non-extensivity implies non-additivity, the converse statement is not true [17]. Indeed, one can show that restoring extensivity does not systematically restores additivity. In order to illustrate this point, we consider the following one-dimensional lattice model:

$$H = \sum_{i>j} \frac{V}{\Lambda_\alpha r_{i,j}^\alpha}, \tag{3.2}$$

where $r_{i,j} = |i - j|$ is the distance between the sites [see Fig. 3.2]. The Kac's factor Λ_α is used to restore energy extensivity. For simplicity, we choose $\alpha = 0$ and divide the system of length L into two equal parts with two particles in each. We find that while $E_1 = E_2 = 2V/L$, the total energy $E_{tot} = 6V/L \neq E_1 + E_2$. This indicates that the system is extensive but non-additive. We now investigate the consequences of Kac's rescaling on the dynamics of classical systems.

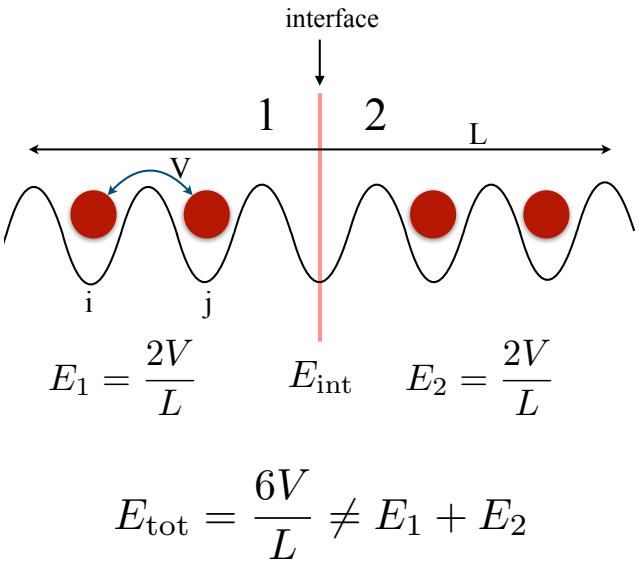

Figure 3.2: Schematic picture of the Hamiltonian Eq. (3.2). A system of size L is divided into two parts 1 and 2 with two particles in each. The potential is considered having an infinite-range ($\alpha = 0$). Since the total energy can not be obtained by summing the energies of the two subsystems, the system is said to be non-additive.

3.2.1 Kac's rescaling in classical systems

The Kac's rescaling is systematically used to study the thermodynamic properties of classical spin models with LR interactions [17, 276–279]. We now show that the dynamical properties with and without Kac's rescaling are the same provided the respective time scales $t_{\rm res}$ and t satisfy $t = t_{\rm res}/\sqrt{\Lambda}$ [289, 290] (for an Hamiltonian with quadratic kinetic

energy). We consider a general classical Hamiltonian $\mathcal{H}(q,p) = T+V$, where $T = p^2/(2m)$ the kinetic term, V the potential and q, p the set of canonical coordinates. The dynamics of such classical system is then governed by the Hamilton equations:

$$\begin{aligned} \dot{p} &= -\frac{\partial \mathcal{H}}{\partial q} \\ \dot{q} &= \frac{\partial \mathcal{H}}{\partial p}. \end{aligned} \tag{3.3}$$

For a quadratic kinetic energy, we can combine the previous equations to obtain

$$\ddot{q} = \frac{\dot{p}}{2m} = -\frac{1}{2m}\frac{\partial \mathcal{H}}{\partial q} = -\frac{1}{2m}\frac{\partial V}{\partial q}. \tag{3.4}$$

If one now considers the new Hamiltonian $\mathcal{H}_{\text{res}}(q,p) = T+\frac{V}{\Lambda}$ with Kac's rescaling, Eq (**??**) becomes

$$\ddot{q} = \frac{\dot{p}}{2m} = -\frac{1}{2m}\frac{\partial \mathcal{H}}{\partial q} = -\frac{1}{2m\Lambda}\frac{\partial V}{\partial q}, \tag{3.5}$$

which can be rewritten as

$$\Lambda \frac{\mathrm{d}^2 q}{\mathrm{d}t_{\text{res}}^2} = -\frac{1}{2m}\frac{\partial V}{\partial q}, \tag{3.6}$$

where t_{res} is the time associated to the Hamiltonian H_{res}. Assuming that the time scales satisfy $t_{\text{res}} = \sqrt{\Lambda}t$, we obtain immediately $\mathrm{d}t_{\text{res}}^2 = \Lambda \mathrm{d}t^2$, and Eq. (3.6) is equivalent to Eq. (3.4). This means that the two Hamiltonians $\mathcal{H}(q,p)$ and $\mathcal{H}_{\text{res}}(q,p)$ feature the same dynamical and thermodynamic properties. However, it can be shown that the latter statement does not hold true in quantum systems. Indeed, the quantum counterparts of the Hamilton equations follow from the Ehrenfest theorem, but only involve the expectation values of the momentum and position operators. In contrast to the classical situation, the dynamics of a quantum system with and without Kac's rescaling are a priori different. It is therefore an interesting question to investigate what other properties such as ground state phases can be fundamentally modified by Kac's rescaling in a generic quantum system.

3.3 Model

We consider an archetypal and still actively studied LR quantum model which consists of one-dimensional (1D) fermions interacting via a $1/r$ (unscreened) Coulomb potential. Schulz showed using bosonization techniques that the ground state of this system is a peculiar metal resembling a classical Wigner crystal, with very slow decay of the charge correlations associated to the plasmon mode [280, 281]. This result was confirmed numerically using DMRG [291] and variational Monte Carlo methods [282–284]. In the presence of a lattice at commensurate fillings, it was shown that while the metallic behavior is surprisingly enhanced as compared to short-range interactions for small system size, the ground state ultimately enters an insulating phase in the thermodynamic limit [285–288].

In the following, we study an extension of this model, with a tunable interaction potential that allow us to explore the whole strong-long regime. We will emphasize striking difference when Kac's prescription is used or not. The Hamiltonian reads as

$$H = -t \sum_{i=1}^{L} \left(a_i^\dagger a_{i+1} + \text{h.c.} \right) + \sum_{i>j} V_{i-j}^{(\alpha)} n_i n_j, \tag{3.7}$$

where the operator a_i ($a_i^\dagger$) annihilates (creates) a hard-core boson on site $i = 1, \cdots, L$, and $n_i = a_i^\dagger a_i$ is the local density. The interaction potential reads

$$V_{i-j}^{(\alpha)} = \frac{V}{\Lambda_\alpha(L) r_{i-j}^\alpha} \qquad V > 0,$$

where $r_{i-j} = (La/\pi)\sin(\pi|i-j|/L)$ for $L \gg 1$ as we assume periodic boundary conditions. A pictural representation of the circular chain is presented in Fig. 3.3. In the following, the nearest neighbor hopping t and lattice spacing a are set to $t \equiv a \equiv 1$. Kac's rescaling of the interaction potential is included via the function $\Lambda_\alpha(L) = 1$ for $\alpha > 1$ (absence of Kac's rescaling), $\Lambda_\alpha(L) = \log(L)$ in the marginal case $\alpha = 1$, and $\Lambda_\alpha(L) = L^{1-\alpha}$ in the strong LR regime $\alpha < 1$. Note that the XXZ Heisenberg model with LR coupling along the z direction and short-range coupling along x and y can be mapped onto hard-core bosons Eq. (3.7) or spinless fermions via a Jordan-Wigner transformation.

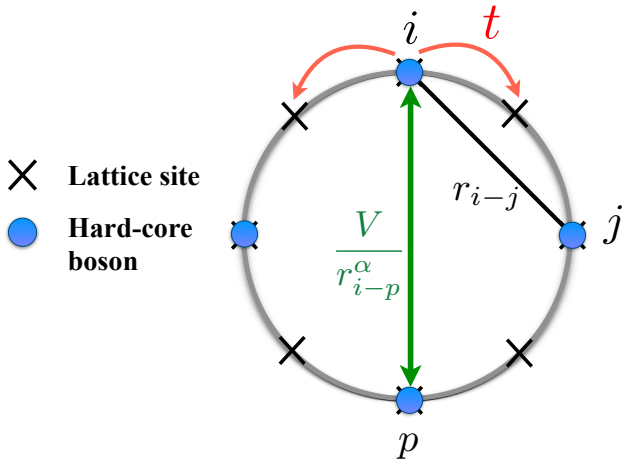

Figure 3.3: Sketch of the physical system described by the Hamiltonian Eq. (1) of the main text, consisting of a circular chain (periodic boundary conditions).

3.4 Low-energy degree of freedom

We have seen previously that the Kac's rescaling restores extensivity in the system. It is therefore convenient to first compute the energy of the ground state $E_0(N)$ (for N particles) and the single-particle gap $\Delta = E_0(N+1) + E_0(N-1) - 2E_0(N)$ for $\alpha = 1$ and different interaction strengths V. These results are shown in Fig. 3.4. The

situation without Kac's rescaling [$\Lambda_1(L) = 1$, Fig. 3.4 **(a)**] has been already investigated in Ref. [286], and features a non-extensive energy [Fig. 3.4 **(b)**]. In this case, we find that the gap $\Delta(L \gg 1) \neq 0$ for any $V > 0$, which indicates an insulating phase in the thermodynamic limit consistently with the conclusion of Ref. [286]. These results are drastically modified when using the Kac's prescription. By rescaling the interaction potential [$\Lambda_1(L) = \log(L)$, Fig. 3.4 **(d)**], we find that while extensivity is clearly restored [Fig. 3.4 **(c)**], $\Delta \sim 1/L$ for all $V > 0$. This result indicates a metallic behavior in the thermodynamic limit observed in the whole range $0 < \alpha \leq 1$ (not shown).

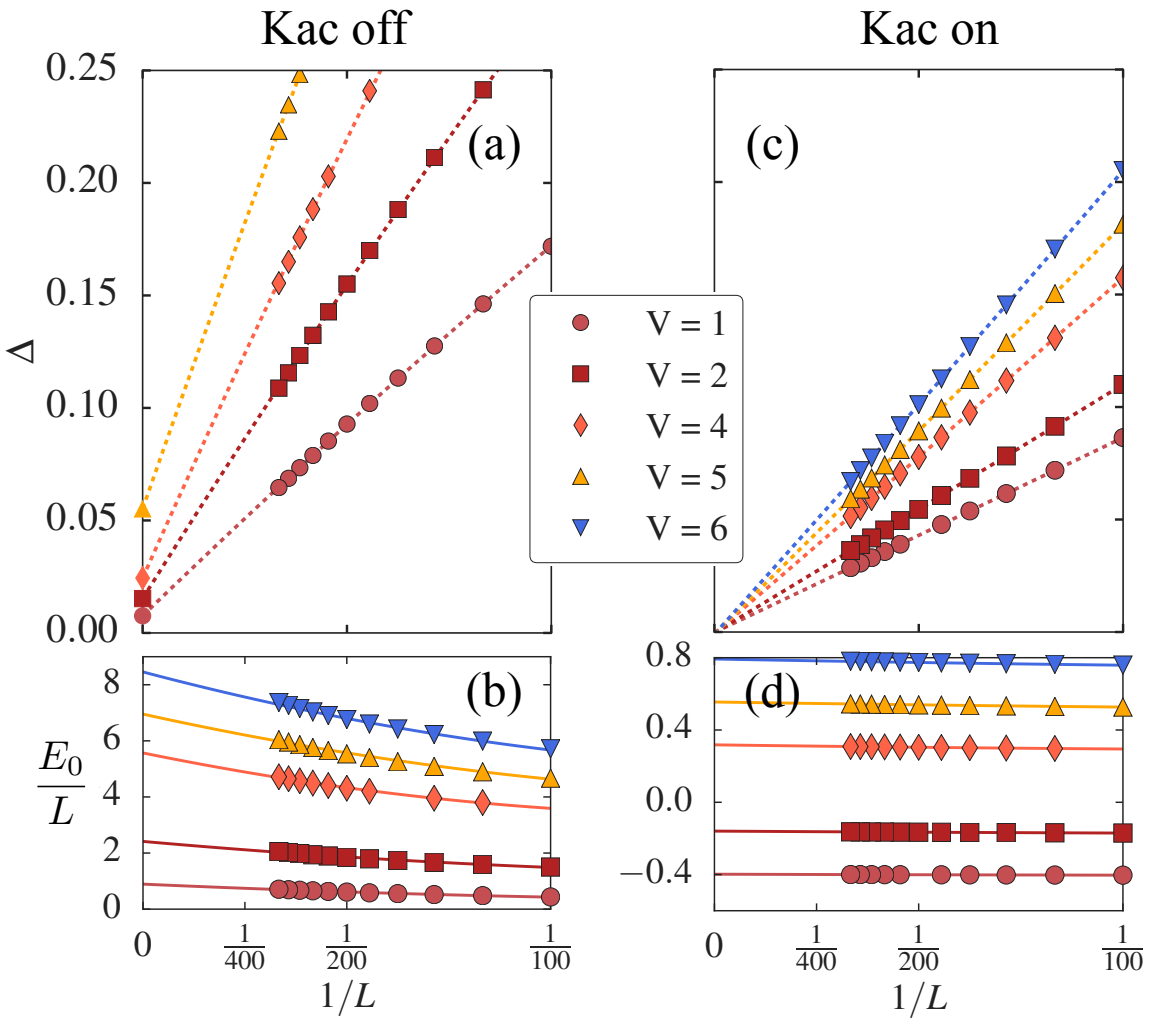

Figure 3.4: Finite-size scaling of the single-particle gap Δ computed with DMRG at half-filling $\langle n_i \rangle = 0.5$, for $\alpha = 1$ and different interaction strengths V (in units of the hopping energy t). In the thermodynamic limit $L \to \infty$, while an insulating phase ($\Delta \neq 0$) is found without Kac's rescaling **(a)**, the latter leads to a metallic phase ($\Delta = 0$) **(b)**. Extrapolation in the thermodynamic limit is obtained by fitting the numerical data with $\Delta(L) = b + \frac{c}{L} + \frac{d}{L^2}$ (dotted lines). The ground state energy E_0/L is shown in **(c)** & **(d)**.

3.5 Luttinger Liquid theory

Now, we have shown that restoring the extensivity drastically modified the ground state properties, we would like to understand the physical origin of the significant difference between the extensive and non-extensive models. To do so, we investigate the low-energy properties of the system using the LL theory. A convenient bosonic representation of H in terms of the continous variable $x \equiv ja$ (with $a \to 0$) can be obtained by treating the interaction potential as a perturbation [252]

$$H = \frac{1}{2\pi}\int dx\; uK\,(\pi\Pi)^2 + \frac{u}{K}\nabla^2\phi - \frac{g}{\pi a^2}\cos\left(4\phi\right), \tag{3.8}$$

where $\Pi(x)$ and $\phi(x)$ and are canonically conjugate bosonic fields depending on the long wavelength fluctuations of the fermion density. The so-called Luttinger parameters u and K are related by the relations [286]

$$\begin{aligned} uK &= v_{\mathrm{F}} \\ \frac{u}{K} &= v_{\mathrm{F}} + \frac{1}{\pi}\sum_{r=1}^{L} V_r^{(\alpha)}\left[1-\cos\left(2k_{\mathrm{F}}r\right)\right] \end{aligned} \tag{3.9}$$

where v_{F} denotes the Fermi velocity and k_{F} the Fermi wave vector. The first two (quadratic) terms of Eq. (3.8) describe how the properties of the non-interacting LL are renormalized by the interactions. In particular, K determines the decay of the single-particle correlation function $\langle a_i^\dagger a_j\rangle \sim r_{i-j}^{-1/(2K)}$. The third term in Eq. (3.8) stems from scattering processes across the Fermi surface where the particle momentum is conserved up to a reciprocal lattice vector. It is usually denoted as umklapp term and scales with the strength

$$g = \sum_{r=1}^{L} V_r^{(\alpha)}\cos\left(2k_{\mathrm{F}}r\right). \tag{3.10}$$

For a finite g, it is possible to show using a renormalization-group study [252] of the Hamiltonian Eq. (3.8) that the system goes from an insulating to a metallic phase as K is increased above a critical value K_c. At half-filling, and neglecting multiple umklapp scattering [292], the critical value is $K_c = 0.5$. Note that in the case of a nearest-neighbor interaction $\alpha \to \infty$, such a metal-insulator transition occurs at $V = 2t$ [293].

We consider a half-filled band $\langle n_i\rangle = 0.5$, which provides $k_{\mathrm{F}} = \pi/2$ and $v_{\mathrm{F}} = 2$. In the absence of Kac's rescaling, the first sum $\sum_r V_r^{(\alpha)}$ entering Eq. (3.9) diverges in the thermodynamic limit $\sim \log(L)$ for $\alpha = 1$ and $\sim L^{1-\alpha}/(1-\alpha)$ for $0 \leq \alpha < 1$. The second sum $\sum_r V_r^{(\alpha)}\cos\left(2k_{\mathrm{F}}r\right)$ entering Eqs. (3.9) and (3.10) is bounded due to the alternating sign. Therefore, while the umklapp scattering strength g remains finite, the Luttinger parameter $K \to 0$ for $0 < \alpha \leq 1$ and $V > 0$ in the thermodynamic limit, consistently with an insulating phase.

We find that rescaling the interaction potential with the factor $\Lambda_\alpha(L) = \log(L)$ for $\alpha = 1$ and $\Lambda_\alpha(L) = L^{1-\alpha}$ for $\alpha < 1$ strongly affects the competition between K and g. In this case, the long-wavelength divergence is removed since $\lim_{L\to\infty}\sum_r V_r^{(\alpha)} = V$ for $\alpha = 1$ and $\lim_{L\to\infty}\sum_r V_r^{(\alpha)} = V/(1-\alpha)$ for $\alpha < 1$. This suggests a metallic phase for

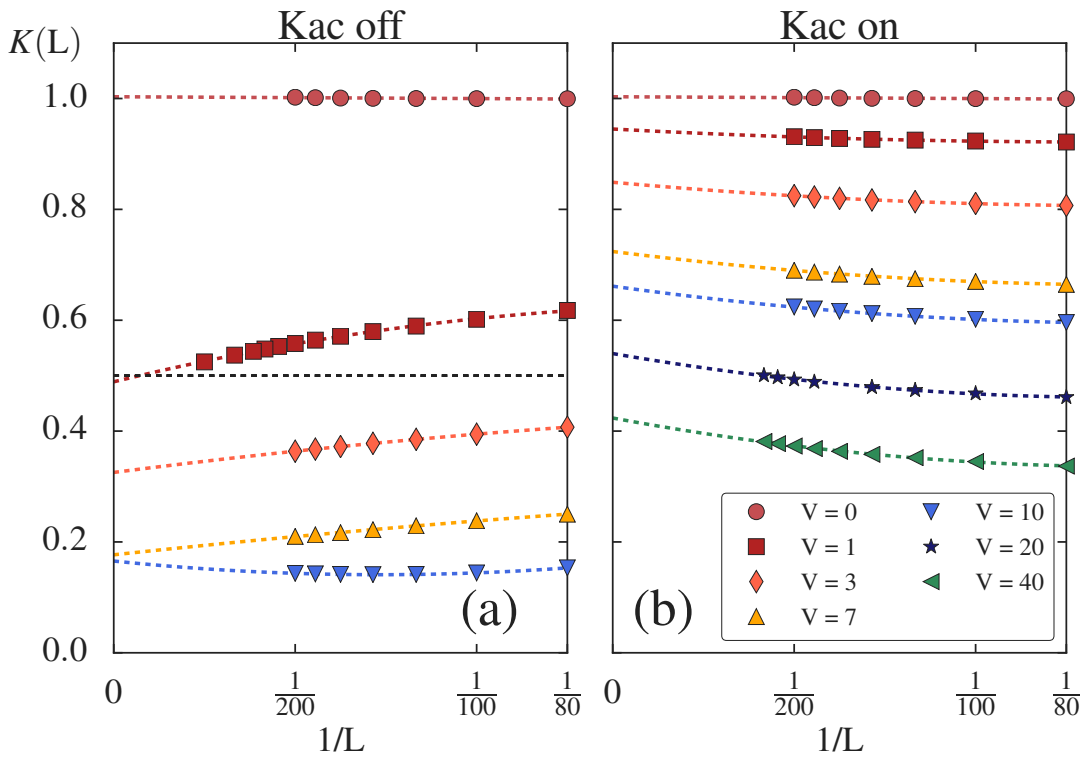

Figure 3.5: Luttinger parameter K computed numerically at half-filling for $\alpha = 0.5$ and different V, by fitting the correlation function $\langle a_i^\dagger a_j \rangle$ [225]. The critical value $K_c = 0.5$ indicating the metal-insulator transition with nearest neighbor interaction is displayed as a black dashed line. In the absence of Kac's rescaling **(a)**, K decreases when increasing L, lying below the critical line for $L \to \infty$ (insulating phase). In contrast, K increases with L in the presence of Kac's rescaling **(b)**, and remains finite even for very large V (metallic phase). Extrapolation in the thermodynamic limit is obtained by fitting the data with the same function as in Fig. 3.4 (dotted lines).

$0 < \alpha \leq 1$, since K remains finite and $g \to 0$ for any finite $V > 0$ in the thermodynamic limit as seen from Eqs. (3.9) and (3.10).

The above arguments cannot be used in the case $\alpha = 0$ since the series $\sum_r V_r^{(\alpha)} \cos(2k_F r)$ does not have a unique limit for $L \to \infty$. Nevertheless, this particular case can be solved exactly using a mean-field approach on the Hamiltonian Eq. (3.7), that we will discuss in detail in a latter section. This leads to a free fermion (metallic) phase with charge correlations $\langle a_i^\dagger a_j \rangle \sim r_{ij}^{-1/2}$, regardless of the presence or absence of Kac's rescaling. However, since a finite gap $\Delta = V + (2\pi t/L)$ is found for $L \to \infty$ in the latter case, this phase was refered to as a strange metal in Ref. [288]. Interestingly, we find that the Kac's prescription $V \to V/L$ leads to a vanishing gap for $L \to \infty$, and the properties of the ground state with extensive energy and $\alpha = 0$ correspond to those of free fermions.

In order to obtain further insights, we first compute the Luttinger parameter K by fitting the correlation function $\langle a_i^\dagger a_j \rangle$, and represent it in Fig. 3.5 for different V and $\alpha = 0.5$. We observe two opposite trends depending on whether Kac's rescaling is present or not. In the latter case [Fig. 3.5 **(a)**], K decreases when increasing L and lies below the critical value $K_c = 0.5$ for $L \to \infty$, which indicates an insulating phase. The case

with Kac's rescaling is shown in Fig. 3.5 **(b)**, where a finite K is found for all V in the thermodynamic limit.

Then, we compute the charge stiffness [252]

$$D = \pi L \left| \frac{\partial^2 E_0(\Phi)}{\partial \Phi^2} \right|_{\Phi=0}, \tag{3.11}$$

which is proportional to the Drude weight [294], and therefore provides valuable information on the metallic or insulating properties of the system. Moreover, it also gives a direct measure of the umklapp scattering strength. A large D corresponds to a good metal, while an insulating phase features $D = 0$. The charge stiffness is computed numerically from the ground state energy E_0 by threading a flux Φ through the circular chain, and represented in Fig. 3.6 as a function of $1/L^2$ for $\alpha = 0.5$. In the absence of Kac's rescaling [Fig. 3.6 **(a)**], D decreases when increasing L for any finite V. The latter drives the system towards an insulating phase ($D \to 0$) in the thermodynamic limit. In contrast, D increases with L in the presence of Kac's rescaling [Fig. 3.6 **(b)**], which confirms the existence of a metallic behavior.

In the thermodynamic limit, we find that $D \approx v_F$ even for very large V, in surprisingly good agreement with the LL prediction $D = uK$ and Eq. (3.9). Note that we have performed a full numerical study showing that the conclusions drawn from Figs. 3.5 and 3.6 can be unambiguously extended to the whole range $0 < \alpha \leq 1$.

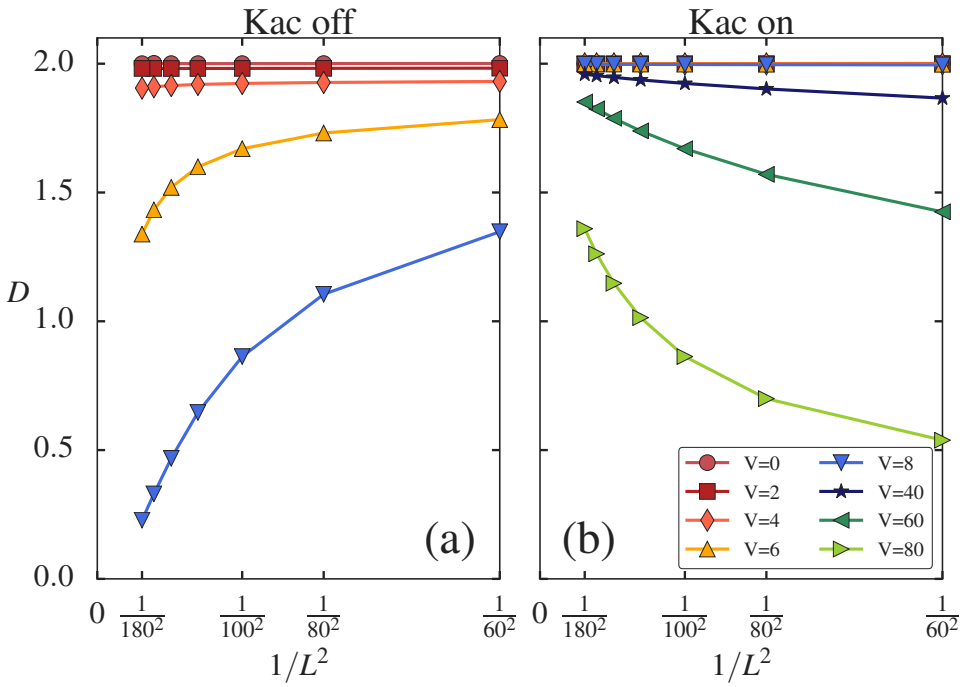

Figure 3.6: Charge stiffness D computed numerically from Eq. (3.11) at half-filling, as a function of $1/L^2$ for $\alpha = 0.5$ and different V. The magnetic flux Φ is implemented via the twisted boundary condition $c_1 = e^{i\Phi} c_{L+1}$ [292]. Two opposite trends are observed depending on whether Kac's rescaling is present **(b)** or not **(a)**. While $D \to 0$ for $L \to \infty$ in the latter case (insulator), D remains finite in the former case (metal).

3.6 Validity of the Luttinger Liquid theory

After having demonstrated in the previous section that the existence of this metallic phase can be inferred qualitatively from the Luttinger liquid theory, it is now important to study the validity of this theory. Up to now, we have only computed the Luttinger parameter K from the single-particle correlation. It is then useful to compare K obtained from different independent observables. Here, we present three of these methods.

The first one, already used in Sec. 3.5, comes from the one-body density matrix $A_{i-j} = \langle a_i^\dagger a_j \rangle$. According to Ref. [225], for a Luttinger liquid on a chain with periodic boundary condition, the one-body matrix depends on K as:

$$\begin{aligned} A(i-j) =& \bar{n}\Big(\frac{1}{\bar{n} r_{i-j}}\Big)^{\frac{1}{2K}} \times \\ & \times \Big[c_0 + \sum_{m=1}^{\infty} c_m \Big(\frac{1}{\bar{n} r_{i-j}}\Big)^{\frac{1}{2K}} \cos(2\pi \bar{n} m |i-j|)\Big] \end{aligned} \tag{3.12}$$

where c_m are model-dependent coefficient and $r_{i-j} = (La/\pi)\sin(\pi|i-j|/L)$ the chord distance. Using this formula with two harmonics ($m = 1, 2$), we perform a fit in order to extract K, denoted $K_{1\mathrm{p}}$ in the following. In Fig. 3.7, we show an example of the decay of the single-particle correlation fitted with eq (3.12) (black line), for $\alpha = 0.5$ and a strong $V = 20$. Note that this power-law behavior also confirms the metallic character observed previously.

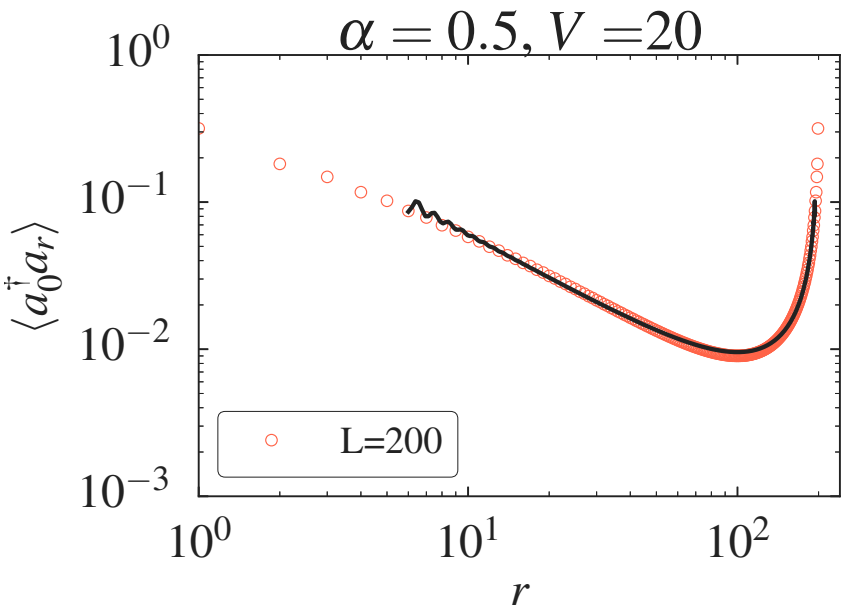

Figure 3.7: Single-particle correlation function $\langle a_0^\dagger a_r \rangle$ fitted with Eq. (3.12) (black line), for $\alpha = 0.5$ and $V = 20$.

The second independent estimate is obtained from the static structure factor:

$$S(q) = \frac{1}{L}\sum_{i,j} e^{\mathrm{i}qr_{i-j}} \left(\langle n_i n_j \rangle - \langle n_i \rangle \langle n_j \rangle\right), \tag{3.13}$$

which is predicted to scale linearly at small momenta q as

$$S_L(q) \approx q\frac{K_{2\mathrm{p}}}{2\pi}, \tag{3.14}$$

where $K_{2\mathrm{p}}$ is the size dependent Luttinger parameter. In a periodic chain with L sites, the smallest non-vanishing momenta is $q = 2\pi/L$, which yields:

$$K_{2\mathrm{p}} = LS_L(q = 2\pi/L) \tag{3.15}$$

Note that these two parameters $K_{1\mathrm{p}}$ and $K_{2\mathrm{p}}$ are size dependent, and we use a standard finite-size analysis in order to extract K in the thermodynamic limit.

Finally, combining the relations $\pi\frac{u}{K} = \frac{\partial\Delta}{\partial(1/L)}$ and $uK = D$ stemming from the LL theory [252], we obtain the third independent estimate:

$$K_{\Delta/\mathrm{D}} = \sqrt{\frac{D}{\pi\frac{\partial\Delta}{\partial(1/L)}}}. \tag{3.16}$$

In Fig. 3.9, we check the validity of the LL theory by comparing the parameter K for $L \to \infty$ and $\alpha = 0.5$ calculated from the single-particle correlation function Eq. (3.12), the static structure factor Eq. (3.15) and from the relation Eq (3.16). In the absence of Kac's rescaling [Fig. 3.9 **(a)**], a discrepancy between the values of K extracted from the two correlation functions is observed, which indicates the breakdown of the LL theory related to the opening of a gap ensuing an insulating phase. The agreement obtained for small V is attributed to the metallic character at finite L consistently with the data shown in Fig. 3.5. In the presence of Kac's rescaling [Fig. 3.9 **(b)**], the values of K extracted from the two correlation functions match well up to very large V. However, these values do not match neither K obtained from Δ and D nor the formula $K = 1/\sqrt{1 + V/[\pi v_{\mathrm{F}}(1-\alpha)]}$ (dotted line) stemming from Eq. (3.9). In Fig. 3.9, we compare the difference $K_{1\mathrm{p}} - K_{2\mathrm{p}}$ and $K_{1\mathrm{p}} - K_{\Delta/\mathrm{D}}$ as function of the exponent α for $V = 1.5$. While for short-range case $\alpha \gg 1$ all these methods gives an equivalent results in agreement with standard the Luttinger liquid theory, in the case $\alpha \leq 1$ a difference appears between the $K_{1\mathrm{p}} = K_{2\mathrm{p}}$ and $K_{\Delta/\mathrm{D}}$, which signals a breakdown of the conventional LL in the entire strong long-range regime. For $\alpha > 0$, this breakdown is only partial since numerics indicate that both $K_{\Delta/\mathrm{D}}$ and $K_{1\mathrm{p},2\mathrm{p}}$ maintain the functional form

$$K = \frac{1}{\sqrt{1 + \gamma V/(\pi v_{\mathrm{F}})}} \tag{3.17}$$

with γ finite for all V [see Fig. 3.9 **(b)**].

In order to gain physical insights we now focus on the extreme case $\alpha = 0$, which has the advantage to be exactly solvable. Here, we will see that the LL theory completely breaks down since $K_{1\mathrm{p},2\mathrm{p}} = 1$ for all V, and thus differs significantly from the functional form Eq. (3.17) ($\gamma = 0$). Interestingly, we find that $K_{\Delta/\mathrm{D}}$ is correctly described by Eq. (3.17) with $\gamma = 1$, which corresponds exactly to the analytic prediction obtained from Eq. (3.9).

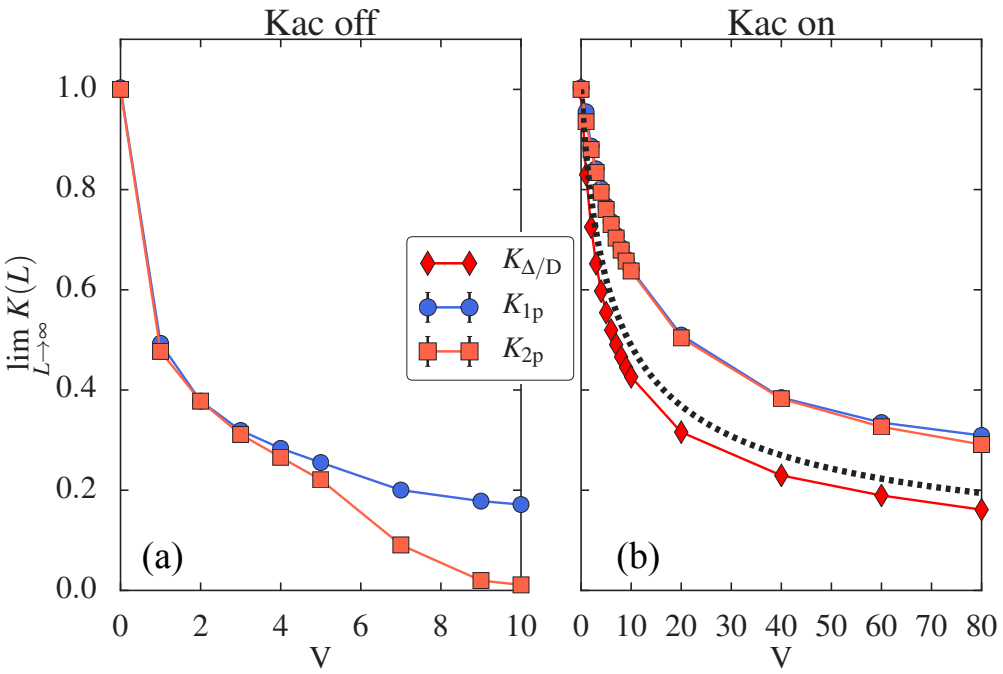

Figure 3.8: Luttinger parameter K extrapolated in the thermodynamic limit versus V at half-filling and for $\alpha = 0.5$, without **(a)** and with **(b)** Kac's rescaling. K is computed in 3 different ways: From the single-particle correlations (K_{1p}), the structure factor (K_{2p}), and from the gap and the charge stiffness ($K_{\Delta/D}$). The formula obtained from Eq. (3.9) is displayed as a dotted line. Inset: $|K_{1p} - K_{2p}|$ and $|K_{1p} - K_{\Delta/D}|$ versus α for $V = 1.5$. A discrepancy between K_{1p} and K_{2p} is observed without Kac's rescaling, which indicates the breakdown of the LL theory (insulator). In contrast, the property $K_{1p} = K_{2p}$ observed with Kac's rescaling even for large V suggests a metallic phase, which is not captured by the conventional LL theory since $K_{\Delta/D}$ does not match $K_{1p,2p}$ for $\alpha < 1$. In the short-range case $\alpha \gg 1$, one recovers $K_{1p,2p} = K_{\Delta/D}$ in agreement with the standard LL theory.

3.6.1 The extreme case $\alpha = 0$

We consider the case $\alpha = 0$ which is exactly solvable using a mean field approach on the Hamiltonian Eq. (3.7). For simplicity, we consider a fermionic Hamiltonian but we note that similar results are found with hard-core bosons.

$$H = -t \sum_{i=0}^{L-1} \left(c_i^\dagger c_{i+1} + \text{h.c.} \right) + \frac{V}{2} \sum_{i \neq j} n_i n_j,$$

where c_i ($c_i^\dagger$) annihilates (creates) a fermion on site $i = 1, \cdots, L$, and $n_i = c_i^\dagger c_i$ is the local density. Writting the density-density interaction as $n_i n_j \approx n_i \langle n_j \rangle + n_j \langle n_i \rangle - \langle n_i \rangle \langle n_j \rangle$, the mean-field Hamiltonian reads

$$H_{\text{mf}} = \sum_k \left[(N-1)\, V - 2t \cos(k) \right] c_k^\dagger c_k - \frac{N\,(N-1)\, V}{2}, \tag{3.18}$$

with $N = L/2$ the number of fermions (at half-filling), and $c_k = \frac{1}{\sqrt{L}} \sum_{j=0}^{L-1} c_j e^{-2i\pi kj/L}$. The energy of the ground state for, e.g., N even, is derived from Eq. (3.18) with anti-periodic

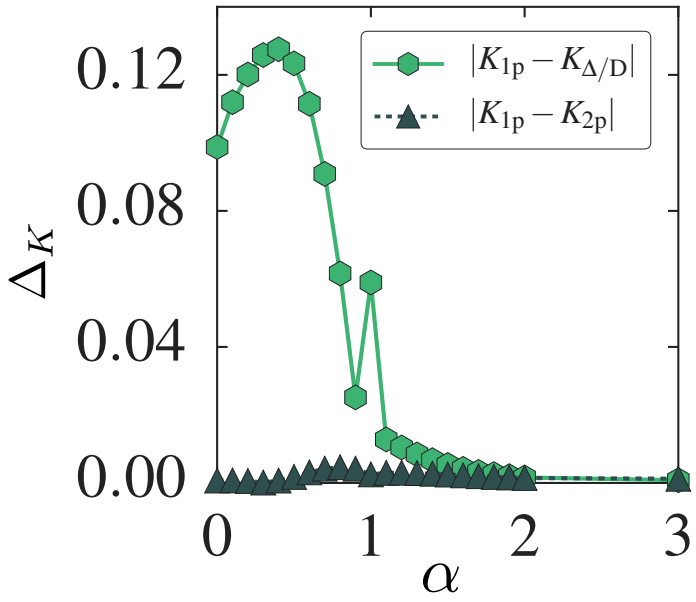

Figure 3.9: Differences $|K_{1p} - K_{2p}|$ and $|K_{1p} - K_{\Delta/D}|$ versus α for $V = 1.5$. In the short-range case $\alpha \gg 1$, one recovers $K_{1p} = K_{2p} = K_{\Delta/D}$ in agreement with the conventional LL theory. However, when $\alpha < 1$, the difference observed between $K_{1p} = K_{2p}$ and $K_{\Delta/D}$ indicates a clear breakdown of the standard Luttinger liquid theory.

boundary conditions as

$$E_0(N) = \frac{N(N-1)V}{2} - 2t \sum_{k=-L/4}^{L/4-1} \cos\left[\frac{2\pi k}{L} + \left(\frac{\pi}{L}\right)\right] = \frac{N(N-1)V}{2} - 2t \csc\left(\frac{\pi}{L}\right).$$

One then has to consider periodic boundary conditions for $N \pm 1$ fermions, which leads to

$$E_0(N+1) = \frac{(N+1)NV}{2} - 2t \sum_{k=-L/4}^{L/4} \cos\left(\frac{2\pi k}{L}\right) = \frac{(N+1)NV}{2} - 2t \cot\left(\frac{\pi}{L}\right)$$

$$E_0(N-1) = \frac{(N-1)(N-2)V}{2} - 2t \sum_{k=-L/4+1}^{L/4-1} \cos\left(\frac{2\pi k}{L}\right) = \frac{(N-1)(N-2)V}{2} - 2t \cot\left(\frac{\pi}{L}\right).$$

The charge gap thus reads $\Delta \equiv E_0(N+1) + E_0(N-1) - 2E_0(N) = V + 4t \tan\left(\frac{\pi}{2L}\right)$, and becomes $\Delta \sim (V + 2\pi t)/L \to 0$ for $L \to \infty$ when using the Kac's prescription $V \to V/L$. The Luttinger parameters u/K and uK can be related to the first derivative

of the single-particle charge gap as $\frac{\partial\Delta}{\partial(1/L)} = \pi\frac{u}{K}$, and to the charge stiffness [252] as

$$D = \pi L \left|\frac{\partial^2 E_0(N,\Phi)}{\partial\Phi^2}\right|_{\Phi=0} = uK$$

Here, $\Phi = 2\pi\phi/\phi_0$ denotes a flux threading the (circular) chain in units of the flux quantum $\phi_0 = h/e$. This flux can be taken into account by multiplying the hopping energy by a phase factor $e^{\pm \mathrm{i}\Phi/L}$ as

$$H(\Phi) = -t\sum_{i=0}^{L-1}\left(e^{\mathrm{i}\Phi/L}c_i^\dagger c_{i+1} + \text{h.c.}\right) + \frac{V}{2}\sum_{i\neq j} n_i n_j.$$

The energy of the Hartree-Fock ground state is derived as

$$E_0(N,\Phi) = \frac{N\,(N-1)\,V}{2} - 2t\csc\left(\frac{\pi}{L}\right)\cos\left(\frac{\Phi}{L}\right),$$

which provides $D = 2t = v_\mathrm{F}$ for $L\to\infty$. The Luttinger parameters extracted from the charge gap and from the charge stiffness thus read

$$uK = v_\mathrm{F} \qquad \frac{u}{K} = v_\mathrm{F}\left[1 + \frac{V}{\pi v_\mathrm{F}}\right], \tag{3.19}$$

and coincide with prediction of the Luttinger liquid theory Eq. (3.9). Since the mean-field Hamiltonian corresponds to that of free fermions, it is straightforward to calculate the Luttinger parameter K from the single-particle correlation function

$$\langle c_i^\dagger c_j\rangle = \frac{1}{L}\sum_k e^{\mathrm{i}k(i-j)}n_k = \frac{1}{2\mathrm{i}\pi}\frac{e^{\mathrm{i}k_\mathrm{F}(i-j)}}{i-j} \sim (i-j)^{-1}, \tag{3.20}$$

and from the long-wavelength limit of the static structure factor

$$\begin{aligned} S(q) &\equiv \frac{1}{L}\sum_{i,j} e^{\mathrm{i}q(i-j)}\left(\langle n_i n_j\rangle - \langle n_i\rangle\langle n_j\rangle\right) \\ &= \frac{1}{L}\sum_{k,k'}\left(\langle c_k^\dagger c_{k-q}c_{k'}^\dagger c_{k'+q}\rangle - \langle c_k^\dagger c_{k-q}\rangle\langle c_{k'}^\dagger c_{k'+q}\rangle\right) \\ &\to_{q\to 0}\frac{1}{L}. \end{aligned} \tag{3.21}$$

Note that the only non-vanishing contribution to the last equation stems from the term $\propto \langle c_k^\dagger c_{k'+q}\rangle\langle c_{k-q}c_{k'}^\dagger\rangle$, which is finite only at the two edges of the Fermi sea where $n_k = 1/2$. Comparing Eqs. (3.20) and (3.21) to the predictions $\langle c_i^\dagger c_j\rangle \sim (i-j)^{-\frac{K+(1/K)}{2}}$ and $K = LS(q\to 0)$ of the Luttinger liquid theory, we thus find $K = 1$. In this case, the free fermion result $K = 1$ extracted from the correlation functions is completely different ($\gamma = 0$) from the functional form $K = 1/\sqrt{1+\gamma V/(\pi v_\mathrm{F})}$. However, K extracted from Δ and D matches exactly the formula obtained from Eq. (3.9) ($\gamma = 1$). The demonstration of this gapless, critical metallic phase that does not fall into the conventional LL theory is a central result of this work.

We have focused so far on the case of half-filling to take the lattice effects into account via the so-called Umklapp scattering [see eq (3.10)]. However, we have seen that the latter becomes completely irrelevant in the presence of Kac's rescaling. This implies that this new unconventional metallic phase actually appears for arbitrary filling. In particular, at low density Schulz showed using bosonization techniques that the ground state of a similar system is a peculiar metal resembling a classical Wigner crystal, with very slow decay of the charge correlations associated to the plasmon mode. It is therefore interesting to understand the impact of Kac's rescaling on the plasmon dispersion relation.

3.7 Effect of energy extensivity on plasmon modes

3.7.1 One-dimensional Luttinger liquid

We consider a general one-dimensional system of length L containing N fermions interacting via the LR potential

$$V^{\alpha}(x) = \frac{V}{(x^2+a^2)^{\alpha/2}} \qquad 0 < \alpha \leq 1.$$

Here, a denotes a short-distance cutoff that can be identified with, e.g., the lattice spacing. In the vicinity of the Fermi level, the low-energy Hamiltonian can be decomposed into the contributions of left (L) and right (R) movers as

$$H = \sum_{k} \sum_{r=\mathrm{L,R}} \hbar v_{\mathrm{F}} \left(\eta_r k - k_{\mathrm{F}}\right) c^{\dagger}_{r,k} c_{r,k} + \frac{1}{2} \int \mathrm{d}x \mathrm{d}x' \rho(x) V^{\alpha}(x-x') \rho(x'), \tag{3.22}$$

where v_{F} is the Fermi velocity, k_{F} the Fermi wave vector, $\eta_{\mathrm{R}} = +1$, $\eta_{\mathrm{L}} = -1$, and $\rho(x) = \sum_{r=\mathrm{L,R}} \rho_r(x)$ with $\rho_r(x) = \frac{1}{L} \sum_{k,q} e^{iqx} c^{\dagger}_{r,k+q} c_{r,k}$. Bosonization assumes that the low-energy properties of the Hamiltonian Eq. (3.22) are governed by the long-wavelength fluctuations of the density $\rho(x)$. Using the standard techniques described in Ref. [252], H can be approximately written (for $L \to \infty$) in the quadratic form

$$H = \frac{1}{2\pi} \sum_{q} u(q) K(q) \pi^2 \Pi(q) \Pi(-q) + \frac{u(q)}{K(q)} q^2 \phi(q) \phi(-q),$$

where $u(q)$ denotes the velocity of the excitations and $K(q)$ is the Luttinger parameter governing the decay of correlations at long distances. The latter satisfy the relations

$$u(q)K(q) = v_{\mathrm{F}} \qquad \frac{u(q)}{K(q)} = v_{\mathrm{F}} \left[1 + \frac{V^{(\alpha)}(q)}{\pi v_{\mathrm{F}}}\right]. \tag{3.23}$$

The Fourier transform of the interaction potential reads

$$V^{\alpha}(q) = \int \mathrm{d}x\, V^{\alpha}(x) e^{-iqx} = V \frac{2\sqrt{\pi}}{\Gamma\left(\frac{\alpha}{2}\right) 2^{\frac{\alpha-1}{2}}} \left(\frac{|q|}{a}\right)^{\frac{\alpha-1}{2}} \mathcal{K}_{\frac{\alpha-1}{2}}(a|q|), \tag{3.24}$$

and the two fields $\Pi(q) = \int \mathrm{d}x\, \Pi(x) e^{-iqx}$ and $\phi(q) = \int \mathrm{d}x\, \phi(x) e^{-iqx}$ are the Fourier transforms of the canonically conjugate fields $\Pi(x) = \frac{1}{\pi}\boldsymbol{\nabla}\theta(x)$ and $\phi(x)$ with

$$\phi(x) = -(N_\mathrm{R} + N_\mathrm{L})\frac{\pi x}{L} - \frac{\mathrm{i}\pi}{L}\sum_{q\neq 0}\frac{1}{q} e^{-\beta|q|/2 - \mathrm{i}qx}\left(\rho_\mathrm{R}(q) + \rho_\mathrm{L}(q)\right)$$
$$\theta(x) = (N_\mathrm{R} - N_\mathrm{L})\frac{\pi x}{L} + \frac{\mathrm{i}\pi}{L}\sum_{q\neq 0}\frac{1}{q} e^{-\beta|q|/2 - \mathrm{i}qx}\left(\rho_\mathrm{R}(q) - \rho_\mathrm{L}(q)\right).$$

Here, β is a (small) cutoff regularizing the theory, $N_r = \sum_k c^\dagger_{r,k} c_{r,k} - \langle c^\dagger_{r,k} c_{r,k}\rangle$, and $\rho_r(q) = \sum_k c^\dagger_{r,k+q} c_{r,k}$. The plasmon dispersion relation follows from Eq. (3.23) and reads

$$\omega(q) = u(q)|q| = v_\mathrm{F}|q|\sqrt{1 + \frac{V^{(\alpha)}(q)}{\pi v_\mathrm{F}}}. \tag{3.25}$$

The potential Eq. (3.24) exhibits a long-wavelength divergence ($q \to 0$), namely $V^\alpha(q) \sim |q|^{\alpha-1}$ for $0 < \alpha < 1$ and $V^\alpha(q) \sim \log|q|$ for $\alpha = 1$. In the latter case, Eq. (3.25) provides the 1D plasmon dispersion $\omega(q) \sim |q|\sqrt{\log|q|}$ stemming from Coulomb interactions [280]. When rescaling the interaction potential by the Kac's factor $\Lambda_\alpha(L) = L^{1-\alpha}$ for $0 \leq \alpha < 1$ and $\Lambda_\alpha(L) = \log(L)$ for $\alpha = 1$, it is easy to check that the long-wavelength divergence of the potential is removed by considering the limit $q = \frac{2\pi}{L} \to 0$. As a consequence, one recovers the sound wave dispersion relation $\omega(q) \sim |q|$ of a metal with short-range interactions. This result is confirmed by looking at the upper bound of the excitation spectrum $\Omega(q) = E(q)/S(q)$ in the Feynman approximation [295] represented in Fig. 3.10, where $E(q) = (t/L)\left[1 - \cos(q)\right]\langle \sum_i a^\dagger_i a_{i+1} + \mathrm{h.c.}\rangle$ and $S(q)$ is the structure factor defined by Eq. (6) of the main text.

3.7.2 Generalization to higher dimensions

This result can be easily generalized to higher dimensions $d = 2, 3$ by looking at the zeros of the dielectric function in the framework of the random phase approximation (RPA):

$$\epsilon(\mathbf{q}, \omega) = 1 - \chi(\mathbf{q}, \omega) V^\alpha(\mathbf{q}) = 0, \tag{3.26}$$

where

$$\chi(\mathbf{q}, \omega) = \frac{1}{\mathcal{V}}\sum_{\mathbf{k}} \frac{n_\mathbf{k} - n_{\mathbf{k}+\mathbf{q}}}{\hbar\omega + E_\mathbf{k} - E_{\mathbf{k}+\mathbf{q}} + \mathrm{i}\eta}$$

denotes the one-spin density-density response function (Lindhard function), $\mathcal{V}$ the volume, and $n_\mathbf{k}$ the occupation number of a state with wave vector $\mathbf{k}$ and energy $E_\mathbf{k} = \frac{\hbar^2|\mathbf{k}|^2}{2m}$ (m is the particle mass). For $\alpha = 1$, the Fourier transform of the Coulomb potential is

$$\begin{aligned} V^1(q) &\sim \log|q| && d = 1 \\ V^1(\mathbf{q}) &\sim \frac{1}{|\mathbf{q}|} && d = 2 \\ V^1(\mathbf{q}) &\sim \frac{1}{|\mathbf{q}|^2} && d = 3. \end{aligned} \tag{3.27}$$

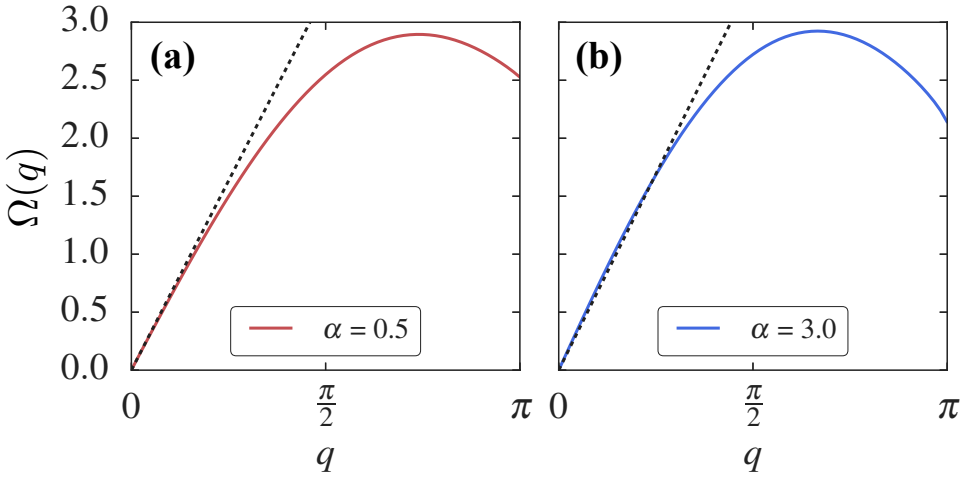

Figure 3.10: Upper bound of the excitation spectrum $\Omega(q)$ (in units of t) in the Feynman approximation (colored lines) computed at half-filling for $V = 0.5$ in the strong LR regime $\alpha = 0.5$ **(a)**, and in the short-range case $\alpha = 3$ **(b)**. The dispersion relation Eq. (3.25) after Kac's rescaling, namely $\omega(q) = v_F q\sqrt{1 + V/\pi}$ for $\alpha = 0.5$ and $\omega(q) = v_F q\sqrt{1 + V/(\sqrt{\pi}\Gamma(3/2)v_F)}$ for $\alpha = 3$ is represented as a black dotted line in the long-wavelength regime $q \to 0$. The proximity of the Mott transition ($V = 2$ for $\alpha \to \infty$) in the short-range case is responsible for the more pronounced minimum at $q = \pi$ (charge density wave).

In the dynamical limit $\omega \gg |\mathbf{q}|v_F$, the Lindhard function can be approximated by $\chi(\mathbf{q}, \omega) = \frac{\rho_0 |\mathbf{q}|^2}{m\omega^2}$ with ρ_0 the average fermion density. Using this expression together with Eq. (3.27) into Eq. (3.26), one finds the plasmon energies

$$\begin{aligned} &\omega \sim |q|\sqrt{\log|q|} && d = 1 \\ &\omega \sim \sqrt{|\mathbf{q}|} && d = 2 \\ &\omega \sim \text{cst} && d = 3. \end{aligned} \tag{3.28}$$

When using the Kac's prescription, namely dividing the potential by the factor L^{d-1}, the long-wavelength divergence ($q = \frac{2\pi}{L} \to 0$) is removed and one recovers the sound wave dispersion relation $\omega \sim |\mathbf{q}|$ for $d = 1, 2, 3$.

3.8 conclusion

In this chapter, we have investigated the ground state properties of one-dimensional hard-core bosons interacting via a variable long-range potential using the density matrix renormalization group.

In the first part of the study, we have demonstrated that restoring energy extensivity in the system, which is done by rescaling the interaction potential with the Kac's prescription, has a profound influence on the low-energy properties of the system. In the thermodynamic limit, while an insulating phase is found in the absence of Kac's rescaling, the latter leads to a metallic phase for finite interaction strengths. We have demonstrated that the numerical results are consistent with the predictions of the Luttinger theory.

In the second part, we have investigated the validity of the Luttinger theory by comparing the Luttinger parameter K obtained from three independent observables, namely the structure factor, the one-body correlations, and the charge gap combined with the charge stiffness. We have found a discrepancy between these parameters, which indicates that the new metallic phase is not captured by the conventional Luttinger theory, although the latter still provides the correct functional behavior in the strong LR regime expect in the case $\alpha = 0$.

In the last part of the study, we have shown that restoring extensivity eliminates the plasmon mode while preserving the LR character of the potential, and with it some inherent properties of the strong LR regime such as non-addivity.

Chapter 4

The fate of Anderson localization under large light-matter coupling

Localization was a different matter: very few believed it at the time, and even fewer saw its importance; among those who failed to fully understand it at first was certainly its author. It has yet to receive adequate mathematical treatment, and one has to resort to the indignity of numerical simulations to settle even the simplest questions about it.

Philip W. Anderson, Nobel Lecture, 8 December, 1977

When a quantum emitter has an internal transition energy resonant with the frequency of a cavity mode, a coupling g between the two can lead to the formation of mixed light-matter states, known as "polaritons", and physics governed by the extensively studied Jaynes-Cummings model [113, 296–298]. In the single-excitation limit the physics is characterized by a vacuum Rabi splitting of two polariton modes proportional to g. Importantly, for an ensemble of N coupled emitters [299, 300], this splitting is enhanced collectively and proportional to the collective coupling $g_c = g\sqrt{N}$, which allowed for experimental observations of vacuum Rabi splittings in optical cavities already in the 80s [301, 302]. The regime of strong coupling regime, i.e when the rate of energy exchange between a cavity mode and the atoms exceeds the dissipation rates set by photon losses and spontaneous emission [114], has been nowadays pursued throughout physics, e.g. in atomic physics [303–306] and with artificial emitter-cavity systems in condensed matter physics [307–314].

Recently, strong and even ultrastrong coupling of molecules [315] to a confined mode of the electromagnetic field has become a promising research direction with possible applications for modifying material properties or chemical reactions [316–325]. A particular interest has been the modification of transport properties for energy [326, 327] or charges [328–333]. Two crucial aspects of molecular systems are the presence of molecular vibrations and large amounts of disorder. Here we focus on heavily disordered, e.g. in the local energy, ensembles of two-level quantum emitters.

While the effect of the disorder is known to hardly affect the polariton splitting [334], it instead can modify the dark states significantly [335]. On the other hand, disordered systems without a cavity have been extensively studied since the discovery of Anderson localization [336, 337]. In this scenario, a disordered medium prevents the diffusion of quantum waves, and the latter are generally localized exponentially by the disorder. Furthermore, it is well known from scaling theory and numerical analysis that a metal-insulator (MI) transition is present in three dimensional models.

Here, we analyze the fate of the Anderson transition between localized and extended

eigenstates for the dark states of a cavity coupled system.

In this chapter, we study an ensemble of disordered quantum emitters strongly coupled to a cavity mode. In Sec. 4.1, we first introduce the model and restrict ourselves to a Hilbert space with a single excitation in the system, which could be an electron-hole pair in the exciton transport problem, for instance. When the excitation is coupled to a cavity mode we already note striking differences for the spatial distribution of the excitation that we analyse as a function of the collective coupling g_c. Then to pursue further the analysis, in Sec. 4.2 , we draw the phase diagram of our model using some localization quantifiers such as the return probability or the inverse participation ratio. We find that in the large coupling regime, a new semi-localized phase appears. We study in detail this novel phase on the paradigm of the Anderson localization with a level statistic analysis and the determination of the fractal dimension. Since we are mainly interested in the transport properties of the system, we then focus on the diffusion in Sec. 4.4 and transfer probability in Sec. 4.5. In both cases, we shed light on the important contribution of the dark states and show that they can significantly enhance energy transfer properties in disordered systems.

Since a deeper analysis of the presented results is still work in progress, this chapter reviews the preliminary results we have obtained so far.

4.1 Model

We consider an Anderson localization model for an ensemble of N quantum emitters on a 3D cubic lattice (lattice constant $a \equiv 1$). The Hamiltonian is $\hat{H} = \hat{H}_T + \hat{H}_D + \hat{H}_C$ with

$$\hat{H}_T = -J \sum_{\langle \boldsymbol{i},\boldsymbol{j} \rangle} \hat{\sigma}_{\boldsymbol{i}}^\dagger \hat{\sigma}_{\boldsymbol{j}} \qquad \hat{H}_D = \sum_{\boldsymbol{i}} w_{\boldsymbol{i}} \hat{\sigma}_{\boldsymbol{i}}^\dagger \hat{\sigma}_{\boldsymbol{i}}. \tag{4.1}$$

Here, $\hat{\sigma}_{\boldsymbol{j}} = |g\rangle \langle e|_{\boldsymbol{i}}$ destroys an excitation on emitter $\boldsymbol{i} = (i_x, i_y, i_z)$ (3D lattice index). $\hat{H}_T$ governs hopping of excitations between nearest neighbors, indicated by the notation $\langle \boldsymbol{i}, \boldsymbol{j} \rangle$. $\hat{H}_D$ contains on-site disorder, and $w_{\boldsymbol{i}}$ is drawn randomly from a uniform distribution $w_{\boldsymbol{i}} \in [-W/2, W/2]$ with width W. Additionally the emitters couple to a cavity mode with bosonic photon annihilation operator $\hat{a}$ with strength g via

$$\hat{H}_C = g \sum_{\boldsymbol{i}} (\hat{a}\hat{\sigma}_{\boldsymbol{i}}^\dagger + \hat{a}^\dagger \hat{\sigma}_{\boldsymbol{i}}). \tag{4.2}$$

Note that we will restrict ourselves to a Hilbert-space with a single excitation in the system, $\sum_{\boldsymbol{i}} \hat{\sigma}_{\boldsymbol{i}}^\dagger \hat{\sigma}_{\boldsymbol{i}} + \hat{a}^\dagger \hat{a} = \mathbb{1}$. Furthermore we consider the cavity frequency ω_c in resonance with the emitters ω_e, and neglect the constant energy $\hat{H}_0 = \omega_e \sum_{\boldsymbol{i}} \hat{\sigma}_{\boldsymbol{i}}^\dagger \hat{\sigma}_{\boldsymbol{i}} + \omega_c \hat{a}^\dagger \hat{a} = (\omega_e)\mathbb{1}$ for $\omega_e = \omega_c$.

Without disorder the Hamiltonian can be brought to a diagonal form

$$\hat{H}_T + \hat{H}_C = \sum_{\boldsymbol{q}} \epsilon_{\boldsymbol{q}} \hat{b}_{\boldsymbol{q}}^\dagger \hat{b}_{\boldsymbol{q}} + \sum_{\mu=\pm} E_\mu \hat{P}_\mu^\dagger \hat{P}_\mu. \tag{4.3}$$

Here, the two polariton operators are defined as $\hat{P}_\pm = (\hat{a} \pm \hat{b}_{\boldsymbol{0}})/\sqrt{2}$ and the quasi-momentum operators are $\hat{b}_{\boldsymbol{q}} = (1/\sqrt{N}) \sum_{\boldsymbol{i}} \exp(-\mathrm{i}\boldsymbol{q} \cdot \boldsymbol{i}) \hat{\sigma}_{\boldsymbol{i}}$, where the discrete quasi-momentum

index can assume values $\boldsymbol{q} = (q_x, q_y, q_z)$, $q_{x,y,z} \in [-\pi, \pi]$ (we assume periodic boundary conditions). The band energies are $\epsilon_{\boldsymbol{q}} = -2J[\cos(q_x) + \cos(q_y) + \cos(q_z)]$. The single bright mode of the system, $\hat{b}_{\boldsymbol{0}} = \hat{b}_{(0,0,0)}$, couples to the cavity forming the two polariton modes with energy $E_\pm = \pm g\sqrt{N}$. Besides the two polaritons, there exist $N-1$ dark state modes $\hat{b}_{\boldsymbol{q}\neq\boldsymbol{0}}$.

In the presence of disorder, the bright and the dark states will mix among each others since in quasi-momentum space for large N

$$\hat{H}_D = \frac{1}{N}\sum_{\boldsymbol{q},\boldsymbol{k}}\sum_{\boldsymbol{i}} w_{\boldsymbol{i}} \mathrm{e}^{\mathrm{i}(\boldsymbol{k}-\boldsymbol{q})\cdot\boldsymbol{i}} \hat{b}^\dagger_{\boldsymbol{q}} \hat{b}_{\boldsymbol{k}} \tag{4.4}$$

$$= \frac{1}{N}\sum_{\boldsymbol{q}} \hat{b}^\dagger_{\boldsymbol{q}} \hat{b}_{\boldsymbol{q}} \sum_{\boldsymbol{i}} w_{\boldsymbol{i}} \tag{4.5}$$

$$+ \frac{2}{N}\sum_{\boldsymbol{q}>\boldsymbol{k}}\sum_{\boldsymbol{i}} w_{\boldsymbol{i}} \cos\left[(\boldsymbol{k}-\boldsymbol{q})\cdot\boldsymbol{i}\right]\left(\hat{b}^\dagger_{\boldsymbol{q}}\hat{b}_{\boldsymbol{k}} + \hat{b}^\dagger_{\boldsymbol{k}}\hat{b}_{\boldsymbol{q}}\right) \tag{4.6}$$

In the collective large coupling regime, i.e. if $g\sqrt{N} \gg J, W$, the spectrum of the full Hamiltonian still contains two distinct polariton states [334]. Here, we are interested in the remaining $N-1$ dark states in the presence of disorder. While without a cavity, N single-excitation states exhibit the well-studied behavior of being either extended or localized, we find that large collective coupling enforces the $N-1$ dark states to spread over N sites on average, which can have important implications as shown in the following.

In Fig. 4.1 panel (a) left and right, we present a sketch of the model without and with the cavity, respectively. In panel (b), we show the disorder averaged (~ 1000 realizations) spatial density distribution of a single excitation, given by the absolute value of the eigenvector $|\Psi_j|^2$. In the left, we present the probability without cavity (red, $g_\mathrm{c} = 0$) and small collective coupling ($g_\mathrm{c} \neq 0$). We see that the excitation decays exponentially in the absence of the cavity in agreement with the prediction of Anderson localization. For small coupling $g_\mathrm{c} < W/2$, after the exponential decay, we observe the appearance of a plateau that extends over all sites in the chain. The corresponding height scales with the coupling g_c. Roughly speaking, the decay can now be described by :

$$|\Psi|^2_W \approx e^{-j/\zeta} + \gamma(g_\mathrm{c}) \tag{4.7}$$

where the subscript W indicates averaging over the disorder distribution, ζ is the localization length and $\gamma(g_\mathrm{c})$ is here an unspecified function of g_c. In the right panel, by increasing the coupling up to $g_\mathrm{c} > W/2$, we find that the plateau saturates to a maximum value. This situation corresponds to a large coupling regime. In the following, we focus on the large coupling regime where the value of the $\gamma(g_\mathrm{c})$ in Eq. (4.7) is maximal. We are interested in investigating its effects to Anderson localization in this regime.

In this chapter, we only focus on this large coupling regime.

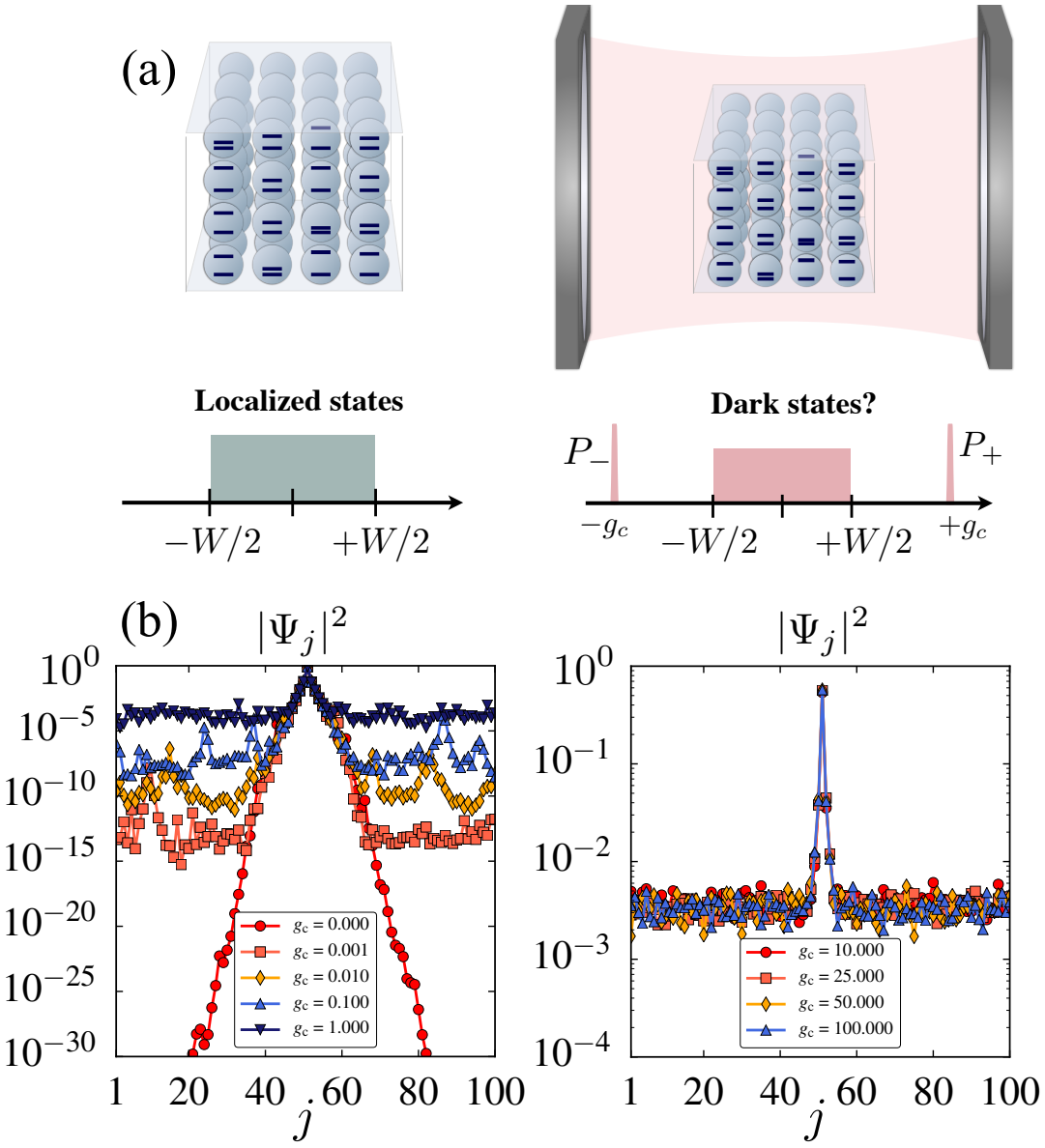

Figure 4.1: Panel (a) left: a strongly disordered system has a band of localized states with a width given by the disorder strength W. Right: When strongly coupled to a cavity mode, two polaritonic states appear (P_- and P_+). Here we study the modified localization properties of the remaining dark states. Panel (b): disorder averaged (~ 1000 realizations) spatial distribution of a single excitation, given by the absolute value of the eigenvector $|\Psi_j|^2$, for different collective coupling strength g_c and a disorder strength $W = 25$. Left : Without the cavity (red), we observe that $|\Psi_j|^2$ decays exponentially as expected by Anderson localization. For a small value of the coupling strength $g_c < W/2$, we see the appearance of a plateau whose height scales with g_c and which is present after an exponential decay at the center ($j = 50$). Right: for large $g_c > W/2$, the plateau saturates, becoming independent of g_c.

4.2 Phase diagram

In this section, we analyze the localization properties of our system by using the return probability, the inverse participation ratio, a level spacing analysis and the fractal dimension.

4.2.1 Return probability and IPR

Let us first consider the so-called return probability that is the probability to stay at the same site as a function of time t, which gives information about the localization phenomenon. Indeed, when a system features the Anderson localization the excitation remains exponentially localized where it was introduced initially, and thus the probability tends to a maximum value of 1. On the contrary, in a diffusive system, the probability to remain on a given site decreases with time due to the possibility to easily jump from site to site.

We initialize the system as $|\psi_0\rangle = |c\rangle$, i.e. the excitation is initially located at the site c. We compute the probability to stay at this site as

$$P_{cc}(t) = |\langle c|\psi_t\rangle|^2 = \langle\psi_t|c\rangle\langle c|\psi_t\rangle.$$

This equation shows that the expectation value of the projector $|c\rangle\langle c|$ equals the probability to stay at the corresponding site with $P_{cc}(0) = 1$, by definition. The time-evolved state can be generally written as

$$|\psi_t\rangle = e^{-iHt}|c\rangle = \sum_\alpha e^{-iE_\alpha t}|\alpha\rangle\langle\alpha|c\rangle$$

where $|\alpha\rangle$ are the eigenstates of the Hamiltonian H, $H|\alpha\rangle = E_\alpha|\alpha\rangle$, with eigenenergies E_α. Using $\langle c|\psi_t\rangle = \sum_\alpha \exp(-iE_\alpha t)|\langle\alpha|c\rangle|^2$ the probability to stay at site c can be written as

$$\begin{aligned} P_{cc}(t) &= \sum_{\alpha,\alpha'} e^{-i(E_\alpha - E_{\alpha'})t}|\langle\alpha|c\rangle|^2|\langle\alpha'|c\rangle|^2 \\ &= \sum_\alpha |\langle\alpha|c\rangle|^4 + \sum_{\alpha\neq\alpha'} e^{-i(E_\alpha - E_{\alpha'})t}|\langle\alpha|c\rangle|^2|\langle\alpha'|c\rangle|^2. \end{aligned} \tag{4.8}$$

From Eq. (4.8) and if one considers the situation of non-degenerate eigenstates, we can compute the time-averaged probability $\overline{P_{cc}(t)} = \int_0^t dt' P_{cc}(t')/t$ to stay at site c as

$$\begin{aligned} \overline{P_{cc}(t)} &= \sum_\alpha |\langle\alpha|c\rangle|^4 + \sum_{\alpha\neq\alpha'} \frac{(e^{-i(E_\alpha - E_{\alpha'})t} - 1)}{-i(E_\alpha - E_{\alpha'})t}|\langle\alpha|c\rangle|^2|\langle\alpha'|c\rangle|^2 \\ &= \sum_\alpha |\langle\alpha|c\rangle|^4 + \sum_{\alpha\neq\alpha'} \frac{\sin[(E_\alpha - E_{\alpha'})t]}{(E_\alpha - E_{\alpha'})t}|\langle\alpha|c\rangle|^2|\langle\alpha'|c\rangle|^2. \end{aligned}$$

Then, the long-time limit of the time-averaged probability $\overline{P_{cc}(t)}$ is given by

$$\Pi_{cc} = \lim_{t\to\infty} \overline{P_{cc}(t)} = \sum_\alpha |\langle\alpha|c\rangle|^4. \tag{4.9}$$

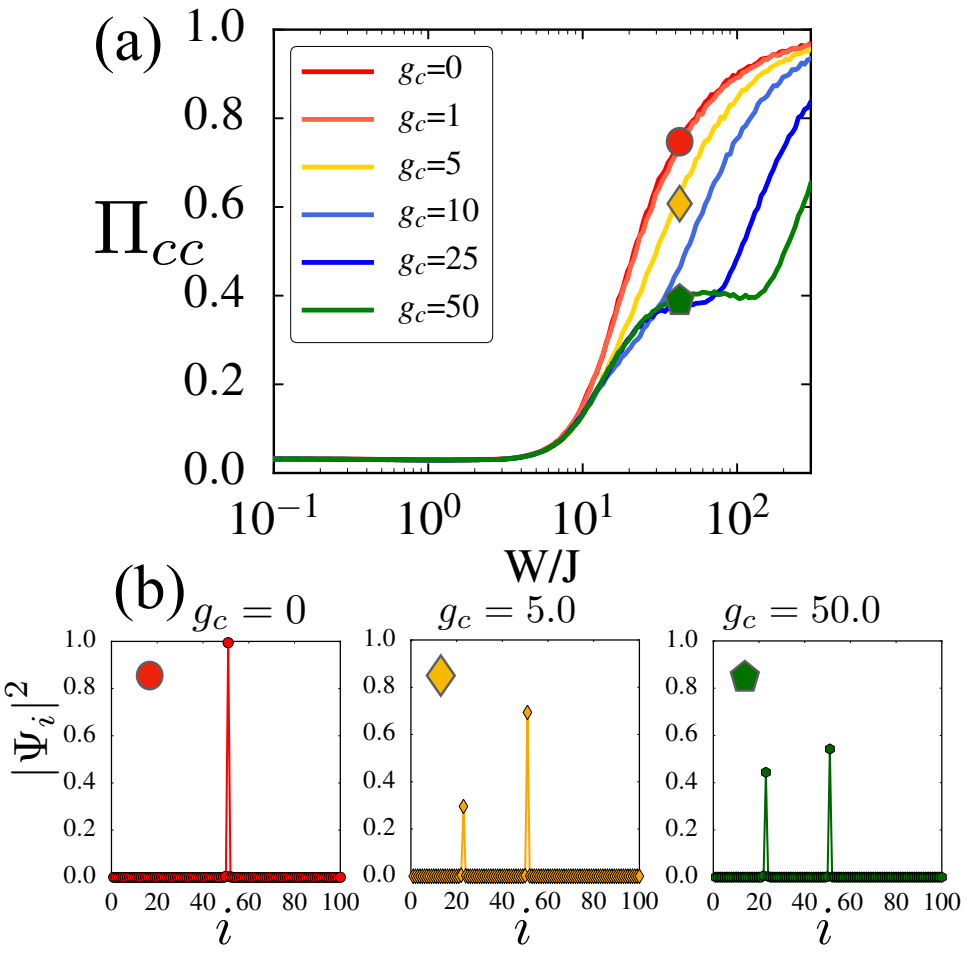

Figure 4.2: Panel (a): long-time disorder averaged (~ 300 realizations) probability (Π_{cc}) to stay at the initial site as function of the disorder strength for different collective coupling strengths g_c and $N = 5^3$ size. For small coupling, we observe that the return probability increases with the disorder, as expected for the Anderson localization. At small finite disorder, this probability is small indicating a delocalized phase. However, in the large coupling regime $g_c \gg W/2$, we see the emergence of an intermediate region, where the probability remains finite $\Pi_{cc} \sim 0.4$. Panel (b): exemplary wave functions for a one-dimensional chain of $N = 100$ for one disorder realization, for $g_c = 0$ (left), $g_c = 5$ (middle), and $g_c = 50$ (right).

Concerning the non-degeneracy of the eigenstates, we remark that in the case without disorder and light-matter coupling, the eigenstates are known to be non-degenerate (Bloch states and corresponding dispersion for open boundary conditions). We assume that this also holds in the situation with disorder and light-matter coupling [1].

In Fig. 4.2, we show the long-time limit of the time-averaged probability Π_{cc} as function of the disorder strength for different collective coupling strength $g_0 = 0, 1, 5, 10, 25, 50$ and a cube of $N = 5^3$. The case without cavity ($g_c = 0$) corresponds to the usual Anderson model. In this case a metal-insulator transition should take place at $W_c = 16.5$ (for energy lying in the middle band spectrum) [338–342]. In Fig. 4.2, we observe two

[1] except for a vanishingly small number of realizations

regimes: I) at small disorder $\Pi_{cc} \sim 0$ indicates that the excitation spreads over the whole sample, i.e. to extended states. II) For strong disorder, the Π_{cc} tends to a maximum value close to one, suggesting a complete localization of the excitation. The two regions are separated by an interesting regime, where the probability rapidly increases with the disorder strength. That region ($15 < W < 30$) corresponds roughly to the prediction of the metal-insulator transition. When we turn on the cavity-coupling, we find that at small collective coupling the behavior of Π_{cc} is qualitatively similar despite a small shift. Interestingly, for a large coupling strength, we observe the emergence of a new intermediate region for $W_c \lesssim W \lesssim 2g_c$, where $\Pi_{cc} \sim 0.4$ [see e.g. $g_c = 50$].

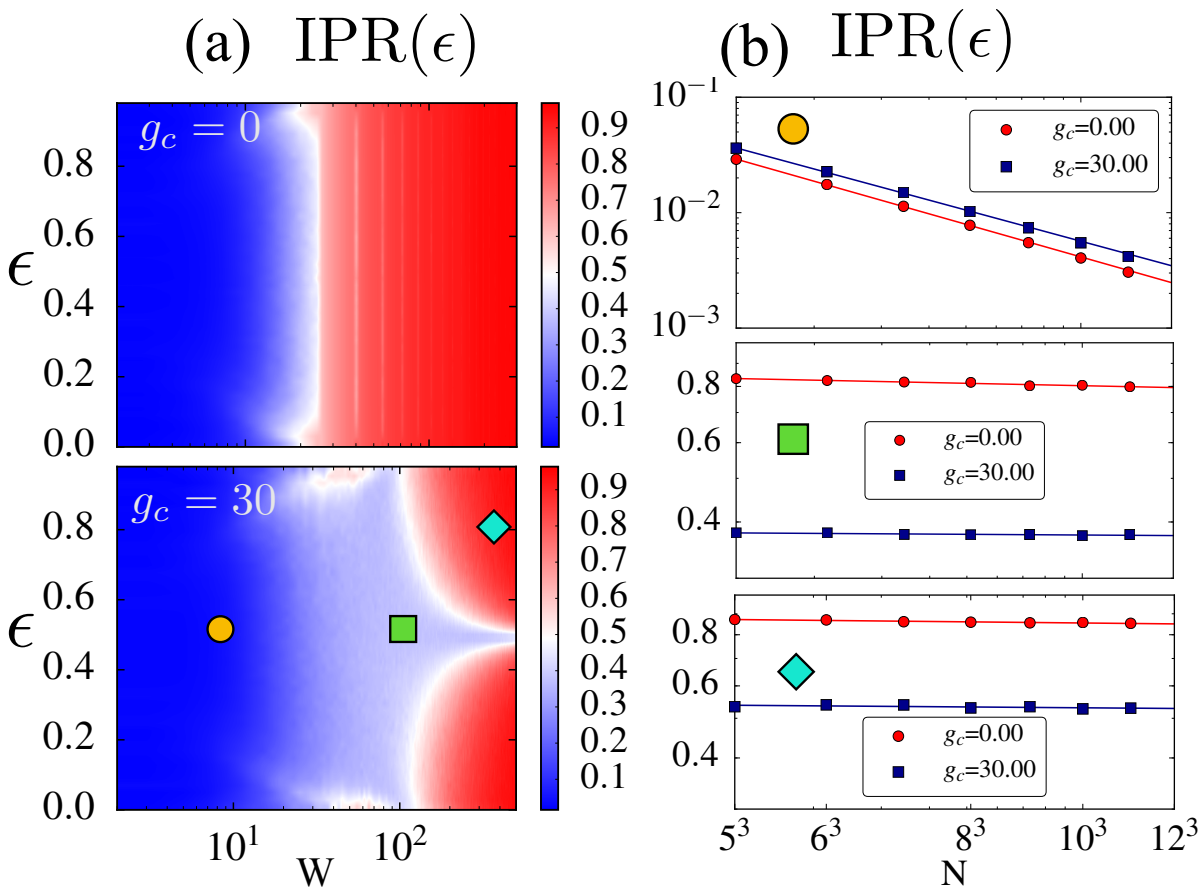

Figure 4.3: Panel (a): Inverse participation ratio I_2 for $N = 5^3$ as function of the disorder strength and the dimensionless rescaled energy ϵ [see Eq. (4.12)], for $g_c = 0$ (upper panel) and $g_c = 30$ (lower panel). Panel (b): finite-size scaling of I_2 for different ϵ and disorder strength W. The values we choose are indicated by the symbols in the lower panel in (a).

One can notice that the expression Eq. (4.9) is reminiscent of the inverse participation ratio (IPR). The IPR quantifies how many sites participate to a given eigenstate, with respect to a certain basis and thus gives a measure of the degree of localization in the system. Here, if one considers the normalized eigenstates $|\alpha\rangle$, the IPR reads:

$$\mathrm{IPR}(\mathrm{E}_\alpha) = \sum_{\mathrm{c}} |\langle \alpha | \mathrm{c} \rangle|^4, \tag{4.10}$$

where E_α is the energy of the corresponding eigenstate $|\alpha\rangle$, c labels the site index.

From the formula Eq. (4.9) and Eq. (4.10), we see that

$$\frac{1}{N}\sum_{c}\Pi_{cc} = \frac{1}{N}\sum_{c}\sum_{\alpha}|\langle\alpha|c\rangle|^4 = \frac{1}{N}\sum_{\alpha}\mathrm{IPR}(\mathrm{E}_\alpha). \tag{4.11}$$

In other words, the mean survival probability is equal to the mean average IPR [2]. So far, we have shown that an intermediate plateau emerges in the survival probability in the large coupling regime and since this observable is closely connected to the IPR, we also expect that the latter changes. The IPR is widely used to characterize localization properties as function of the energy spectrum, since an IPR scaling to a finite value in the thermodynamic limit indicates a localized phase, while an IPR scaling to zero as $1/L^D$ (D is the dimension) indicates a delocalized phase. Furthermore, the IPR allows to observe a separation in energy between localized and delocalized states, i.e. a mobility edge. It is well known that a single-particle mobility edge is present in the standard Anderson model, which according to the argument of Lifshitz appears first to the band tail [343]. It is therefore an interesting question to see how this picture is modified within the large coupling regime. Here, in order to compare the energy between different states and over different realizations of the disorder (~ 200), we define a dimensionless energy:

$$\epsilon = \frac{E_\alpha - \min(\mathrm{E}_\alpha)}{\max(\mathrm{E}_\alpha) - \min(\mathrm{E}_\alpha)}. \tag{4.12}$$

When the polaritons are discarded, as in Fig. 4.3, then $\max(\mathrm{E}_\alpha) = \mathrm{W}/2$ and $\min(\mathrm{E}_\alpha) = -\mathrm{W}/2$. In the numerics, we bin the IPR (~ 100 realizations) into groups of equal energy windows ($\epsilon \pm \delta_\epsilon = 0.02$) and average within each bin.

Fig. 4.3 (a) shows the Inverse Participation Ratio as function of the disorder strength (in log scale) and the dimensionless energy for a cube of $N = 5^3$ sites. The upper panel presents the standard Anderson model, where we see a clear separation between extended and localized states as W increases. We can not identify precisely the mobility edge and the transition point, which we attribute to important finite-size effects. In the lower panel, $g_\mathrm{c} = 30$ and we find that a new intermediate region appears with a *constant* value of the IPR close to 0.4 for all the spectrum [see Fig.4.2]. This *large* coupling regime corresponds approximatively to $W_c \lesssim W \lesssim 2g_\mathrm{c}$ as expected from the return probability [see Fig.4.2]. For a disorder $2g_\mathrm{c} \lesssim W$, the usual localized phase appears again, starting from the band tails, which implies an energy separation between this new intermediate region and the fully localized phases. Furthermore, we note that the IPR for mid-spectrum modes remains close to values of about 0.4 up to very strong disorder, suggesting an important robustness of this novel phase against disorder. In Fig. 4.3 (b), we then show a finite size analysis in three regions [symbols in Fig. 4.3 panel (a)]. From that, we observe that the IPR scales similarly in both regimes, without cavity (red) and in the large coupling regime (blue). We however note a shift of the value of the IPR. This similar scaling suggests at first glance that the localization properties are not deeply modified by the presence of the cavity. In order to investigate this point in more detail, in the next section, we focus on this novel intermediate region.

[2] The complete basis should be used to obtain this equality, which implies to take into account the photon state, we expect that the latter is getting less relevant in the limit $N \gg 1$.

4.2.2 Energy level statistics & Fractal Dimension

By looking at the level spacing distribution and the fractal dimension, we now analyse and characterize in detail this novel phase.

First, we consider the spectrum of the eigenenergies which is known to be qualitatively different for an insulator (localized regime), a critical phase and a metal (delocalized regime). The quantitative difference can notably be measured by looking at the level spacing between subsequent eigenenergies:

$$s_n = E^{\alpha}_{n+1} - E^{\alpha}_{n}. \tag{4.13}$$

Indeed, the probability distribution $P(s)$ features diffferent behaviour depending on whether the systems is metallic, critical or localized [344].

For a metallic system, the random matrix theory states that $P(s)$ follows a universal behaviour, which depends only on the physical symmetry present in the system. The generalized distribution can be formulated as follows:

$$P_{\beta}(s) = a_{\beta} s^{\beta} \exp\left(-b_{\beta} s^2\right) \tag{4.14}$$

where $\beta = 1, 2, 4$, for orthogonal, unitary and symplectic symmetry, respectively. The coefficient a_{β} and b_{β} are obtained from the normalization condition, i.e. $\int \mathrm{d}s P(s) = \int \mathrm{d}s P(s) s = 1$. In our case, it can be shown that the eigenenergies of our Hamiltonian H with small disorder are characterized by a function $P(s)$ that belongs to the Wigner-Dyson of the Gaussian Orthogonal Ensemble (GOE), which yields to the form ($\beta = 1$):

$$P_{\beta=1}(s) = \frac{\pi}{2} s \exp\left(-\frac{4}{\pi} s^2\right) \tag{4.15}$$

One important characteristic of the Wigner-Dyson distribution is the level repulsion, i.e. $P(s) \to 0$ for $s \to 0$, which implies an absence of degeneracy in the metallic (delocalized) spectrum due to the overlap of the wave function.

For an insulator the situation is different as the spectrum is now governed by random energies and thus the levels are completely uncorrelated. In this case, the distribution $P(s)$ is close to the Poisson distribution [345]:

$$P_{\mathrm{loc}}(s) = \exp(-s). \tag{4.16}$$

Indeed, site with levels close in energies can now be separated by a large distance, preventing the overlap of their respective wave-functions. We then expect that in the localized regime, the level spacing is Poisson distributed.

Interestingly, the transition between a metal and an insulator is characterized by a universal (independent of the system size) statistics. At the critical point, the distribution has been widely studied [341, 346–349]. Those studies suggest that $P(s)$ features elements from both Poisson and Wigner distribution. Despite the fact that the analytical form is not known, the numerical analysis has shown that $P(s)$ behaves as $s^{\beta=1}$ for $s \ll 1$ and with an exponential tail for $s \gg 1$. Several predictions have been proposed to describe the distribution of $P(s)$, e.g. a simple distribution intermediate between the WD and

the Poisson distributions can be obtained by taking the middle of a Poissonian sequence. The latter was denoted Semi-poisson [350] and is given by:

$$P_{\text{semi-poisson}}(s) = 4s\exp(-2s) \tag{4.17}$$

Unfortunately, even with numerical results the different predictions can not be distinguished [351]. One fundamental reason could be that boundary conditions play a crucial role in the distribution behavior [352].

In order to study numerically the level spacing, we study a cube of different N and different disorder strength. We diagonalize the corresponding Hamiltonian with open boundary conditions for several disorder realizations and compute the rescaled energies (see Eq. (4.12)). We consider only dimensionless energies close to 0.5, i.e. mid-spectrum, where the density of states can be considered as constant. Then, we compute the consecutive energy difference $s_n = \epsilon^{\alpha}_{n+1} - \epsilon^{\alpha}_{n}$ and normalize the latter by the mean spacing average. Results of the level spacing are presented in Fig. 4.3, for two disorder strengths $W = 5$ (left) and $W = 50$ (right). In panels (a) and (c), we consider the standard Anderson model for weak and strong disorder, respectively, and we find a complete agreement with previous studies [353]. At small disorder (extended states, panel (a)) the distribution is Wigner-Dyson type while in the localized regime (strong disorder, panel (b)), $P(s)$ is Poissonian distributed. Hence, in panels (b) and (d) we consider the large coupling regime $g_c = 30$. First, we observe that in the delocalized [see panel (b)] regime, the situation is similar to that without cavity. However, at strong disorder [see panel (d)] $P(s)$ has a semi-poissonian form, which confirms the presence of a new type of localized phase that we denote semi-localized phase.

Note that this semi-poisson distribution seems reminiscient of the universal distribution encoutered at the metal-insulator (MI) transition. At this transition, the wave functions undergo a multifractal behavior, as defined below, describing their strong fluctuations at the criticality. In other words, the system shows scale invariance at the criticality. This behavior can be observed using the generalized inverse participation ratio which is given by

$$\mathrm{I_q(E_\alpha)} = \sum_{\mathrm{c}} |\,\langle \alpha|\mathrm{c}\rangle\,|^{2\mathrm{q}}. \tag{4.18}$$

In the thermodynamic limit, the generalized IPR scales according to:

$$I_q \sim L^{-D_q(q-1)}, \tag{4.19}$$

where D_q is the fractal dimension, D the dimension of the model considered and L the system size. We then distinguish 3 different regimes:

I) $D_q \to D$ independenly of q indicates extended states.

II) $D_q \to \gamma(q)$, a finite value which depends of q. This is called a multifractal behavior.

III) $D_q \to 0$ independently of q indicates fully localized states.

To determine if the wave function features a particular fractal behavior, we realize a finite-size analysis of I_q to extract the fractal dimension in our model, for $W = 50$. In Fig. 4.5 panel (a) and panel (b), we present a finite-size scaling analysis of the generalized inverse participation ratio I_q, for eigenenergies lying in the middle of the spectrum, i.e.

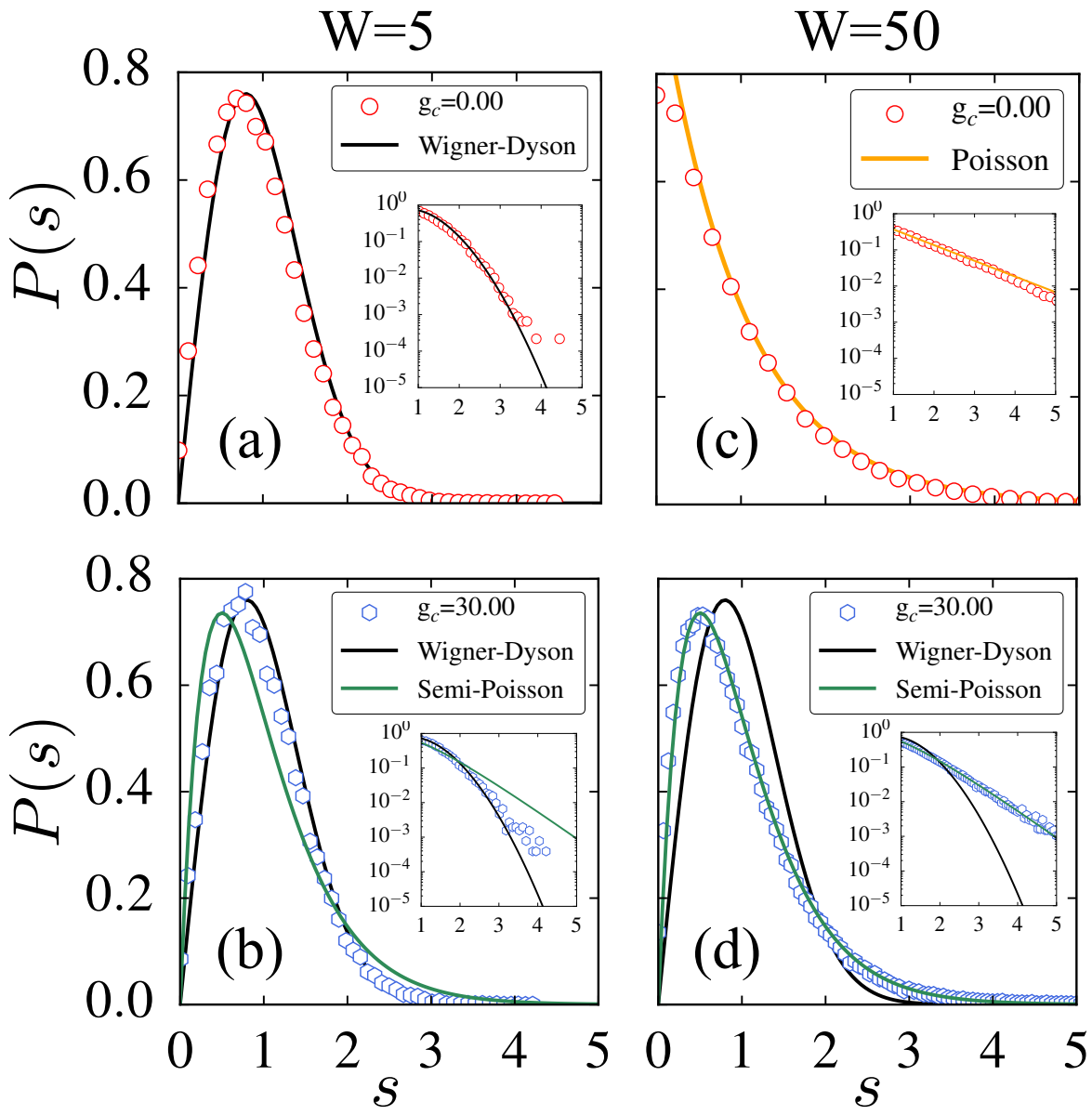

Figure 4.4: Panel (a) and (c) : Level spacing distribution $P(s)$ for the 3D Anderson model ($g_c = 0$ (red circle)) for a disorder strength $W = 5$ and $W = 50$, respectively. At small disorder the level spacing follows a Wigner-Dyson distribution [see (a) black line], indicating a delocalized phase. At strong disorder the level spacing is Poisson distributed [see (c) orange line], indicating a localized phase. These results are in agreement with what we expect for the standard Anderson model. Panel (b) and (d), 3D Anderson model coupled to a cavity mode in the large coupling limit ($g_c = 30$ (blue diamond)) for a disorder strength $W = 5$ and $W = 50$, respectively. At small disorder (b), the behavior is similar that in (a) [see (b) black line], however, for strong disorder, the level spacing follows now a Semi-Poissonian distribution [see (d) green line] in stark contrast with the Poisson distribution observed in (c). Insets show the tail of the level spacing distribution on a logarithmic scale.

$\epsilon = 0.5 \pm 0.02$, for $g_c = 0$ and $g_c = 30$, respectively. We then perform a fit using Eq. (4.19) to extract the effective fractal dimension D_q, and the resulting exponents are shown in Fig. 4.5 panel (c). We find that both cases feature the same behavior; D_q seems to go to 0 independently of q, which indicates an absence of multi-fractality in our system. Here, due to the small value of D_q and the strong disorder, obtaining a relevant precision is challenging. The results suggest that there is no multi-fractal behavior in the large coupling regime. Note that, a similar analysis might become more relevant at the transition point of the MI transition.

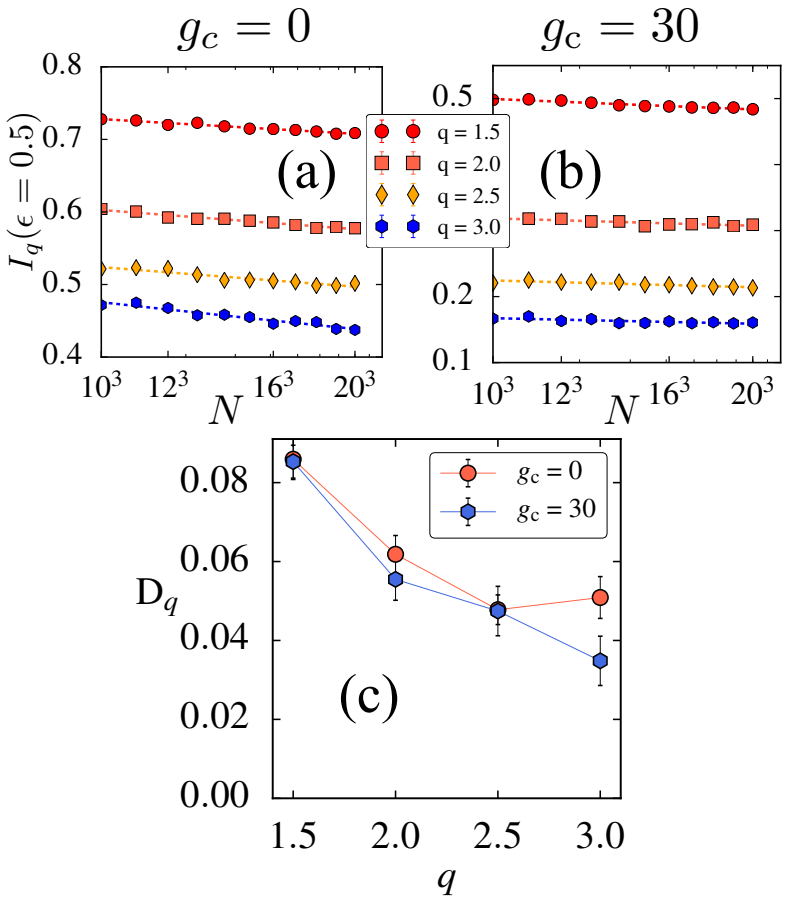

Figure 4.5: Panel (a) and (b): Finite-size scaling for the generalized inverse participation ratio I_q, averaged over eigenvalues in the middle of the spectrum $\epsilon = 0.5 \pm 0.02$, for two collective coupling strength $g_c = 0$ [see panel (a)] and $g_c = 30$ [see panel (b)], respectively and disorder strength $W = 40$. The dashed lines are a fit of the form $I_q = N^{-D_q(q-1)/D}$, and the resulting exponents are shown in the panel (c).

4.3 Limit of large coupling ($g_c \gg W/2$)

To obtain physical insights, we now perform a perturbation theory. In this work, the dynamics is restricted to the single-excitation subspace, where $|i\rangle$ denotes an excitation at site i and $|\mathrm{p}\rangle$ a single-photon state, i.e. when the excitation is found in the light field. We choose those states as the basis (of dimension $N + 1$) for a generic single-excitation

state

$$|\psi\rangle = \sum_{i=1}^{N} \alpha_i |i\rangle + \beta |\mathrm{p}\rangle \tag{4.20}$$

with $\sum_{i=1}^{N} |\alpha_i|^2 + |\beta|^2 = 1$. As discussed below, the light-matter coupling induces the formation of two eigenstates with energy $\pm g_c$, where $g_c = g\sqrt{N}$. In the following, we are interested in the limit of large coupling and consider the parameter regime $g_c \gg W \gg J = 1$. In order to get an insight in the structure of the eigenstates, we simplify the analysis by neglecting the tunneling J, being a very small parameter in the problem. With this, the problem becomes independent of the dimension. In this limit, the Hamiltonian $H \simeq H_0 + V$ only includes the light-matter interaction

$$H_0 = g \sum_{i=1}^{N} \big(|i\rangle\langle \mathrm{p}| + |\mathrm{p}\rangle\langle i| \big)$$

and the on-site energies $V = \sum_{i=1}^{N} \epsilon_i |i\rangle\langle i|$. As $g_c \gg W$, we now consider a perturbation theory with H_0 as the dominant part and V as the perturbation. We first rewrite the dominant part H_0 as

$$H_0 = g_c \big(|\mathrm{B}\rangle\langle \mathrm{p}| + |\mathrm{p}\rangle\langle \mathrm{B}| \big) ,$$

where $|\mathrm{B}\rangle = \frac{1}{\sqrt{N}} \sum_i |i\rangle$ is denoted as the bright mode. This shows that the light field only couples to the bright mode, with a coupling strength g_c. This coupling gives rise to the formation of an upper polariton $|u\rangle$ and a lower polariton $|l\rangle$ as eigenstates of H_0, here defined as,

$$|u\rangle \equiv \frac{1}{\sqrt{2}} \big(|\mathrm{B}\rangle + |\mathrm{p}\rangle \big) , \quad |l\rangle \equiv \frac{1}{\sqrt{2}} \big(|\mathrm{B}\rangle - |\mathrm{p}\rangle \big)$$

with $H_0 |u\rangle = g_c |u\rangle$ and $H_0 |l\rangle = -g_c |l\rangle$.

The remaining eigenstates $\{|d_j\rangle\}_{j=1\ldots N-1}$ of H_0 have to be orthogonal to $|u\rangle$ and $|l\rangle$, and with this to each linear combination of both polaritons. They are thus orthogonal to the photon state,

$$\langle \mathrm{p}|\mathrm{d_j}\rangle = 0 \tag{4.21}$$

with $|\mathrm{p}\rangle = \frac{1}{\sqrt{2}} \big(|u\rangle - |l\rangle \big)$. In other words, the states $|d_j\rangle$ do not carry any photon weight and are called *dark states*. The dark states $|d_j\rangle$ are also orthogonal to the bright mode,

$$\langle \mathrm{B}|\mathrm{d_j}\rangle = 0 \tag{4.22}$$

with $|\mathrm{B}\rangle = \frac{1}{\sqrt{2}} \big(|u\rangle + |l\rangle \big)$.

According to the Eqs. (4.21) and (4.22), each normalized dark state $|d_j\rangle$ has to fulfill the conditions

$$\beta = 0, \quad \sum_{i=1}^{N} \alpha_i = 0, \quad \sum_{i=1}^{N} |\alpha_i|^2 = 1 . \tag{4.23}$$

Each dark state has zero energy, $H_0 |d_j\rangle = 0$, and besides the conditions in Eq. (4.23), the dominant part H_0 does not impose any further restriction on the choice for a basis of the dark-state subspace. The dark-state subspace is thus degenerate with respect to H_0 and, as a consequence, degenerate perturbation theory has to be applied.

In order to remove the degeneracies, V will be diagonalized within the dark-states subspace $\{|d_j\rangle\}$. We call the corresponding dark states $\{|D_j\rangle\}$ from now on. They fulfill the conditions

$$\langle D_i| V |D_j\rangle = \lambda_i \delta_{ij} \,. \tag{4.24}$$

We are interested in the coefficients $\langle j|D_i\rangle$ for the dark states as defined by the previous conditions [354, 355]. Those states are also eigenstates of H in the limit $g_c/W \to \infty$. Defining $h_j = \langle \mathrm{B}| V |D_j\rangle$, and using the completeness relation $\mathbf{1} = \sum_j |D_j\rangle\langle D_j| + |\mathrm{B}\rangle\langle \mathrm{B}| + |\mathrm{p}\rangle\langle \mathrm{p}|$, together with Eq. (4.24), we obtain

$$\begin{aligned}\frac{1}{\sqrt{N}} h_j &= \langle i|\mathrm{B}\rangle \langle \mathrm{B}| V |D_j\rangle = \langle i| \big(\mathbf{1} - \sum_m |D_m\rangle\langle D_m| - |\mathrm{p}\rangle\langle \mathrm{p}|\big) V |D_j\rangle \\ &= \langle i| V |D_j\rangle - \sum_m \langle i|D_m\rangle \lambda_m \delta_{mj} = \big(\epsilon_i - \lambda_j\big) \langle i|D_j\rangle\end{aligned}$$

where we used $\langle p| V = 0$. The amplitude of dark-state $|D_j\rangle$ at site $|i\rangle$ is thus given by

$$\langle i|D_j\rangle = \mathcal{N}_j \frac{1}{\epsilon_i - \lambda_j} \,, \tag{4.25}$$

where h_j enters the normalization $\mathcal{N}_j = \frac{h_j}{\sqrt{N}}$. According to Eqs. (4.23) and (4.25), one finds $\sum_i (\epsilon_i - \lambda_j)^{-1} = 0$. The dark-state energies λ_j $(j = 1, \ldots, N-1)$ are thus the $N-1$ solutions of the equation

$$\sum_{i=1}^{N} \frac{1}{\epsilon_i - \lambda} = 0. \tag{4.26}$$

By using to Eq. (4.24) - Eq. (4.26), we can now compute the dark states and their corresponding energies purely from a perturbation theory. In order to check validity of this expansion in Fig. 4.6, we present the level spacing distribution for $g_c = 30$ obtained by full diagonalization of the Hamiltonian [see Sec. 4.1] (red circle) and obtained by the perturbation theory (hexagon blue) by diagonalizing V within the dark-state subspace Eq. (4.24). The agreement with the Semi-Poisson form of the level spacing distribution is quite remarkable.

After having checked that perturbation gives a good agreement with the numerical analysis, we would like to understand the origin of this specific distribution. In Fig. 4.7, we sketch a graphical representation of $N = 3$ sites without cavity and in the large coupling regime with cavity. From Eq. (4.26), we note that the $N-1$ dark state energies are distributed between the N initial random energies [334]. In a rough approximation, we suppose that the distance between the two dark states are given by $\Delta = \frac{x+y}{2}$, i.e. the mean distance spacing between the N states. In addition, we know that without cavity the distribution of the level spacing follows a Poissonian distribution $(\exp(-x))$. Let us

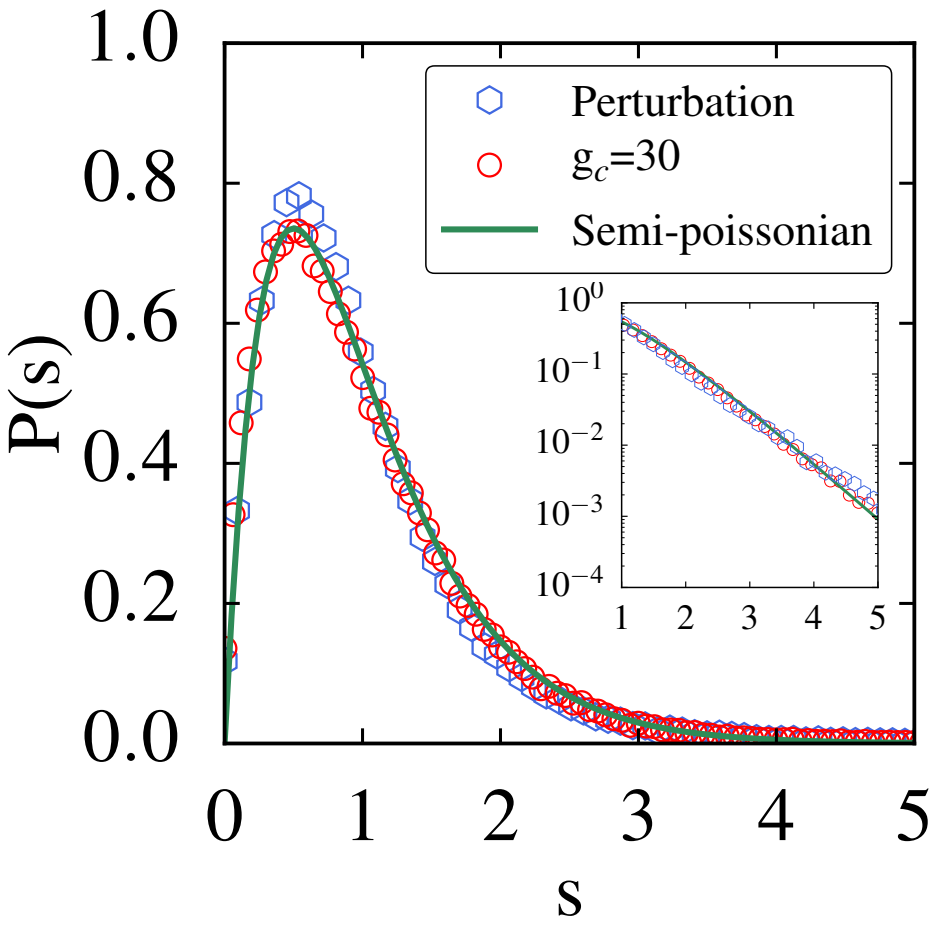

Figure 4.6: Comparison of the distribution of the level spacing from the complete Hamiltonian (red circle) and from the dark state build with the perturbation theory (blue hexagon) for a disorder strength $W = 50$ and $N = 100$ sites. The green line is the analytical semi-poissonian distribution. Inset shows the tail of the level spacing distribution on a logarithmic scale.

now derive the distribution of the dark states under this approximation. To do so, we calculate

$$\begin{aligned} P_{\rm ds}(s) &= \int_x \int_y \delta(\Delta - \tfrac{x+y}{2}) \exp(-x) \exp(-y) \mathrm{d}x \mathrm{d}y \\ &= 2 \int_0^{2\Delta} \mathrm{d}y \exp\{-2\Delta\} = 4\Delta \exp(-2\Delta). \end{aligned} \tag{4.27}$$

Remarkably, we find that $P_{\rm ds}(s)$ is Semi-Poissonian distributed [356].

As a final comment, we note that when tunnelling is neglected, the perturbation theory is valid at any dimension, which extends the aforementioned results (semi-localized phase) to all dimensions (something we have checked, but which is not shown). In the end of this chapter, for convenience, we restrict the analysis to a one-dimensional chain.

4.4 Anomalous Diffusion

In the previous section, we have emphasized some new properties within the large coupling regime. We would now like to turn to transport properties, such as the diffusion of the

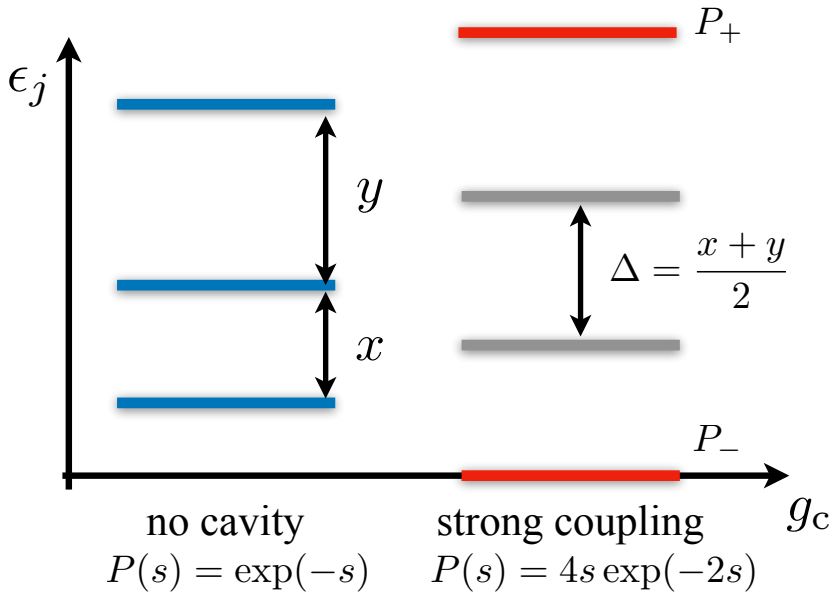

Figure 4.7: Graphical representation of 3 levels and the corresponding dark states and two polaritons when coupled to a cavity.

wave-packet or the transfer probability. In the Anderson model, a strong localization leads to an absence of diffusion. The question is what happens to the diffusion properties in the presence of a coupling to the cavity?

More specifically, we first focus on the dynamics and the long-time behavior of the spreading $(\Delta x)_t^2$ and we put the hopping term to zero ($J = 0$). In the following, we restrict the analysis of the dynamics to the following initial condition

$$|\psi(0)\rangle = |\frac{N+1}{2}\rangle, \tag{4.28}$$

with N an odd number. By this, the system is initialized with one excitation in the middle of the chain and no photon in the cavity mode. We will first focus on the quantity

$$(\Delta x)_t^2 = \langle x^2\rangle_t - \langle x\rangle_t^2 \tag{4.29}$$

which measures the spreading of the excitation over the chain, where

$$\langle x\rangle_t = \sum_{j=1}^{N} jP_j(t), \quad \langle x^2\rangle = \sum_{j=1}^{N} j^2P_j(t) \tag{4.30}$$

and $P_j(t) = \frac{|\alpha_j(t)|^2}{\sum_{l=1}^{N}|\alpha_l(t)|^2}$. In the definition of the local density P_j of excitations we discard the photon state $|\mathrm{p}\rangle$, as no position can be attributed to its global excitation character.

In Fig. 4.8 (a), we show the Mean Square Displacement (MSD) $(\Delta x)_t^2$ as function of the time t and different number of sites $N = 60, 80, 100$. The black line is a guide for the eye presenting the scaling of the usual diffusive type propagation. We find that a sub-diffusive propagation emerges in the presence of the cavity, despite an absence of tunneling. Furthermore, in panel (b), we focus on the short-time dynamics, showing an initial rapid oscillation of the MSD, that we relate to the Rabi-type oscillations due to the polaritons (see black line and Eq. (4.31)).

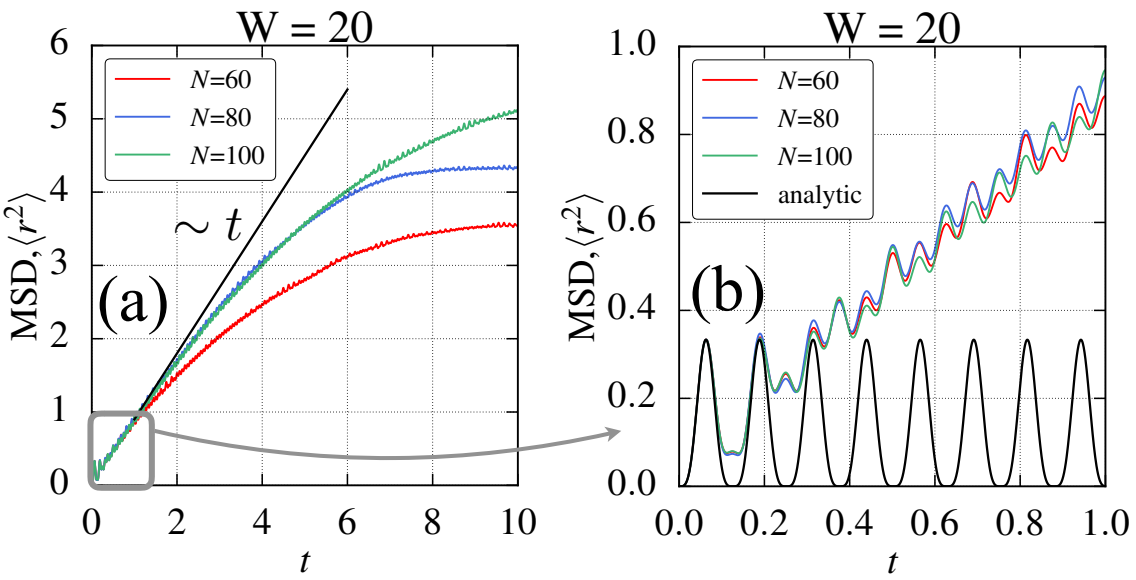

Figure 4.8: Panel (a) : Mean square displacement for $g_c = 50$, a disorder strength $W = 20$ and different number of sites $N = 60, 80, 100$ (see color code). The hopping term J is set to zero. We note the presence of a sub-diffusive behavior, the black line is a guide for the eye and presents the diffusive scaling $\sim t$. In panel (b), we zoom on the short-time behavior (see panel (a)). The black line corresponds to the full polaritonic expansion obtained in Eq. (4.32) and fits precisely the ultra-short time dynamics.

4.4.1 Diffusion due to polaritons

We here derive an expression for the ultra-short time behavior of the system's dynamics in the limit of large coupling. Its final result is given by Eq. (4.32), which is represented by the black line in Fig. 4.8 (b).

The time evolution of the system is described by the state vector with

$$|\psi(t)\rangle = \exp(-\mathrm{i}Ht)\,|\psi(0)\rangle = \sum_{\alpha=1}^{N+1} \exp(-iE_\alpha t)\,|\alpha\rangle\langle\alpha|\,|\psi(0)\rangle\ ,$$

In the following, the system is initialized with a single excitation at site j_0, $|\psi(0)\rangle = |j_0\rangle$, chosen as the center of the chain of length N. In the limit of large light-matter coupling in the disordered regime ($g\sqrt{N} \gg W \gg J$), the evolved state can be approximately written as [see Sec. 4.3]

$$|\psi(t)\rangle = \exp(-ig_0 t)\,|u\rangle\langle u|\,|j_0\rangle + \exp(ig_0 t)\,|\ell\rangle\langle\ell|\,|j_0\rangle + \sum_j \exp(-i\lambda_j t)\,|D_j\rangle\langle D_j|\,|j_0\rangle$$

Using $|u\rangle\langle u| + |\ell\rangle\langle\ell| + \sum_{j=1}^{N-1} |D_j\rangle\langle D_j| = \mathbf{1}$, this can be written as

$$\begin{aligned}|\psi(t)\rangle - |j_0\rangle =& \big(\exp(-ig_c t) - 1\big)\,|u\rangle\langle u|\,|j_0\rangle \\ &+ \big(\exp(+ig_c t) - 1\big)\,|\ell\rangle\langle\ell|\,|j_0\rangle \\ &+ \sum_j \big(\exp(-i\lambda_j t) - 1\big)\,|D_j\rangle\langle D_j|\,|j_0\rangle\end{aligned}$$

We assume $g_c = g\sqrt{N} \gg W/2 \geq \max\{|\lambda_j|\}$ and consider times $|\lambda_j|t \ll 1$. The amplitude on site j is then given by

$$\begin{aligned}\langle j|\psi(t)\rangle - \delta_{j,j_0} =&\big(\cos(g_c t) - i\sin(g_c t) - 1\big)(2N)^{-1}\\ &+\big(\cos(g_c t) + i\sin(g_c t) - 1\big)(2N)^{-1}\\ &+\mathcal{O}(\lambda_j t)\end{aligned}$$

where we used $\langle u|j'\rangle = (2N)^{-1/2} = \langle \ell|j'\rangle$ for each site $j' = j, j_0$. Finally, one obtains

$$\langle j|\psi(t)\rangle = \delta_{j,j_0} + N^{-1}\big(\cos(g_c t) - 1\big) + \mathcal{O}(\lambda_j t).$$

The corrections due to the dark states $\mathcal{O}(\lambda_j t)$ are neglected from now on. The amplitude at site $j = j_0$ reads

$$\alpha_{j_0} = \langle j_0|\psi_t\rangle \simeq 1 + N^{-1}\big(\cos(g_c t) - 1\big)\,,$$

and with it the probability to be at site $j = j_0$

$$P_{j=j_0} = |\alpha_{j_0}|^2 \simeq \Big(1 + N^{-1}\big(\cos(g_c t) - 1\big)\Big)^2.$$

In contrast to this, the amplitude at each site $j \neq j_0$, different from the site j_0 where the excitation is found initially, reads

$$\alpha_{j\neq j_0} = \langle j \neq j_0|\psi_t\rangle \simeq N^{-1}\big(\cos(g_c t) - 1\big)\,,$$

and with it the probability to be at site $j \neq j_0$

$$P_{j\neq j_0} = |\alpha_{j\neq j_0}|^2 = N^{-2}\big(\cos(g_c t) - 1\big)^2\,.$$

The chain is coupled to the light field. The corresponding amplitude β for the photon state reads

$$\begin{aligned}\beta = \langle p|\psi(t)\rangle =&\big(\cos(g_c t) - i\sin(g_c t) - 1\big)\,\langle p|u\rangle\,\langle u|j_0\rangle\\ &+\big(\cos(g_c t) + i\sin(g_c t) - 1\big)\,\langle p|\ell\rangle\,\langle \ell|j_0\rangle\ .\end{aligned}$$

As $\langle p|D_j\rangle = 0$, this expression is exact when one considers the eigenstates $\big\{\,|u\rangle\,,|l\rangle\,,|D_j\rangle_{j=1,\ldots,N-1}\,\big\}$ in the limit $g\sqrt{N} \gg W$. With $\langle p|u\rangle = 1/\sqrt{2}$, $\langle p|\ell\rangle = -1/\sqrt{2}$ and $\langle j_0|u\rangle = (2N)^{-1/2} = \langle j_0|\ell\rangle$, one gets

$$\begin{aligned}\beta = \langle p|\psi(t)\rangle =&\big(\cos(g_c t) - i\sin(g_c t) - 1\big)\frac{1}{2\sqrt{N}}\\ &+\big(\cos(g_c t) + i\sin(g_c t) - 1\big)\frac{-1}{2\sqrt{N}}\\ &= -\,i\sin(g_c t)/\sqrt{N}\end{aligned}$$

The probability for a photon reads

$$P_{ph} = |\beta|^2 = \frac{\sin^2(g_c t)}{N}.$$

With this, the probability to find the excitation within the chain is therefore given by

$$\sum_{j=1}^{N} P_j = \sum_{j=1}^{N} |\alpha_j|^2 = 1 - |\beta|^2 = 1 - P_{ph} = 1 - \sin^2(g_c t)/N.$$

This allows to compute 'renormalized' probabilities $\tilde{P}_j = P_j / \sum_j P_j$ for the excitation in the chain

$$\tilde{P}_{j=j_0} = \frac{\Big(1 + N^{-1}\big(\cos(g_c t) - 1\big)\Big)^2}{1 - \sin^2(g_c t)/N},$$
$$\tilde{P}_{j\neq j_0} = \frac{N^{-2}\big(\cos(g_c t) - 1\big)^2}{1 - \sin^2(g_c t)/N}.$$

The spreading of the excitation over the chain for an odd number $N = 2\tilde{N} + 1$ of sites is given by

$$\big\langle x^2 \big\rangle_t = \sum_j \tilde{P}_j (ja)^2 = a^2 \tilde{P}_{j\neq c} 2 \sum_{j=1}^{\tilde{N}} j^2,$$

with a the lattice spacing. We here assume that the excitation is initially found at the center $j_0 = c$ of the chain. Using the relation $\sum_{j=1}^{\tilde{N}} j^2 = \tilde{N}(\tilde{N}+1)(2\tilde{N}+1)/6$ with $\tilde{N} = (N-1)/2$, one obtains

$$\sum_{j=1}^{\tilde{N}} j^2 = \frac{N-1}{2}\frac{N+1}{2}\frac{N}{6} = \frac{N^3(1-N^{-2})}{24}.$$

The spreading of the excitation thus reads

$$\frac{\langle x^2\rangle_t}{a^2} = \tilde{P}_{j\neq c}\frac{N^3(1-N^{-2})}{12} = \frac{N^{-2}\big(\cos(g_c t) - 1\big)^2}{1 - \sin^2(g_c t)/N}\frac{N^3(1-N^{-2})}{12} \tag{4.31}$$

which gives

$$\frac{\langle x^2\rangle_t}{a^2} = \frac{N\big(\cos(g_c t) - 1\big)^2}{12\big(1 - \sin^2(g_c t)/N\big)}\Big(1 - \frac{1}{N^2}\Big) \simeq N\frac{(g_c t)^4}{48}, \tag{4.32}$$

where the last expression is an approximation for sufficiently small times $t \ll g_c^{-1}$ and large N.

4.5 Transfer probability

Similarly to the derivation of the survival probability, we now investigate the probability that an excitation is transfer to a site f, when the excitation was initially located at site c. The transfer probability reads

$$P_{c\to f}(t) = |\langle f|e^{-iHt}|c\rangle|^2. \tag{4.33}$$

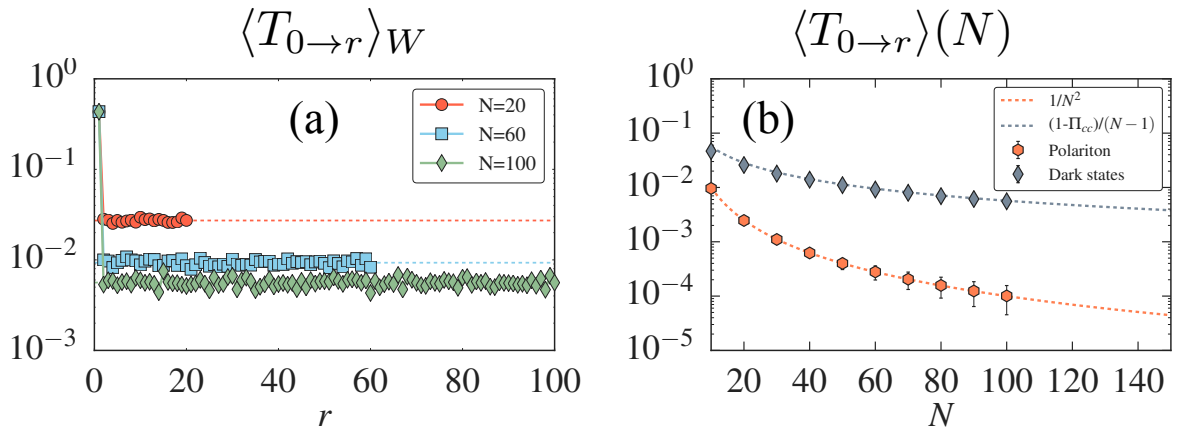

Figure 4.9: Panel (a): averaged probability to transfer an exciton from site 0 to r , with r the site distance, for $J = 0$, a disorder strength $W = 20$, a collective coupling $g_c = 50$ and for different number of sites $N = 20, 60, 100$ [see color code]. We see that this average probability is constant for all site, independent of the distance, but its value varies with the number of sites N. In panel (b), we report the average value of this plateau as function of the number of total sites N. We have separated the contribution from the dark states and the polaritons, showing that the two contributions scale differently. The polaritons scale as $\sim 1/N^2$ (orange), while the dark states scale as $\sim 1/N$ (grey).

In the case of non-degenerate eigenstates, the long-time averaged transfer probability $\mathrm{T}_{c\to f}$ reads

$$\mathrm{T}_{c\to f} = \lim_{t\to\infty} \int_0^t dt' P_{c\to f}(t')/t = \sum_\alpha |\langle\alpha|c\rangle|^2 |\langle\alpha|f\rangle|^2. \tag{4.34}$$

Note that $\mathrm{T}_{0\to 0}$ corresponds to the return probability.

In Fig. 4.9 (a), we show the averaged (~ 1000 realizations) transfer probability $\mathrm{T}_{0\to r}$, as function of the site distance r, for $J = 0$, a disorder strength $W = 20$, a collective coupling $g_c = 50$ and different number of sites $N = 20, 60, 100$ [see legend]. We observe that this probability goes to a constant value for all distances [see panel (a)] but scales with the total number of sites N [see panel (b)]. The dotted line in panel (a) corresponds to the mean values of the plateau that we report as a function of N in Fig. 4.9 (b). When separating the contribution of the dark states and polaritons, we find that the polaritons scale as $\sim 1/N^2$ (orange), while the dark states scale as $\sim 1/N$ (grey). In order to understand the dark states' scaling, we postulate that the excitation can be (on average!) equally distributed over all the sites except the initial one. We can then express the average probability to transfer excitation on another site as $(1 - \Pi_{\mathrm{cc}})/(N - 1)$. This suggested scaling behavior is in good agreement with the numerical data [see dotted grey line in Fig. 4.9 (b)].

4.6 Conclusion

In this chapter, we have analysed the modification of the Anderson localization under the coupling to cavity mode. We first investigated observables such as the return probability and the inverse participation ratio. We have shown that striking differences are found in the regime of strong disorder ($W \gg J$) and large coupling limit ($g\sqrt{N} \gg W/2$), which we characterize as semi-localized phase. Indeed, in this regime, the level statistics shows semi-poissonian behavior, charaterized by level repulsion (as in the metallic phase) and exponential behavior in the long tail (as in the localized phase). The analysis of the general inverse participation ratio shows no evidence for the behavior of multi-fractality. Treating the disorder as a perturbation, we obtain analytic estimates for the eigenstates as well as the statistics of eigenenergies, which well reproduce the numerical results discussed before. Finally, in order to study transport properties, we focus on the diffusion (time-evolution of the mean square displacement), which we analyse both numerically and analytically. It is found that the polaritons determine the short-time behavior, while the dark states are responsible for diffusion in the long-time limit, that shows anomalous behavior. We close the discussion with an analysis of the averaged transfer probability. Here, we were able to separate the contributions from the polaritons (scaling as $\sim 1/N^2$) and the dark states (scaling as $\sim 1/N$). Interestingly, the latter scaling corresponds to the one for Bloch states, which are present in the delocalized regime. Therefore, the semi-localized phase shows localization properties similar to the insulator phase and transfer properties similar to the delocalized phase. In this phase, in contrast to an exponential localization of the excitation in space, the structure of the dark states indicates a spreading of the excitation that obeys an algebraic behavior according to the site energies.

It would be interesting to study localization and transport properties in the small coupling regime ($g\sqrt{N} < W/2$) and at the crossover ($g\sqrt{N} \sim W/2$), where we expect a favorable mixing between polaritons and dark states. Furthermore, in the small coupling regime, a perturbative approach for the cavity coupling [354] can give insight on the plateau value observed in Fig. 4.1.

Conclusion & Outlook

I must finish what I've started, even if, inevitably, what I finish turns out not to be what I began.

Salman Rushdie, Midnight's Children

In this Ph.D work, I studied the impact of long-range couplings on the quantum phases of strongly-correlated many-body systems. For this purpose, I have focused on different one-dimensional systems with various long-range couplings.

In the first chapter, we investigated the interplay between long-range couplings and the localization phenomenon induced by disorder. We have considered one-dimensional disordered chains of fermions and spins with long-range interactions that decay with the distance ℓ as a power-law $1/\ell^{\alpha}$. We first considered an extension of the Kitaev model with long-range pairing. By using the integrability of the model, we have determined its complete phase diagram. The latter features rich properties including a new delocalized regime with high energy states protected against disorder. The existence of this regime can be traced back to the presence of a divergence in the excitation spectrum induced by the long-range potential. It can however be shown that this phase disappears in the thermodynamic limit. We have shown that the correlation functions in the localized phase display an algebraic decay at large distance, with an exponent that does not depends on the strength of the disorder but only of the power law exponent α. The strength of these results relies especially on an analytical evidence obtained from a perturbative approach. We have also looked at the correlation functions in another model featuring density-density interactions, namely the long-range Ising model in a transverse field. Interestingly, similar algebraic decay were observed. Our results are in stark contrast to the results expected for short-range systems and generalize recent results for the decay of the wave-functions in quadratic models. We argue that the fact that these results are found for both non-interacting and interacting models suggests a possible universal behavior due to long-range couplings. These results are of immediate interest for experiments with cold ions, molecule, Rydberg atoms and quantum emitters embbeded in cavity-type resonators. Since the initial Anderson model was devoted to the study of diffusion in a disordered medium, understanding how the *algebraic* localization manifests itself in the transport properties appears as a natural extension of this work.

In the second chapter, we studied an extension of the Hubbard model where fermions can hop between nearest-neighboring sites with rate t, and interact via both an on-site potential U and a repulsive finite-range soft-shoulder potential V which typically extends over a few sites of the lattice. This soft-shoulder potential is directly inspired by experiments with Rydberg-dressed cold gases. Starting from the classical limit ($t = 0$), we have shown

that the competition between the length scale associated to the range of the potential and the average inter-particle distance can lead to a degenerate ground state. This effect relies on frustration, i.e. when the system can not minimized simultaneously all the terms present in the Hamiltonian, which leads to the appearance of two new phases made of cluster of particles. The first phase corresponds to the so-called cluster Luttinger liquid (CLL), and the second one to a CLL with on-site pairs of fermions (CLL_d). Importantly, these phases do not fall into the standard Tomonaga-Luttinger liquid (TLL) class. Furthermore, we have found that a transition between these two phases occurs at $V = \frac{2}{3}U$. Then focusing on the quantum model ($t \equiv 1$), we have determined the complete phase diagram in the whole range of parameter U and V using a density matrix renormalization group algorithm. At large V or large U, we have unambiguously demonstrated that the cluster phases predicted classically survive in the presence of quantum fluctuations. At intermediate U, we have characterized in detail the CLL phase and the TLL-CLL and CLL-CLL_d transitions. All the phases are characterized by a central charge $c = 2$, consistent with a liquid phase featuring a separation between the spin and charge degrees of freedom. However, since the single-particle gap is finite in the CLL, the granularity of the liquid has been interpreted as clusters of particles instead of single particles. We have found that the conventional Tomonaga Luttinger Liquid (TLL) is separated by a critical line with a central charge $c = 5/2$, along which the two (spin and charge) bosonic degrees of freedom (corresponding to $c = 1$ each) combine in a supersymmetric way with an emergent fermionic excitation ($c = 1/2$). We have also demonstrated that there are no significant spin correlations. Finally, we have provided evidences of a first-order transition between the CLL and the CLL_d. It would be an interesting question to investigate the quantum phase transition in a two-dimensional model, and look for exotic quantum phases such as frustration-induced super-stripes [110], superglass [357], and emergent gauge fields [358]. Furthermore, the emergent supersymmetry between bosonic and fermionic modes paves the way to identify the fundamental features that could lead to new extended critical phases in higher dimensions. Since emergent supersymmetric modes have been shown to be related to Majorana fermions, it could be also interesting to investigate possible applications of these extended critical phases in the context of quantum information.

In the third chapter, we have shown that restoring energy extensivity of a quantum system in the strong long-range regime, which is done by rescaling the potential with a volume-dependent factor called Kac's prescription, has a profound influence on the low-energy properties. We have considered a long-range quantum model consisting of one-dimensional fermions interacting via a $1/r^\alpha$ potential at half filing. Using a combination of bosonization and numerical results, we have demonstrated that the ground state of the system strongly depends on whether Kac's prescription is used or not. In the thermodynamic limit, while an insulating phase is found in the absence of Kac's rescaling, the latter leads to a metallic phase for finite interaction strengths. Interestingly, we have found that this new metallic phases is not completely captured by the Luttinger theory, although the latter still provides the correct functional behavior except for an infinite range potential ($\alpha = 0$). In the latter case, we have demonstrated the full

breakdown of the Luttinger liquid theory by solving the model exactly via a mean field approach. Finally, we have shown that restoring extensivity eliminates the plasmon mode while preserving the LR character of the potential, and with it some inherent properties of the strong LR regime such as non-addivity. It is an interesting prospect to investigate the properties of such an unconventional liquid with restored energy extensivity in higher dimensions [359]. Since cavity-mediated two-body interactions are naturally LR and extensive [117], another perspective of this work is the exploration of the non-trivial thermodynamics of cold atoms in cavity-QED. For instance, the case $\alpha = 0$ can be typically obtained when the spatial extent of the atomic cloud is much smaller than the cavity wavelength [118].

Finally, in chapter 4, we have studied an three-dimensional Anderson localization model with nearest-neighbor tunnelling J and random local energy disorder within $[-W, W]$. We considered a situation where the excitation is collectively coupled to a common cavity mode with strength $g_c = g\sqrt{N}$, where N is the system size. Here, a cavity photon can mediate long-range hopping between the individual sites. We put our focus on the analysis of localization and transfer properties in the regime of large collective coupling ($g_c \gg W/2 \gg J$). In this parameter regime, we find the appearance of a novel semi-localized phase, not present in the Anderson model, and which is characterized by a level spacing distribution following a semi-poissonian distribution. Indeed, the eigenstates and eigenenergies within this phase are computed via a perturbative treatment, from which we can derive a semi-poissonian distribution for the level spacing under a certain simplification. Moreover, we have found that the long-time limit of the diffusion shows anomalous behavior. Crucially, we found that the modified dark states, besides polaritonic states can play an important role for excitation transport. On average, those dark states can spread the excitation over long distances in the chain, with a transmission probability decaying only as $\sim 1/N$.

In order to complete the analysis, it would be interesting to study the system in the perturbative limit of small coupling ($g\sqrt{N} < W/2$) in more detail. Furthermore, the crossover regime ($g\sqrt{N} \sim W/2$) should be studied further. There, we expect a favorable mixing between polaritons and dark states. This includes the appearance of a possible novel phase transition between semi-localized and localized phase [354]. A further perspective is the analysis of conductance and transfer properties with the help of the Green's functions. These findings can have impact on studies of cavity modified transport properties in several experimental setup.

Bibliography

[1] P. W. Anderson, "Absence of diffusion in certain random lattices," Phys. Rev. **109**, 1492 (1958).

[2] C. Schneider, D. Porras, and T. Schätz, "Experimental quantum simulations of many-body physics with trapped ions," Reports on Progress in Physics **75**, 024401 (2012).

[3] P. Richerme, Z.-X. Gong, A. Lee, C. Senko, J. Smith, M. Foss-Feig, S. Michalakis, A. V. Gorshkov, and C. Monroe, "Non-local propagation of correlations in quantum systems with long-range interactions," Nature (London) **511**, 198 (2014).

[4] P. Jurcevic, B. P. Lanyon, P. Hauke, C. Hempel, P. Zoller, R. Blatt, and C. F. Roos, "Quasiparticle engineering and entanglement propagation in a quantum many-body system," Nature (London) **511**, 202 (2014).

[5] J. W. Britton, B. C. Sawyer, A. C. Keith, C. C. J. Wang, J. K. Freericks, H. Uys, M. J. Biercuk, and J. J. Bollinger, "Engineered two-dimensional Ising interactions in a trapped-ion quantum simulator with hundreds of spins," Nature (London) **484**, 489 (2012).

[6] A. Bermudez, T. Schäetz, and M. B. Plenio, "Dissipation-assisted quantum information processing with trapped ions," Phys. Rev. Lett. **110**, 110502 (2013).

[7] E. Shahmoon and G. Kurizki, "Nonradiative interaction and entanglement between distant atoms," Phys. Rev. A **87**, 033831 (2013).

[8] V. D. Vaidya, Y. Guo, R. M. Kroeze, K. E. Ballantine, A. J. Kollár, J. Keeling, and B. L. Lev, "Tunable-Range, Photon-Mediated Atomic Interactions in Multimode Cavity QED," Phys. Rev. X **8**, 011002 (2018).

[9] D. Vodola, L. Lepori, E. Ercolessi, A. V. Gorshkov, and G. Pupillo, "Kitaev chains with long-range pairing," Phys. Rev. Lett. **113**, 156402 (2014).

[10] M. Mattioli, M. Dalmonte, W. Lechner, and G. Pupillo, "Cluster luttinger liquids of rydberg-dressed atoms in optical lattices," Phys. Rev. Lett. **111**, 165302 (2013).

[11] C. L. Kane, A. Stern, and B. I. Halperin, "Pairing in luttinger liquids and quantum hall states," Phys. Rev. X **7**, 031009 (2017).

[12] J. Ruhman and E. Altman, "Topological degeneracy and pairing in a one-dimensional gas of spinless Fermions," Phys. Rev. B **96**, 085133 (2017).

[13] H.-C. Jiang, Z.-X. Li, A. Seidel, and D.-H. Lee, "Symmetry protected topological luttinger liquids and the phase transition between them," Science Bulletin **63**, 753 (2018).

[14] G. Magnifico, D. Vodola, E. Ercolessi, S. P. Kumar, M. Müller, and A. Bermudez, "Symmetry-protected topological phases in lattice gauge theories: Topological qed_2," Phys. Rev. D **99**, 014503 (2019).

[15] http://itensor.org/.

[16] T. Dauxois, S. Ruffo, E. Arimondo, and M. Wilkens, "Dynamics and thermodynamics of systems with long-range interactions: An introduction," in *Dynamics and Thermodynamics of Systems with Long-Range Interactions*, edited by T. Dauxois, S. Ruffo, E. Arimondo, and M. Wilkens (Springer Berlin Heidelberg, 2002) pp. 1–19.

[17] A. Campa, A. Giansanti, and D. Moroni, "Canonical solution of classical magnetic models with long-range couplings," Journal of Physics A: Mathematical and General **36**, 6897 (2003).

[18] D. Ruelle, "Classical statistical mechanics of a system of particles," Helvetica Physica Acta **36**, 183 (1963).

[19] J. Barré, D. Mukamel, and S. Ruffo, "Inequivalence of ensembles in a system with long-range interactions," Phys. Rev. Lett. **87**, 030601 (2001).

[20] D. Ruelle, *Statistical Mechanics: Rigorous Results* (World Scientific, 1999).

[21] D. Ruelle, "Superstable interactions in classical statistical mechanics," Commun. Math. Phys. **18**, 127 (1970).

[22] A. Campa, T. Dauxois, and S. Ruffo, "Statistical mechanics and dynamics of solvable models with long-range interactions," Phys. Rep. **480**, 57 (2009).

[23] M. Kastner, "Nonequivalence of ensembles for long-range quantum spin systems in optical lattices," Phys. Rev. Lett. **104**, 240403 (2010).

[24] Y. Levin, R. Pakter, F. B. Rizzato, T. N. Teles, and F. P. Benetti, "Nonequilibrium statistical mechanics of systems with long-range interactions," Physics Reports **535**, 1 (2014), nonequilibrium statistical mechanics of systems with long-range interactions.

[25] N. W. Ashcroft and N. D. Mermin, *Solid State Physics* (Holt, 1976).

[26] C. Kittel, *Introduction to Solid State Physics* (Wiley, 2004).

[27] T. Moriya, "Theory of itinerant electron magnetism," Journal of Magnetism and Magnetic Materials **100**, 261 (1991).

[28] L. Hedin and S. Lundqvist, "Effects of electron-electron and electron-phonon interactions on the one-electron states of solids," in *Solid State Physics*, Vol. 23, edited by F. Seitz, D. Turnbull, and H. Ehrenreich (Academic Press, United States, 1969) pp. 1–181, doi:10.1016/S0081-1947(08)60615-3.

[29] D. Pines and P. Nozieres, "The theory of quantum liquids," American Journal of Physics **36**, 279 (1968), https://doi.org/10.1119/1.1974502 .

[30] G. F. Giuliani and G. Vignale, *Quantum theory of the electron liquid* (Cambridge Univ. Press, Cambridge, 2005).

[31] D. Pines and D. Bohm, "A collective description of electron interactions: Ii. collective vs individual particle aspects of the interactions," Phys. Rev. **85**, 338 (1952).

[32] D. Pines, "A collective description of electron interactions: Iv. electron interaction in metals," Phys. Rev. **92**, 626 (1953).

[33] M. Gell-Mann and K. A. Brueckner, "Correlation energy of an electron gas at high density," Phys. Rev. **106**, 364 (1957).

[34] D. Pines, *Elementary excitations in solids.* (W.A. Benjamin, New York, 1963) pp. xii, 200 p.

[35] H. Yukawa, "On the Interaction of Elementary Particles I," Proc. Phys. Math. Soc. Jap. **17**, 48 (1935), [Prog. Theor. Phys. Suppl.1,1(1935)].

[36] L. Landau and E. Lifshitz, *Statistical Physics*, vol. 5 (Elsevier Science, 2013).

[37] J. Bardeen, L. N. Cooper, and J. R. Schrieffer, "Microscopic theory of superconductivity," Phys. Rev. **106**, 162 (1957).

[38] D. van Delft and P. Kes, "The discovery of superconductivity," Phys. Today **63**, 38 (2010).

[39] V. L. Ginzburg and L. D. Landau, "On the theory of superconductivity," in *On Superconductivity and Superfluidity: A Scientific Autobiography* (Springer Berlin Heidelberg, Berlin, Heidelberg, 2009) pp. 113–137.

[40] E. Ising, "Beitrag zur theorie des ferromagnetismus," Zeitschrift für Physik **31**, 253 (1925).

[41] R. Baxter, *Exactly Solved Models in Statistical Mechanics*, Dover books on physics (Dover Publications, 2007).

[42] N. F. Mott, "Metal-insulator transition," Rev. Mod. Phys. **40**, 677 (1968).

[43] "Electron correlations in narrow energy bands III. An improved solution," (1964), [Online; accessed 27. Oct. 2019].

[44] R. O. Zaĭtsev, E. V. Kuz'min, and S. G. Ovchinnikov, "Fundamental ideas on metal-dielectric transitions in 3d-metal compounds," Sov. Phys. Usp. **29**, 322 (1986).

[45] A. O. Anokhin, V. Y. Irkhin, and M. I. Katsnelson, "On the theory of the Mott transition in the paramagnetic phase," J. Phys.: Condens. Matter **3**, 1475 (1991).

[46] M. J. Rozenberg, G. Kotliar, and X. Y. Zhang, "Mott-Hubbard transition in infinite dimensions. II," Phys. Rev. B **49**, 10181 (1994).

[47] M. Imada, A. Fujimori, and Y. Tokura, "Metal-insulator transitions," Rev. Mod. Phys. **70**, 1039 (1998).

[48] S.-i. Tomonaga, "Remarks on Bloch's Method of Sound Waves applied to Many-Fermion Problems," Progress of Theoretical Physics **5**, 544 (1950), http://oup.prod.sis.lan/ptp/article-pdf/5/4/544/5430161/5-4-544.pdf .

[49] J. M. Luttinger, "An exactly soluble model of a many-fermion system," Journal of Mathematical Physics **4**, 1154 (1963), https://doi.org/10.1063/1.1704046 .

[50] F. D. M. Haldane, "Effective harmonic-fluid approach to low-energy properties of one-dimensional quantum fluids," Phys. Rev. Lett. **47**, 1840 (1981).

[51] D. Jérome, "Organic superconductors," Solid State Communications **92**, 89 (1994).

[52] Z. Yao, H. W. C. Postma, L. Balents, and C. Dekker, "Carbon nanotube intramolecular junctions," Nature **402**, 273 EP (1999).

[53] M. Bockrath, D. H. Cobden, J. Lu, A. G. Rinzler, R. E. Smalley, L. Balents, and P. L. McEuen, "Luttinger-liquid behaviour in carbon nanotubes," Nature **397**, 598 (1999).

[54] J. Reynolds, B. Thompson, and T. Skotheim, *Handbook of Conducting Polymers, Fourth Edition - 2 Volume Set*, Handbook of Conducting Polymers (Taylor & Francis Group, 2019).

[55] A. M. Chang, L. N. Pfeiffer, and K. W. West, "Observation of chiral Luttinger behavior in electron tunneling into fractional quantum hall edges," Phys. Rev. Lett. **77**, 2538 (1996).

[56] A. M. Chang, "Chiral Luttinger liquids at the fractional quantum hall edge," Rev. Mod. Phys. **75**, 1449 (2003).

[57] T. Kinoshita, T. Wenger, and D. S. Weiss, "Observation of a One-Dimensional Tonks-Girardeau Gas," Science **305**, 1125 (2004).

[58] B. Paredes, A. Widera, V. Murg, O. Mandel, S. Folling, I. Cirac, G. V. Shlyapnikov, T. W. Hansch, and I. Bloch, "Tonks-girardeau gas of ultracold atoms in an optical lattice," Nature (London) **429**, 277 (2004).

[59] E. Haller, R. Hart, M. J. Mark, J. G. Danzl, L. Reichsollner, M. Gustavsson, M. Dalmonte, G. Pupillo, and H.-C. Nagerl, "Pinning quantum phase transition for a luttinger liquid of strongly interacting bosons," Nature (London) **466**, 597 (2010).

[60] B. Yang, Y.-Y. Chen, Y.-G. Zheng, H. Sun, H.-N. Dai, X.-W. Guan, Z.-S. Yuan, and J.-W. Pan, "Quantum criticality and the tomonaga-luttinger liquid in one-dimensional bose gases," Phys. Rev. Lett. **119**, 165701 (2017).

[61] S. R. White, "Density matrix formulation for quantum renormalization groups," Phys. Rev. Lett. **69**, 2863 (1992).

[62] U. Schollwöck, "The density-matrix renormalization group," Rev. Mod. Phys. **77**, 259 (2005).

[63] D. M. Ceperley and B. J. Alder, "Ground state of the electron gas by a stochastic method," Phys. Rev. Lett. **45**, 566 (1980).

[64] A. W. Sandvik, "Computational studies of quantum spin systems," AIP Conference Proceedings **1297**, 135 (2010), https://aip.scitation.org/doi/pdf/10.1063/1.3518900 .

[65] F. D. M. Haldane, "Model for a quantum hall effect without landau levels: Condensed-matter realization of the "parity anomaly"," Phys. Rev. Lett. **61**, 2015 (1988).

[66] J. M. Kosterlitz and D. J. Thouless, "Ordering, metastability and phase transitions in two-dimensional systems," Journal of Physics C: Solid State Physics **6**, 1181 (1973).

[67] A. Y. Kitaev, "Unpaired Majorana fermions in quantum wires," Physics-Uspekhi **44**, 131 (2001).

[68] D. Vodola, L. Lepori, E. Ercolessi, and G. Pupillo, "Long-range Ising and Kitaev models: phases, correlations and edge modes," New J. Phys. **18**, 015001 (2016).

[69] J. Dalibard and C. Cohen-Tannoudji, "Laser cooling below the doppler limit by polarization gradients: simple theoretical models," J. Opt. Soc. Am. B **6**, 2023 (1989).

[70] H. Metcalf and P. van der Straten, *Laser Cooling and Trapping*, Graduate Texts in Contemporary Physics (Springer New York, 2012).

[71] M. Lewenstein, A. Sanpera, V. Ahufinger, B. Damski, A. Sen(De), and U. Sen, "Ultracold atomic gases in optical lattices: mimicking condensed matter physics and beyond," Advances in Physics **56**, 243 (2007), https://doi.org/10.1080/00018730701223200 .

[72] I. Bloch, J. Dalibard, and W. Zwerger, "Many-body physics with ultracold gases," Rev. Mod. Phys. **80**, 885 (2008).

[73] D. Jaksch and P. Zoller, "The cold atom hubbard toolbox," Annals of Physics **315**, 52 (2005), special Issue.

[74] P. Berman, E. Arimondo, and C. Lin, *Advances in Atomic, Molecular, and Optical Physics*, ISSN (Elsevier Science, 2013).

[75] J. I. Cirac and P. Zoller, "Goals and opportunities in quantum simulation," Nature Physics **8**, 264 (2012).

[76] M. Greiner and S. Fölling, "Optical lattices," Nature **453**, 736 (2008).

[77] I. Bloch, "Ultracold quantum gases in optical lattices," Nat. Phys. **1**, 23 (2005).

[78] C. Chin, R. Grimm, P. Julienne, and E. Tiesinga, "Feshbach resonances in ultracold gases," Rev. Mod. Phys. **82**, 1225 (2010).

[79] M. Greiner, O. Mandel, T. Esslinger, T. W. Hansch, and I. Bloch, "Quantum phase transition from a superfluid to a mott insulator in a gas of ultracold atoms," Nature (London) **415**, 39 (2002).

[80] J. Billy, V. Josse, Z. Zuo, A. Bernard, B. Hambrecht, P. Lugan, D. Clement, L. Sanchez-Palencia, P. Bouyer, and A. Aspect, "Direct observation of Anderson localization of matter waves in a controlled disorder," Nature (London) **453**, 891 (2008).

[81] G. Roati, C. D'Errico, L. Fallani, M. Fattori, C. Fort, M. Zaccanti, G. Modugno, M. Modugno, and M. Inguscio, "Anderson localization of a non-interacting Bose-Einstein condensate," Nature (London) **453**, 895 (2008).

[82] R. Nandkishore and D. A. Huse, "Many-Body Localization and Thermalization in Quantum Statistical Mechanics," Annu. Rev. Condens. Matter Phys. **6**, 15 (2015).

[83] D. A. Abanin, E. Altman, I. Bloch, and M. Serbyn, "Colloquium: Many-body localization, thermalization, and entanglement," Rev. Mod. Phys. **91**, 021001 (2019).

[84] E. A. Cornell and C. E. Wieman, "Nobel lecture: Bose-einstein condensation in a dilute gas, the first 70 years and some recent experiments," Rev. Mod. Phys. **74**, 875 (2002).

[85] M. H. Anderson, J. R. Ensher, M. R. Matthews, C. E. Wieman, and E. A. Cornell, "Observation of bose-einstein condensation in a dilute atomic vapor," Science **269**, 198 (1995), http://www.sciencemag.org/content/269/5221/198.full.pdf .

[86] C. C. Bradley, C. A. Sackett, J. J. Tollett, and R. G. Hulet, "Evidence of bose-einstein condensation in an atomic gas with attractive interactions," Phys. Rev. Lett. **75**, 1687 (1995).

[87] K. B. Davis, M. O. Mewes, M. R. Andrews, N. J. van Druten, D. S. Durfee, D. M. Kurn, and W. Ketterle, "Bose-einstein condensation in a gas of sodium atoms," Phys. Rev. Lett. **75**, 3969 (1995).

[88] B. Yan, S. A. Moses, B. Gadway, J. P. Covey, K. R. A. Hazzard, A. M. Rey, D. S. Jin, and J. Ye, "Observation of dipolar spin-exchange interactions with lattice-confined polar molecules," Nature (London) **501**, 521 (2013).

[89] K. R. A. Hazzard, M. van den Worm, M. Foss-Feig, S. R. Manmana, E. G. Dalla Torre, T. Pfau, M. Kastner, and A. M. Rey, "Quantum correlations and entanglement in far-from-equilibrium spin systems," Phys. Rev. A **90**, 063622 (2014).

[90] L. Reichsöllner, A. Schindewolf, T. Takekoshi, R. Grimm, and H.-C. Nägerl, "Quantum engineering of a low-entropy gas of heteronuclear bosonic molecules in an optical lattice," Phys. Rev. Lett. **118**, 073201 (2017).

[91] H. P. Büchler, E. Demler, M. Lukin, A. Micheli, N. Prokof'ev, G. Pupillo, and P. Zoller, "Strongly correlated 2d quantum phases with cold polar molecules: Controlling the shape of the interaction potential," Phys. Rev. Lett. **98**, 060404 (2007).

[92] A. Micheli, G. Pupillo, H. P. Büchler, and P. Zoller, "Cold polar molecules in two-dimensional traps: Tailoring interactions with external fields for novel quantum phases," Phys. Rev. A **76**, 043604 (2007).

[93] T. Lahaye, C. Menotti, L. Santos, M. Lewenstein, and T. Pfau, "The physics of dipolar bosonic quantum gases," Rep. Prog. Phys. **72**, 126401 (2009).

[94] G. Pupillo, A. Micheli, Büchler, and P. Zoller, "Condens. matter phys. with cold polar molecules," in *Cold Molecules: Theory, Experiment, Applications*, edited by R. Krems, B. Friedrich, and S. W. C. (CRC Press, 2009).

[95] A. Trautmann, P. Ilzhöfer, G. Durastante, C. Politi, M. Sohmen, M. J. Mark, and F. Ferlaino, "Dipolar quantum mixtures of erbium and dysprosium atoms," Phys. Rev. Lett. **121**, 213601 (2018).

[96] S. Lepoutre, J. Schachenmayer, L. Gabardos, B. Zhu, B. Naylor, E. Maréchal, O. Gorceix, A. M. Rey, L. Vernac, and B. Laburthe-Tolra, "Out-of-equilibrium quantum magnetism and thermalization in a spin-3 many-body dipolar lattice system," Nature Communications **10**, 1714 (2019).

[97] H. Weimer, R. Löw, T. Pfau, and H. P. Büchler, "Quantum critical behavior in strongly interacting Rydberg gases," Phys. Rev. Lett. **101**, 250601 (2008).

[98] M. Saffman, T. G. Walker, and K. Mølmer, "Quantum information with Rydberg atoms," Rev. Mod. Phys. **82**, 2313 (2010).

[99] R. Löw, H. Weimer, J. Nipper, J. B. Balewski, B. Butscher, H. P. Büchler, and T. Pfau, "An experimental and theoretical guide to strongly interacting rydberg

gases," Journal of Physics B: Atomic, Molecular and Optical Physics **45**, 113001 (2012).

[100] J. Honer, H. Weimer, T. Pfau, and H. P. Büchler, "Collective many-body interaction in rydberg dressed atoms," Phys. Rev. Lett. **105**, 160404 (2010).

[101] A. Piñeiro Orioli, A. Signoles, H. Wildhagen, G. Günter, J. Berges, S. Whitlock, and M. Weidemüller, "Relaxation of an isolated dipolar-interacting Rydberg quantum spin system," Phys. Rev. Lett. **120**, 063601 (2018).

[102] M. D. Lukin, M. Fleischhauer, R. Cote, L. M. Duan, D. Jaksch, J. I. Cirac, and P. Zoller, "Dipole blockade and quantum information processing in mesoscopic atomic ensembles," Phys. Rev. Lett. **87**, 037901 (2001).

[103] D. Tong, S. M. Farooqi, J. Stanojevic, S. Krishnan, Y. P. Zhang, R. Côté, E. E. Eyler, and P. L. Gould, "Local blockade of rydberg excitation in an ultracold gas," Phys. Rev. Lett. **93**, 063001 (2004).

[104] K. Singer, M. Reetz-Lamour, T. Amthor, L. G. Marcassa, and M. Weidemüller, "Suppression of excitation and spectral broadening induced by interactions in a cold gas of rydberg atoms," Phys. Rev. Lett. **93**, 163001 (2004).

[105] D. Barredo, S. Ravets, H. Labuhn, L. Béguin, A. Vernier, F. Nogrette, T. Lahaye, and A. Browaeys, "Demonstration of a strong Rydberg blockade in three-atom systems with anisotropic interactions," Phys. Rev. Lett. **112**, 183002 (2014).

[106] J. B. Balewski, A. T. Krupp, A. Gaj, S. Hofferberth, R. Löw, and T. Pfau, "Rydberg dressing: understanding of collective many-body effects and implications for experiments," New Journal of Physics **16**, 063012 (2014).

[107] F. Cinti, P. Jain, M. Boninsegni, A. Micheli, P. Zoller, and G. Pupillo, "Supersolid droplet crystal in a dipole-blockaded gas," Phys. Rev. Lett. **105**, 135301 (2010).

[108] M. Boninsegni and N. V. Prokof'ev, "Colloquium: Supersolids: What and where are they?" Rev. Mod. Phys. **84**, 759 (2012).

[109] N. Prokof'ev and B. Svistunov, "Supersolid state of matter," Phys. Rev. Lett. **94**, 155302 (2005).

[110] G. Masella, A. Angelone, F. Mezzacapo, G. Pupillo, and N. V. Prokof'ev, "Supersolid stripe crystal from finite-range interactions on a lattice," Phys. Rev. Lett. **123**, 045301 (2019).

[111] D. Porras and J. I. Cirac, "Effective quantum spin systems with trapped ions," Phys. Rev. Lett. **92**, 207901 (2004).

[112] U. Schneider, L. Hackermuller, J. P. Ronzheimer, S. Will, S. Braun, T. Best, I. Bloch, E. Demler, S. Mandt, D. Rasch, and A. Rosch, "Fermionic transport and out-of-equilibrium dynamics in a homogeneous hubbard model with ultracold atoms," Nat. Phys. **8**, 213 (2012).

[113] J. M. Raimond, M. Brune, and S. Haroche, "Manipulating quantum entanglement with atoms and photons in a cavity," Rev. Mod. Phys. **73**, 565 (2001).

[114] H. J. Kimble, "Strong interactions of single atoms and photons in cavity QED," Phys. Scr. **T76**, 127 (1998).

[115] J. S. Douglas, H. Habibian, C. L. Hung, A. V. Gorshkov, H. J. Kimble, and D. E. Chang, "Quantum many-body models with cold atoms coupled to photonic crystals," Nat. Photonics **9**, 326 (2015).

[116] M. Litinskaya, E. Tignone, and G. Pupillo, "Broadband photon-photon interactions mediated by cold atoms in a photonic crystal fiber," Scientific Reports **6**, 25630 (2016).

[117] H. Ritsch, P. Domokos, F. Brennecke, and T. Esslinger, "Cold atoms in cavity-generated dynamical optical potentials," Rev. Mod. Phys. **85**, 553 (2013).

[118] S. Schütz and G. Morigi, "Prethermalization of atoms due to photon-mediated long-range interactions," Phys. Rev. Lett. **113**, 203002 (2014).

[119] P. Münstermann, T. Fischer, P. Maunz, P. W. H. Pinkse, and G. Rempe, "Observation of cavity-mediated long-range light forces between strongly coupled atoms," Phys. Rev. Lett. **84**, 4068 (2000).

[120] B. L. Altshuler, Y. Gefen, A. Kamenev, and L. S. Levitov, "Quasiparticle lifetime in a finite system: A nonperturbative approach," Phys. Rev. Lett. **78**, 2803 (1997).

[121] D. Basko, I. Aleiner, and B. Altshuler, "Metal–insulator transition in a weakly interacting many-electron system with localized single-particle states," Ann. Phys. **321**, 1126 (2006).

[122] V. Oganesyan and D. A. Huse, "Localization of interacting fermions at high temperature," Phys. Rev. B **75**, 155111 (2007).

[123] I. V. Gornyi, A. D. Mirlin, and D. G. Polyakov, "Interacting Electrons in Disordered Wires: Anderson Localization and Low-T Transport," Phys. Rev. Lett. **95**, 206603 (2005).

[124] M. Žnidarič, T. c. v. Prosen, and P. Prelovšek, "Many-body localization in the Heisenberg xxz magnet in a random field," Phys. Rev. B **77**, 064426 (2008).

[125] J. Biddle, B. Wang, D. J. Priour, and S. Das Sarma, "Localization in one-dimensional incommensurate lattices beyond the Aubry-André model," Phys. Rev. A **80**, 021603 (2009).

[126] J. Biddle and S. Das Sarma, "Predicted mobility edges in one-dimensional incommensurate optical lattices: An exactly solvable model of Anderson localization," Phys. Rev. Lett. **104**, 070601 (2010).

[127] J. Biddle, D. J. Priour, B. Wang, and S. Das Sarma, "Localization in one-dimensional lattices with non-nearest-neighbor hopping: Generalized Anderson and Aubry-André models," Phys. Rev. B **83**, 075105 (2011).

[128] A. Pal and D. A. Huse, "Many-body localization phase transition," Phys. Rev. B **82**, 174411 (2010).

[129] B. Bauer, L. Huijse, E. Berg, M. Troyer, and K. Schoutens, "Supersymmetric multicritical point in a model of lattice fermions," Phys. Rev. B **87**, 165145 (2013).

[130] A. D. Luca and A. Scardicchio, "Ergodicity breaking in a model showing many-body localization," EPL (Europhys. Lett.) **101**, 37003 (2013).

[131] R. Vosk and E. Altman, "Many-Body Localization in One Dimension as a Dynamical Renormalization Group Fixed Point," Phys. Rev. Lett. **110**, 067204 (2013).

[132] R. Vosk and E. Altman, "Dynamical Quantum Phase Transitions in Random Spin Chains," Phys. Rev. Lett. **112**, 217204 (2014).

[133] Y. Bar Lev and D. R. Reichman, "Dynamics of many-body localization," Phys. Rev. B **89**, 220201 (2014).

[134] Y. Bar Lev, G. Cohen, and D. R. Reichman, "Absence of Diffusion in an Interacting System of Spinless Fermions on a One-Dimensional Disordered Lattice," Phys. Rev. Lett. **114**, 100601 (2015).

[135] D. J. Luitz, N. Laflorencie, and F. Alet, "Many-body localization edge in the random-field Heisenberg chain," Phys. Rev. B **91**, 081103 (2015).

[136] D. J. Luitz, "Long tail distributions near the many-body localization transition," Phys. Rev. B **93**, 134201 (2016).

[137] P. Naldesi, E. Ercolessi, and T. Roscilde, "Detecting a many-body mobility edge with quantum quenches," SciPost Phys. **1**, 010 (2016).

[138] H. Kadau, M. Schmitt, M. Wenzel, C. Wink, T. Maier, I. Ferrier-Barbut, and T. Pfau, "Observing the Rosensweig instability of a quantum ferrofluid," Nature **530**, 194 EP (2016).

[139] S. Lepoutre, L. Gabardos, K. Kechadi, P. Pedri, O. Gorceix, E. Maréchal, L. Vernac, and B. Laburthe-Tolra, "Collective spin modes of a trapped quantum ferrofluid," Phys. Rev. Lett. **121**, 013201 (2018).

[140] S. Baier, D. Petter, J. H. Becher, A. Patscheider, G. Natale, L. Chomaz, M. J. Mark, and F. Ferlaino, "Realization of a strongly interacting Fermi gas of dipolar atoms," Phys. Rev. Lett. **121**, 093602 (2018).

[141] Y. Tang, W. Kao, K.-Y. Li, and B. L. Lev, "Tuning the dipole-dipole interaction in a quantum gas with a rotating magnetic field," Phys. Rev. Lett. **120**, 230401 (2018).

[142] M. Viteau, P. Huillery, M. G. Bason, N. Malossi, D. Ciampini, O. Morsch, E. Arimondo, D. Comparat, and P. Pillet, "Cooperative excitation and many-body interactions in a cold Rydberg gas," Phys. Rev. Lett. **109**, 053002 (2012).

[143] P. Schauß, M. Cheneau, M. Endres, T. Fukuhara, S. Hild, A. Omran, T. Pohl, C. Gross, S. Kuhr, and I. Bloch, "Observation of spatially ordered structures in a two-dimensional Rydberg gas," Nature (London) **491**, 87 (2012).

[144] C. Carr, R. Ritter, C. G. Wade, C. S. Adams, and K. J. Weatherill, "Nonequilibrium phase transition in a dilute Rydberg ensemble," Phys. Rev. Lett. **111**, 113901 (2013).

[145] Y. Y. Jau, A. M. Hankin, T. Keating, I. H. Deutsch, and G. W. Biedermann, "Entangling atomic spins with a Rydberg-dressed spin-flip blockade," Nature Physics **12**, 71 (2015).

[146] T. M. Weber, M. Höning, T. Niederprüm, T. Manthey, O. Thomas, V. Guarrera, M. Fleischhauer, G. Barontini, and H. Ott, "Mesoscopic rydberg-blockaded ensembles in the superatom regime and beyond," Nature Physics **11**, 157 EP (2015).

[147] R. Faoro, C. Simonelli, M. Archimi, G. Masella, M. M. Valado, E. Arimondo, R. Mannella, D. Ciampini, and O. Morsch, "van der Waals explosion of cold Rydberg clusters," Phys. Rev. A **93**, 030701 (2016).

[148] H. Labuhn, D. Barredo, S. Ravets, S. de Léséleuc, T. Macrì, T. Lahaye, and A. Browaeys, "Tunable two-dimensional arrays of single Rydberg atoms for realizing quantum ising models," Nature **534**, 667 (2016).

[149] H. Gorniaczyk, C. Tresp, P. Bienias, A. Paris-Mandoki, W. Li, I. Mirgorodskiy, H. P. Büchler, I. Lesanovsky, and S. Hofferberth, "Enhancement of Rydberg-mediated single-photon nonlinearities by electrically tuned Förster resonances," Nature Communications **7**, 12480 (2016).

[150] J. Zeiher, R. van Bijnen, P. Schauß, S. Hild, J.-y. Choi, T. Pohl, I. Bloch, and C. Gross, "Many-body interferometry of a Rydberg-dressed spin lattice," Nature Physics **12**, 1095 (2016).

[151] H. Bernien, S. Schwartz, A. Keesling, H. Levine, A. Omran, H. Pichler, S. Choi, A. S. Zibrov, M. Endres, M. Greiner, V. Vuletić, and M. D. Lukin, "Probing many-body dynamics on a 51-atom quantum simulator," Nature **551**, 579 (2017).

[152] G. A. Álvarez, D. Suter, and R. Kaiser, "Localization-delocalization transition in the dynamics of dipolar-coupled nuclear spins," Science **349**, 846 (2015).

[153] W. R. Anderson, J. R. Veale, and T. F. Gallagher, "Resonant dipole-dipole energy transfer in a nearly frozen rydberg gas," Phys. Rev. Lett. **80**, 249 (1998).

[154] W. R. Anderson, M. P. Robinson, J. D. D. Martin, and T. F. Gallagher, "Dephasing of resonant energy transfer in a cold rydberg gas," Phys. Rev. A **65**, 063404 (2002).

[155] G. D. Scholes and G. Rumbles, "Excitons in nanoscale systems," Nature Materials **5**, 683 (2006).

[156] F. Dubin, R. Melet, T. Barisien, R. Grousson, L. Legrand, M. Schott, and V. Voliotis, "Macroscopic coherence of a single exciton state in an organic quantum wire," Nature Physics **2**, 32 (2005).

[157] F. Dubin, J. Berrehar, R. Grousson, M. Schott, and V. Voliotis, "Evidence of polariton-induced transparency in a single organic quantum wire," Phys. Rev. B **73**, 121302 (2006).

[158] X. P. Vögele, D. Schuh, W. Wegscheider, J. P. Kotthaus, and A. W. Holleitner, "Density enhanced diffusion of dipolar excitons within a one-dimensional channel," Phys. Rev. Lett. **103**, 126402 (2009).

[159] S. Wüster, C. Ates, A. Eisfeld, and J. M. Rost, "Excitation transport through Rydberg dressing," New Journal of Physics **13**, 073044 (2011).

[160] G. Günter, H. Schempp, M. Robert-de Saint-Vincent, V. Gavryusev, S. Helmrich, C. S. Hofmann, S. Whitlock, and M. Weidemüller, "Observing the dynamics of dipole-mediated energy transport by interaction-enhanced imaging," Science **342**, 954 (2013).

[161] F. Robicheaux and N. M. Gill, "Effect of random positions for coherent dipole transport," Phys. Rev. A **89**, 053429 (2014).

[162] D. W. Schönleber, A. Eisfeld, M. Genkin, S. Whitlock, and S. Wüster, "Quantum simulation of energy transport with embedded Rydberg aggregates," Phys. Rev. Lett. **114**, 123005 (2015).

[163] H. Schempp, G. Günter, S. Wüster, M. Weidemüller, and S. Whitlock, "Correlated exciton transport in Rydberg-dressed-atom spin chains," Phys. Rev. Lett. **115**, 093002 (2015).

[164] D. Barredo, H. Labuhn, S. Ravets, T. Lahaye, A. Browaeys, and C. S. Adams, "Coherent excitation transfer in a spin chain of three Rydberg atoms," Phys. Rev. Lett. **114**, 113002 (2015).

[165] I. Rosenberg, D. Liran, Y. Mazuz-Harpaz, K. West, L. Pfeiffer, and R. Rapaport, "Strongly interacting dipolar-polaritons," Science Advances **4** (2018), 10.1126/sciadv.aat8880.

[166] F. Pientka, L. I. Glazman, and F. von Oppen, "Topological superconducting phase in helical Shiba chains," Phys. Rev. B **88**, 155420 (2013).

[167] F. Pientka, L. I. Glazman, and F. von Oppen, "Unconventional topological phase transitions in helical Shiba chains," Phys. Rev. B **89**, 180505 (2014).

[168] D. T. Liu, J. Shabani, and A. Mitra, "Long-range Kitaev chains via planar Josephson junctions," Phys. Rev. B **97**, 235114 (2018).

[169] D. T. Liu, J. Shabani, and A. Mitra, "Floquet majorana zero and π modes in planar josephson junctions," Phys. Rev. B **99**, 094303 (2019).

[170] P. Hauke and L. Tagliacozzo, "Spread of correlations in long-range interacting quantum systems," Phys. Rev. Lett. **111**, 207202 (2013).

[171] Z.-X. Gong, M. Foss-Feig, S. Michalakis, and A. V. Gorshkov, "Persistence of locality in systems with power-law interactions," Phys. Rev. Lett. **113**, 030602 (2014).

[172] M. Foss-Feig, Z.-X. Gong, C. W. Clark, and A. V. Gorshkov, "Nearly Linear Light Cones in Long-Range Interacting Quantum Systems," Phys. Rev. Lett. **114**, 157201 (2015).

[173] F. Liu, R. Lundgren, P. Titum, G. Pagano, J. Zhang, C. Monroe, and A. V. Gorshkov, "Confined quasiparticle dynamics in long-range interacting quantum spin chains," Phys. Rev. Lett. **122**, 150601 (2019).

[174] J. Zhang, P. W. Hess, A. Kyprianidis, P. Becker, A. Lee, J. Smith, G. Pagano, I. D. Potirniche, A. C. Potter, A. Vishwanath, N. Y. Yao, and C. Monroe, "Observation of a discrete time crystal," Nature **543**, 217 EP (2017).

[175] O. Viyuela, D. Vodola, G. Pupillo, and M. A. Martin-Delgado, "Topological massive Dirac edge modes and long-range superconducting Hamiltonians," Phys. Rev. B **94**, 125121 (2016).

[176] Z.-X. Gong, M. F. Maghrebi, A. Hu, M. L. Wall, M. Foss-Feig, and A. V. Gorshkov, "Topological phases with long-range interactions," Phys. Rev. B **93**, 041102 (2016).

[177] L. Lepori and L. Dell'Anna, "Long-range topological insulators and weakened bulk-boundary correspondence," New Journal of Physics **19**, 103030 (2017).

[178] K. Patrick, T. Neupert, and J. K. Pachos, "Topological quantum liquids with long-range couplings," Phys. Rev. Lett. **118**, 267002 (2017).

[179] O. Viyuela, L. Fu, and M. A. Martin-Delgado, "Chiral topological superconductors enhanced by long-range interactions," Phys. Rev. Lett. **120**, 017001 (2018).

[180] L. Lepori, D. Giuliano, and S. Paganelli, "Edge insulating topological phases in a two-dimensional superconductor with long-range pairing," Phys. Rev. B **97**, 041109 (2018).

[181] F. Ares, J. G. Esteve, F. Falceto, and A. R. de Queiroz, "Entanglement in fermionic chains with finite-range coupling and broken symmetries," Phys. Rev. A **92**, 042334 (2015).

[182] Z.-X. Gong, M. Foss-Feig, F. G. S. L. Brandão, and A. V. Gorshkov, "Entanglement area laws for long-range interacting systems," Phys. Rev. Lett. **119**, 050501 (2017).

[183] N. Roy, A. Sharma, and R. Mukherjee, "Quantum simulation of long range XY quantum spin glass with strong area-law violation using trapped ions," arXiv:1812.08938 (2018).

[184] L. S. Levitov, "Absence of localization of vibrational modes due to dipole-dipole interaction," Europhysics Letters (EPL) **9**, 83 (1989).

[185] L. S. Levitov, "Delocalization of vibrational modes caused by electric dipole interaction," Phys. Rev. Lett. **64**, 547 (1990).

[186] A. D. Mirlin, Y. V. Fyodorov, F.-M. Dittes, J. Quezada, and T. H. Seligman, "Transition from localized to extended eigenstates in the ensemble of power-law random banded matrices," Phys. Rev. E **54**, 3221 (1996).

[187] A. Rodríguez, V. A. Malyshev, and F. Domínguez-Adame, "Quantum diffusion and lack of universal one-parameter scaling in one-dimensional disordered lattices with long-range coupling," J. Phys. A **33**, L161 (2000).

[188] A. Rodríguez, V. A. Malyshev, G. Sierra, M. A. Martín-Delgado, J. Rodríguez-Laguna, and F. Domínguez-Adame, "Anderson Transition in Low-Dimensional Disordered Systems Driven by Long-Range Nonrandom Hopping," Phys. Rev. Lett. **90**, 027404 (2003).

[189] F. A. B. F. de Moura, A. V. Malyshev, M. L. Lyra, V. A. Malyshev, and F. Domínguez-Adame, "Localization properties of a one-dimensional tight-binding model with nonrandom long-range intersite interactions," Phys. Rev. B **71**, 174203 (2005).

[190] G. L. Celardo, R. Kaiser, and F. Borgonovi, "Shielding and localization in the presence of long-range hopping," Phys. Rev. B **94**, 144206 (2016).

[191] X. Deng, V. E. Kravtsov, G. V. Shlyapnikov, and L. Santos, "Duality in power-law localization in disordered one-dimensional systems," Phys. Rev. Lett. **120**, 110602 (2018).

[192] T. Koffel, M. Lewenstein, and L. Tagliacozzo, "Entanglement entropy for the long-range Ising chain in a transverse field," Phys. Rev. Lett. **109**, 267203 (2012).

[193] P. Hauke and M. Heyl, "Many-body localization and quantum ergodicity in disordered long-range Ising models," Phys. Rev. B **92**, 134204 (2015).

[194] H. Li, J. Wang, X.-J. Liu, and H. Hu, "Many-body localization in Ising models with random long-range interactions," Phys. Rev. A **94**, 063625 (2016).

[195] C. L. Baldwin, C. R. Laumann, A. Pal, and A. Scardicchio, "Clustering of nonergodic eigenstates in quantum spin glasses," Phys. Rev. Lett. **118**, 127201 (2017).

[196] D. A. Abanin and Z. Papić, "Recent progress in many-body localization," Annalen der Physik **529**, 1700169 (2017).

[197] A. L. Burin, "Many-body delocalization in a strongly disordered system with long-range interactions: Finite-size scaling," Phys. Rev. B **91**, 094202 (2015).

[198] A. O. Maksymov, N. Rahman, E. Kapit, and A. L. Burin, "Comment on "Many-body localization in Ising models with random long-range interactions"," Phys. Rev. A **96**, 057601 (2017).

[199] E. Lieb, T. Schultz, and D. Mattis, "Two soluble models of an antiferromagnetic chain," Ann. Phys. (N.Y.) **16**, 407 (1961).

[200] S. Ganeshan, J. H. Pixley, and S. Das Sarma, "Nearest neighbor tight binding models with an exact mobility edge in one dimension," Phys. Rev. Lett. **114**, 146601 (2015).

[201] R. Modak and S. Mukerjee, "Many-body localization in the presence of a single-particle mobility edge," Phys. Rev. Lett. **115**, 230401 (2015).

[202] H. P. Lüschen, S. Scherg, T. Kohlert, M. Schreiber, P. Bordia, X. Li, S. Das Sarma, and I. Bloch, "Single-particle mobility edge in a one-dimensional quasiperiodic optical lattice," Phys. Rev. Lett. **120**, 160404 (2018).

[203] F. M. Izrailev and A. A. Krokhin, "Localization and the mobility edge in one-dimensional potentials with correlated disorder," Phys. Rev. Lett. **82**, 4062 (1999).

[204] G. Vidal, J. I. Latorre, E. Rico, and A. Kitaev, "Entanglement in quantum critical phenomena," Phys. Rev. Lett. **90**, 227902 (2003).

[205] X. Li, S. Ganeshan, J. H. Pixley, and S. Das Sarma, "Many-body localization and quantum nonergodicity in a model with a single-particle mobility edge," Phys. Rev. Lett. **115**, 186601 (2015).

[206] S. D. Geraedts, R. Nandkishore, and N. Regnault, "Many-body localization and thermalization: Insights from the entanglement spectrum," Phys. Rev. B **93**, 174202 (2016).

[207] F. Ares, J. G. Esteve, F. Falceto, and E. Sánchez-Burillo, "Excited state entanglement in homogeneous fermionic chains," J. Phys. A: Math. Theor. **47**, 245301 (2014).

[208] P. Calabrese and J. Cardy, "Entanglement entropy and quantum field theory," J. Stat. Mech: Theory Exp. **2004**, P06002 (2004).

[209] I. Peschel, "Calculation of reduced density matrices from correlation functions," J. Phys. A: Math. Gen. **36**, L205 (2003).

[210] J. J. Sakurai and J. Napolitano, *Modern Quantum Mechanics*, 2nd ed. (Addison-Wesley, 2011).

[211] K. Gottfried and T.-M. Yan, *Quantum Mechanics: Fundamentals* (Springer-Verlag, 2003).

[212] A. Altland and B. Simons, *Condensed Matter Field Theory* (Cambridge University Press, Cambridge, England, 2006).

[213] H. Bruus and K. Flensberg, *Many-Body Quantum Theory in Condensed Matter Physics: An Introduction* (Oxford University Press, Oxford, 2004).

[214] M. Abramowitz and I. A. Stegun, *Handbook of Mathematical Functions* (Dover, 1964).

[215] F. W. J. Olver, D. W. Lozier, R. F. Boisvert, and C. W. Clark, *NIST Handbook of Mathematical Functions* (Cambridge University Press, Cambridge, England, 2010).

[216] U. Schollwöck, "The density-matrix renormalization group," Rev. Mod. Phys. **77**, 259 (2005).

[217] L. Lepori, D. Vodola, G. Pupillo, G. Gori, and A. Trombettoni, "Effective theory and breakdown of conformal symmetry in a long-range quantum chain," Ann. Phys. **374**, 35 (2016).

[218] I. Peschel and T. T. Truong, "Corner transfer matrices and conformal invariance," Z. Phys. B **69**, 385 (1987).

[219] T. T. Truong and I. I. Peschel, "Diagonalisation of finite-size corner transfer matrices and related spin chains," Z. Phys. B **75**, 119 (1989).

[220] I. Peschel, M. Kaulke, and O. Legeza, "Density-matrix spectra for integrable models," Ann. Phys. (Leipzig) **8**, 153 (1999).

[221] I. Peschel, "Calculation of reduced density matrices from correlation functions," J. Phys. A **36**, L205 (2003).

[222] I. Peschel, "Special review: Entanglement in solvable many-particle models," Braz. J. Phys. **42**, 267 (2012).

[223] T. Giamarchi, *Quantum Physics in One Dimensions*, International Series of Monographs on Physics, Vol. 121 (Clarendon, Oxford, 2004).

[224] E. O. Gogolin, E. A. Nersesyan, and M. Tsvelik, *Bosonization and Strongly Correlated Systems* (1998).

[225] M. A. Cazalilla, "Bosonizing one-dimensional cold atomic gases," Journal of Physics B: Atomic, Molecular and Optical Physics **37**, S1 (2004).

[226] M. A. Cazalilla, R. Citro, T. Giamarchi, E. Orignac, and M. Rigol, "One dimensional bosons: From condensed matter systems to ultracold gases," Rev. Mod. Phys. **83**, 1405 (2011).

[227] T. Giamarchi, "Some experimental tests of tomonaga–luttinger liquids," International Journal of Modern Physics B **26**, 1244004 (2012), https://doi.org/10.1142/S0217979212440043 .

[228] C. Kim, A. Y. Matsuura, Z.-X. Shen, N. Motoyama, H. Eisaki, S. Uchida, T. Tohyama, and S. Maekawa, "Observation of spin-charge separation in one-dimensional $srcuo_2$," Phys. Rev. Lett. **77**, 4054 (1996).

[229] P. Segovia, D. Purdie, M. Hengsberger, and Y. Baer, "Observation of spin and charge collective modes in one-dimensional metallic chains," Nature **402**, 504 (1999).

[230] O. Auslaender, H. Steinberg, A. Yacoby, Y. Tserkovnyak, B. I Halperin, K. W Baldwin, L. N Pfeiffer, and K. West, "Spin-charge separation and localization in one dimension," Science (New York, N.Y.) **308**, 88 (2005).

[231] B. J. Kim, H. Koh, E. Rotenberg, S. J. Oh, H. Eisaki, N. Motoyama, S. Uchida, T. Tohyama, S. Maekawa, Z. X. Shen, and C. Kim, "Distinct spinon and holon dispersions in photoemission spectral functions from one-dimensional srcuo2," Nature Physics **2**, 397 EP (2006).

[232] Y. Jompol, C. J. B. Ford, J. P. Griffiths, I. Farrer, G. A. C. Jones, D. Anderson, D. A. Ritchie, T. W. Silk, and A. J. Schofield, "Probing spin-charge separation in a tomonaga-luttinger liquid," Science **325**, 597 (2009), https://science.sciencemag.org/content/325/5940/597.full.pdf .

[233] T. L. Yang, P. Grišins, Y. T. Chang, Z. H. Zhao, C. Y. Shih, T. Giamarchi, and R. G. Hulet, "Measurement of the dynamical structure factor of a 1d interacting Fermi gas," Phys. Rev. Lett. **121**, 103001 (2018).

[234] S. Sachdev, *Quantum Phase Transitions*, 2nd ed. (Cambridge University Press, 2011).

[235] M. Dalmonte, W. Lechner, Z. Cai, M. Mattioli, A. M. Läuchli, and G. Pupillo, "Cluster Luttinger liquids and emergent supersymmetric conformal critical points in the one-dimensional soft-shoulder Hubbard model," Phys. Rev. B **92**, 045106 (2015).

[236] S. Rossotti, M. Teruzzi, D. Pini, D. E. Galli, and G. Bertaina, "Quantum critical behavior of one-dimensional soft bosons in the continuum," Phys. Rev. Lett. **119**, 215301 (2017).

[237] M. Nakamura, "Tricritical behavior in the extended hubbard chains," Phys. Rev. B **61**, 16377 (2000).

[238] T. F. Gallagher, *Rydberg Atoms*, Cambridge Monographs on Atomic, Molecular and Chemical Physics (Cambridge University Press, 1994).

[239] J. Lim, H.-g. Lee, and J. Ahn, "Review of cold rydberg atoms and their applications," Journal of the Korean Physical Society **63**, 867 (2013).

[240] N. Henkel, F. Cinti, P. Jain, G. Pupillo, and T. Pohl, "Supersolid vortex crystals in rydberg-dressed bose-einstein condensates," Phys. Rev. Lett. **108**, 265301 (2012).

[241] N. Henkel, R. Nath, and T. Pohl, "Three-dimensional roton excitations and supersolid formation in rydberg-excited bose-einstein condensates," Phys. Rev. Lett. **104**, 195302 (2010).

[242] L. Santos, G. V. Shlyapnikov, P. Zoller, and M. Lewenstein, "Bose-einstein condensation in trapped dipolar gases," Phys. Rev. Lett. **85**, 1791 (2000).

[243] G. Pupillo, A. Micheli, M. Boninsegni, I. Lesanovsky, and P. Zoller, "Strongly correlated gases of rydberg-dressed atoms: Quantum and classical dynamics," Phys. Rev. Lett. **104**, 223002 (2010).

[244] T. Macrì and T. Pohl, "Rydberg dressing of atoms in optical lattices," Phys. Rev. A **89**, 011402 (2014).

[245] M. Henkel, *Conformal Invariance and Critical Phenomena* (Springer, New York, 1999).

[246] P. di Francesco, P. Mathieu, and D. Senechal, *Conformal Field Theory* (Springer, 1997).

[247] P. Fendley, B. Nienhuis, and K. Schoutens, "Lattice fermion models with supersymmetry," Journal of Physics A: Mathematical and General **36**, 12399 (2003).

[248] S.-S. Lee, "Emergence of supersymmetry at a critical point of a lattice model," Phys. Rev. B **76**, 075103 (2007).

[249] T. Padmanabhan, "Statistical mechanics of gravitating systems," Physics Reports **188**, 285 (1990).

[250] L. D. Landau and E. M. Lifshitz, *Electrodynamics of continuous media*, 1st ed., Course of theoretical physics (Pergamon Press, Oxford, 1960).

[251] D. R. Nicholson, *Introduction to Plasma Theory*, 1st ed., Wiley series in plasma physics (Wiley, New York, 1983).

[252] T. Giamarchi, *Quantum Physics in One Dimensions*, International Series of Monographs on Physics, Vol. 121 (Clarendon, Oxford, 2004).

[253] J. Stuhler, A. Griesmaier, T. Koch, M. Fattori, T. Pfau, S. Giovanazzi, P. Pedri, and L. Santos, "Observation of dipole-dipole interaction in a degenerate quantum gas," Phys. Rev. Lett. **95**, 150406 (2005).

[254] K.-K. Ni, S. Ospelkaus, M. H. G. de Miranda, A. Pe'er, B. Neyenhuis, J. J. Zirbel, S. Kotochigova, P. S. Julienne, D. S. Jin, and J. Ye, "A high phase-space-density gas of polar molecules," Science **322**, 231 (2008).

[255] L. D. Carr, D. DeMille, R. V. Krems, and J. Ye, "Cold and ultracold molecules: Science, technology and applications," New J. Phys. **11**, 055049 (2009).

[256] D. S. Jin and J. Ye, "Introduction to Ultracold Molecules: New Frontiers in Quantum and Chemical Physics," Chem. Rev. **112**, 4801 (2012).

[257] S. Baier, M. J. Mark, D. Petter, K. Aikawa, L. Chomaz, Z. Cai, M. Baranov, P. Zoller, and F. Ferlaino, "Extended bose-hubbard models with ultracold magnetic atoms," Science **352**, 201 (2016).

[258] M. Schmitt, M. Wenzel, F. Böttcher, I. Ferrier-Barbut, and T. Pfau, "Self-bound droplets of a dilute magnetic quantum liquid," Nature **539**, 259 (2016).

[259] L. Chomaz, R. M. W. van Bijnen, D. Petter, G. Faraoni, S. Baier, J. H. Becher, M. J. Mark, F. Wächtler, L. Santos, and F. Ferlaino, "Observation of roton mode population in a dipolar quantum gas," Nature Physics **14**, 442 (2018).

[260] Y. Tang, W. Kao, K.-Y. Li, and B. L. Lev, "Tuning the Dipole-Dipole Interaction in a Quantum Gas with a Rotating Magnetic Field," Phys. Rev. Lett. **120**, 230401 (2018).

[261] N. Defenu, A. Trombettoni, and S. Ruffo, "Anisotropic long-range spin systems," Phys. Rev. B **94**, 224411 (2016).

[262] N. Defenu, A. Trombettoni, and S. Ruffo, "Criticality and phase diagram of quantum long-range o(n) models," Phys. Rev. B **96**, 104432 (2017).

[263] N. Defenu, T. Enss, M. Kastner, and G. Morigi, "Dynamical critical scaling of long-range interacting quantum magnets," Phys. Rev. Lett. **121**, 240403 (2018).

[264] A. Dutta and J. K. Bhattacharjee, "Phase transitions in the quantum ising and rotor models with a long-range interaction," Phys. Rev. B **64**, 184106 (2001).

[265] N. Laflorencie, I. Affleck, and M. Berciu, "Critical phenomena and quantum phase transition in long range heisenberg antiferromagnetic chains," Journal of Statistical Mechanics: Theory and Experiment **2005**, P12001 (2005).

[266] D. Peter, S. Müller, D. Wessel, and H. P. Büchler, "Anomalous behavior of spin systems with dipolar interactions," Phys. Rev. Lett. **109**, 025303 (2012).

[267] P. Hauke, F. M. Cucchietti, M. Müller-Hermes, A. Bañuls, J. I. Cirac, and M. Lewenstein, "Complete devil's staircase and crystal–superfluid transitions in a dipolar xxz spin chain: a trapped ion quantum simulation," New J. Phys. **12**, 113037 (2010).

[268] I. Frérot, P. Naldesi, and T. Roscilde, "Entanglement and fluctuations in the XXZ model with power-law interactions," Phys. Rev. B **95**, 245111 (2017).

[269] T. Botzung, D. Vodola, P. Naldesi, M. Müller, E. Ercolessi, and G. Pupillo, "Algebraic localization from power-law interactions in disordered quantum wires," ArXiv e-prints (2018), arXiv:1810.09779 [cond-mat.dis-nn] .

[270] F. J. Burnell, M. M. Parish, N. R. Cooper, and S. L. Sondhi, "Devil's staircases and supersolids in a one-dimensional dipolar Bose gas," Phys. Rev. B **80**, 174519 (2009).

[271] L. Pollet, J. D. Picon, H. P. Büchler, and M. Troyer, "Supersolid Phase with Cold Polar Molecules on a Triangular Lattice," Phys. Rev. Lett. **104**, 125302 (2010).

[272] B. Capogrosso-Sansone, C. Trefzger, M. Lewenstein, P. Zoller, and G. Pupillo, "Quantum phases of cold polar molecules in 2d optical lattices," Phys. Rev. Lett. **104**, 125301 (2010).

[273] M. F. Maghrebi, Z.-X. Gong, and A. V. Gorshkov, "Continuous symmetry breaking in 1d long-range interacting quantum systems," Phys. Rev. Lett. **119**, 023001 (2017).

[274] D. Mukamel, "Statistical mechanics of systems with long range interactions," AIP Conference Proceedings **970**, 22 (2008).

[275] M. Kac, G. E. Uhlenbeck, and P. C. Hemmer, "On the van der waals theory of the vapor-liquid equilibrium. i. discussion of a one-dimensional model," Journal of Mathematical Physics **4**, 216 (1963).

[276] S. A. Cannas and F. A. Tamarit, "Long-range interactions and nonextensivity in ferromagnetic spin models," Phys. Rev. B **54**, R12661 (1996).

[277] F. Tamarit and C. Anteneodo, "Rotators with long-range interactions: Connection with the mean-field approximation," Phys. Rev. Lett. **84**, 208 (2000).

[278] T. Dauxois, V. Latora, A. Rapisarda, S. Ruffo, and A. Torcini, "The hamiltonian mean field model: From dynamics to statistical mechanics and back," in *Dynamics and Thermodynamics of Systems with Long-Range Interactions*, edited by T. Dauxois, S. Ruffo, E. Arimondo, and M. Wilkens (Springer Berlin Heidelberg, Berlin, Heidelberg, 2002) pp. 458–487.

[279] M. Kastner and O. Schnetz, "On the mean-field spherical model," Journal of Statistical Physics **122**, 1195 (2006).

[280] H. J. Schulz, "Wigner crystal in one dimension," Phys. Rev. Lett. **71**, 1864 (1993).

[281] D. W. Wang, A. J. Millis, and S. Das Sarma, "Coulomb luttinger liquid," Phys. Rev. B **64**, 193307 (2001).

[282] M. Casula, S. Sorella, and G. Senatore, "Ground state properties of the one-dimensional coulomb gas using the lattice regularized diffusion monte carlo method," Phys. Rev. B **74**, 245427 (2006).

[283] G. E. Astrakharchik and M. D. Girardeau, "Exact ground-state properties of a one-dimensional coulomb gas," Phys. Rev. B **83**, 153303 (2011).

[284] R. M. Lee and N. D. Drummond, "Ground-state properties of the one-dimensional electron liquid," Phys. Rev. B **83**, 245114 (2011).

[285] D. Poilblanc, S. Yunoki, S. Maekawa, and E. Dagotto, "Insulator-metal transition in one dimension induced by long-range electronic interactions," Phys. Rev. B **56**, R1645 (1997).

[286] S. Capponi, D. Poilblanc, and T. Giamarchi, "Effects of long-range electronic interactions on a one-dimensional electron system," Phys. Rev. B **61**, 13410 (2000).

[287] B. Valenzuela, S. Fratini, and D. Baeriswyl, "Charge and spin order in one-dimensional electron systems with long-range coulomb interactions," Phys. Rev. B **68**, 045112 (2003).

[288] Z.-H. Li, "Ground states of long-range interacting fermions in one spatial dimension," Journal of Physics: Condensed Matter **31**, 255601 (2019).

[289] C. Anteneodo and C. Tsallis, "Breakdown of exponential sensitivity to initial conditions: Role of the range of interactions," Phys. Rev. Lett. **80**, 5313 (1998).

[290] C. Anteneodo, "Nonextensive scaling in a long-range hamiltonian system," Physica A: Statistical Mechanics and its Applications **342**, 112 (2004), proceedings of the VIII Latin American Workshop on Nonlinear Phenomena.

[291] G. Fano, F. Ortolani, A. Parola, and L. Ziosi, "Unscreened coulomb repulsion in the one-dimensional electron gas," Phys. Rev. B **60**, 15654 (1999).

[292] P. Schmitteckert and R. Werner, "Charge-density-wave instabilities driven by multiple umklapp scattering," Phys. Rev. B **69**, 195115 (2004).

[293] F. Franchini, *An Introduction to Integrable Techniques for One-Dimensional Quantum Systems*, Lecture Notes in Physics (Springer International Publishing, 2017).

[294] W. Kohn, "Theory of the insulating state," Phys. Rev. **133**, A171 (1964).

[295] G. G. Batrouni, F. F. Assaad, R. T. Scalettar, and P. J. H. Denteneer, "Dynamic response of trapped ultracold bosons on optical lattices," Phys. Rev. A **72**, 031601 (2005).

[296] E. T. Jaynes and F. W. Cummings, "Comparison of quantum and semiclassical radiation theories with application to the beam maser," Proc. IEEE **51**, 89 (1963).

[297] B. W. Shore and P. L. Knight, "The Jaynes-Cummings Model," J. Mod. Opt. **40**, 1195 (1993).

[298] H. J. Kimble, "Strong interactions of single atoms and photons in cavity QED," Phys. Scr. **T76**, 127 (1998).

[299] M. Tavis and F. W. Cummings, "Exact Solution for an N-Molecule—Radiation-Field Hamiltonian," Phys. Rev. **170**, 379 (1968).

[300] Y. Zhu, D. J. Gauthier, S. E. Morin, Q. Wu, H. J. Carmichael, and T. W. Mossberg, "Vacuum Rabi splitting as a feature of linear-dispersion theory: Analysis and experimental observations," Phys. Rev. Lett. **64**, 2499 (1990).

[301] L. A. Orozco, M. G. Raizen, M. Xiao, R. J. Brecha, and H. J. Kimble, "Squeezed-state generation in optical bistability," J. Opt. Soc. Am. B **4**, 1490 (1987).

[302] M. G. Raizen, R. J. Thompson, R. J. Brecha, H. J. Kimble, and H. J. Carmichael, "Normal-mode splitting and linewidth averaging for two-state atoms in an optical cavity," Phys. Rev. Lett. **63**, 240 (1989).

[303] R. J. Thompson, G. Rempe, and H. J. Kimble, "Observation of normal-mode splitting for an atom in an optical cavity," Phys. Rev. Lett. **68**, 1132 (1992).

[304] M. Brune, F. Schmidt-Kaler, A. Maali, J. Dreyer, E. Hagley, J. M. Raimond, and S. Haroche, "Quantum Rabi Oscillation: A Direct Test of Field Quantization in a Cavity," Phys. Rev. Lett. **76**, 1800 (1996).

[305] P. W. H. Pinkse, T. Fischer, P. Maunz, and G. Rempe, "Trapping an atom with single photons," Nature **404**, 365 (2000).

[306] Y. Colombe, T. Steinmetz, G. Dubois, F. Linke, D. Hunger, and J. Reichel, "Strong atom–field coupling for Bose–Einstein condensates in an optical cavity on a chip," Nature **450**, 272 (2007).

[307] Y. Nakamura, Yu. A. Pashkin, and J. S. Tsai, "Coherent control of macroscopic quantum states in a single-Cooper-pair box," Nature **398**, 786 (1999).

[308] D. Vion, A. Aassime, A. Cottet, P. Joyez, H. Pothier, C. Urbina, D. Esteve, and M. H. Devoret, "Manipulating the Quantum State of an Electrical Circuit," Science **296**, 886 (2002).

[309] J. M. Martinis, S. Nam, J. Aumentado, and C. Urbina, "Rabi Oscillations in a Large Josephson-Junction Qubit," Phys. Rev. Lett. **89**, 117901 (2002).

[310] I. Chiorescu, Y. Nakamura, C. J. P. M. Harmans, and J. E. Mooij, "Coherent Quantum Dynamics of a Superconducting Flux Qubit," Science **299**, 1869 (2003).

[311] A. Wallraff, D. I. Schuster, A. Blais, L. Frunzio, R.-S. Huang, J. Majer, S. Kumar, S. M. Girvin, and R. J. Schoelkopf, "Strong coupling of a single photon to a superconducting qubit using circuit quantum electrodynamics," Nature **431**, 162 (2004).

[312] T. Yoshie, A. Scherer, J. Hendrickson, G. Khitrova, H. M. Gibbs, G. Rupper, C. Ell, O. B. Shchekin, and D. G. Deppe, "Vacuum Rabi splitting with a single quantum dot in a photonic crystal nanocavity," Nature **432**, 200 (2004).

[313] K. Hennessy, A. Badolato, M. Winger, D. Gerace, M. Atatüre, S. Gulde, S. Fält, E. L. Hu, and A. Imamoğlu, "Quantum nature of a strongly coupled single quantum dot–cavity system," nature **445**, 896 (2007).

[314] H. Deng, H. Haug, and Y. Yamamoto, "Exciton-polariton Bose-Einstein condensation," Rev. Mod. Phys. **82**, 1489 (2010).

[315] C. Ciuti, G. Bastard, and I. Carusotto, "Quantum vacuum properties of the intersubband cavity polariton field," Phys. Rev. B **72**, 115303 (2005).

[316] I. Pockrand, A. Brillante, and D. Möbius, "Exciton–surface plasmon coupling: An experimental investigation," J. Chem. Phys. **77**, 6289 (1982).

[317] D. G. Lidzey, D. D. C. Bradley, M. S. Skolnick, T. Virgili, S. Walker, and D. M. Whittaker, "Strong exciton–photon coupling in an organic semiconductor microcavity," Nature **395**, 53 (1998).

[318] J. Bellessa, C. Bonnand, J. C. Plenet, and J. Mugnier, "Strong Coupling between Surface Plasmons and Excitons in an Organic Semiconductor," Phys. Rev. Lett. **93**, 036404 (2004).

[319] J. Dintinger, S. Klein, F. Bustos, W. L. Barnes, and T. W. Ebbesen, "Strong coupling between surface plasmon-polaritons and organic molecules in subwavelength hole arrays," Phys. Rev. B **71**, 035424 (2005).

[320] V. M. Agranovich, Yu. N. Gartstein, and M. Litinskaya, "Hybrid Resonant Organic–Inorganic Nanostructures for Optoelectronic Applications," Chem. Rev. **111**, 5179 (2011).

[321] J. A. Hutchison, T. Schwartz, C. Genet, E. Devaux, and T. W. Ebbesen, "Modifying Chemical Landscapes by Coupling to Vacuum Fields," Angew. Chem. Int. Ed. **51**, 1592 (2012).

[322] A. Shalabney, J. George, J. Hutchison, G. Pupillo, C. Genet, and T. W. Ebbesen, "Coherent coupling of molecular resonators with a microcavity mode," Nat. Commun. **6**, 5981 (2015).

[323] R. Chikkaraddy, B. de Nijs, F. Benz, S. J. Barrow, O. A. Scherman, E. Rosta, A. Demetriadou, P. Fox, O. Hess, and J. J. Baumberg, "Single-molecule strong coupling at room temperature in plasmonic nanocavities," nature **535**, 127 (2016).

[324] Y. Zhang, Q.-S. Meng, L. Zhang, Y. Luo, Y.-J. Yu, B. Yang, Y. Zhang, R. Esteban, J. Aizpurua, Y. Luo, J.-L. Yang, Z.-C. Dong, and J. G. Hou, "Sub-nanometre control of the coherent interaction between a single molecule and a plasmonic nanocavity," Nat. Commun. **8**, 15225 (2017).

[325] D. Wang, H. Kelkar, D. Martin-Cano, D. Rattenbacher, A. Shkarin, T. Utikal, S. Götzinger, and V. Sandoghdar, "Turning a molecule into a coherent two-level quantum system," Nat. Phys. **15**, 483 (2019).

[326] J. Feist and F. J. Garcia-Vidal, "Extraordinary Exciton Conductance Induced by Strong Coupling," Phys. Rev. Lett. **114**, 196402 (2015).

[327] J. Schachenmayer, C. Genes, E. Tignone, and G. Pupillo, "Cavity-Enhanced Transport of Excitons," Phys. Rev. Lett. **114**, 196403 (2015).

[328] E. Orgiu, J. George, J. A. Hutchison, E. Devaux, J. F. Dayen, B. Doudin, F. Stellacci, C. Genet, J. Schachenmayer, C. Genes, G. Pupillo, P. Samorì, and T. W. Ebbesen, "Conductivity in organic semiconductors hybridized with the vacuum field," Nat. Mater. **14**, 1123 (2015).

[329] D. Hagenmüller, J. Schachenmayer, S. Schütz, C. Genes, and G. Pupillo, "Cavity-Enhanced Transport of Charge," Phys. Rev. Lett. **119**, 223601 (2017).

[330] D. Hagenmüller, S. Schütz, J. Schachenmayer, C. Genes, and G. Pupillo, "Cavity-assisted mesoscopic transport of fermions: Coherent and dissipative dynamics," Phys. Rev. B **97**, 205303 (2018).

[331] N. Bartolo and C. Ciuti, "Vacuum-dressed cavity magnetotransport of a two-dimensional electron gas," Phys. Rev. B **98**, 205301 (2018).

[332] G. L. Paravicini-Bagliani, F. Appugliese, E. Richter, F. Valmorra, J. Keller, M. Beck, N. Bartolo, C. Rössler, T. Ihn, K. Ensslin, C. Ciuti, G. Scalari, and J. Faist, "Magneto-transport controlled by Landau polariton states," Nat. Phys. **15**, 186 (2018).

[333] C. Naudet-Baulieu, N. Bartolo, G. Orso, and C. Ciuti, "Dark vertical conductance of cavity-embedded semiconductor heterostructures," New J. Phys. **21**, 093061 (2019).

[334] R. Houdré, R. P. Stanley, and M. Ilegems, "Vacuum-field Rabi splitting in the presence of inhomogeneous broadening: Resolution of a homogeneous linewidth in an inhomogeneously broadened system," Phys. Rev. A **53**, 2711 (1996).

[335] C. Gonzalez-Ballestero, J. Feist, E. Gonzalo Badía, E. Moreno, and F. J. Garcia-Vidal, "Uncoupled Dark States Can Inherit Polaritonic Properties," Phys. Rev. Lett. **117**, 156402 (2016).

[336] P. W. Anderson, "Absence of Diffusion in Certain Random Lattices," Phys. Rev. **109**, 1492 (1958).

[337] F. Evers and A. D. Mirlin, "Anderson transitions," Rev. Mod. Phys. **80**, 1355 (2008).

[338] A. MacKinnon and B. Kramer, "One-parameter scaling of localization length and conductance in disordered systems," Phys. Rev. Lett. **47**, 1546 (1981).

[339] E. Hofstetter and M. Schreiber, "Finite-size scaling and critical exponents. a new approach and its application to anderson localisation," Europhysics Letters (EPL) **21**, 933 (1993).

[340] I. K. Zharekeshev and B. Kramer, "Scaling of level statistics at the disorder-induced metal-insulator transition," Phys. Rev. B **51**, 17239 (1995).

[341] B. I. Shklovskii, B. Shapiro, B. R. Sears, P. Lambrianides, and H. B. Shore, "Statistics of spectra of disordered systems near the metal-insulator transition," Phys. Rev. B **47**, 11487 (1993).

[342] B. Kramer and A. MacKinnon, "Localization: theory and experiment," Rep. Prog. Phys. **56**, 1469 (1993).

[343] I. M. Lifshitz, "Energy Spectrum Structure and quantum States of disordered condensed systems," Soviet Physics Uspekhi **7**, 549 (1965).

[344] M. P. Sörensen and T. Schneider, "Level-spacing statistics for the anderson model in one and two dimensions," Zeitschrift für Physik B Condensed Matter **82**, 115 (1991).

[345] F. Haake, "Random-matrix theory," in *Quantum Signatures of Chaos* (Springer Berlin Heidelberg, Berlin, Heidelberg, 2010) pp. 61–143.

[346] J. Brndiar and P. Markoš, "Universality of the metal-insulator transition in three-dimensional disordered systems," Phys. Rev. B **74**, 153103 (2006).

[347] L. Ujfalusi and I. Varga, "Quantum percolation transition in three dimensions: Density of states, finite-size scaling, and multifractality," Phys. Rev. B **90**, 174203 (2014).

[348] F. Evers and A. D. Mirlin, "Anderson transitions," Rev. Mod. Phys. **80**, 1355 (2008).

[349] S. N. Evangelou and D. E. Katsanos, "Energy level statistics in disordered metals with an anderson transition," Journal of Statistical Physics **85**, 525 (1996).

[350] Y. Y. Atas, E. Bogomolny, O. Giraud, and G. Roux, "Distribution of the ratio of consecutive level spacings in random matrix ensembles," Phys. Rev. Lett. **110**, 084101 (2013).

[351] M. Arndt, R. Stannarius, H. Groothues, E. Hempel, and F. Kremer, "Length scale of cooperativity in the dynamic glass transition," Phys. Rev. Lett. **79**, 2077 (1997).

[352] D. Braun, G. Montambaux, and M. Pascaud, "Boundary conditions at the mobility edge," Phys. Rev. Lett. **81**, 1062 (1998).

[353] P. Markoš, "Numerical analysis of the anderson localization," Acta Physica Slovaca. Reviews and Tutorials **56** (2006), 10.2478/v10155-010-0081-0.

[354] G. Celardo, A. Biella, L. Kaplan, and F. Borgonovi, "Interplay of superradiance and disorder in the anderson model," Fortschritte der Physik **61**, 250 (2013), https://onlinelibrary.wiley.com/doi/pdf/10.1002/prop.201200082 .

[355] V. V. Sokolov, I. Rotter, D. V. Savin, and M. Müller, "Interfering doorway states and giant resonances. i. resonance spectrum and multipole strengths," Phys. Rev. C **56**, 1031 (1997).

[356] E. B. Bogomolny, U. Gerland, and C. Schmit, "Models of intermediate spectral statistics," Phys. Rev. E **59**, R1315 (1999).

[357] A. Angelone, F. Mezzacapo, and G. Pupillo, "Superglass phase of interaction-blockaded gases on a triangular lattice," Phys. Rev. Lett. **116**, 135303 (2016).

[358] C. Lacroix, P. Mendels, and F. Mila, *Introduction to Frustrated Magnetism: Materials, Experiments, Theory*, Springer Series in Solid-State Sciences (Springer Berlin Heidelberg, 2011).

[359] I. S. Tupitsyn and N. V. Prokof'ev, "Stability of dirac liquids with strong coulomb interaction," Phys. Rev. Lett. **118**, 026403 (2017).